*Year :* 2020

# MALT1 protease function – from ubiquitin binding to substrate cleavage

## Schairer Rebekka

**UNIL | Université de Lausanne**

# Faculté de biologie
# et de médecine

**Département de Biochimie**

# MALT1 protease function – from ubiquitin binding to substrate cleavage

**Thèse de doctorat ès sciences de la vie (PhD)**

présentée à la

Faculté de biologie et de médecine
de l'Université de Lausanne

par

# Rebekka SCHAIRER

Master en Biochimie de l'Université de Tübingen

**Jury**

Prof. Fabio Martinon, Président
Prof. Margot Thome-Miazza, Directrice de thèse
Prof. Kay Hofmann, Expert
Prof. Geert van Loo, Expert

Lausanne, 2020

# Imprimatur

Vu le rapport présenté par le jury d'examen, composé de

| | | | | |
|---|---|---|---|---|
| **Président·e** | Monsieur | Prof. | Fabio | **Martinon** |
| **Directeur·trice de thèse** | Madame | Prof. | Margot | **Thome Miazza** |
| **Expert·e·s** | Monsieur | Prof. | Kay | **Hoffmann** |
| | Monsieur | Prof. | Geert | **van Loo** |

le Conseil de Faculté autorise l'impression de la thèse de

## Madame Rebekka Schairer

Master of science, Eberhard Karls Universität, Allemagne

intitulée

## MALT1 protease function – from ubiquitin binding to substrate cleavage

Lausanne, le 4 juin 2020

pour le Doyen
de la Faculté de biologie et de médecine

Prof. Niko GELDNER
Directeur de l'Ecole Doctorale

# Acknowledgements

Finishing a PhD is like climbing a high mountain. It is a tough way with ups and downs, in which you have to be patient and learn to appreciate every single step. I would not have been able to reach the top without the help, support and the company of countless people to whom I would like to give my gratitude here.

First of all, I would like to thank Prof. Margot Thome-Miazza for the great opportunity to do my PhD in your lab. I appreciate your leadership, expertise and the freedom and trust that you gave me to follow my own ideas in the lab. Your open door, the direct supervision and the availability for instructive discussions are the things I want to thank the most. Your optimism and enthusiasm made me confident in my research and strengthened me to hold on things and to believe in myself. Thank you for everything that I could learn from you from an academic, but also from a personal point of view.

I also thank all the members of my thesis committee, Prof. Fabio Martinon, Prof. Kay Hofmann and Prof. Geert van Loo, for the time that you invested in the evaluation of my research and thesis. I especially thank Prof. Fabio Martinon, who always followed my research and my whole path as my PhD representative.

I am also grateful for having the company and help of amazing colleagues in the Thome lab in the past and present. I cannot mention all of them, but I want to thank Chantal, Monserrat, Mélanie, Julie, Daniela, Laurence, Colin, Silvia, Tatjana, David, Nagham, Quentin, Ivana and Ming for the always friendly and positive atmosphere in the lab. I enjoyed the daily serious and non-serious discussions, the singing, dancing and any other joy in the lab that made it a wonderful workplace to me. Special thanks go to Chantal for her intensive technical help in the lab. I appreciated your precision in all kind of lab work, your vast knowledge about different methods and your helpful suggestions. It was a pleasure to work with you. I also want to thank Julie for your help with french translations.

Overall, I want to thank all the members of the Department of Biochemistry for their scientific help and advice, especially the groups of the fourth floor for interesting and instructive joint group meetings. I also want to acknowledge all the secretaries of the DB for the help with formalities and for allowing everything to run so smoothly.

Outside of the University of Lausanne, I also want to thank our collaboration partners from the University of Leicester and from LifeArc, Stevenage for their great contribution to this work. Special thanks go to Gareth Hall and Mark Carr for the always constructive phone meetings. I am grateful for working together with you and looking forward to future projects.

Finally, this work could not have been done without the support of my family and friends in Germany. I am glad for my parents Rainer and Isolde, who eternally believe in me, for offering me unconditional support during my entire life, even though you not always precisely understood what I am actually doing. I thank my sister Nadja and her family for their advices and encouragement. Last but not least I thank Andi for his love, patience, trust and support of the last three years and I am infinitely grateful for having you on my side to climb the next mountain in my life.

# Table of Content

# 1 Abstract

(English)

The protease MALT1 has a key function in the activation of lymphocytes and the regulation of the immune response, by promoting the activation of pro-inflammatory transcription factors such as NF-κB. Dysregulation of MALT1 is implicated in immunodeficiency, autoimmune diseases, lymphomagenesis and non-lymphoid malignancies. Therefore, MALT1 proteolytic activity has appeared as a possible pharmaceutical target, however, the precise mechanism of MALT1 protease activation and the role of individual substrate cleavage events remain incompletely defined. Thus, the aims of this study are to firstly elucidate the molecular mechanism of MALT1 activation and second, to explore the role of the MALT1-dependent cleavage of one particular substrate namely, A20.

The protease activity of MALT1 is tightly controlled by conjugation of monoubiquitin to its third auto-inhibitory Ig-like domain, but the mechanism governing the release of the protease domain by a single ubiquitin moiety remains unknown. Here, we identify the Ig3 domain of MALT1 as a novel ubiquitin-binding domain, responsible for MALT1 monoubiquitination, which is essential for MALT1 proteolytic activity and lymphocyte activation. Furthermore, we reveal an allosteric communication from the monoubiquitination site through the protease-Ig3 interaction surface to the catalytic active site of the protease domain.

One of the first substrates of MALT1 that has been identified is A20, a potent anti-inflammatory protein. A20 is a well-described negative regulator of the NF-κB signaling pathway downstream of different pro-inflammatory stimuli and a regulator of cell death. Although MALT1-dependent A20 cleavage is generally thought to promote NF-κB activity, the functional role of A20 cleavage remains controversial and not well defined. This is due to the fact that the originally described single cleavage site in A20 is not conserved among species and only a small proportion of cellular A20 undergoes cleavage. Here, we demonstrate that MALT1 cleaves A20 at a total of four distinct sites in B and T lymphocytes, including three novel cleavage sites with unusual sequence properties, which are conserved in the mouse and other species. The cleavage fragments lost their capacity to regulate the NF-κB pathway, but are stable within the cell, suggesting that they retain an unknown physiological function in lymphocytes.

Collectively, our findings provide fundamentally new insights into the mechanism of MALT1 protease activation and its cleavage site specificity, and suggest that MALT1-dependent A20 cleavage has roles that go beyond the enhancement of NF-κB activity.

(French)

La protéase MALT1 a une fonction clé dans l'activation des lymphocytes et la régulation de la réponse immunitaire, en favorisant l'activation de facteurs de transcription pro-inflammatoires comme le NF-κB. La dérégulation de MALT1 est impliquée dans l'immunodéficience, les maladies auto-immunes, la lymphomagénèse et les tumeurs malignes non-lymphoides. Par conséquent, l'activité protéolytique de MALT1 est apparue comme une cible thérapeutique possible, cependant le mécanisme précis de l'activation de la protéase MALT1 et le rôle du clivage de chacun de ses substrats restent en partie incompris. Ainsi les objectifs de cette étude sont d'abord d'élucider le mécanisme moléculaire d'activation de MALT1 puis d'explorer le rôle du clivage dépendant de MALT1 d'un substrat en particulier nommé A20.

L'activité protéase de MALT1 est étroitement contrôlée par la conjugaison d'une monoubiquitine à son troisième domaine auto-inhibiteur de type Ig, mais le mécanisme régissant la libération du domaine protéase par un seul fragment d'ubiquitine reste inconnu. Ici, nous avons identifié le domaine Ig3 de MALT1 comme un nouveau domaine de liaison à l'ubiquitine, responsable de la monoubiquitination de MALT1, qui est essentielle pour son activité protéolytique et l'activation lymphocytaire. De plus, nous avons révélé une transmission allostérique du site de monoubiquitination à travers la surface d'interaction protéase-Ig3 au site catalytique actif du domaine protéase.

L'un des premiers substrats de MALT1 qui a été identifié est A20, une protéine anti-inflammatoire puissante. A20 est un régulateur négatif bien décrit de la voie de signalisation NF-κB en aval de différents stimuli pro-inflammatoires et un régulateur de la mort cellulaire. Bien que le clivage de A20 dépendant de MALT1 soit généralement vu comme un promoteur de l'activité de NF-κB, le rôle fonctionnel du clivage de A20 reste controversé et mal défini. Cela est dû au fait que le site de clivage originellement découvert de A20 n'est pas conservé chez les autres espèces et que seulement une petite partie de la protéine cellulaire est clivée. Ici, nous démontrons que MALT1 clive A20 sur un total de quatre sites distincts dans les lymphocytes B et T. Nous avons également identifié trois nouveaux sites de clivage avec des motifs inhabituels, sites qui sont conservés chez la souris et d'autres espèces. Les fragments issus du clivage ont perdu leur capacité à réguler la voie NF-κB, mais sont stables dans la cellule, suggérant qu'ils gardent une fonction physiologique inconnue dans les lymphocytes.

Ensemble, nos résultats apportent de nouvelles informations fondamentales sur le mécanisme d'activation de la protéase MALT1 et sur la spécificité de ses sites de clivage, et suggèrent que le clivage de A20 dépendant de MALT1 a un rôle qui va au-delà d'une simple activation de NF-κB.

# 2 List of Abbreviations

| | | | |
|---|---|---|---|
| ABC | Activated B cell-like | DLBCL | Diffuse large B cell lymphoma |
| AGTR1 | Angiotensin II receptor 1 | DSS | Dextran sulfate sodium |
| ATLL | Acute T cell leukemia/lymphoma | EAE | Experimental autoimmune encephalitis |
| AP-1 | Activator protein 1 | EDC4 | Enhancer of mRNA-decapping protein 4 |
| BCL10 | B cell lymphoma 10 | | |
| BCR | B cell receptor | EGFR | Epidermal growth factor receptor |
| BENTA | B cell expansion with NF-κB and T cell anergy | ERK | Extracellular signal regulated kinase |
| BLNK | B-cell linker protein | | |
| BTK | Bruton's tyrosine kinase | FCS | Fetal calf serum |
| β-TRCP | β-transducin repeat-containing protein | FL | Follicular lymphoma |
| | | fmk | fluoromethyl ketone |
| CARD | Caspase recruitment domain | FOXP3 | Forkhead box protein P3 |
| CARMA1 | CARD-containing MAGUK protein 1 | GADS | Grb2-related adaptor downstream of shc |
| CaMKII | Ca$^{2+}$/calmodulin-dependent kinase II | GEF | Guanine nucleotide exchange factors |
| CBM | CARD-CC-protein-BCL10-MALT1 | GPCR | G-protein coupled receptor |
| CC | Coiled coil | GUK | Guanylate kinase |
| cIAP | Cellular inhibitor of apoptosis | HECTD3 | Homologous to the E6-associated protein carboxyl terminus domain containing 3 |
| CLL | Chronic lymphoid leukemia | | |
| CTCL | Cutaneous T cell lymphoma | | |
| CXCR | C-X-C chemokine receptor | HER2 | Human epidermal growth factor receptor 2 |
| CYLD | Cylindromatosis protein D | | |
| DAG | Diacylglycerol | HOIL-1 | Heme-oxidized iron-responsive element-binding protein 2 ubiquitin ligase 1 |
| DAP12 | DNAX-activating protein of 12 kDa | | |
| DC | Dendritic cell | HOIP | HOIL-1 interacting protein |
| DD | Death domain | ICOS | Inducible T cell co-stimulator |
| DDX6 | DEAD box protein 6 | | |

| | | | |
|---|---|---|---|
| Ig | Immunoglobulin | MCPIP1 | Monocyte chemotactic protein-induced protein 1 |
| IKK | IκB kinase | MHC | Major histocompatibility complex |
| IκB | Inhibitor of NF-κB | | |
| IPEX | Immunodysregulation polyendocrinopathy enteropathy X-linked | MMP9 | Matrix-metalloproteinase 9 |
| | | MZ | Marginal zone |
| IP₃ | Inositole triphosphate | NEMO | NF-κB essential modulator |
| ITK | IL-2-inducible T cell kinase | NFAT | Nuclear factor of activated T cells |
| ITAM | Immunoreceptor tyrosine-based activation motif | NF-κB | Nuclear factor κB |
| JNK | c-Jun-N-terminal kinase | NIK | NF-κB-inducing kinase |
| κB | 'kappa-light-chain-enhancer' of activated B cells | NK | Natural killer |
| | | NLR | NOD-like receptors |
| KSHV | Kaposi's sarcoma herpes virus | NOD2 | Nucleotide-binding oligomerization domain-containing protein 2 |
| LAT | Linker for activation of T cells | | |
| | | N4BP1 | NEDD4-binding protein 1 |
| Lck | Lymphocyte-specific protein tyrosine kinase | OTU | Ovarian tumor protease |
| | | PAGE | Poly-acrylamid gel electrophoresis |
| LIMA1 | LIM domain and actin-binding protein 1 | PAR1 | Protease-activated receptor 1 |
| LPAR | Lysophosphatidic acid receptor | | |
| | | PD | Protease dead |
| LUBAC | Linear ubiquitin chain assembly complex | PEL | Primary effusion lymphoma |
| | | PIP2 | Phosphatidylinositole 4,5-bisphosphate |
| Lyn | LCK/YES novel tyrosine kinase | | |
| | | PKC | Protein kinase C |
| MAGUK | Membrane-associated guanylate kinase | PLCγ | Phospholipase γ |
| | | PMA | Phorbol-12-myristate-13-acetate |
| MALT | Mucosa associated lymphoid tissue | | |
| | | PRP | Pityriasis rubra pilaris |
| MALT1 | MALT lymphoma translocation protein 1 | PRR | Pattern recognition receptor |
| | | PTCL | Peripheral T cell lymphoma |
| MAPK | Mitogen-activated protein kinase | RHD | Rel homology domain |
| | | RIG-I | Retinoic acid-inducible gene I |
| MCL | Mantle cell lymphoma | | |

| | |
|---|---|
| RIPK1 | Receptor-interacting S/T kinase 1 |
| RTK | Receptor tyrosine kinase |
| SCF | Skp1/Cul1/F-box |
| SDS | Sodium dodecyl sulfate |
| SHARPIN | Shank-associated RH domain interactor |
| SH3 | SRC homology 3 |
| SLP76 | SH2 domain-containing leukocyte phosphoprotein of 76 kDa |
| SRC | Sarcoma |
| SYK | Spleen tyrosine kinase |
| TAB | TAK1-binding protein |
| TAD | Transactivation domain |
| TAK1 | TGFβ activating kinase 1 |
| TCR | T cell receptor |
| TGF | Tumor growth factor |
| TNF | Tumor necrosis factor |
| TNFAIP3 | TNF alpha-induced protein 3 |
| TRAF | TNF receptor associated factor |
| Treg | Regulatory T cells |
| UBAN | Ubiquitin binding in ABIN and NEMO |
| Ubc13 | E2 ubiquitin-conjugating enzyme 13 |
| UTR | Untranslated region |
| ZAP70 | $\zeta$ chain-associated protein of 70 kDa |
| ZnF | Zinc finger |

# 3  Introduction

The gene encoding mucosa-associated lymphoid tissue lymphoma translocation protein 1 (MALT1) was originally identified from mucosa-associated lymphoid tissue (MALT) lymphomas, which are B cell malignancies driven by an oncogenic chromosomal translocation, mainly within the MALT1 gene locus.[1-3]  In view of its similarity to proteases of the caspase family, MALT1 has also been defined as a paracaspase. MALT1 is the only member of this family in humans.[4,5]  However, MALT1 orthologs are found in mammals and other metazoans, in zebrafish and *C. elegans*. Metacaspases of different plants, fungi and protozoa are distantly related proteins.[4] The biological function of MALT1 in mammals is defined by its incorporation into multiprotein signaling complexes.

In the introduction, I will describe the molecular nature of these complexes and their roles in individual signaling pathways and detail the role of MALT1 in pathways important for lymphocyte activation. I will then focus on the protease activity of MALT1, the molecular mechanisms that control its activity and finally, describe the implications of MALT1 protease activity in different pathologies and depict recent progress in the targeting of MALT1 by small molecule drugs for therapeutic purposes.

## 3.1  MALT1 as a component of different CBM complexes

Biochemical and genetic studies of this protein have revealed crucial roles for MALT1 as a signaling protein in various inflammatory and tumorigenic cellular processes. Today we know that in mammals, MALT1 is found in complex with the adaptor protein B cell lymphoma 10 (BCL10) in a catalytic inactive form in the cytoplasm.[4,6]  Like for MALT1, the gene encoding BCL10 was originally identified as a gene undergoing chromosomal translocation in MALT lymphoma patients.[7,8]  MALT1 and BCL10 are signaling proteins characterized by well-defined protein domain structures. MALT1 contains a caspase-like domain, which is here referred to as protease domain. Additionally, MALT1 contains a death domain (DD) and two immunoglobulin (Ig)-like domains upstream and a third Ig domain downstream the protease domain (**Fig. 1**).[4,9] The interaction of MALT1 with BCL10 is mediated by the N-terminal DD of MALT1, which interacts with the N-terminal caspase recruitment domain (CARD) of BCL10 (**Fig. 1**).[10]  Upon different extracellular stimuli, BCL10-MALT1 complexes are recruited to CARD and coiled coil (CC) domain-containing proteins.[11-17]  The CARD-CC protein family comprises four proteins, CARD9, CARD10, CARD11 and CARD14. The latter

three additionally have PDZ, SRC homology 3 (SH3) and guanylate kinase-like (GUK) domains, together defined as membrane-associated guanylate kinase (MAGUK) region. Therefore CARD10, CARD11 and CARD14 are also referred to as CARD-containing MAGUK (CARMA) proteins, CARMA3, CARMA1 and CARMA2, respectively (**Fig. 1**).[18] Unlike for MALT1 and BCL10, which are ubiquitously expressed, the CARD-CC-containing proteins are cell type-specific and get activated by triggering of cell surface receptors such as immunoreceptor tyrosine-based activation motifs (ITAM)-containing receptors, G-protein-coupled receptors (GPCR), or receptor tyrosine kinases (RTK).[6] Generally, stimulation of those receptors leads to the formation of the CARD-CC-protein-BCL10-MALT1 (CBM) complex, including the cell type-specific CARD-CC protein, which serves as a scaffold to recruit BCL10 and MALT1. CBM formation results in the activation of the transcription factor, nuclear factor 'kappa-light-chain-enhancer' of activated B cells (NF-κB), which is important for inflammatory processes in a variety of different cell types.
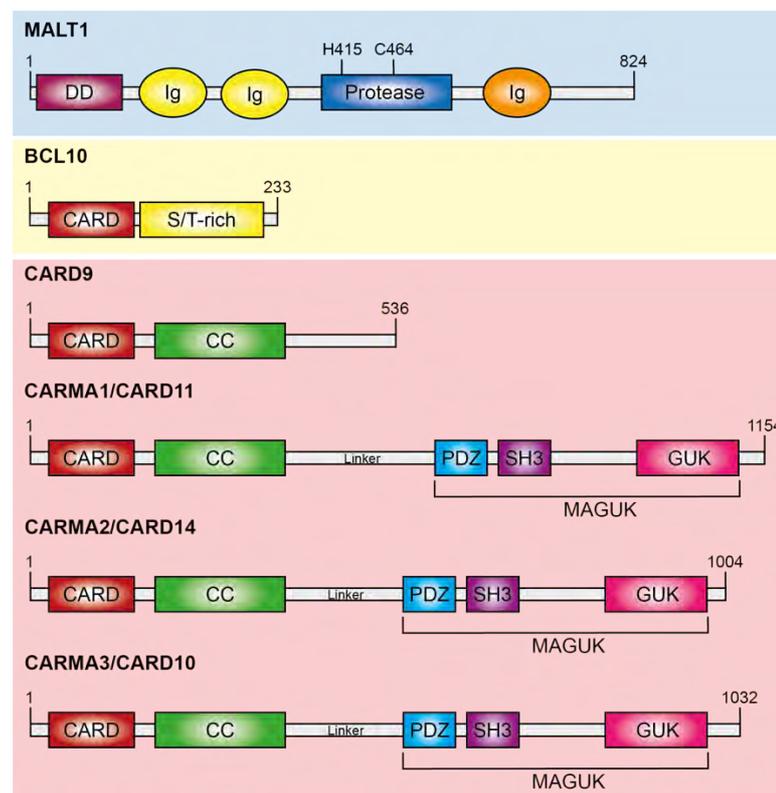


**Figure 1: Structure and domains of CBM complex components.** MALT1 contains an N-terminal death domain (DD), followed by two immunoglobulin-like domains (Ig) and a protease domain with an adjacent Ig at the C-terminus. The protease domain includes two conserved residues (H415 and C464) that are necessary for the protease function. BCL10 possesses an N-terminal CARD followed by a C-terminal S/T-rich domain. CARD-CC proteins contain an N-terminal CARD, followed by a coiled-coil structure (CC). CARMA1/2/3 additionally contain a long linker region and share features of proteins of the membrane-associated guanylate kinase (MAGUK) family at the C-terminus, which contains a PDZ (PSD95, Dlg1, ZO-1), SH3 (Src homology 3), and GUK (guanylate kinase) domain.

CARD9, which is expressed in myeloid cells such as dendritic cells (DC), macrophages and neutrophils, is part of a CBM complex that is formed upon stimulation of several pattern recognition receptors (PRR) and other innate immune receptors.[13,19,20] The CARD9-BCL10-MALT1 signalosome mediates innate anti-fungal immune responses from C-type lectin receptors like Dectin1, Dectin2 and Mincle together with various FcRγ- and/or DNAX-activating protein of 12 kDa (DAP12)-associated receptors.[13,19,21,22] Furthermore, intracellular pathogens such as certain RNA and DNA viruses and invasive bacteria that are detected by retinoic acid-inducible gene I (RIG-I), RAD50 or nucleotide-binding oligomerization domain-containing protein 2 (NOD2), respectively, are relayed by the CARD9-BCL10-MALT1 signalosome.[23-25]

In lymphoid cells and natural killer (NK) cells the CBM complex is formed with CARMA1/CARD11. This CBM complex is the best characterized one. Downstream of antigen receptors, the T cell receptor (TCR) and B cell receptor (BCR), on T cells or B cells, respectively, CARMA1 gets activated through its phosphorylation by serine/threonine protein kinase C (PKC) family members.[26-29] In NK cells, the CARMA1-associated CBM complex is crucial for the downstream signal transduction of activating NK cell receptors, such as NK1.1, Ly49D, Ly49H, and NKG2D.[30,31] Additionally, CARMA1 is present in mast cells and a role of CARMA1 in combination with BCL10 and MALT1 in NF-κB activation downstream of the IgE receptor, FcεRI, has been proposed.[32,33]

CARMA2/CARD14 is expressed in several tissues but the only described function of CARMA2 so far is in keratinocytes. Here, CARMA2 forms the CBM complex upon Dectin1 and IL-17R triggering.[15,16,34]

CARMA3/CARD10 is broadly expressed in non-hematopoietic cells and tissues.[35] The CARMA3-coupled CBM complex controls inflammation in these tissues in response to infections, hormones and metabolic signals, relayed by GPCRs.[14,36,37] The CARMA3-BCL10-MALT1 signalosome was also found downstream of oncogenic RTKs of the epidermal growth factor receptor (EGFR) family in breast cancer and lung cancer, but the physiological function of the CBM complex engagement by EGFRs remain unknown.[38-40] Taken together, MALT1 forms part of different CBM complexes downstream of several surface and intracellular receptors in numerous cell types and tissues.

## 3.2 Importance of MALT1 in immunity

The identification and characterization of MALT1-deficient patients and the generation of MALT1-knockout mice identified a crucial role for MALT1 in the activation of the pro-inflammatory transcription factor NF-κB in different cell types and demonstrate the importance of MALT1 in general immunity.

### 3.2.1 Characterization of MALT1-deficient mice

To assess the physiological role of MALT1 and BCL10, mice lacking expression of these proteins have been generated. MALT1$^{-/-}$ mice are born at the expected Mendelian ratios, are fertile and seem to be healthy.[41,42] In contrast, BCL10-deficient mice have substantial developmental problems, including neural tube closure failures leading to a partial embryonic lethality, indicating that BCL10 has MALT1-independent functions during embryonic development.[43] Nevertheless, surviving BCL10$^{-/-}$ mice and MALT1$^{-/-}$ mice are both highly immunodeficient.[42,43] MALT1-deficient mice have defects in the development of marginal zone (MZ) and B1 B cells, resulting in decreased basal serum immunoglobulin levels. Furthermore, IgM and IgG1 production upon a T cell-dependent and T cell-independent challenge is strongly decreased in MALT1-deficient mice. Moreover, T cell activation and subsequent proliferation are impaired in MALT1-deficient mice.[41,42] Upon aging MALT1$^{-/-}$ mice develop atopic-like dermatitis, due to a decrease in regulatory T (Treg) cell frequency and functionality and an increase of Th2 cells following higher IgE levels.[44] Due to the fact that the CARMA1-BCL10-MALT1 signalosome is essential for signal transduction of activating NK cell receptors, MALT1-deficient mice show impaired NK cell activation, resulting in reduced cytokine and chemokine production but do not affect NK-cell differentiation or killing.[31] DCs from MALT1-deficient mice are impaired in NF-κB activation upon a fungal stimuli, similar to DCs from BCL10$^{-/-}$ and CARD9$^{-/-}$ mice.[13]

### 3.2.2 MALT1 deficiency in humans

A few cases of MALT1 deficiencies upon germline loss-of-function mutations in humans have been described. In five patients the partial or complete loss of MALT1 expression results in combined immunodeficiency with normal B and T cell numbers but impaired cellular and humoral immunity, resembling the phenotype of MALT1$^{-/-}$ mice.[45-48] For one patient the MALT1 deficiency causes an immunodysregulation polyendocrinopathy enteropathy X-linked (IPEX)-like disease combined with severe immunodeficiency.[49] IPEX-like syndromes are generally found in patients with mutations in genes essential

for Treg differentiation and function, such as forkhead box protein P3 (FOXP3).[50] The patient suffers from autoimmune enteropathy, dermatitis and increased IgE serum levels with severe immunodeficiency, close to the phenotype of aged MALT1-deficient mice.[49] Overall, the mouse and human data confirm the importance of MALT1 in innate and adaptive immunity with a major function in lymphocyte activation.

## 3.3 Lymphocyte activation

T lymphocytes and B lymphocytes are the two major elements of the adaptive immunity. T cells ensure a cell-transmitted immune response and support B cells, which are themselves responsible for the humoral immunity. During lymphopoiesis, lymphocytes acquire structurally unique surface receptors to detect antigens due to somatic recombination and hypermutations.[51,52] Contrary to B lymphocytes, which can detect free antigens, conventional T lymphocytes recognize processed antigens presented by major histocompatibility complex (MHC) molecules on the surface of antigen-presenting cells or infected cells. Mature naïve lymphocytes patrol the body to search for pathogens by continuously moving from one lymphoid organ to another. When a lymphocyte binds via its antigen receptor to its specific antigen, the lymphocyte becomes activated, starts to proliferate and differentiates to initiate its effector functions. Co-stimulatory signals, for example provided by the surface proteins CD28 on T cells or CD40 on B cells, but also by cytokines, are essential for proper lymphocyte activation.[52] A common important feature in B and T cell activation is the formation of the CARMA1-composed CBM complex and subsequent activation of the transcription factors NF-κB, nuclear factor of activated T cells (NFAT) and activator protein 1 (AP-1), but the signaling pathways leading to the assembly of the CBM complex are distinctive in T- and B cells.

### 3.3.1 Early TCR signaling to CBM complex formation

The antigen-specific TCR is composed of highly variable αβ or γδ heterodimers that are constitutively coupled to invariant CD3 dimers (γε,δε and ζζ).[53,54] The CD3 chains contain ITAMs that upon an antigen-binding to the receptor become phosphorylated by the sarcoma (Src)-family tyrosine kinases, lymphocyte-specific protein tyrosine kinase (Lck) and Fyn (**Fig. 2**).[55,56] Phosphorylated ITAMs form a high-affinity binding site for the spleen tyrosine kinase (Syk)-family member, ζ-chain-associated protein kinase 70 (ZAP70) that itself becomes phosphorylated and activated by Lck and Fyn.[57] The target of ZAP70 in T cells is the adaptor protein linker for activation of T cells (LAT)

that is a scaffold to recruit phospholipase Cγ (PLCγ) and the Grb2-related adaptor downstream of shc (GADS)- SH2 domain-containing leukocyte phosphoprotein of 76 kDa (SLP76) complex together with IL-2-inducible T cell kinase (ITK). ITK phosphorylates and thereby activates PLCγ that converts phosphatidylinositol bisphosphate (PIP2) to inositol trisphosphate (IP3) and diacylglycerol (DAG). IP3 induces the release of calcium from the ER, increasing the cytosolic calcium concentration. The high intracellular calcium level activates calcineurin, which induces the nuclear translocation of the transcription factor NFAT. DAG binds to proteins with a conserved cysteine-rich domain such as guanine nucleotide exchange factors (GEF), which activates RAS and the downstream mitogen-activated protein kinase (MAPK) pathway ending in the phosphorylation of extracellular signal-regulated kinase (ERK) and the activation of the AP-1 transcription factor. Another DAG-binding protein is PKCθ. This serine/threonine kinase phosphorylates CARMA1 leading to CBM complex formation and activation of the transcription factors NF-κB and AP-1 (**Fig. 2**).[58]
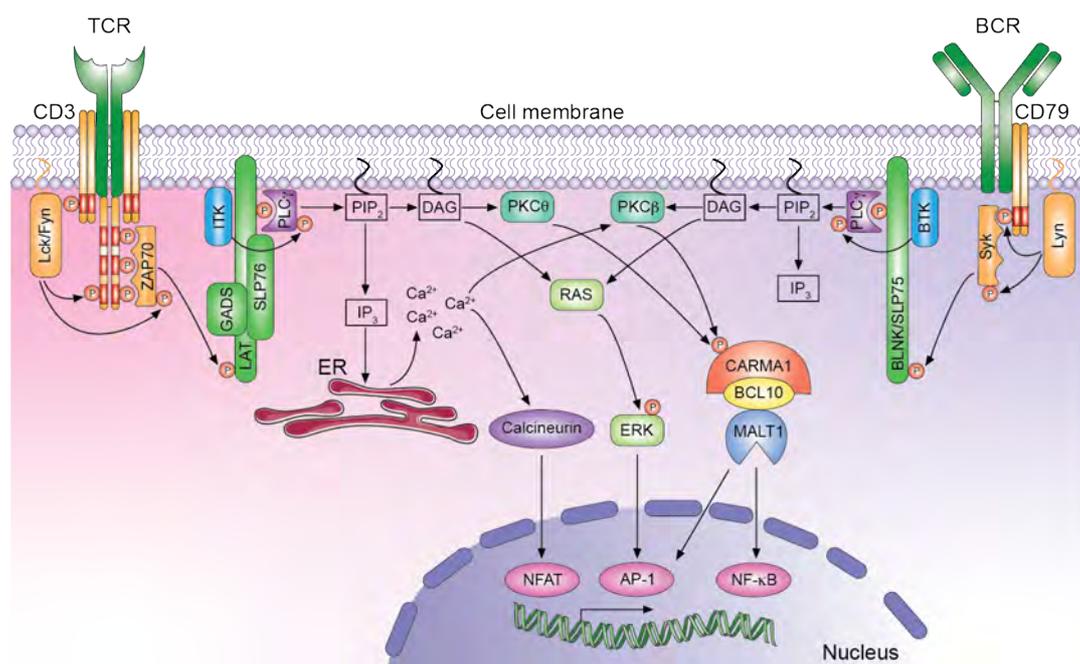


**Figure 2: Early antigen receptor signaling in lymphocytes.** Signaling from the antigen receptor (TCR or BCR) with associated ITAM-containing chains (CD3 or CD79) via Src (Lck/Fyn or Lyn) and Syk (ZAP70 or Syk) family members to the activation of PLCγ and production of IP$_3$ and DAG to the PKC-dependent (PKCθ or PKCβ) formation of the CBM complex (CARMA1-BCL10-MALT1) and transcription factor activation (NFAT, AP-1 and NF-κB).

## 3.3.2 Early BCR signaling to CBM complex formation

The antigen-specific receptor on B cells, named BCR, is a highly variable membrane-bound IgM or IgD, coupled to CD79a/b heterodimers. The early signaling pathway is similar to the one in T cells, however the involved proteins are different (**Fig. 2**). Like

the CD3 chains in T cells, the CD79 subunits in B cells harbor ITAMs that become phosphorylated by the Src kinase, Lck/Yes novel tyrosine kinase (Lyn), leading to the recruitment and activation of the Syk family member, Syk. A B-cell adapter protein combining functions of both, LAT and SLP76, is the B-cell linker protein (BLNK), also known as SLP65, that recruits PLCγ. Instead of ITK, BLNK recruits bruton's tyrosine kinase (BTK), which leads to the phosphorylation and activation of PLCγ in B cells. Similar as in T cells, an increased calcium concentration and DAG generation activates the NFAT and the AP-1 transcription factors in B cells.[58,59] However, the CBM complex formation and subsequent NF-κB activation is regulated by PKCβ, which depends on both calcium and DAG (**Fig. 2**).[60]

### 3.3.3 CARMA1-BCL10-MALT1 signalosome assembly in lymphocytes

In resting conditions, CARMA1 is inactive and dissociated from BCL10-MALT1 heterodimers in the cytoplasm. In the inactive closed conformation of CARMA1, the CARD domain is not accessible because of an intramolecular interaction of the CARD domain with sites in the linker region and the CC domain.[61,62] Upon antigen receptor engagement, PKCθ/PKCβ phosphorylates residues within the linker region of CARMA1, leading to the release of the CARD domain.[63-66] Furthermore, $Ca^{2+}$/calmodulin-dependent kinase II (CaMKII)-mediated CARMA1 phosphorylation at the CARD domain and AKT-dependent phosphorylation within the linker region contribute to CARMA1 activation. These kinases are activated by the increase of cytoplasmic calcium concentration and by co-stimulatory signals.[67,68]

Activated CARMA1 oligomerizes within lipid rafts and recruits BCL10-MALT1 dimers through CARD-CARD interactions between CARMA1 and BCL10.[63,64] Furthermore, this triggers an energetically favored process of unidirectional self-polymerization of BCL10 via its CARD domain, resulting in a helical filament with BCL10 as core and MALT1 facing the periphery (**Fig. 3**). Oligomerized CARMA1, which is not within the filaments, serves as a seed to nucleate BCL10 filaments, thereby several BCL10 strands can arise from one CARMA1 seed. Thereby, CBM complex formation results in a massive amplification of the antigen receptor signal (**Fig. 3**).[69,70]

The BCL10-MALT1 filament is a left-handed helix with 3.571 subunits per helical turn. MALT1, which binds to BCL10 in a 1:1 stoichiometry, is not directly involved in the filament formation but it was shown that the BCL10-MALT1 binding is essential for the interaction of BCL10 CARD with the CARD domain of nucleating CARMA1, most probably by a conformational shift of BCL10. Impairment of BCL10-MALT1 filament

formation abrogates any further downstream signaling critical for lymphocyte activation.[10] Thus, the CBM complex is not a simple tripartite complex but a tightly regulated high molecular weight signalosome able to amplify initial immunoreceptor signals (**Fig. 3**).
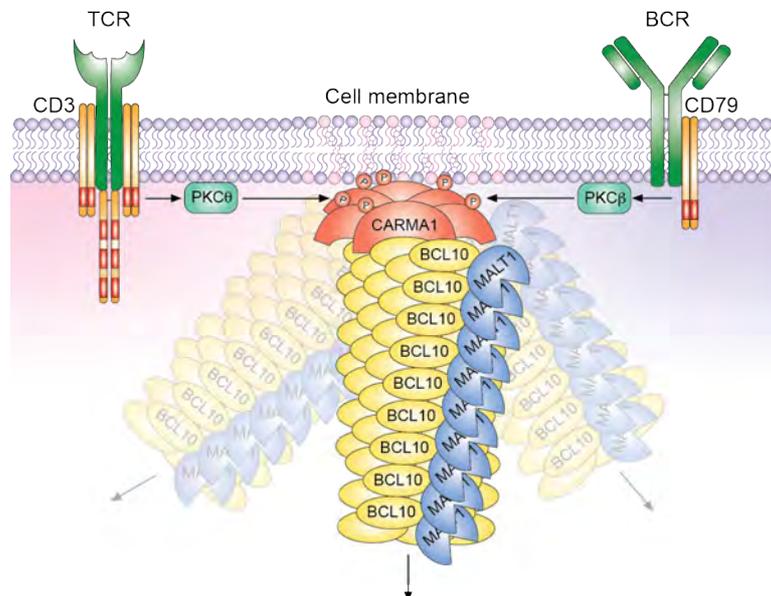


**Figure 3: High-order assembly of the CARMA1-BCL10-MALT1 signalosome.** Upon lymphocyte stimulation, CARMA1 gets phosphorylated by PKCθ/β and oligomerizes within lipid rafts. Oligomerized CARMA1 recruits BCL10-MALT1 heterodimers via CARD-CARD interaction of CARMA1 and BCL10 and thus acts as a nucleator for the formation of BCL10 filaments. The filament assembly is built via CARD-CARD interactions between BCL10 molecules and MALT1 is facing the periphery. Several BCL10 filaments can arise from one CARMA1 seed, leading to signal amplification.

### 3.3.4 Late signaling events in lymphocyte activation

The CBM complex serves as a central scaffold in activated lymphocytes in which MALT1 is the major player in engaging different protein kinases and ubiquitin regulators (**Fig. 4**). The E2 ubiquitin-conjugating enzyme 13 (Ubc13) can bind to the Ig3 domain of MALT1.[9] MALT1 has several tumor necrosis factor (TNF) receptor-associated factor 6 (TRAF6)-binding motives, which help to recruit TRAF6 to the CBM complex.[71-73] TRAF6 is an E3 ubiquitin ligase that in complex with Ubc13 attaches K63-linked ubiquitin chains to itself and to several lysine residues in the C-terminus of MALT1.[71,74] Interestingly, Meininger *et al.* identified that in humans two alternative splice isoforms of MALT1 exist. They differ by inclusion (MALT1A) or exclusion (MALT1B) of exon7, encoding eleven amino acids (aa309-319) that form a TRAF6-binding motive. Thus, MALT1A contains a total of three and MALT1B just two TRAF6-binding motives. The expression patterns of the two isoforms of MALT1 are still unclear, however, in naïve CD4^{+} T cells mainly MALT1B is expressed and upon an TCR signal the ratio of MALT1A/MALT1B increases. [75] This suggests that upon lymphocyte activation, the cell

strengthens its capabilities to recruit TRAF6 to the CBM complex via alternative splicing of MALT1.

Furthermore, MALT1 recruits cellular inhibitor of apoptosis 1 and 2 (cIAP1/2) that link K63-ubiquitin chains to BCL10.[76,77] Additionally, BCL10 becomes modified by M1-linked ubiquitin chains, which are added by the linear ubiquitin chain assembly complex (LUBAC). LUBAC is composed of three subunits known as SHANK-associated RH domain interacting protein (SHARPIN), heme-oxidized IRP2 ubiquitin ligase 1 (HOIL-1) and HOIL-1-interacting protein (HOIP), which harbors the E3 ubiquitin ligase activity (**Fig. 4**).[78] Although a physical interaction between CARMA1 and HOIP has been proposed, the exact mechanism of LUBAC recruitment to the CBM complex and the role of its recruitment remains controversial.[78,79]
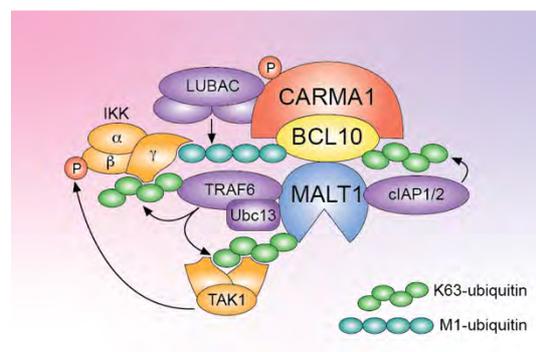


**Figure 4: CBM scaffold in lymphocytes.** The CBM complex recruits several E3 ubiquitin ligases (violet) that attach either K63-linked or M1-linked ubiquitin chains to CBM complex components. These ubiquitin chains further recruit the IKK and TAK1 kinase complexes (orange), allowing the TAK1 complex to activate the IKK complex by phosphorylation.

The K63-linked ubiquitin chains on the CBM complex are responsible for tumor growth factor (TGF)β-associated kinase 1 (TAK1) recruitment via the ubiquitin-binding proteins, TAK1-binding protein 2 (TAB2) and TAB3.[71] Additionally, K63-linked ubiquitination together with the linear ubiquitination engage the inhibitor of NF-κB (IκB) kinase (IKK) complex. The IKK complex is a tripartite complex formed by IKKα, IKKβ and IKKγ, which is also known as NF-κB essential modulator (NEMO). This subunit mediates the physical recruitment of the IKK complex to the CBM ubiquitin chains via its ubiquitin binding in ABIN and NEMO (UBAN) motif and the C-terminal K63-specific zinc finger (ZnF).[71,76,78,80] IKKβ has kinase activity that is activated by TAK1-dependent phosphorylation (**Fig. 4**).[71] However, also TRAF6 and LUBAC-dependent ubiquitination of the NEMO subunit itself contributes to IKK complex activation.[81] The active IKK complex phosphorylates the NF-κB inhibitor IκBα at S32 and S36, which generates a DSG motif (DpSGφXpS) that is recognized by Skp1/Cul1/F-box (SCF)-β-transducin repeat-containing protein (β-TRCP).[82] SCF-β-TRCP is an E3 ubiquitin ligase

that attaches K48-linked ubiquitin chains to K21 and K22 of IκBα, which targets it for degradation by the 26S proteasome. Released NF-κB dimers are now allowed to translocate into the nucleus and initiate gene expression.[82,83]

*NF-κB transcription factor family*

NF-κB is a specific transcription factor that is present in all mammalian cells and tissues. NF-κB binds to a specific DNA motive, called κB enhancer, within the promoter of numerous targeted genes. NF-κB target genes include inflammatory cytokines (e.g. IL-1, IL-2, IL-6 and TNFα), chemokines (e.g. RANTES, CXCL1 and CXCL10) and adhesion molecules (e.g. ICAM-1 and VCAM-1) but also factors regulating cell proliferation, apoptosis (e.g. Fas, c-FLIP and IAPs), morphogenesis and differentiation. Thus, NF-κB is generally involved in inflammation development and progression.[84]

The NF-κB family includes five Rel homology domain (RHD)-containing proteins, of which three members have additionally a transactivation domain (TAD). Thus, the NF-κB family is further divided into Class I (without TAD) and Class II (with TAD) proteins. Class I family members, including NF-κB1 (also known as p105/p50) and NF-κB2 (also known as p100/p52) are translated as large precursors that undergo proteasomal processing to generate functional NF-κB subunits. In contrast to NF-κB1, which is constitutively processed by the proteasome, NF-κB2 remains in its inactive precursor in the cytoplasm, until an NF-κB-inducing kinase (NIK)-stabilizing and activating signal. NIK activates and links IKKα to NF-κB2/p100 that is subsequently phosphorylated, ubiquitinated and further processed by the proteasome. This signaling cascade leading to processing and activation of NF-κB2 is known as the non-canonical NF-κB activation pathway.[85]

NF-κB Class I family members have to dimerize with a Class II family member, including RelA (also known as p65), RelB and c-Rel, to activate target gene transcription. Normally, NF-κB1 forms a heterodimer with RelA or c-Rel (canonical NF-κB dimers), whereas NF-κB2 is found in complex with RelB (non-canonical NF-κB dimers).[85,86] Furthermore, NF-κB1 or NF-κB2 homodimers negatively regulate target gene transcription by competing with NF-κB heterodimers for binding to the κB enhancer.[87,88] Antigen receptor signals in T and B cells that are transduced by the CBM complex activate canonical NF-κB dimers containing NF-κB1 in combination with RelA or c-Rel, which are indispensable for lymphocyte activation. [85]

*Involvement of the CBM complex in AP-1 activation*

In addition to the already described, ERK-dependent activation of the transcription factor AP-1 upon an antigen receptor signal, the CBM complex also contribute to the

activation of AP-1 by various means. BCL10 recruits c-Jun N-terminal kinase (JNK) 2 that is phosphorylated and activated by TAK1. JNK2 is known to be crucial for the TCR-induced accumulation of c-Jun, an important member of the AP-1 transcription factor family. [33] Additionally, a CBM complex-dependent stabilization and activation of several other AP-1 transcription factor family members have been described in B lymphocytes.[89,90] However, the exact role of the CBM complex in AP-1 activation remains incompletely defined.

In conclusion, the CBM complex acts as a signaling platform for the engagement of various signaling complexes essential for NF-κB and AP-1 activation.

## 3.4 MALT1 proteolytic activity

A second function of the CBM complex is the initiation of the catalytic activity of MALT1. Structural analysis of MALT1 identified a catalytically active section with homology to caspases with a conserved histidine (H415) and cysteine (C464) residue forming the catalytic dyad essential for cysteine-dependent proteases (**Fig. 1**).[4,91,92] For about a decade MALT1 was thought to be a protease-dead protein, which lost its catalytic function during evolution. However, outstanding scientific investigations of the last twelve years discovered the proteolytic activity of MALT1 within the CBM complex, identified ten substrates, determined the prerequisites and the mechanism of MALT1 activation and *in vivo* studies uncovered the physiological relevance of MALT1 protease function.

### 3.4.1 MALT1 protease activation mechanism

Structural studies identified that the minimal unit of activity of MALT1 consists of the protease domain and the adjacent third Ig-like domain. This MALT1$_{Protease-Ig3}$ requires dimerization, a feature that is also essential for caspase activation. MALT1 dimerization is mediated by the two protease domains forming an asymmetric unit with the protease active site facing opposite directions (**Fig. 5**). The protease-protease interface is facilitated by interactions between the β6 and α5 of one unit with their respective symmetry mates. [91,92] Impairment of MALT1 dimerization abrogates its cleavage activity.[92,93] The Ig3 domain is closely packed onto the protease domain and in the dimeric structure, Ig3 domains are pointing away from each other (**Fig. 5**). The protease-Ig3 interaction is mediated by a combination of hydrogen bonds and hydrophobic interactions between α2 and β2 of the protease domain and the β2/β3, β4/β5 and β5/β6 loops of the Ig3 fold.[91,92]

The structure of MALT1$_{Protease-Ig3}$ changes upon binding to the peptide-based active site inhibitor z-VRPR-fmk.[92] This inhibitor was designed based on the optimal substrate tetrapeptide sequence of the metacaspase AtmC9 of *Arabidopsis thaliana*, a close homolog of MALT1.[94] The binding of this inhibitor to the active site leads to a conformational change of the protease domain, resembling the active conformation of MALT1, based on comparison with the structure of active caspases. Additionally, peptide binding favors MALT1 dimerization. Strikingly, along with the protease domain, also the Ig3 domain shows dramatic conformational changes upon peptide binding. The α1 helix of the Ig3 rotates by approximately 45° and elongates by one turn, which most probably weakens the interactions between the protease and the Ig3 domain.[92] By interaction with the protease domain, the Ig3 domain has been shown to have an inhibitory function, possibly by holding the protease domain in an inactive conformation.[95] However, the precise mechanism of the autoinhibition and its release were unknown when I started my thesis.
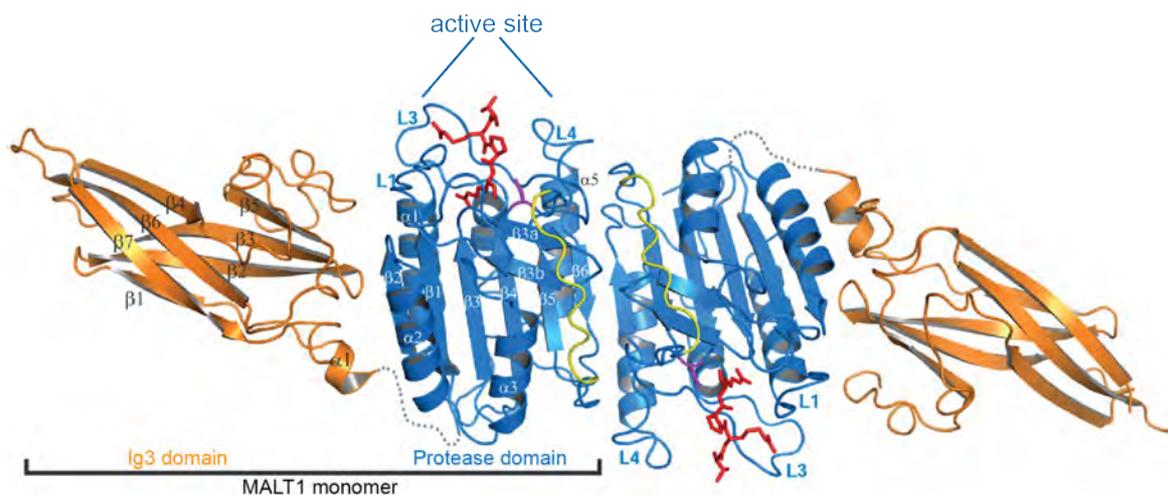


**Figure 5: Dimeric MALT1 crystal structure.** MALT1 homodimer (residues 339-719) crystal structure bound to the peptide inhibitor (z-VRPR-fmk; red). Each MALT1 monomer contains a protease domain (blue) and an Ig3 domain (orange). The α-helices and β-sheets of the protease domain and the Ig3 domain are numbered based on the sequence. The active site with the loops L1-L4 is indicated. Adapted from Yu, *J. et al.*, PNAS (2011)

*In vivo*, MALT1 proteolytic function gets activated by an antigen receptor signal and formation of the CBM complex. CBM signalosome formation impairment by single point mutations within BCL10 abrogates MALT1 proteolytic activity. Thus, CBM complex formation promotes MALT1 activity most likely by providing the platform for its dimerization.[10] Furthermore, the structure of MALT1$_{DD-Ig1-Ig2}$ suggests that the N-terminal Ig-like domains of MALT1 might contribute to MALT1 dimerization and/or oligomerization.[96] However, the domains upstream of the protease domain are

dispensable for dimerization and protease activation *in vitro*[92], thus, the role of these domains in MALT1 activation remains controversial.

In addition to dimerization and CBM complex formation, MALT1 monoubiquitination is a third prerequisite for the proteolytic activity. Upon an antigen-receptor signal MALT1 becomes monoubiquitinated with a delay of approximately 15 min, in line with the induction of the proteolytic activity, indicating that MALT1 protease function is initiated after CBM complex formation and after initial NF-κB activation (since IκBα phosphorylation peaks at approximately 5 min under similar experimental conditions). MALT1 monoubiquitination happens within the Ig3 domain on K644 (**Fig. 6**). Mutation of K644 to an arginine dramatically decreases the proteolytic activity of this monoubiquitination-deficient MALT1 in cells. Interestingly, fusion of a single ubiquitin moiety to the C-terminus of MALT1 rescues MALT1 cleavage activity of MALT1(K644R). MALT1 monoubiquitination is proposed to promote MALT1 cleavage activity by stabilizing MALT1 dimers.[93,95] However, the mechanism of MALT1 monoubiquitination and how a single ubiquitin moiety activates the protease function of MALT1 have remained unclear.
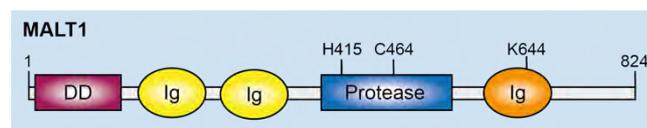


**Figure 6: Structure and domains of MALT1.** MALT1 contains a N-terminal death domain (DD), followed by two immunoglobulin-like domains (Ig) and a protease domain with an adjacent Ig at the C-terminus. The protease domain includes two conserved residues (H415 and C464) that are necessary for the protease function. The side of monoubiquitination within the Ig3 domain is indicated (K644).

In conclusion, MALT1 protease function is activated upon an antigen receptor signal leading to CBM complex formation, which most probably initiates MALT1 dimerization by the recruitment of numerous MALT1 monomers to the CBM complex. MALT1 monoubiquitination promotes the proteolytic activity in a manner that remains elusive.

## 3.4.2 Physiological role of MALT1 protease function

Mice expressing a catalytically inactive MALT1 mutant (C472A, resembling C464A in humans) phenocopy MALT1-deficient mice in several aspects. As for MALT1 knockout mice, mice expressing protease-dead MALT1 (MALT1-PD) have severely reduced numbers of B1 and MZ B cells and thereby decreased serum levels of a subset of Igs, although to a lesser extent than MALT1-deficient mice. Additionally, T cell proliferation and T cell-dependent and -independent immune responses are similarly impaired.[97-100] Also NK cell and dendritic cell activation is reduced in both MALT1-KO and MALT1-

PD mice, indicating the importance of MALT1 protease function in different CBM complexes and cell types.[97,100]

Interestingly, *ex vivo* stimulation of primary T and B lymphocytes from MALT1-PD mice shows normal levels of IKK activation compared to wild-type mice, whereas MALT1-KO mice are completely abolished in IKK activation.[97,99] Nevertheless, IL-2 production of stimulated MALT1-PD T cells is remarkably reduced. Cell line-based experiments using MALT1 active site inhibitors, which inhibit MALT1 protease activation in an irreversible manner, confirmed these observations. Cells pre-treated with MALT1 inhibitors show normal IKK complex activation and nuclear NF-κB translocation but are strongly impaired in IL-2 production.[94,101] These findings suggest that MALT1 proteolytic activity is dispensable for phosphorylation of IκBα and initial NF-κB activation but prolongs or enhances NF-κB activity later on.[97]

Surprisingly, in contrast to MALT1-deficient mice, MALT1-PD mice develop spontaneous autoimmune phenotypes such as ataxia and multiorgan inflammations comprising the gastro-intestinal tract, salivary glands, the lung and peripheral nerves. Early disease onset around the age of six weeks, suggests that MALT1 protease activity plays a role in immune homeostasis.[97-100] The systemic inflammation in MALT1-PD mice is due to an imbalance between effector CD4$^+$ T cells and Treg cells in a T cell-intrinsic manner.[102] Like MALT1-KO mice, MALT1-PD mice are impaired in the development of thymic and peripheral FoxP3$^+$ Treg cells. However, only MALT1-PD mice show a massive increase of B and T cells in the lymph nodes at the age of disease onset. These T cells have an activated T cell phenotype with high surface expression of CD44 and low levels of CD62L, together with increased production of IFNγ and IL-4.[97-99] Since these cells are not present in MALT1-KO mice or in wild-type mice, these observations indicate that the MALT1-PD and MALT1-KO mice have a defect in the development of Treg cells that leads to an activation of effector T cells, which highly depends on MALT1 scaffold function, leading to early onset severe autoinflammation in MALT1-PD mice but only to a mild atopic-like dermatitis in aged MALT1-KO mice.[44,102] In line with this, reconstitution of young MALT1-PD mice with MALT1-sufficient Treg cells rescues autoimmune symptoms.[97]

### 3.4.3 MALT1 substrate cleavage

So far, ten MALT1 substrates have been identified, including MALT1 itself[103,104], its binding partner BCL10[94], the deubiquitinases A20[105] and cylindromatosis (CYLD)[106], the NF-κB family member RelB[107], the LUBAC subunit HOIL-1[108], and the mRNA-

binding proteins Regnase1[109], Roquin1/2[110] and NEDD4-binding protein 1 (N4BP1).[111] All MALT1 substrates are cleaved after an arginine, which is seen similarly for metacaspases.[112] Based on the cleavage sites of the known substrates the preferred consensus cleavage site is $\phi$-X-P/S-R′-G, including an arginine at the P1 position, a preference for proline or serine at P2, a variable residue at P3 and a preferred hydrophobic amino acid at P4. The residue following the P1 arginine is normally a small amino acid such as glycine (**Table 1**).[113] The role of the cleavage of these substrates has been investigated mainly downstream of antigen receptors of B and T cells.

| Substrate | Cleavage site |
|---|---|
| MALT1 | $LCCR_{149}A$ |
| MALT1 | $HCSR_{781}T$ |
| BCL10 | $LRSR_{228}T$ |
| A20 | $GASR_{439}G$ |
| CYLD | $FMSR_{324}G$ |
| RelB | $LVSR_{85}G$ |
| HOIL-1 | $LQPR_{165}G$ |
| Regnase-1 | $LVPR_{111}G$ |
| Roquin-1 | $LIPR_{510}G$ |
| Roquin-1 | $MVPR_{579}G$ |
| Roquin-2 | $LISR_{509}S$ |
| N4BP1 | $FVSR_{509}G$ |
| **Cons. seq.** | $\phi XS/PR′G$ |

**Table 1: MALT1 consensus cleavage site sequence.** MALT1 substrates with their specific cleavage sites. MALT1 and Roquin-1 are cleaved twice. Comparisons leading to the consensus cleavage site sequence of a hydrophobic residue followed by a variable amino acid, serine or proline and the essential arginine at P1, followed by a small amino acid (mainly G, but also A or T). The A20 cleavage site is atypical in that it contains a small amino acid (G) instead of a hydrophobic aa in position P4.

*MALT1 auto-processing*

Similarly to caspases, MALT1 has an auto-proteolytic activity. However, unlike caspases, MALT1 does not cleave itself within the protease domain and auto-processing is dispensable for its catalytic activity. MALT1 instead cleaves itself at R149, between the DD and the first Ig-like domain, and at R781, which is within the C-terminal extension (**Fig. 7**).[103,104] The N-terminal auto-processing site is essential for NF-κB transcriptional activity, although it is dispensable for phosphorylation of IκBα or initial NF-κB activation.[103,114] The N-terminal auto-processing site partially contributes to the loss of Treg cells in mice, however, unlike MALT1-PD mice, mice expressing MALT1 uncleavable at the N-terminus do not show signs of autoimmunity, indicating the existence of a Treg threshold that is still sufficient to prevent autoimmunity.[114]

The role of the C-terminal auto-processing site is not clear yet. Basically, cleavage of MALT1 at R781 leads to the loss of one TRAF6-binding site. This auto-cleavage dependent loss of the TRAF6-binding motif has no effect on NF-κB activity or substrate cleavage induced by MALT1 isoform A, which still retains two TRAF6-binding motives.[104] However, NF-κB activity and substrate cleavage induced by MALT1 isoform

B is dramatically reduced, due to the alternative splicing and loss of exon 7 that encodes the first TRAF6-binding motif of MALT1.[75,104] Thus, the hypothesis is that C-terminal auto-cleavage serves as a negative feedback for MALT1B activation during weak or tonic TCR signals. Strong TCR engagement leads to upregulation of MALT1A, for which C-terminal auto-processing has no effect anymore. Nevertheless, the amount of MALT1 that is auto-processed at the C-terminus is small, maybe due to the fact that the cleavage sequence is a rather poor MALT1 consensus cleavage sequence with a positively charged histidine at P4. *In vivo* experiments are needed to characterize the physiological role of the C-terminal cleavage site.
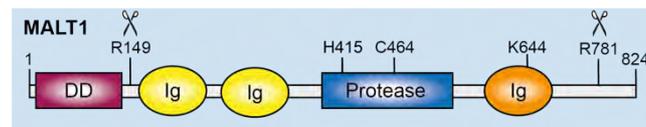


**Figure 7: Structure and domains of MALT1.** MALT1 contains an N-terminal death domain (DD), followed by two immunoglobulin-like domains (Ig) and a protease domain with an adjacent Ig at the C-terminus. The protease domain includes two conserved residues (H415 and C464) that are necessary for the protease function. The site of monoubiquitination within the Ig3 domain (K644) and the auto processing sites (R149 and R781) are indicated.

*BCL10*

The constitutive binding partner of MALT1, BCL10, is cleaved after R228 upon a TCR signal. This cleavage removes the last five amino acids of BCL10. MALT1-mediated cleavage of BCL10 is not essential for NF-κB activation or target gene transcription, nevertheless expression of an uncleavable BCL10(R228G) mutant in T cells impairs TCR-induced β1 integrin-dependent cell adhesion to fibronectin by a mechanism that is still unknown, but possibly relies on changes in cytoskeletal interactions.[94]

*CYLD*

CYLD is a deubiquitinating enzyme involved in the negative regulation of NF-κB and AP-1 activation.[115,116] However, the mechanism of CYLD-mediated regulation of NF-κB and AP-1 activation in lymphocytes is unclear. MALT1-dependent cleavage of CYLD after R324 impairs CYLD function and promotes AP-1 but not NF-κB target gene transcription in stimulated B and T cells.[117] Although the authors demonstrate that MALT1-dependent CYLD cleavage is necessary for the phosphorylation of JNK and subsequent AP-1 activation, this finding remains controversial, since MALT1 protease activity is dispensable for antigen receptor-induced phosphorylation of JNK in MALT1-PD mice.[97]

*RelB*

Antigen receptor-induced NF-κB activation relies on the canonical NF-κB family members, including RelA-NF-κB1 and c-Rel-NF-κB1 complexes.[118] RelB, on the other

hand, is a known negative regulator of canonical NF-κB target gene transcription in lymphocytes, most probably by acting as a competitor of DNA-binding and by direct interaction-mediated inhibition of RelA and c-Rel.[119-121] MALT1-mediated RelB cleavage after R85 induces the proteasomal degradation of RelB upon lymphocyte activation. Like this, MALT1 proteolytic activity is enhancing DNA binding of RelA and c-Rel and furthermore promotes NF-κB target gene transcription.[107]

*HOIL-1*

The LUBAC subunit HOIL-1 is cleaved by MALT1 after R165 upon antigen receptor stimulation in B and T cells.[108,122] Although there is evidence that MALT1-mediated cleavage of HOIL-1 enhances NF-κB activity in a LUBAC and IKK-independent manner[123], the more important role of MALT1-dependent cleavage seems to be the inactivation of LUBAC and subsequent termination of antigen receptor signaling.[108,122,124] Indeed, HOIL-1 cleavage, resulting in a small N-terminal fragment that is responsible for HOIP-binding and a larger C-terminal fragment, which after cleavage diffuses from the LUBAC complex, destabilizes the whole LUBAC complex and subsequently leads to degradation of HOIP. Thus, overall linear ubiquitination events decrease and terminate IKK complex activation.[108,122] Hence, MALT1 proteolytic activity is not just enhancing NF-κB activity but also leads to the termination of initial antigen receptor signals.

*Regnase-1*

Regnase-1, which is also known as monocyte chemotactic protein-induced protein (MCPIP1), is an RNAse that can bind to a specific stem loop element in the 3′ untranslated region (UTR) of mRNAs and promotes their transcript degradation. Target mRNAs of Regnase-1 are mainly immunoregulatory transcripts, such as IL-2, IL-6, IL-12b, c-Rel, inducible T cell co-stimulator (ICOS) and OX40. Mice with full body or T cell-specific knockout of Regnase-1 have an autoimmune phenotype with systemic inflammation, driven by an exaggerated T cell response.[109,125]

MALT1-mediated cleavage of Regnase-1 after R111 upon antigen receptor stimulation leads to Regnase-1 degradation. Thereby, MALT1 protease activity stabilizes Regnase-1 target transcripts and strengthens T cell immune response.[109]

*Roquin-1/2*

Like Regnase-1, also Roquin-1 and its homologue Roquin-2 bind to a stem loop structure of the constitutive decay element of the 3′-UTR of different mRNAs.[126] Thereby Roquin-1/2 promote mRNA decay by recruiting the helicase DEAD box protein 6 (DDX6), enhancer of mRNA-decapping protein 4 (EDC4) and the CCR4–CAF1–NOT1

deadenylase complex.[126,127] Roquin-1/2 target mRNAs include ICOS, OX40, IL-6, TNF, IRF4, c-Rel, IκBNS, IκBζ and CTLA-4. Combined T cell-specific loss of Roquin-1 and Roquin-2 results in Th17-driven inflammation and lung pathologies, suggesting an important role of Roquins in Th17 cell differentiation.[110] Indeed, IL-6 promotes Th17 cell differentiation and impairs Treg cell differentiation.[128] Furthermore, IRF4, c-Rel, IκBNS and IκBζ are critical factors for Th17 cell differentiation.[110,129-131] Finally, ICOS is increasing Th17 cell proliferation.[132]

MALT1 cleaves Roquin-1 at R510 and R579 and Roquin-2 at R509 upon lymphocyte activation and thereby stabilizes the specific transcripts. Collectively, MALT1-mediated cleavage of Roquin-1/2 induces the differentiation of T cells into Th17 effector T cells.[110]

*N4BP1*

N4BP1 is an interactor and negative regulator of the E3 ubiquitin ligase ITCH that is a central regulator of the immune responses by marking proteins, such as the AP-1 family member c-Jun, for proteasomal degradation.[133] Additionally, by interacting with the deubiquitinase Cezanne, N4BP1 acts as an effective negative regulator of NF-κB signaling in neuroblastoma cells.[134]

N4BP1 was recently found to be involved in the regulation of HIV-1 latency and reactivation by binding and degrading viral mRNAs. Upon TCR stimulation of HIV-1 infected T cells, MALT1 inactivates N4BP1 by cleavage after R509. Thereby, MALT1 protease activity contributes to HIV-1 reactivation in T cells.[111] However, the functional role of N4BP1 in regulating host mRNAs and the physiological role of MALT1-mediated N4BP1 cleavage remains elusive.

*A20*

Together with BCL10, the deubiquitinase A20, also known as TNF alpha-induced protein 3 (TNFAIP3), is one of the first two MALT1 substrates identified.[94,105] The original publication reported cleavage of a small proportion of A20 in activated T cells and identified a single cleavage site in human A20 that is not conserved in mice.[105] Thus, the role of its cleavage by MALT1 remains to be determined.

The ubiquitin-editing enzyme A20 is an anti-inflammatory protein, known to act as an inhibitor of NF-κB signaling and regulator of cell death.[135] Thus, A20-deficient mice develop a severe inflammatory phenotype and die perinatally of multiorgan inflammation and cachexia.[136] A20 contains an N-terminal ovarian tumor (OTU) domain, characteristic of the OTU subfamily of deubiquitinases[137], and seven ZnF domains (**Fig. 8**).[138]
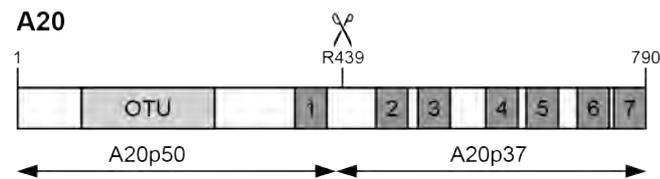
**Figure 8: Structure and domains of A20.** A20 contains an N-terminal ovarian tumor (OTU) domain followed by seven zinc fingers. The MALT1-dependent cleavage site is indicated (R439). Cleavage at this site is resulting in an N-terminal A20p50 and a C-terminal A20p37 fragment.[105]

A20 acts downstream of different NF-κB-activating receptors, such as TNFR1, IL-1R, PRRs, NOD-like receptors (NLRs), and T- and B cell receptors, but its function is best characterized in TNFR1-mediated NF-κB activation.[135] Here it counteracts NF-κB activation by the OTU-mediated cleavage of non-degradative K63-linked ubiquitin chains from TNFR1 and from the signaling mediators receptor-interacting S/T kinase 1 (RIPK1) and NEMO.[138-140] Additionally, A20 further desensitizes cells to TNF via its ZnF4-mediated E3 ubiquitin ligase activity, by marking RIPK1 with K48-linked ubiquitin chains, inducing its proteasomal degradation.[138] Moreover, A20 diminishes TNFR1 signaling by antagonizing the interaction between the E2 ubiquitin conjugating enzyme Ubc13 and the E3 ubiquitin ligases TRAF2 and cIAP1, two essential signaling mediators assembling K63-linked ubiquitin chains. Furthermore, A20 induces the polyubiquitination and proteasomal degradation of Ubc13.[141] However, neither mice expressing DUB-inactive A20 nor ZnF4-mutant A20 develop the severe phenotype of A20-deficient mice.[140,142,143] Consequently, this indicates that neither the DUB nor the proposed E3 ubiquitin ligase activity of A20 are crucial for its anti-inflammatory function *in vivo*.

Lately, the ubiquitin binding capacity of A20 came into the focus of many scientists as a way to explain its biological activity. Taken together, *in vitro* and *in vivo* studies demonstrated that ZnF4 specifically binds to K63-linked ubiquitin chains and ZnF7 to M1-linked linear ubiquitin chains.[140,144-148] Combined inactivation of A20 ZnF4 and ZnF7 in mice was recently found to induce a severe inflammatory phenotype and postnatal lethality, similarly as seen in A20-deficient mice.[149,150] In conclusion, these findings suggest that the ubiquitin-binding capacities of A20 are more important in the anti-inflammatory function than its ubiquitin-editing abilities. However, the underlying mechanism remains incompletely understood.

In general, the basal expression of A20 is low in most cell types and becomes rapidly induced through NF-κB activity.[151] Interestingly, in T lymphocytes the expression level of A20 is already high at steady-state, and rapidly but transiently downregulated upon T cell activation, suggesting an important role for A20 in these

cells.[101,152]  However, mice with T cell-specific A20 deficiency develop normally and survive without any inflammatory phenotype for at least one year.[153,154]  Two different groups showed that the total T cell numbers in these mice are normal, but have a slightly more activated phenotype of the A20-deficient CD4+ and CD8+ T cells, determined by higher CD69 expression levels.[153,154]  While one group showed an augmented activation with increased IFNγ and TNF production of isolated CD8+ T cells from A20-deficient mice[154], another group stated that A20-deficient CD4+ T cells were activated as readily as A20-sufficient T cells, based on antigen stimulation-induced CD69, CD44 and IL-2 expression levels.[153]  Thus, A20 has a major function in the regulation of CD8+ T cells but does not affect CD4+ T cell activation. Nevertheless, A20-deficient CD4+ T cells proliferate more upon TCR triggering, but conversely, A20 is also obligatory for activated CD4+ T cell survival and expansion *in vivo*, most probably by promoting autophagy and protecting the cells from necroptosis.[153,155] Similarly, A20 enhances the survival of activated CD8+ T cells *in vivo* by reduction of necroptotic cell death. Additionally, A20 diminishes NF-κB-induced upregulation of Fas and protects CD8+ T cells from activation-induced apoptosis.[154]  In conclusion, A20 seems to control T cell activation to prevent overwhelming T cell proliferation and cytokine production and additionally protects activated T cells from cell death in several ways.

Studies using a Jurkat T cell line gave further insights in the underlying mechanism of A20-mediated regulation of T cell activation. A20 inhibits TCR-mediated NF-κB activation and target gene expression, such as IL-2.[101,105]  Upon TCR triggering, A20 is rapidly degraded by the proteasome by a still unknown mechanism, nevertheless the rapid degradation of A20 is necessary for initial IKK complex activation.[101,152]  After NF-κB is activated, the A20 expression increases again in the cells, which is supposed to serve as a negative feedback regulation of NF-κB activity. In detail, A20 cleaves K63 ubiquitin chains that are linked to MALT1 in an OTU-dependent manner and thereby inhibits the recruitment and activation of the IKK complex.[101]

Intriguingly, upon TCR triggering, a proportion of A20 is cleaved by MALT1 after R439. MALT1-dependent cleavage of A20 results in an N-terminal fragment of 50 kDa, comprising the OTU domain and the first ZnF (p50) and a C-terminal fragment of 37 kDa with the last six ZnFs (p37) (**Fig. 8**). The C-terminal p37 fragment is rapidly degraded by the proteasome, however the p50 fragment is stable. Nevertheless, p37 and p50 cleavage fragments are partially (p37) or completely (p50) incompetent to suppress CBM-driven NF-κB activation.[105]  This would suggest that MALT1-dependent

cleavage and inactivation of A20 serves as a positive feedback prolonging NF-κB activity via the maintenance of crucial K63-linked ubiquitin chains attached to MALT1. However, inhibition of the catalytic activity of MALT1 neither has an effect on initial phosphorylation and degradation of IκBα nor on the duration of NF-κB activity.[94,97,101] Thus, the role of MALT1-dependent A20 cleavage in lymphocytes remains elusive.

Overall, with the identification of specific MALT1 substrates, the involvement of MALT1 protease activity in different events in lymphocytes has been demonstrated. As a scaffold protein, MALT1 leads to IKK-dependent initiation of NF-κB activity, while the catalytic activity of MALT1 is essential for the enhancement and prolongation of NF-κB activity. Furthermore, MALT1 scaffold and enzymatic activities are also required for proper AP-1 activity. By cleavage of BCL10, the catalytic activity of MALT1 additionally contributes to cell adhesion. Finally, MALT1-mediated cleavage of different mRNA interactors and repressors further regulates lymphocyte activation, proliferation and differentiation and contributes to HIV-1 reactivation by the regulation of the stability of specific mRNA subsets. The role of the MALT1-dependent cleavage of the deubiquitinase A20, however, merits further exploration.

## 3.4.4 MALT1 protease activity in non-lymphoid cells

Although the biological role of MALT1 protease activity is best explored in lymphocytes, MALT1 proteolytic activity is also found in myeloid cells, keratinocytes and endothelial cells, where MALT1 activation depends on CARD9, CARMA2 and CARMA3, respectively.[16,106,156,157] In myeloid cells, MALT1 gets activated in complex with CARD9 upon triggering of Dectin-1/2, Mincle or FcγR and is supposed to contribute to the inflammatory response to fungus or autoantibodies.[156,157] In keratinocytes, MALT1 protease activity is induced by Dectin-1 triggering and is important for the expression of inflammatory genes such as TNFα, IL-17C and CXCL8. Furthermore, the catalytic activity of MALT1 in keratinocytes is essential for the production of antimicrobial peptides such as cathelicidin and defensins promoting bacterial killing. Although MALT1 induces cleavage of RelB, BCL10, A20, CYLD and Regnase-1 in keratinocytes, the exact mechanism by which substrate cleavage promotes keratinocyte-mediated bacterial killing remains unknown.[16] MALT1-mediated cleavage of CYLD in endothelial cells is essential for thrombin induced microtubule disruption, endothelial cell retraction and an acute permeability response and thereby promotes the transmigration of activated immune cells to infected tissues.[106] Hence, due to the ubiquitous expression of MALT1, the proteolytic activity can be induced by CBM complex formation including all four

CARD-CC proteins, suggesting a broad involvement of the catalytic activity of MALT1 in different cells downstream of different receptors.

## 3.5 MALT1 inhibitors and their potential to treat diverse pathologies

MALT1 is the only known human paracaspase, which makes it a specific druggable target to alter NF-κB activation.[5] In a wide range of pathologies MALT1 inhibition could be a promising new treatment option, including autoimmune and inflammatory diseases, lymphoid malignancies and other cancer types.[113,158] Thus, it is of great interest to develop small molecule MALT1 inhibitors for therapeutic reasons. Several MALT1 inhibitors already exist that either irreversibly bind to the active site or reversibly inhibit MALT1 proteolytic activity through an allosteric site.[94,159-162] The following paragraphs will depict the pathologies in which the proteolytic activity of MALT1 is involved and the investigations on the development of MALT1 inhibitors that are done so far.

### 3.5.1 MALT1 in lymphoid malignancies

Several diverse lymphoid malignancies are driven by constitutive MALT1 activity, resulting in NF-κB activation and subsequent cell survival and proliferation of B or T cells. The reasons for continuous MALT1 activation are often gain-of-function or loss-of-function mutations in upstream regulators, chromosomal translocation of the MALT1 gene or MALT1 activation by latent viral infection.[163] Thus, inhibiting MALT1 could be a new treatment option for patients suffering of these B and T cell malignancies.[113]

*B cell malignancies with deregulated MALT1*

A constitutive active BCR signaling pathway is found in different types of B cell malignancies, such as activated B cell diffuse large B cell lymphoma (ABC DLBCL), mantle cell lymphoma (MCL), chronic lymphocytic leukemia (CLL) and in follicular lymphoma (FL).[113,164] Either self-antigen recognition of the BCR or somatic gain-of-function or loss-of-function mutations in genes encoding for CD79, CARMA1 or A20 are leading to MALT1 activation and drive lymphomagenesis.[165-168] Additionally, several germline gain-of-function mutations of CARMA1 are associated with B cell expansion with NF-κB and T cell anergy (BENTA) syndrome, an inherited lymphoproliferative immunodeficiency.[169-171] Typically, gain-of-function mutations of CARMA1 are found in the coiled-coil domain or the adjacent linker region (**Fig. 1**) that disrupt CARMA1 autoinhibition, which makes it independent from upstream signals.[172]

*MALT lymphoma*

MALT lymphoma is a special B cell malignancy of mucosa-associated lymphoid tissues initiated by prolonged inflammation caused by a chronic inflammatory infection for instance with *Helicobacter pylori* or by autoimmune diseases like Sjögren syndrome or Hashimoto thyreoiditis.[173,174] Several organs can be affected including the stomach, lung, liver, skin, eyes, thyroid and the intestine.

In a later stage the disease is driven by antigen-independent constitutive activation of NF-κB via oncogenic chromosomal translocations, mainly affecting the genes encoding MALT1 or BCL10.[173] The most common chromosomal translocation (t(11;18)(q21;q21)) encodes an oncogenic IAP2-MALT1 fusion protein that promotes canonical NF-κB activation via recruitment of TRAF6 and constitutive MALT1 proteolytic activity, resulting in cleavage of NF-κB negative regulators such as A20.[9,105,175] Additionally, IAP2-MALT1 activates non-canonical NF-κB2 complexes by MALT1-dependent cleavage and stabilization of NIK. Interestingly, NIK is a specific substrate of the IAP2-MALT1 fusion protein and is not cleaved by conventional MALT1.[176] Furthermore, also LIM domain and actin-binding protein 1 (LIMA1) is an unambiguous substrate of IAP2-MALT1. LIMA1 cleavage abolishes its tumor suppressor function and generates a fragment with oncogenic properties.[177]

Other chromosomal translocations that are found in MALT lymphoma are t(14;18)(q32;q21), t(1;14)(p22;q32) and t(1;2)(p22;p12), which bring the MALT1 gene or the BCL10 gene under the control of immunoglobulin heavy chain or light chain enhancer promoter elements, resulting in overexpression of MALT1 or BCL10 and thereby driving aberrant NF-κB activation.[7,8,178,179]

*Primary effusion lymphoma (PEL)*

PEL is a rare and incurable B cell malignancy associated with a latent infection with Kaposi's sarcoma herpes virus (KSHV) in immunocompromised patients. Viral latency and malignant growth of the infected cells is dependent on constitutive NF-κB activity.[180] The viral latency genes K13 and K15 promote NF-κB activation via the protease MALT1.[181] Although the exact mechanisms of K13 and K15-dependent MALT1 activation is not clear, MALT1 inhibition could be a treatment option for patients with incurable PEL.

*T cell malignancies with deregulated MALT1*

Similarly as in B cells, MALT1 activating mutations can also drive T cell lymphomagenesis and give rise to acute T cell leukemia/lymphoma (ATLL), peripheral T cell lymphoma (PTCL), cutaneous T cell lymphoma (CTCL) and leukemic CTCL, also

known as Sézary syndrome.[113]  Somatic gain-of-function mutations driving these T cell malignancies have been found in PLCγ1, PKCβ, CARMA1 and also involve different gene fusions with the co-activating receptor CD28.[182-185]

## 3.5.2 MALT1 in autoimmune and inflammatory diseases

Due to the importance of MALT1 proteolytic activity in the innate and adaptive immune response, MALT1 inhibition might contribute to the treatment of autoimmune pathologies and inflammatory diseases, such as multiple sclerosis, rheumatoid arthritis, psoriasis, allergic asthma and inflammatory bowel disease.[113,186]

First hints of the contribution of MALT1 in autoimmune and inflammatory diseases came from MALT1-deficient mice. MALT1 full-body knockout mice are resistant to the induction of experimental autoimmune encephalitis (EAE), a mouse model of human multiple sclerosis, an autoreactive T cell-mediated autoimmune disease of the central nervous system.[187,188]  Furthermore, also MALT1-PD mice are completely protected from development of autoimmune encephalomyelitis.[97,99] Additionally, MALT1-PD mice develop just mild symptoms upon induction of a T cell-driven autoimmune colitis.[97]  These findings have raised hopes that MALT1 inhibitors could be useful to alleviate symptoms of autoimmune diseases.

*MALT1 implications in psoriasis*

MALT1 proteolytic activity is also involved in the inflammatory skin disease psoriasis, suggesting that psoriasis patients could benefit from topical MALT1 inhibition in two distinct ways, which will be described below.

Psoriasis is a common chronic autoinflammatory skin disorder that arises from an interplay between activated keratinocytes and infiltrating, activated immune cells, mainly T lymphocytes.[189]  Both, T cell activation and keratinocyte activation depend on signal transduction through CARMA1 and CARMA2 CBM signalosomes, respectively. Germline alterations in CARMA2 are associated with an increased psoriasis risk, familial psoriasis and the rare psoriasis-related skin disorder, pityriasis rubra pilaris (PRP).[190,191]  These alterations include gain-of-function mutations in CARMA2, which similarly as gain-of-function mutations in CARMA1, drive constitutive MALT1 activation and nuclear translocation of NF-κB in keratinocytes.[192] Subsequent pro-inflammatory gene expression in keratinocytes, including cytokines such as TNFα, CXCL8 and IL-17C, recruits and activates immune cells that further contribute to skin inflammation.[16,192] Thus, psoriasis patients might benefit from topical MALT1 inhibitors by decreasing keratinocyte and immune cell activation.

## 3.5.3 MALT1 in non-lymphoid malignancies

Within the last few years until today the interest raises in targeting MALT1 proteolytic activity for the therapy of different non-lymphoid malignances. Firstly, a reliance of tumor cell growth on CBM-dependent activation of NF-κB was discovered for different types of carcinoma.[113,193]  Secondly, the dependence on MALT1 protease activity for Treg cell development and function indicates that MALT1 inhibitors might improve antitumor immunity.[194]  Accordingly, MALT1 inhibitors may exert their tumor growth inhibitory effects both, by directly acting on tumor cells and indirectly, by impeding Treg-mediated diminishing of the antitumor immune response.

*Direct MALT1 contribution to tumor cell growth*
Several publications indicate a role for inappropriate MALT1 signaling in the development of non-lymphoid malignancies. In malignant melanoma cells a high expression level of MALT1 is associated with poor disease-free survival by promoting cell proliferation and motility and enhancing melanoma cell survival through activation of AP-1 and NF-κB.[195]  Furthermore, the increased malignancy of glioblastoma that is related to NF-κB activity relies on MALT1 overexpression, mediated by the loss of the MALT1-targeting miRNA, miR-181d.[196]  Additionally, MALT1 is involved in NF-κB-dependent DNA damage resistance of tumor cells.[197]  Indeed, NF-κB is a known pro-survival regulator in the context of irradiation and chemotherapy by inducing cell cycle arrest and allowing DNA damage repair.[198]  Interestingly, MALT1 expression is necessary for chemotherapeutic NF-κB induction[197], however, the contribution of the proteolytic activity in this process remains elusive.

Similar to overexpression of MALT1, overexpression of CARMA3 is associated with different malignancies, such as non-small cell lung cancer, colon cancer, breast cancer, glioma, pancreatic cancer, renal cell carcinoma, bladder cancer and ovarian cancer. High CARMA3 expression levels in these tumors are positively related with the primary tumor size and stage and the degree of lymph node and distant metastasis. Silencing of CARMA3 in cell lines of the different types of tumors in general leads to decreased proliferation and cell invasion and to an increased susceptibility to chemotherapeutics.[193]  However, whether CARMA3 overexpression also induces CBM complex formation and MALT1 activation in the tumor cells and how this contributes to the pathogenesis is still unclear.

In addition, enhanced CARMA3-CBM complex activation has been found in different cancer cells without a basal increase of the expression levels of CBM complex components. This increased CBM complex activity is due to upregulation or gain-of-

function mutations of the upstream GPCRs or RTKs. For example, gain-of-function mutations of the oncogene EGFR drives cell proliferation, migration and invasion of lung cancer cells in a CARMA3, BCL10 and MALT1-dependent manner.[39]   Human epidermal growth factor receptor 2 (HER2) or angiotensin II receptor 1 (AGTR1) overexpression, which is often found in breast cancer, promote tumorigenesis via CARMA3-CBM complex-mediated NF-κB activation.[40,199]   Furthermore, the CARMA3-CBM signalosome is involved in oncogenic signal transduction of the GPCRs, C-X-C chemokine receptor type 4 (CXCR-4) and lysophosphatidic acid receptor (LPAR), in oral squamous cell carcinoma and ovarian cancer, respectively.[200,201]   Although MALT1 silencing reduced signal transduction and subsequent tumor growth, the contribution of the proteolytic activity to tumorigenesis still needs to be investigated. Interestingly, recent findings indicate an involvement of MALT1 proteolytic activity in tumor metastasis.[202]   Indeed, the GPCR, protease-activated receptor 1 (PAR1), which is implicated in the promotion of metastasis of a wide range of epithelial and mesenchymal tumors, activates NF-κB via the CARMA3-CBM complex.[203]   In an osteosarcoma cell line and in breast cancer cell lines, PAR1-induced NF-κB activation is dependent on MALT1. Furthermore, PAR1 stimulation leads to MALT1-dependent cleavage of RelB in these cell lines, indicating that MALT1 proteolytic activity contributes to NF-κB-dependent tumor metastasis of osteosarcoma, breast cancer and putatively also of other epithelial and mesenchymal tumors.[202]

In conclusion, MALT1 seems to be involved in tumorigenesis, tumor growth and metastasis of a wide range of tumors, indicating that MALT1 inhibitors could be of interest in the therapy of different non-lymphoid malignancies.

### *MALT1 as a target to boost antitumor immunity*

In solid tumors, infiltrating effector T cells are able to control tumor cell growth, however also Treg cells are found inside the tumors that restrict the antitumoral response of effector T cells. Thus, specifically targeting Treg cell function promotes antitumor immune response.[204]   The first hint that MALT1 inhibition may impair Treg cells comes from MALT1-PD mice that show impaired natural Treg cell development and function.[97-100,102]   Furthermore, the generation of Treg-specific CARMA1-deficient, BCL10-deficient and MALT1 protease-dead mice confirmed the potential of MALT1 inhibition to promote antitumoral immune response.[194,205,206]   Partial conditional genetic deletion of CARMA1 in Treg cells improves the antitumor immune response in combination with PD-1 blockade via the increased production of IFNγ by CARMA1-deficient Treg cells with subsequent macrophage activation and upregulation of MHC-I molecules on melanoma cells.[205]   Similarly, conditional deletion of BCL10 in Treg cells

impairs tumor growth of melanoma cells.[206] Mice with Treg-specific heterozygous expression of MALT1-PD display a better antitumor response to transferred lymphoma cells due to a lower Treg cell tumor infiltration.[194] Interestingly, also full-body MALT1-PD expressing mice show improved tumor growth control of injected lymphoma cells or colon carcinoma cells.[114,194] Hence, effector T cells and other immune cells responsible for antitumor response are not dramatically affected by the abrogation of MALT1 protease function. Thus, MALT1 inhibitors might be suitable to impair Treg cells and thereby increase the antitumor immune response of cancer patients.

## 3.5.4 Development of MALT1 inhibitors

The first MALT1 inhibitor that was created is z-VRPR-fmk that was designed based on the optimal tetrapeptide substrate of the metacaspase AtmC9 of *Arabidopsis thaliana*.[94] The tetrapeptide of valine-arginine-proline-arginine (VRPR) is conjugated to fluoromethyl ketone (fmk), which alkylates the active site cysteine irreversibly. Specificity of the inhibitor is mediated by the tetrapeptide.[94,207] Its efficiency to inhibit MALT1 was tested *in vitro* and on lymphoid cell lines. [94] The next generation of this active site inhibitor, z-LVSR-fmk was designed later based on the optimal tetrapeptide sequence of MALT1, which was determined by peptide screens and which is present in the MALT1 substrate RelB.[107,208] Although, these peptide-based inhibitors are efficient to inhibit MALT1 and reduce the growth of ABC DLBCL and MCL cell lines *in vitro*, they have pharmacologic limitations for therapeutic purposes *in vivo*.[209-211]

By screening chemical libraries, several small molecule MALT1 inhibitors have been identified that show potential for therapeutic applications.[159-162] Amongst these, MI-2 binds and inhibits MALT1 irreversibly in a similar mechanism as for fmk peptide inhibitors, but with a higher affinity for the active site of MALT1.[159] Currently, several groups are chemically altering MI-2 to pharmacologically and pharmacodynamically improve this compound to enable clinical trials.[212,213] Another group of small molecule MALT1 inhibitors are phenothiazines, such as mepazine, thioridazine and promazine. These compounds are efficient, noncompetitive, reversible MALT1 inhibitors that are also clinically used as antipsychotics.[160,214,215] Phenothiazine derivatives bind to a pocket in the interface of the protease domain and the Ig3 domain and most probably prevent the structural change of the protease to its active conformation.[216] Recently, also β-lapachone derivatives were found to irreversibly inhibit MALT1 by binding to the active site and inhibit the growth of an ABC DLBCL cell line.[161] However, whereas MI-2 and phenothiazine derivatives have been pre-clinically tested in the context of different pathologies, the efficacy of β-lapachones *in vivo* remains to be determined.

*Treatment of lymphoid malignances with MALT1 inhibitors*

MI-2 and phenothiazines are efficient to block the growth of ABC DLBCL cell lines *in vitro* and *in vivo* in xenograft mouse models.[159,160] Furthermore, also primary human DLBCL and CLL are growing less well upon MI-2 treatment *ex vivo*. [159,217] Strikingly, also ABC DLBCL cell lines that are resistant to the BTK inhibitor, ibrutinib, are susceptible to mepazine, indicating that a combinatorial treatment with ibrutinib and MALT1 inhibitors could improve the therapeutic effectiveness for ABC DLBCL patients.[218] Furthermore, also the growth of KSHV-infected PEL cell lines is impaired *in vitro* and in xenograft mouse models by thioridazine or mepazine administration.[181] In conclusion, MALT1 inhibitors are indeed of interest in the treatment of lymphoid malignancies such as ABC DLBCL, CLL, PEL, and potentially also of other MALT1 protease-dependent lymphoid malignancies for which further pre-clinical investigations have to be done.

*Treatment of autoimmune and inflammatory diseases with MALT1 inhibitors*

MALT1 inhibitors have been tested for their usefulness in the treatment of a variety of inflammatory conditions. One inflammatory condition in which MI-2 was found to protect mice is LPS-induced lung injuries and death, most probably by the stabilization of Regnase-1 in myeloid cells.[219] Another chronic inflammatory disease that is driven by myeloid cells is rheumatoid arthritis, in which joint destruction is mediated by leukocyte infiltration and an increased osteoclast activity. MI-2 administration and thereby blockage of MALT1 proteolytic activity improves the outcome of collagen-induced arthritis in mice.[220] Additionally, MI-2 or mepazine administration attenuate dextran sulfate sodium (DSS)-induced experimental colitis, which is a mouse model of ulcerative colitis that shares features with human inflammatory bowel disease.[221,222] Interestingly, in addition of decreasing MALT1 protease-induced NF-κB activity, MI-2 also diminishes NLRP3 inflammasome formation in a MALT1-independent mechanism that contributes to symptoms attenuation.[221] Thus, patients with ulcerative colitis might profit from this double-edged function of MI-2, however it also indicates that MI-2 may in part exert its effects by acting on off-targets, independently of the MALT1 protease. In view to the treatment of autoimmune disorders, mepazine has been efficiently tested in attenuation of EAE, prophylactically and after disease onset in mice.[223] Thus, MALT1 inhibition could be beneficial for patients suffering from autoimmune and inflammatory diseases. Nonetheless, it should be pointed out that most of these studies have applied MALT1 inhibitors only for limited times and the fact that genetic inactivation of MALT1 catalytic function compromises immune homeostasis is raising concerns about the safety of systemic long-term applications of

MALT1 inhibitors.[97-100,102]  Thus, the safety of systemic long-term application needs to be carefully determined by preclinical and clinical trials to secure the potential of MALT1 inhibitors in the therapy of chronic autoimmune and inflammatory diseases.

*Treatment of non-lymphoid malignancies with MALT1 inhibitors*

So far, the efficacy of MALT1 inhibitors to suppress tumor progression of non-lymphoid malignancies is poorly investigated. However, MI-2 and z-VRPR-fmk are efficient to block PAR1-driven upregulation of the two metastasis-associated genes, IL-1β and matrix-metalloproteinase 9 (MMP9) in an osteosarcoma cell line, indicating a general involvement of MALT1 substrate cleavage in PAR1-dependent tumor metastasis.[202]  In mice, administration of mepazine shows promising effects on tumor growth in a model of malignant melanoma. [206]  However, in another mouse model of malignant melanoma administration of MI-2 or mepazine shows only a mild effect on the tumor growth.[205]  This discrepancy might be due to the differences in the immunogenicity of the different melanoma models. Indeed, in the study in which pharmacological MALT1 inhibition had only little effects on tumor growth the melanoma cell line that was transplanted carried only a negligible mutational load, thus having a low immunogenicity. Strikingly, pharmacological MALT1 inhibition seems to improve the response to immune checkpoint therapy in this mouse model by interfering with Treg cell function and increasing the number of infiltrating cytotoxic T lymphocytes and NK cells.[205]  Thus, MALT1 inhibitors are able to improve antitumor immune response directly or in combination with immune checkpoint therapy.


In conclusion, all these small molecule compounds demonstrate efficiency in MALT1 inhibition *in vitro* and *in vivo*, and indicate promising efficacy to treat lymphoid and non-lymphoid malignancies.  MALT1 inhibitors also showed promising therapeutic effects in mouse models of autoimmune/inflammatory diseases, but whether prolonged treatment of autoimmunity patients with MALT1 inhibitors is safe needs to be assessed in future studies. Of note, recent studies have revealed that the specificity of MI-2 and phenothiazines to MALT1 is not optimal or rather low and that these compounds have MALT1-independent off-target effects.[224,225]  Thus, further chemical adjustments of these initial compounds or the discovery of new MALT1 inhibiting substances are needed to improve the selectivity and to avoid off-target effects.

# 4  Aim of the thesis

MALT1 is a ubiquitously expressed protein that serves as a scaffold in complex with CARD-CC-containing proteins and BCL10 to induce the activation of pro-inflammatory transcription factors, such as NF-κB, downstream of different receptors in various cell types. Furthermore, the proteolytic function of MALT1 enhances and prolongs NF-κB activity by cleavage and inactivation of negative regulators, such as A20, but also further promotes inflammatory processes by other means. Dysregulation of MALT1 activity is implicated in immunodeficiency, lymphomagenesis, autoimmune and inflammatory diseases as well as in non-lymphoid malignancies. Therefore, targeting the proteolytic activity of MALT1 is of high interest in the therapy of a wide range of pathologies.

Despite the recognized physiological relevance of MALT1 protease function, relatively little is known about the mechanism of MALT1 protease activation and regulation. The protease activity of MALT1 was recently found to be tightly controlled by monoubiquitin conjugation to the third Ig-like domain[95], but how MALT1 becomes monoubiquitinated and the mechanism governing the unshackling of the protease domain by a single ubiquitin moiety, remain unknown. In the first part of this work, we have thus investigated the intramolecular mechanism connecting monoubiquitination of the Ig3 domain with the activation of the protease domain. This has allowed us to identify the Ig3 domain of MALT1 as a ubiquitin-binding domain that promotes recruitment and conjugation of ubiquitin to MALT1, and to identify an allosteric mechanism of MALT1 activation by monoubiquitination. The results of this part of the project provide insights into the basic mechanism of MALT1 activation that could be helpful for the development and identification of new MALT1 protease activity modulating substances that will be of benefit in the treatment of different pathologies.

Another aspect of MALT1 function that is poorly understood is the consequence of the MALT1-dependent cleavage of A20, one of the first identified substrates of MALT1.[105] In T cells, A20 was found to cleave K63 ubiquitin chains that are linked to MALT1 and to thereby inhibit the recruitment and activation of the IKK complex.[101] MALT1-dependent cleavage of A20 results in two non-functional products *in vitro*, suggesting that MALT1-dependent cleavage of A20 prolongs or amplifies IKK complex activity. However, inhibition of the catalytic activity of MALT1 has no effect on IKK activation or phosphorylation of IκBα.[94,97,101] Thus, the role of MALT1-dependent A20 cleavage in lymphocytes and potentially in other cell types remains elusive. Mice expressing non-cleavable A20 would be useful to investigate the physiological role of

A20 cleavage. However, the published human A20 cleavage site is not conserved in mouse A20 or among other species. Nevertheless, there is additional evidence that A20 is cleaved by MALT1 between ZnF3 and ZnF4 in mice, though the specific cleavage site remains unknown.[105] Furthermore, several publications showed that human A20 is cleaved by MALT1 on additional, yet unidentified sites.[101,209,226] Thus, the aim of the second project was to examine the precise location of the cleavage sites in human and mouse A20 and to investigate on the functional relevance of MALT1-dependent A20 cleavage in T lymphocytes. The results presented here demonstrate that human A20 is cleaved at 4 distinct sites, 3 of which are conserved in the mouse, and let to a refinement of the known substrate cleavage motif of MALT1. The functional relevance of the individual cleavage sites is the target of ongoing investigations.

# 5 Project 1: Allosteric activation of MALT1 by its ubiquitin-binding Ig3 domain

<u>Rebekka Schairer</u>, Gareth Hall, Ming Zhang, Richard Cowan, Roberta Baravalle, Fred Muskett, Peter J. Coombs, Chido Mpamhanga, Lisa R. Hale, Barbara Saxty, Justyna Iwaszkiewicz, Chantal Décaillet, Mai Perroud, Mark D. Carr, and Margot Thome

For details see article in *Annex I*

## 5.1 Summary of Results

To activate MALT1 protease function, the Ig3 domain needs to become monoubiquitinated at K644. Mutation of K644 to an arginine dramatically decreases the proteolytic activity of this monoubiquitination-deficient MALT1 in cells, however fusion of a single ubiquitin moiety to the C-terminus of MALT1 rescues cleavage activity of MALT1(K644R). Interestingly, the MALT1-Ubiquitin fusion protein (MALT1-Ub) is able to cleave substrates *in vitro* without the presence of any other CBM complex components. Moreover, mutation of I44 within the fused ubiquitin to alanine dampens the MALT1 cleavage activity.[95] I44 is localized in a hydrophobic surface patch of ubiquitin that is commonly used for the interaction of ubiquitin with several ubiquitin-binding domains (UBD).[227] This suggests that MALT1 is activated in an intra- and/or intermolecular way by monoubiquitination of the Ig3 domain. The study from Pelzer *et al.* further identified MALT1 as a ubiquitin-binding protein and the interaction site was mapped to the C-terminal part of MALT1, including the protease domain, the third Ig3 domain and the unstructured C-terminal extension.[95] Taken together, these data suggested that MALT1 is activated by a MALT1-ubiquitin interaction within its C-terminal part. However, the exact ubiquitin-interaction site within MALT1 had remained unknown.

By using 2D-NMR approaches and an Octet system, we and our collaboration partners from the University of Leicester identified that ubiquitin interacts with MALT1 via positively charged residues surrounding I44 of ubiquitin. The ubiquitin-binding site within MALT1 was found to be a negatively charged patch at the surface of the Ig3 domain. Mutations of key residues in MALT1 (E696/D697 to lysine (ED/KK)) or in

ubiquitin (K6, K48 and H68 to alanine), which are involved in the MALT1-ubiquitin binding, impaired the interaction.

To gain insights into the role of MALT1-ubiquitin binding, we tested the ubiquitin-binding-deficient MALT1 mutants (E696/D697 to alanine (ED/AA) or lysine (ED/KK)) functionally. MALT1 ED/AA and ED/KK showed normal scaffold function, but were strongly impaired in their proteolytic activity. The reduced proteolytic activity of the ubiquitin-binding-deficient MALT1 mutants was due to a defect in MALT1 monoubiquitination. Interestingly, similarly as for monoubiquitination-deficient MALT1 (K644R), the functional defect of the ubiquitin binding-deficient MALT1 mutants could be overcome by fusion of ubiquitin to the C-terminus of the MALT1 mutants. On the other hand, mutations of the residues within ubiquitin, which were found essential for MALT1-ubiquitin interaction, decreased the catalytic activity of the MALT1-Ub fusion protein. Thus, the ED motif in the Ig3 domain is required for ubiquitin recruitment and conjugation to MALT1 but, once conjugated onto MALT1, ubiquitin promotes MALT1 activation by additional means.

Furthermore, to investigate the outcome of disruption of the MALT1-ubiquitin interaction, we assessed the effect of the ubiquitin-binding-deficient MALT1 mutants on lymphocyte activation. We generated a CRISPR/Cas9-mediated knockout of MALT1 in a Jurkat T-lymphocyte cell line and reconstituted the cells by lentiviral transduction with either MALT1 wild-type, catalytically-inactive mutant (C464A), monoubiquitination-deficient mutant (K644R) or the ubiquitin-binding-deficient mutants (ED/AA and ED/KK). With this approach we confirmed that ubiquitin-binding-deficient MALT1 retains its scaffold function but is dramatically impaired in cleaving known MALT1 substrates upon stimulation of the cells. Proper lymphocyte activation, differentiation and cytokine production needs both, the scaffold and the protease function of MALT1.[97,107] Thus, we further examined the effect of MALT1 ED/KK mutation on stimulation-induced IL-2 transcription and secretion in Jurkat T cells and in primary human CD4^{+} T lymphocytes. The transcription and secretion of IL-2 was strongly decreased in cells expressing ubiquitin-binding-deficient MALT1, similarly to cells expressing catalytically-inactive or monoubiquitination-deficient MALT1. Thus, ubiquitin binding by the MALT1 Ig3 domain, promotes ubiquitin conjugation to K644 and subsequent proteolytic activity, which is crucial for proper lymphocyte activation.

However, the exact mechanism by which ubiquitin binding and conjugation to the Ig3 domain activates the protease domain remained unknown. Analysis of the MALT1 crystals (MALT1$_{Protease-Ig3}$; 334-719 aa) show that the C-terminal Ig3 domain interacts with the protease domain via a combination of hydrogen bonds and

hydrophobic contacts, stabilizing or forcing the structure to adopt an inactive conformation.[91,92]   We found that artificial interference with the hydrophobic interactions between the Ig3 and the protease domain results in an uncontrolled and hyperactive MALT1 mutant. The activation was independent of ubiquitin binding and conjugation, but still depended on MALT1 dimerization.

Analysis of the strongest hyperactive MALT1 mutant (Y657A) revealed that impairment of the protease-Ig3 interaction affects the loop connecting the monoubiquitination site (K644) to the protease-Ig3 interaction site (Y657). Additionally, residues in the active site of the protease were affected. Taken together, this suggests a signal transfer from the ubiquitin-conjugation site (K644) via the protease-Ig3 interaction surface to the active site of the protease.

To conclude, we identified the Ig3 domain as a novel ubiquitin-binding domain, which is crucial for monoubiquitin conjugation to the Ig3 domain. Monoubiquitination of MALT1 signals through the loop, including Y657, to the protease-Ig3 interaction surface and weakens the hydrophobic interactions involving Y657, to allow the protease domain to adopt its active conformation and to cleave substrates.

On this article I share first authorship with Gareth Hall and Ming Zhang. For this study I designed, performed and analyzed the majority of the biochemical experiments, shown in Figure 2, Figure 3, Figure 4 B, C, F, G and supplementary Figures S2, S3, S4 A and S5. Furthermore, I assembled all the Figures and contributed to the writing and revision of the manuscript.

## 5.2 Discussion

Activation of lymphocytes, during antigen-receptor signaling and lymphomagenesis, is dependent on CBM complex formation and activation of the protease function of MALT1. So far, the catalytic activation of MALT1 was thought to rely on two events. Firstly, MALT1 has to homo-dimerize via its protease domain, prospectively encouraged by CARMA1 and BCL10-dependent oligomerization and filament formation.[69] Secondly, MALT1 needs to get monoubiquitinated at the Ig3 domain and then undergoes an intra- or intermolecular physical interaction with this ubiquitin moiety.[95]

### 5.2.1 MALT1 monoubiquitination mechanism

Here, we identified the MALT1 Ig3 domain as a novel ubiquitin-binding domain that interacts with ubiquitin via a conserved hydrophobic patch, which is known to be crucial for the interaction with many other ubiquitin-binding domains.[227] Indeed, the binding is mediated by negatively charged residues on the surface of the Ig3 domain (E696 and D697) and positively charged amino acids surrounding I44 of ubiquitin (K6, K48, H68 and R72).

Ubiquitin binding to the Ig3 domain is essential for the conjugation of monoubiquitin to the Ig3 domain at K644 and subsequently for the proteolytic activation of MALT1. MALT1 monoubiquitination may be catalyzed by a yet unknown E3 ubiquitin ligase. Alternatively, MALT1 possibly mediates its own monoubiquitination in an E3 ubiquitin ligase-independent manner as it was shown for other UBD-containing proteins.[228] Different UBDs, including UBA, UIM, UBM, NFZ, and UBZ, can directly cooperate with Ub-charged E2 enzymes to promote their own monoubiquitination.[228] This could explain why so far no E3 ubiquitin ligase involved in MALT1 monoubiquitination has been identified. Indeed, previous studies demonstrated that the Ig3 domain interacts with the E2 ubiquitin-conjugating enzyme unit Ubc13/Mms2.[9,81] Silencing of Ubc13 dampened NF-κB activation through a decrease in NEMO ubiquitination.[9,81] It would be interesting to check whether MALT1 ED/KK is still able to bind Ubc13 and whether MALT1 monoubiquitination is affected by diminishing Ubc13 expression, which would contribute to the reduction of NF-κB activity.

Interestingly, the monoubiquitination site in the Ig3 domain is also one of the proposed eleven lysine residues linked to K63-ubiquitin chains, assembled by TRAF6.[74,95] This could mean that MALT1 first becomes polyubiquitinated by TRAF6 and

later on a deubiquitinating enzyme might trim the ubiquitin chain until only one ubiquitin moiety is left conjugated to K644 in MALT1. However, TRAF6 was found dispensable for MALT1 monoubiquitination and proteolytic activation by ourselves (unpublished data) and by the group of Frederic Bornancin.[104]  Recently, also the homologous to the E6-associated protein carboxyl terminus domain containing 3 (HECTD3) E3 ubiquitin ligase has been found to mediate polyubiquitination of MALT1.[229]  This ubiquitin ligase was previously discovered as a MALT1 interaction partner, stabilizing MALT1 and promoting chemotherapeutical resistance of breast cancer cells.[230]  The study of Cho *et al.* demonstrated the dependence of HECTD3 expression for EAE development in mice and revealed that HECTD3 is necessary for stimulation-induced nuclear translocation of RelA in CD4$^+$ T cells. Further, they identified K648 of MALT1 being linked to K27 or K29 polyubiquitin chains via HECTD3 in CD4$^+$ T cells.[229]  Although the authors demonstrated that K648R mutation has no effect on the proteolytic activity of MALT1, it would be interesting to determine the level of proteolytic activity of MALT1 in cells deficient for HECTD3. In addition to K648, HECTD3 might target the neighboring K644 and thereby promote MALT1 activation. Moreover, it would be interesting to test whether ubiquitin-binding deficiency affects the described MALT1-HECTD3 interaction.

Here, we demonstrated that T lymphocytes that express ubiquitin-binding deficient mutants of MALT1 showed poor cleavage of the MALT1 substrates CYLD and Roquin-1 upon stimulation. In contrast, MALT1 scaffold function was not affected, as evident from equal amounts of IκBα and JNK phosphorylation. This indicates that TRAF6-mediated MALT1 polyubiquitination, which is critical for MALT1 scaffold function[74], is not dependent on ubiquitin binding. Nevertheless, lymphocyte activation, survival and cytokine production are dependent on MALT1 scaffold and protease function.[94,97,101,107]  Indeed, production and secretion of IL-2 was clearly reduced by impairment of MALT1-ubiquitin binding.

Interestingly, as for monoubiquitination-deficient MALT1, the activity of ubiquitin-binding-deficient MALT1 could be restored by C-terminal fusion of ubiquitin.[95] Remarkably, the activity of MALT1-Ub fusion protein was impaired by mutation of the ubiquitin residues that are essential for MALT1-ubiquitin interaction. This indicates that as soon as ubiquitin is conjugated to MALT1, the monoubiquitination-dependent MALT1 activity does not rely on the identified UBD but still depends on the same surface on ubiquitin. This implies that there is a second UBD within MALT1 that is essential for monoubiquitination-dependent MALT1 activation, but which has not been identified yet. Of note, the 2D-NMR analysis did not show any additional chemical shift

perturbations and thus provided no indication for a second UBD. This might be because the 2D-NMR approach uses recombinant monomeric MALT1, but in the cleavage assays in cells, MALT1 most probable dimerizes or oligomerizes, which may lead to a conformational change or formation of a composite ubiquitin-binding site that is normally hidden in monomeric MALT1. This hypothesis remains to be investigated in future studies.

## 5.2.2 Monoubiquitination-mediated MALT1 activation

Furthermore, we investigated the mechanism of monoubiquitination-dependent MALT1 proteolytic activation. The Ig3 domain that was previously found to repress the catalytic activity of MALT1 interacts with the protease domain through several hydrogen bonds and extensive Van-der-Waals contacts (**Fig. 9A, B**).[91,95]
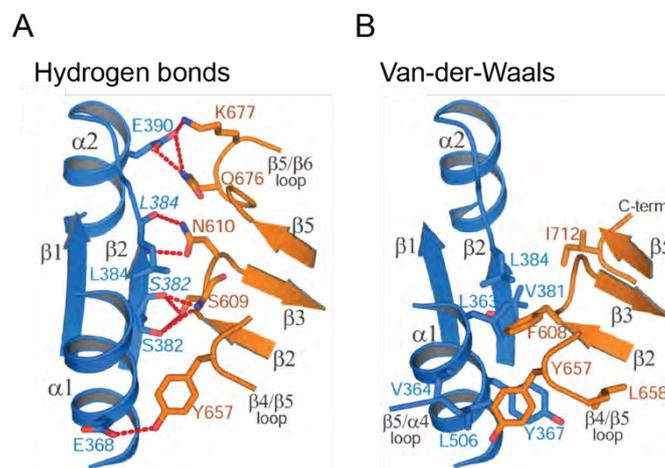


**Figure 9: Protease-Ig3 interactions.** A stereoview of the hydrogen bonds (A) and the Van-der-Waals interactions (B) between the protease domain (blue) and the Ig3 domain (orange). Key residues involved in the protease-Ig3 interaction are indicated. Hydrogen bonds are highlighted as red dashed lines. Adapted from Yu, J. *et al.*, PNAS (2011)

A study comparing the dimeric crystal structure of MALT1$_{Protease-Ig3}$ with or without the active site inhibitor and peptide analog, z-VRPR-fmk, revealed that ligand-bound MALT1 protease adopts an active conformation. Comparison of the structure of ligand-free (inactive) MALT1$_{Protease-Ig3}$ with ligand-bound (active) MALT1$_{Protease-Ig3}$ showed that also the Ig3 domain of MALT1 undergoes substantial conformational changes upon ligand binding. The α1 helix of the Ig3 rotates by approximately 45° and elongates by one turn and thereby weakens the previously described interaction of the Ig3 with the protease domain.[92] Based on that, we hypothesized that artificially diminishing the interaction of the protease domain with the Ig3 domain may affect the catalytic activity. Among others, tyrosine 657 of the Ig3 domain was proposed to participate in the protease-Ig3 interaction. It forms a hydrogen bond to E368 of the protease domain

(**Fig. 9A**) and Van-der-Waals interactions with L363, Y367 and L506 (**Fig. 9B**).[91] Additionally, Y657 undergoes a considerable shift upon ligand binding to the active site, resulting in the assumption that Y657 is an important player for the protease-Ig3 interaction.[92] Indeed, interference with the protease-Ig3 interaction by Y657A mutation turns MALT1 into a constitutively active protease *in vivo* and *in vitro*. The interference with the corresponding Van-der-Waals interactions seemed to be the reason for this, since substitution of Y657 to phenylalanine, which impairs the hydrogen bond to E368 but not the hydrophobic interactions, had no activating effect. Additionally, also individual mutations of hydrophobic residues of the protease domain within the Ig3 interaction site (Y367, L506 and N508) activated MALT1 protease function.

By comparing the $^{15}N/^1H$ TROSY spectra of MALT1 WT with MALT1 Y657A, we found chemical shift perturbations in the Ig3 domain and in the protease domain. In the Ig3 domain, residues within the loop connecting Ig3β4 and Ig3β5, containing the monoubiquitination site (K644) and the protease-Ig3 interaction site (Y657), were strongly affected by Y657A mutation. In the protease domain, mainly residues of the α1, including L363 and Y367, and the β5/α4 loop, containing L506 and N508 at the protease-Ig3 interaction surface were affected. Interestingly, also amino acids at the protease active site, including H415 and C464, showed chemical shift perturbations upon Y657A mutation. This data suggests a signal transfer from the ubiquitin-conjugation site (K644) via the protease-Ig3 interaction surface to the active site of the protease. In agreement, the activity of MALT1 Y657A was independent of ubiquitin-binding and conjugation, leading to the conclusion that signal transduction from the Ig3 domain to the protease domain is a consequence of monoubiquitination. However, the activity of MALT1 Y657A was still dependent on MALT1 dimerization.

The dimer interface between two MALT1 monomers is formed by interactions between β6 and α5 of the protease domain with their respective symmetry mates β6′ and α5′ (**Fig. 5**). As in caspases, this leads to the formation of a dimer with the active sites positioned on opposite faces. Additionally, this crystallographic structure uncovered the position of the C-terminal Ig3 domains pointing away from each other and from the center of the dimeric structure (**Fig. 5**).[91,92] The discovery of CBM complex filaments gave new insights into MALT1 protease activation. Within the BCL10 filaments, MALT1 binds to BCL10 with its N-terminal DD. The C-terminal protease and Ig3 domain protrude from this core to enroll mediators and substrates at the filament periphery. Like this, filament formation likely brings MALT1 monomers into proximity to promote their dimerization.[10]

In conclusion, based on the dimeric structure of MALT1 (**Fig. 5**) and on the new findings of the assembly of the CBM complex, we propose a model in which BCL10 filament formation promotes MALT1 dimerization upon an antigen receptor signal. Subsequent recruitment of the still unknown E2/E3 ubiquitin conjugating complex by the identified ubiquitin-binding domain of the Ig3, leads to MALT1 monoubiquitination. Conjugated ubiquitin of one MALT1 moiety most probably interacts with a still unidentified ubiquitin-binding site of a neighboring MALT1 dimer along the BCL10 filament. These physical connections between dimers may structurally change the position of the loop extending from K644 to Y657, which may in turn alter the activity of the enzyme by disrupting the previously reported inhibitory, hydrophobic interaction between the protease and the adjacent Ig3 domain, allowing the adaption of a catalytically active conformation of the MALT1 dimers.

Overall, our results provide fundamentally new insights into the mechanism of MALT1 activation and might help for the development and identification of new MALT1 protease activity-modulating substances that will be useful in the treatment of different pathologies. Indeed, our results uncovered a new interface that could be targeted by substances, which might allosterically alter MALT1 proteolytic activity, similarly as phenothiazine derivatives. These MALT1 inhibitors bind in a pocket in the interface of the protease domain and the Ig3-connecting helix $\alpha$1 and are supposed to prevent the structural change of the protease to its active conformation.[216] Equally, substances that are able to bind to the MALT1 protease-Ig3 interface, including the critical Y657, could function as MALT1 inhibitors or activators with high target specificity. Thus, further screenings of chemical libraries could identify MALT1 protease activity-modulating substances that act via binding to our identified allosteric pocket.

# 6 Project 2: Identification and characterization of novel A20 cleavage sites

## 6.1 Materials and Methods

*Antibodies*

Primary antibodies used in this project include anti-A20 (D13H3), anti-CYLD (D1A10), anti-p-IκBα (S32/S36, 5A5) and anti-CARMA1 (1D12) from Cell Signaling Technology, anti-Tubulin (B-5-1-2), anti-p-ERK (T202/Y204 in ERK1; T185/Y187 in ERK2; MAPK-YT) and anti-VSV-G (P5D4) from Sigma Aldrich and an affinity-purified rabbit anti-MALT1 antibody that were described by Rebeaud *et al.*[94] Horseradish peroxidase-conjugated anti-mouse (115-035-146) and anti-rabbit (111-035-144) secondary antibodies were purchased from Jackson ImmunoResearch laboratories.

*Plasmids*

N-terminal VSV-tagged A20 and Strep-tagged MALT1 were subcloned in an pCR3-based expression vector. N-terminal HA-tagged CARMA1(L244P) was subloned in a pcDNA3 vector. Point mutants were generated by mutagenesis PCR using PfuUltra High-Fidelity DNA Polymerase AD from Agilent. For CRISPR/Cas9-mediated A20 silencing, the lentiCRISPRv2 vector from GeCKO was used with an A20-specific sgRNA sequence (5′-TCAGTACATGTGGGGCGTTC-3′). For the control a non-specific sgRNA sequence (5′-CTTCGAAATGTCCGTTCGGT-3′) was used. For the reconstitution of A20-KO cells with A20 constructs the pWPI vector from Addgene was used. For that we induced a silent point mutation within the A20 nucleotide sequence (g348a) to make the A20 constructs Cas9-stable.

*Cell culture, transfection and transduction*

HEK293T were cultured in DMEM supplemented with 10% fetal calf serum (FCS) (Biowest). Jurkat cells and the ABC DLBCL cell lines HBL-1, OCI-Ly3 and TMD8 were cultured in RPMI1640 supplemented with 10% or 20% FCS, respectively. All cell lines were grown at an atmosphere of 37°C and 5% $CO_2$.

Transient transfection of HEK293T cells was performed by calcium-phosphate precipitation. For this the plasmids were mixed in a 250mM $CaCl_2$ solution and added by a 2xHeBS-Buffer (0.28μM NaCl, 50mM HEPES, 15mM anhydrous $Na_2HPO_4$, pH 7.05). After 10 min of incubation at room temperature the mixture was added to the cells (40-60% confluency).

For lentiviral transduction of Jurkat cells to either silence A20 by CRISPR/Cas9 or to reconstitute the cells with A20 constructs, lentiviral particles were produced by transfection of HEK293T cells with the lentiviral plasmid of interest and the packaging plasmids psPAX2 and pVSVg. After 48h the supernatant containing lentiviral particles was collected and virus were concentrated with polyethylene glycol (PEG8000). Jurkat cells were incubated with lentiviruses for 48h and transduced cells were isolated by puromycin selection (1µg/ml Alexis; for CRISPR/Cas9 transduced cells) or by GFP$^+$ cell sorting (for transduced cells with reconstitution constructs).

*Primary T and B cell isolation from human blood samples*
Peripheral blood mononuclear cells were isolated by density centrifugation of blood samples from healthy, informed and consenting donors obtained from the Interregional Blood Transfusion SRC Ltd. CD4$^+$ T cells and CD19$^+$ B cells were obtained using CD4 or CD19 MicroBeads from Miltenyi, respectively. Primary B and T cells were resuspended in RPMI1640 with 10% FCS in a ratio of approximately 5-10x10$^6$ cells per 1ml and incubated at 37°C for 30 minutes before cell treatment and stimulation.

*Splenocyte isolation from mice*
Splenocytes of 9 weeks old knock-in mice expressing a catalytically inactive C472A mutant of MALT1 as described previously[97] and a heterozygous littermate were isolated by mechanical tissue separation and incubation of the cells with ACK lysing buffer to eradicate the red blood cells. Washed splenocytes were resuspended in RPMI1640 with 10% FCS in a ratio of approximately 2x10$^7$ cells per 1ml and incubated at 37°C for 30 minutes before cell stimulation.

*Cell treatment and stimulation*
For immunoblot analysis, Jurkat T cells and primary human B and T cells at 5-10x10$^6$ cells per 1ml and splenocytes from mice at 2x10$^7$ cells per 1ml were either left untreated or pre-treated with z-LVSR-fmk (2µM; Bachem), MG132 (10µM; Cabliochem) or Thioridazine (10µM; Sigma Aldrich) for one hour. Subsequent stimulation of the cells were performed by using PMA (80ng/ml; Alexis) and ionomycin (1µM; Cabliochem) or a combination of anti-human CD3 (10µg/ml; OKT3; BioLegend) and anti-human CD28 (10µg/ml; CD28.2; BioLegend), followed by the addition of crosslinking goat anti-mouse (13µg/ml; Jackson ImmunoResearch) for two hours or as indicated. The ABC DLBCL-derived cell lines HBL-1, OCI-Ly3 and TMD8 were treated with z-LVSR-fmk (2µM; Bachem) for 24 hours before cell lysis and immunoblot analysis. For the analysis of IL-2 secretion, Jurkat T cells at 2.5x10$^5$ cells per 1ml were stimulated with PMA (20ng/ml; Alexis) and ionomycin (1µM; Cabliochem) for 16 hours.

*Cell lysis and immunoblot analysis*

Cells were lysed in lysis buffer (50mM HEPES pH 7.4, 150mM NaCl and 1% Triton-X100) supplemented with protease inhibitors (Complete; Roche) and phosphatase inhibitors (50mM NaF, 10mM $Na_4P_2O_7$ and 10mM $NaVO_4$) for 10 minutes on ice. After centrifugation for 10 minutes by 13,000 rpm, protein concentration was determined by Bradford and cell lysate was mixed with reducing sodium dodecyl sulfate (SDS) sample buffer and denatured for 10 minutes at 95°C. Cell extracts were resolved by SDS-polyacrylamide gel electrophoresis (PAGE) and proteins were transferred to a nitrocellulose membrane and analyzed with the antibodies mentioned above.

*IL-2 ELISA*

The IL-2 concentration in the supernatants of stimulated Jurkat cells as described above was evaluated using BD OptEIA Human IL-2 ELISA set from BD Biosciences according to manufacturer's instructions.

*Statistical analysis*

Parametric two-tailed Student's t test were used for statistical analysis and P values $\leq$ 0.05 were considered as statistically significant.

## 6.2 Results

### 6.2.1 A20 is cleaved by MALT1 at several sites upon lymphocyte activation

One of the first substrates of MALT1 that has been identified is the NF-κB negative regulator A20.[105] However, the role of MALT1-dependent A20 cleavage in lymphocytes remains poorly characterized. Furthermore, several publications showed that A20 is cleaved by MALT1 on additional sites.[101,209,226] To check whether A20 is effectively cleaved by MALT1 more than once, the Jurkat T lymphocyte cell line was stimulated for two hours by CD3/CD28-crosslinking, to mimic a TCR and a co-stimulatory signal, or by a combination of phorbol myristate acetate (PMA) and the calcium ionophore ionomycin, which activate PKCs and promote calcium release from the ER, respectively (**Fig. 10A, B**). Both stimulation strategies were previously established to activate MALT1 protease function.[94] Efficient stimulation of the cells was assessed by monitoring phosphorylation of IκBα and MALT1 protease activity was evaluated by cleavage of the MALT1 substrate CYLD, which results in an N-terminal cleavage fragment of approximately 40 kDa.[117] By using a specific antibody for the amino terminus of A20, the presence of A20 cleavage fragments in the stimulated cells was revealed by immunoblot. Stimulation of Jurkat cells by CD3/CD28 crosslinking resulted in several N-terminal A20 cleavage fragments of an approximate molecular weight of 42, 48, 60 and 70 kDa (**Fig. 10A**), which were even more pronounced upon stimulation with PMA/ionomycin (**Fig. 10B**). To investigate whether the stimulation-induced A20 cleavage fragments are MALT1 protease-dependent, the cells were treated with the MALT1 protease inhibitor z-LVSR-fmk for one hour before stimulation (**Fig. 10A, B**). Pre-treatment with the MALT1 inhibitor abolished the appearance of A20 cleavage fragments similarly as for CYLD, indicating that the cleavage fragments are indeed dependent on MALT1 protease activity. Furthermore, we assessed the stability of A20 fragments by pre-treatment of the cells with the proteasome inhibitor MG132 (**Fig. 10B**). MG132 efficiently blocked the proteasomal degradation of phosphorylated IκBα as expected, but had no effect on A20 cleavage fragments. Thus, MALT1 protease-dependent A20 cleavage leads to the generation of stable N-terminal A20 fragments.
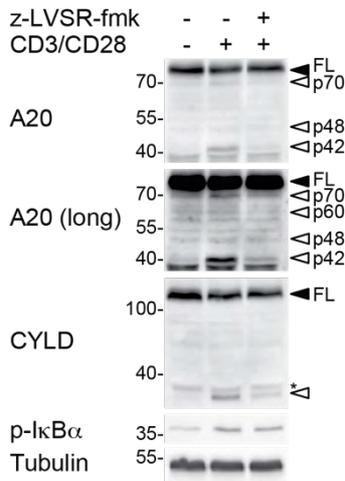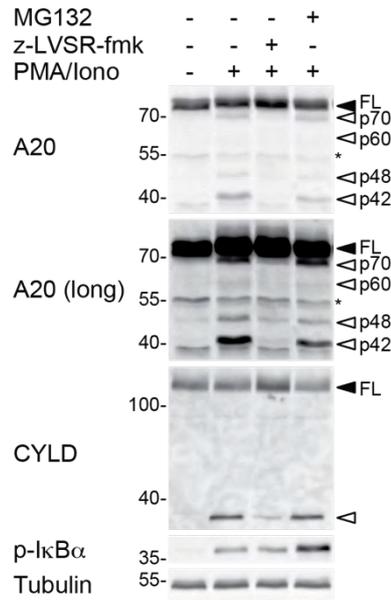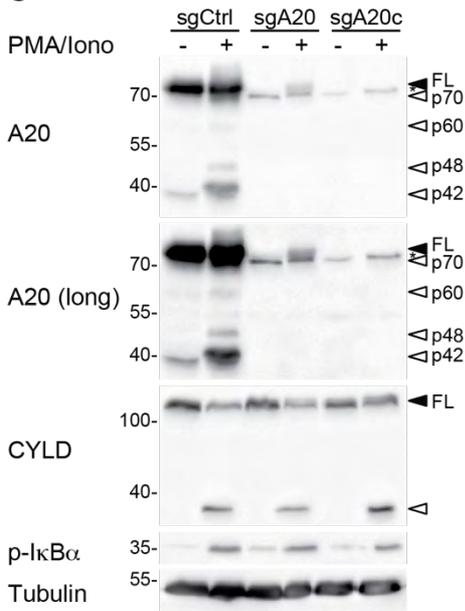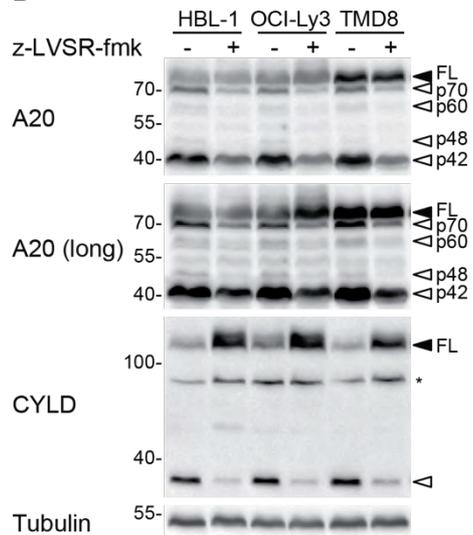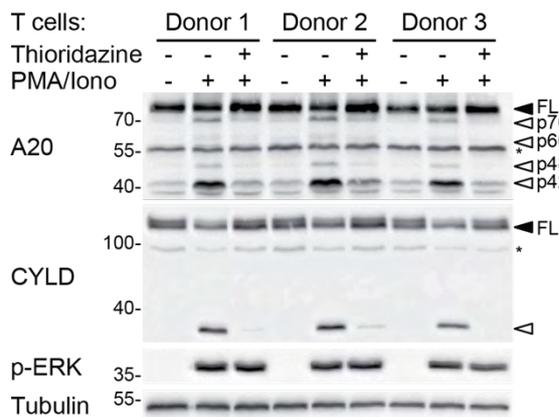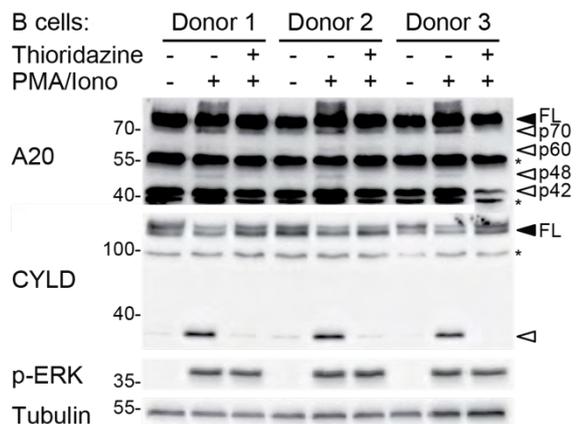
**Figure 10: A20 is cleaved by MALT1 at several sites upon lymphocyte activation.** Assessment of A20 cleavage in (A, B) Jurkat T cells pre-treated for one hour with z-LVSR-fmk and/or MG132, as indicated, and stimulated with anti-CD3, anti-CD28 and a crosslinking antibody (A) or PMA/ionomycin (B) for two hours, (C) Jurkat T cell populations that were infected with a control sgRNA (sgCtrl) or an sgRNA targeting A20 (sgA20), and a single cell clone of this population (sgA20c) were stimulated with PMA/ionomycin for two hours, (D) three ABC DLBCL-derived cell lines that were incubated with z-LVSR-fmk for 24 hours, (E, F) Primary human T (E) and B cells (F) from three healthy donors, pre-treated for one hour with Thioridazine and stimulated with PMA/ionomycin for two hours.
Unstimulated control samples were incubated with the appropriate amount of solvent (DMSO) alone. Cells were analyzed by immunoblot as indicated. Filled arrowheads indicate positions of full length (FL) A20 and CYLD and empty arrowheads mark cleavage fragments. Positions of molecular weight markers (in kDa) are indicated. Tubulin serves a loading control. *, unspecific band. Data are representative of two (A, C, E, F) and three (B, D) independent experiments.

To confirm that the A20 bands that appear upon cell stimulation are indeed fragments of A20, we silenced A20 by CRISPR/Cas9 in Jurkat cells and assessed band appearance using the same A20 antibody as before (**Fig. 10C**). Cells that were infected with a non-targeting control single-guide RNA (sgCtrl) showed the same pattern of A20 bands as before in non-infected Jurkat cells (**Fig. 10B**). However, a sgRNA targeting the A20 gene (sgA20) silenced the expression of full length (FL) A20 and abolished the appearance of the faster migrating fragments upon stimulation, both in the sgA20-transduced cell population and the A20-KO single cell clone (sgA20c) derived from this population (**Fig. 10C**). This confirms that the stimulation-induced fragments are indeed N-terminal fragments of A20.

MALT1 protease function is also activated in B lymphocytes upon a BCR signal[94] and in malignant B cells derived from patients with ABC DLBCL that are characterized by constitutive BCR signaling and exhibit MALT1 protease activity at steady-state.[209] Thus, we further investigated A20 cleavage in B cell lines, which were derived from ABC DLBCL patients (**Fig. 10D**). As expected, A20 was constitutively cleaved in these cell lines, resulting in cleavage fragments of the same molecular weight as seen in the stimulated Jurkat T cells (**Fig. 10B**). Treatment of these cells with z-LVSR-fmk for 24 hours depleted A20 cleavage fragments (**Fig. 10D**). Hence, MALT1-dependent A20 cleavage occurs in T and in B lymphocytes in response to antigen receptor signaling.

To assess MALT1-dependent A20 cleavage in primary human T and B lymphocytes, CD4+ T cells and CD79+ B cells were isolated from blood samples of three healthy volunteers (**Fig. 10E, F**). After isolation, cells were left untreated or stimulated with PMA/ionomycin for two hours and stimulation efficiency was determined by phosphorylation of ERK. Stimulated primary T cells of all donors displayed all N-terminal A20 cleavage fragments (p42, p48, p60 and p70). Similar results were obtained in stimulated primary B cells, but unfortunately, the presence of the p42 cleavage band could not be reliably detected in primary B cells due to comigration with a potential nonspecific band of the same molecular weight (**Fig. 10F**). Pre-treatment

of the cells with the small molecule MALT1 inhibitor, Thioridazine, also abolished CYLD and A20 cleavage in primary T and B cells (**Fig. 10E, F**). To conclude, lymphocyte activation induces the MALT1-dependent cleavage of A20 at a total of four sites, leading to the generation of stable N-terminal cleavage fragments of putative physiological relevance.

## 6.2.2 Human A20 is cleaved by MALT1 at R439, R479, R596 and R706

To determine the exact sites of A20 cleavage, we set up a MALT1-dependent A20 cleavage system in HEK293T cells. Transient transfection of HEK293T cells with MALT1 together with an oncogenic, constitutively active mutant of CARMA1(L244P)[166] has been shown to induce the cleavage of co-expressed, N-terminally VSV-tagged A20 (**Fig. 11A**). The N-terminal cleavage fragments detected either by the A20 antibody or by a VSV-specific antibody had the same molecular weight as in stimulated lymphocytes (**Fig. 10**), indicating that in this HEK293T system overexpressed VSV-A20 is cleaved at the same sites as endogenous A20. Furthermore, overexpression of the catalytically inactive MALT1(C464A) mutant abolished A20 cleavage, confirming the dependence on MALT1 proteolytic activity (**Fig. 11A**). To identify which cleavage fragment corresponds to the already known MALT1-dependent A20 cleavage site at R439[105], R439 was mutated to alanine to prevent A20 cleavage at this specific site. Overexpression of MALT1 WT and CARMA1(L244P) with VSV-A20(R439A) still resulted in the p48, p60 and p70 fragment, however the p42 fragment was not detectable anymore, indicating that the previously described N-terminal A20p50 fragment (comprising 1-439aa) corresponds to the p42 fragment in our system (**Fig. 11A, B**).

In view of the molecular weight of the remaining A20 cleavage fragments, it seems obvious that the other three cleavage sites are situated downstream of the known R439 cleavage site. Therefore, we individually mutated different arginine residues (R479, R562, R572, R581, R596, R706 and R713) within the C-terminal half of VSV-A20 to alanine and evaluated the cleavage of these mutants in HEK293T cells (**Fig. 11B, C, D**). Mutation of R479 to alanine eliminated the p48 cleavage fragment and double mutation of R439 and R479 to alanine eradicated both, the p42 and p48 fragments (**Fig. 11B and Fig. 12A**). Similarly, substitution of R596 and R706 to alanine abolished the p60 and p70 cleavage fragment, respectively (**Fig. 11C, D and Fig. 12A**). Mutation of R562, R572, R581 and R713 had no effect on the A20 cleavage fragment pattern (**Fig. 11C, D**). Taken together, MALT1 cleaves A20 at R439, R479, R596 and R706, resulting in the N-terminal cleavage fragments p42 (previously published as p50[105]), p48, p60 and p70, respectively (**Fig. 11E**).
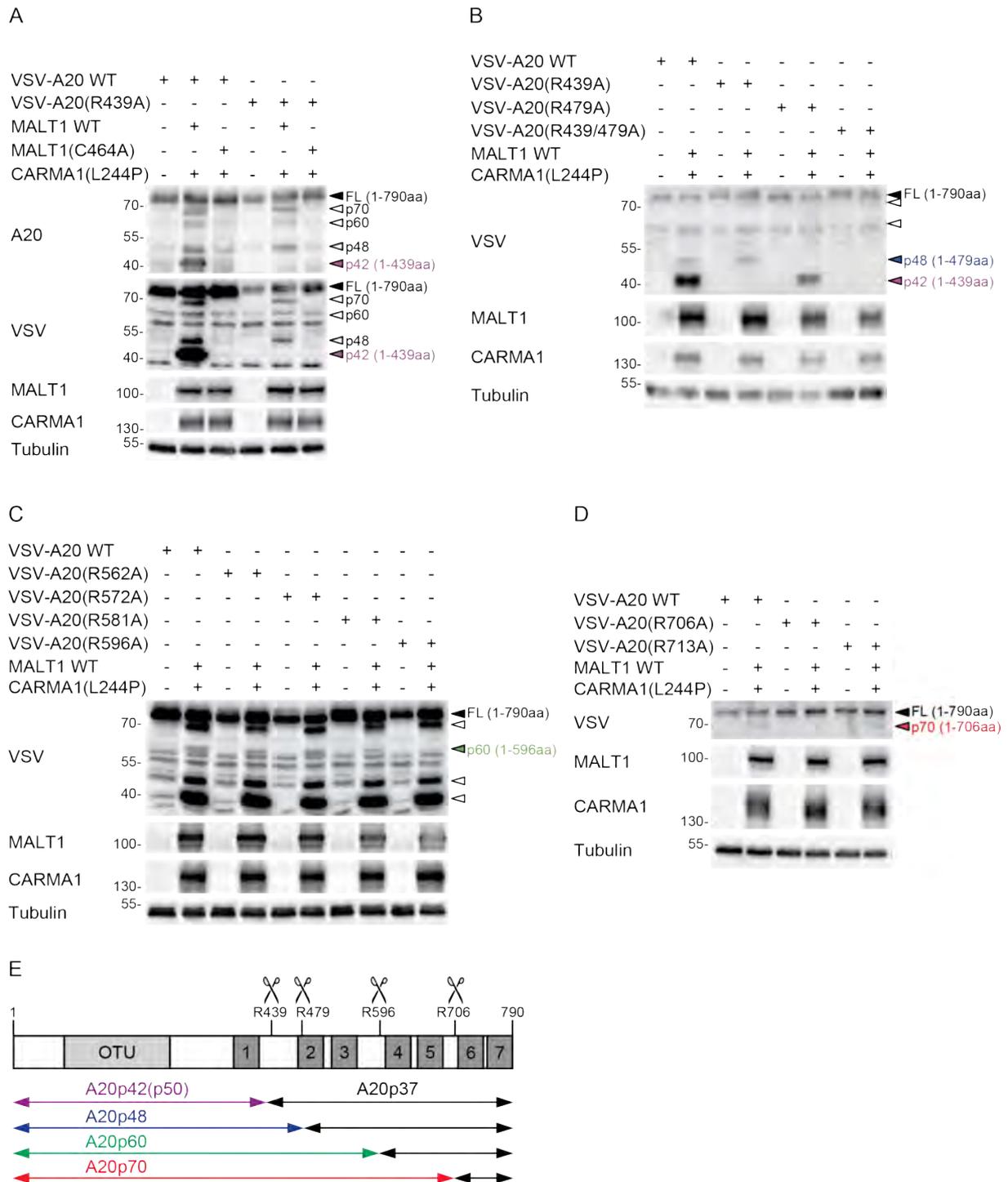
**Figure 11: Human A20 is cleaved by MALT1 at R439, R479, R596 and R706.** (A-D) HEK293T cells transiently transfected with the indicated constructs of A20, MALT1 and CARMA1 were analyzed by immunoblot as indicated. Filled arrowheads indicate the positions full length (FL) VSV-A20 and empty arrowheads mark cleavage fragments. Identified cleavage fragments are indicated with purple (p42), blue (p48), green (p60) and red (p70) arrowheads. Positions of molecular weight markers (in kDa) are indicated. Tubulin serves as a loading control. Data are representative of two independent experiments. (E) Illustration of A20 with the indicated MALT1-dependent cleavage sites and the resulting cleavage fragments.

Furthermore, since mutation of one cleavage site had no effect on the abundance of the other A20 fragments (**Fig. 12A**), none of the cleavage sites seem to be prerequisite for the cleavage at another site. Moreover, substitution of all four

arginines to alanine (R439A, R479A, R596A, R706A) led to a non-cleavable A20 mutant (VSV-A20 NC), which confirms that there are no additional MALT1-dependent cleavage sites in A20 (**Fig. 12B**).
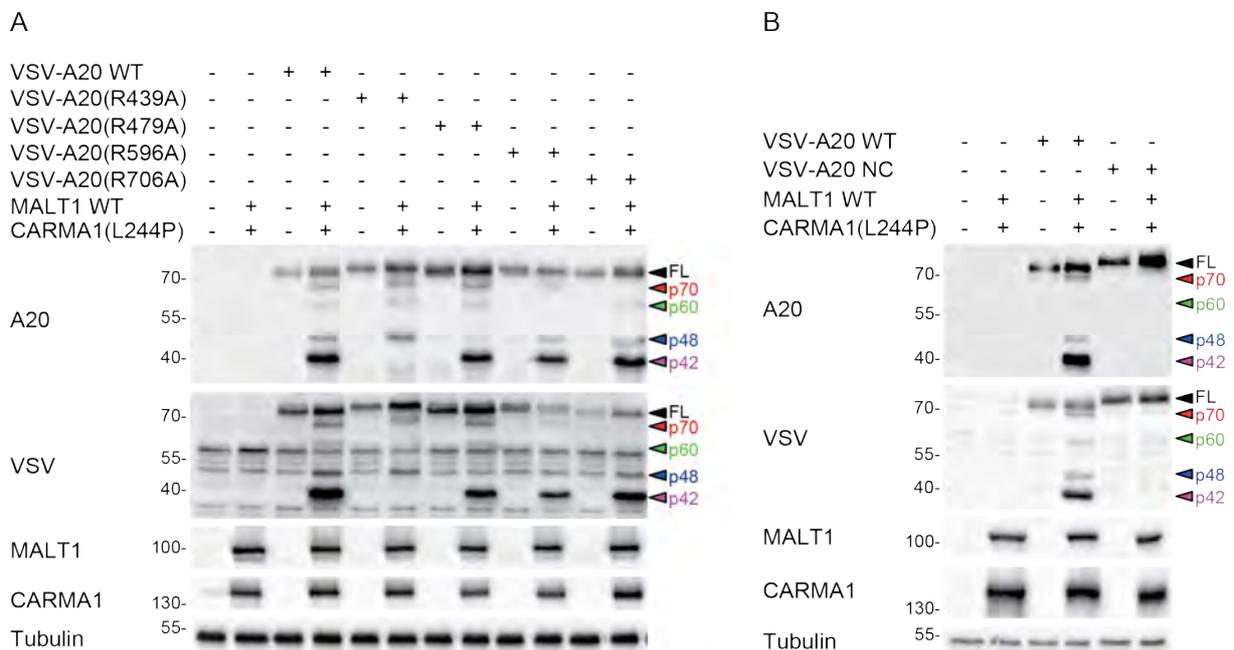


**Figure 12: A20(R439A, R479A, R596A and R706A) is not cleaved any longer.** (A, B) HEK293T cells transiently transfected with the indicated constructs of A20, MALT1 and CARMA1 were analyzed by immunoblot as indicated. (B) VSV-A20 NC = VSV-A20(R439A, R479A, R596A, R706A).
Filled arrowheads indicate the position of full length (FL) VSV-A20 and identified cleavage fragments are indicated with purple (p42), blue (p48), green (p60) and red (p70) arrowheads. Positions of molecular weight markers (in kDa) are indicated. Tubulin serves a loading control. Data are representative of three independent experiments.

## 6.2.3 A20 cleavage fragments are unable to regulate IL-2 cytokine production

To gain further insights into the function of MALT1-dependent A20 cleavage in lymphocytes, the A20-KO Jurkat cells described above (**Fig. 10C**) were reconstituted with either a mock vector, A20 WT, A20(R439A) or non-cleavable A20 (**Fig. 13A**). Stimulation of these cells with PMA/ionomycin led to the cleavage of the reconstituted A20 WT and A20(R439A) as expected and, similar to the results obtained in HEK293T cells, Jurkat cells that were reconstituted with non-cleavable A20 showed no residual cleavage upon cell stimulation (**Fig. 13A**). The stimulation efficiency was assessed by phosphorylation of ERK, which was comparable between the cell lines. As expected, phosphorylation of IκBα was strongly impaired upon reconstitution of the A20-KO Jurkat cells with A20 constructs. However, considering the differences in expression levels, no major difference in IκBα phosphorylation was detectable in cells expressing wild-type A20 or non-cleavable A20. This indicates that MALT1-dependent cleavage of A20 in lymphocytes has no effect on the initial, IKK-dependent NF-κB activation.
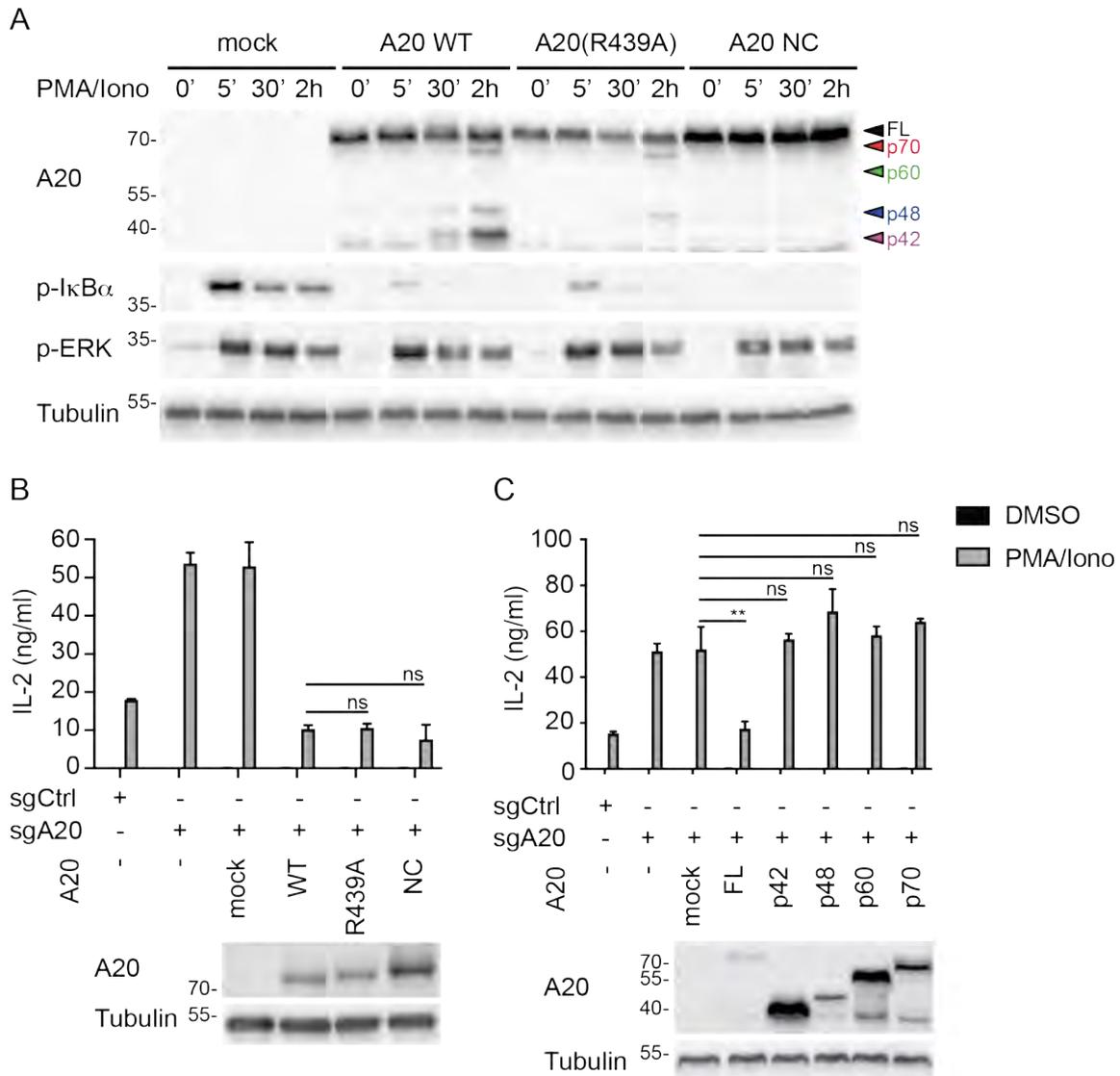
**Figure 13: A20 cleavage fragments are unable to regulate IL-2 cytokine production.** (A) A20-KO Jurkat cells reconstituted with mock or the designated A20 constructs were stimulated with PMA/ionomycin for 0, 5, 30 min or 2 h and analyzed by immunoblot as indicated. (B, C) IL-2 secretion by Jurkat cells infected with either sgCtrl or sgA20 and indicated A20 expression vectors followed by DMSO or PMA/ionomycin treatment for 16 hours. Expression levels of A20 constructs were evaluated by immunoblot. Bars represent means ±SD; ns, nonsignificant, **p<0,01.
Filled arrowheads indicate the position of full length (FL) VSV-A20 and identified cleavage fragments are indicated with purple (p42), blue (p48), green (p60) and red (p70) arrowheads. Positions of molecular weight markers (in kDa) are indicated. Tubulin serves a loading control. Data are representative of two (A) and three (B, C) independent experiments.

Nevertheless, two groups already showed that A20 dampens NF-κB activity and IL-2 cytokine production of stimulated T lymphocytes.[101,105] Furthermore, Coornaert *et al.* demonstrated that the N- and C-terminal A20 cleavage fragments created upon cleavage at R439 were not or less capable to decrease NF-κB activity in an NF-κB promoter luciferase assay. This suggests that MALT1-dependent A20 cleavage impairs its NF-κB regulatory function and might promote NF-κB target gene expression in an IKK-independent manner. To investigate this hypothesis and to determine the NF-κB regulatory function of the other N-terminal cleavage fragments, we measured IL-2

production of stimulated Jurkat cells expressing A20 WT or A20 NC or the different N-terminal cleavage fragments by ELISA (**Fig. 13B, C**). As expected, Jurkat cells that were silenced for A20 by CRISPR/Cas9 with an A20-specific sgRNA produced drastically more IL-2 compared to control cells. Reconstitution with an A20 WT construct rescued this phenotype, whereas a mock vector had no effect on IL-2 production. Interestingly, neither A20(R439A) nor the non-cleavable A20 mutant were more efficient to control IL-2 production compared to A20 WT, indicating that MALT1-dependent A20 cleavage has no impact on IL-2 production (**Fig. 13B**). Nevertheless, reconstitution of the A20-KO cells with the N-terminal cleavage fragments had no impact on the amount of IL-2 produced, although they were more strongly expressed than full length A20, indicating that the cleavage fragments by themselves are indeed not able to control IL-2 production (**Fig. 13C**). Taken together, our data suggest that MALT1-dependent cleavage of A20 results in N-terminal cleavage fragments that are no longer able to control NF-κB target gene expression, but A20 cleavage has no impact on IL-2 production *per se*, which might be due to the fact that only a small proportion of total A20 is cleaved by MALT1 upon lymphocyte stimulation and the remaining full length A20 is sufficient to control NF-κB activity and IL-2 production.
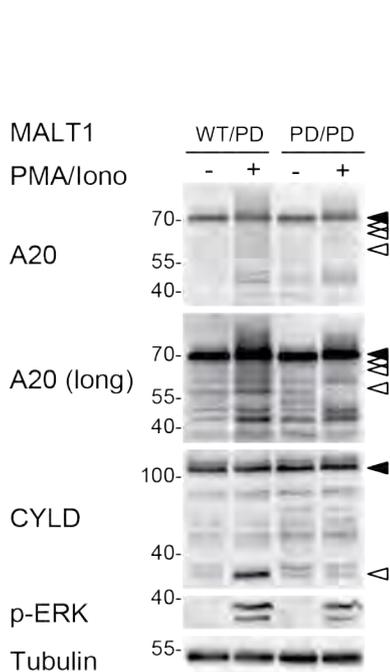
## 6.2.4 Murine A20 is cleaved by MALT1 at conserved cleavage sites

The physiological relevance of MALT1-dependent A20 processing could not be studied so far, because the known cleavage site of A20 is not conserved in mice.[105] However, Coornaert *et al.* could show that murine A20 is cleaved by murine MALT1 upon overexpression in HEK293T cells. Amino acid sequence alignment of A20 from different species identified that the first cleavage site is indeed not conserved in the mouse or even other species (**Fig. 14A**), however, the here newly identified cleavage sites are highly conserved (2nd site) or at least more conserved (3rd and 4th sites) than the first cleavage site in mammals. Thus, we further investigated whether murine A20 is cleaved by MALT1 and whether the here identified human cleavage sites are also used in mice.

A

| Species | 1. Site | 2. Site | 3. Site | 4. Site |
|---------|---------|---------|---------|---------|
| *human* | ALGAS$R_{439}$GEAY | TAMKC$R_{479}$SPGC | LSQAA$R_{596}$TPGD | RRDVP$R_{706}$TTQS |
| *mouse* | GLG--- ---- | TAMKC$R_{471}$SPGC | LSQAA$R_{581}$TPGD | HRDMP$R_{691}$TTQV |
| *rat* | GLG--- ---- | TAMKC$R_{509}$SPGC | LSQTS$R_{620}$TPAD | RREMP$R_{730}$TTQG |
| *rabbit* | ALGAP$R_{435}$GEAC | TAMKC$R_{476}$SPGC | LPPAA$R_{593}$TPVD | RRDVP$R_{703}$TTQS |
| *chicken* | GSGSSC$_{439}$GKAC | TAMKC$R_{479}$TPDC | LAHAP$R_{596}$ALEE | RRDLQ$R_{723}$AALT |
| *zebrafish* | NQT--- ---- | HAMKC$K_{462}$TPGC | ----SG$_{537}$QTWQ | ARPP-- -PPV |

B



C
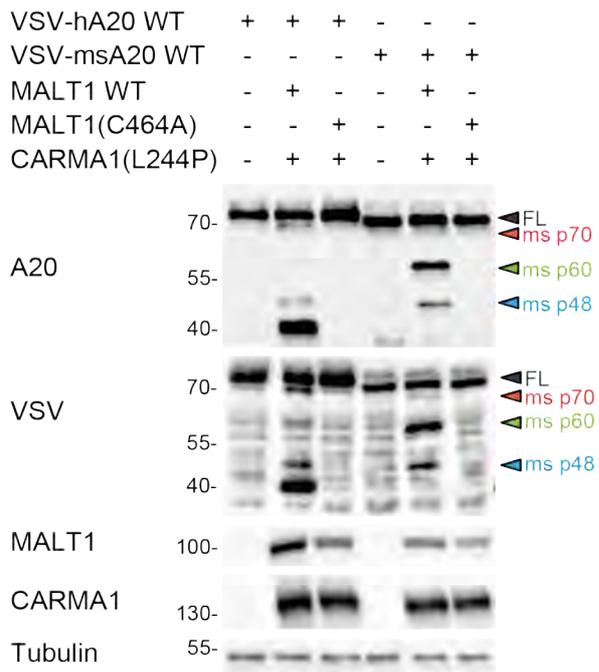


D
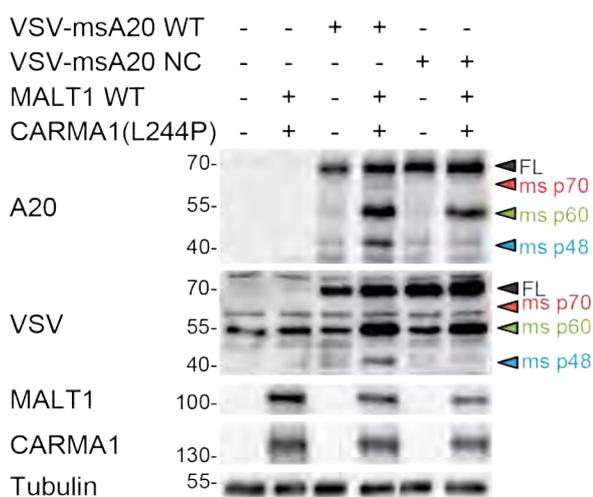
**Figure 14: Murine A20 is cleaved by MALT1 at conserved cleavage sites.** (A) Table showing the conservation of the four identified MALT1-dependent cleavage sites of A20 from different species using Clustal Omega-Multiple sequence alignment tool. The P1 arginine is indicated by a bold letter and with the corresponding amino acid number. (B) Isolated splenocytes from a heterozygous (WT/PD) and homozygous (PD/PD) MALT1-PD mouse were stimulated with PMA/ionomycin for two hours and analyzed by immunoblot as indicated. Unstimulated samples were incubated with the appropriate amount of solvent (DMSO) alone. Filled arrowheads indicate full length (FL) A20 and CYLD and empty arrowheads mark positions of cleavage fragments. (C, D) HEK293T cells transiently transfected with constructs of human or murine A20, human MALT1 and human CARMA1 and analyzed by immunoblot as indicated. Filled arrowheads indicate full length (FL) VSV-A20 and identified cleavage fragments are indicated with purple (p42), blue (p48), green (p60) and red (p70) arrowheads. (D) VSV-msA20 NC = VSV-msA20(R471A, R581A and R691A).
Positions of molecular weight markers (in kDa) are indicated. Tubulin serves a loading control. Data are representative of three (B-D) independent experiments.

In order to confirm that murine A20 is cleaved in a MALT1-dependent manner, splenocytes, isolated from previously described MALT1 protease-deficient (PD/PD) mice [97] expressing a catalytically inactive murine MALT1(C472A), or from a heterozygous (WT/PD) littermate, were stimulated with PMA/ionomycin (**Fig. 14B**). Jaworski *et al.* have shown that one WT allele of MALT1 is sufficient for proper substrate cleavage. The loss of MALT1 protease activity in these mice was confirmed by the absence of cleaved CYLD and appropriate splenocyte stimulation was monitored by ERK phosphorylation. Furthermore, we assessed A20 cleavage with the previously used anti-human A20 antibody, which cross-reacts with murine A20. Indeed, a strong band of the expected molecular weight of full length murine A20 was detectable in splenocytes of both mice. Unfortunately, the antibody showed strong background staining of the murine splenocyte lysates. Nevertheless, three potential A20 cleavage fragments could be identified in heterozygous mice that were not present in MALT1-PD mice (**Fig. 14B**). The molecular weights of these fragments were all between 60 and 70 kDa.

To gain further insights into MALT1-dependent murine A20 cleavage, N-terminally VSV-tagged murine A20 was overexpressed in HEK293T cells together with human MALT1 and CARMA1(L244P) (**Fig. 14C**) and the A20 cleavage fragment pattern was assessed by immunoblot. Convincingly, murine A20 was cleaved in a MALT1 protease-dependent manner and the resulting three cleavage fragments had similar molecular weights as the human A20 p48, p60 and p70 fragments. This suggests that human MALT1 is cleaving murine A20 at the same three sites that we identified and described above, but not at the site corresponding to the human p42 fragment (**Fig. 14C**). To determine whether the conserved, new A20 cleavage sites are indeed responsible for murine A20 cleavage, we mutated all analogous arginine residues (R471, R581 and R691) in the murine A20 to alanine (VSV-msA20 NC) and assessed its cleavage in HEK293Ts (**Fig. 14D**). Interestingly, mutation of all three arginines eliminated generation of the p48- and the p70-related fragments but not of the p60-

related fragment. Thus, MALT1 most likely cleaves murine A20 at a site distinct from but close to R581, or another protease is involved in the cleavage of murine A20.

## 6.3  Discussion

In this second project we showed that upon an antigen receptor signal, A20 gets cleaved more than once in a MALT1-dependent manner in B and T lymphocytes. This results in stable N-terminal cleavage fragments of a molecular weight of 42, 48, 60 and 70 kDa. The cleavage sites were mapped to R439, confirming the former findings of Coornaert *et al.*[105], and the newly identified sites R479, R596 and R706 (**Fig. 15**). Cleavage at R439, previously described to generate an N-terminal fragment of 50 kDa, resulted in a p42 fragment in our hands. Cleavage after R479, R596 and R706 led to formation of p48, p60 and p70 fragments, respectively. Furthermore, we demonstrated that the created N-terminal cleavage fragments are unable to control IL-2 production of stimulated A20-silenced Jurkat cells. Finally, we verified cleavage of murine A20 in primary mouse splenocytes. Our results suggest that murine A20 can be cleaved at sites corresponding to those identified in human A20, but it remains to be confirmed *in vivo*.
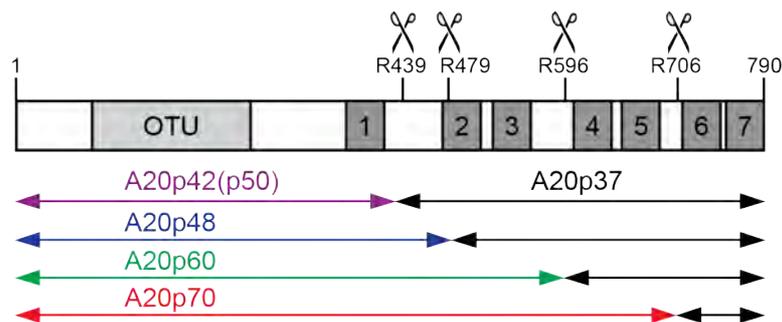


**Figure 15: MALT1-dependent cleavage of human A20.** Human A20 is cleaved by MALT1 after R439, R479, R596 and R706, resulting in N-terminal cleavage fragments and at least to one C-terminal cleavage fragment as indicated.

## 6.3.1 MALT1 substrate specificity

Through the identification of novel MALT1 cleavage sites within A20, we also expanded our knowledge about MALT1 substrate specificity. Based on the crystallographic structure of MALT1 and peptide library screens, the consensus cleavage site sequence of MALT1 substrates is supposed to be $\phi$-X-P/S-R'-G, which matches the majority of known substrates.[92,208]  However, the already published cleavage site in A20, $GASR_{439}G$[105], and also the here identified novel cleavage sites, $MKCR_{479}S$, $QAAR_{596}T$ and $DVPR_{706}T$ are rather distinctive from the previously established consensus sequence.

At P1' a small, uncharged amino acid is preferred, which is the case for all four cleavage sites in A20 (**Table 2**). At P2 proline or serine seems to be the favored amino

acid, however also alanine was shown to be tolerated, which is given in three of the four cleavage sites in A20.[92,208]  The tolerance of a cysteine residue at P2 was never tested by tetrapeptide screens, however due to the presence of a cysteine at P2 in the second cleavage site within A20 and the first MALT1 auto-processing site (LCCR$_{149}$A)[103], also cysteine at P2 seems to be accepted. MALT1 exhibits the greatest tolerance in the P3 position, nevertheless the preferred amino acid in P3 is valine, followed by other non-polar hydrophobic amino acids, but also polar charged residues are well tolerated.[208]

| A20 | 1. Site | 2. Site | 3. Site | 4. Site |
|---|---|---|---|---|
| | LGASR$_{439}$G | AMKCR$_{479}$S | SQAAR$_{596}$T | RDVPR$_{706}$T |

**Table 2:** Four MALT1-dependent cleavage sites in human A20.

From the crystallographic structure and peptide library screens, MALT1 seems to have a clear preference for hydrophobic residues in P4. So far, only the second MALT1 auto-processing site (HCSR$_{781}$T)[104], and the special substrate of the oncogenic IAP2-MALT1 fusion protein, NIK (CLSR$_{325}$G), have been reported to have no hydrophobic residue at P4. Our data confirm that non-hydrophobic residues at P4 are indeed well tolerated since the first and the third cleavage site of A20 have a polar amino acid at P4 (G and Q) and the fourth site even has a negatively charged aspartate residue at P4 (**Table 2**). Staal *et al.* and Hachmann *et al.* suggested that the P5 leucine of the first cleavage site in A20 rescues the missing hydrophobic amino acid in P4.[208,231]  For the third and the fourth cleavage site of A20, the P5 amino acid is not hydrophobic, however both the amino acids in P3 and P2 are hydrophobic (**Table 2**). This suggests that a non-hydrophobic amino acid in P4 can be tolerated, if the surrounding amino acids (P5, P3 and possibly P2) are hydrophobic. Although this hypothesis remains to be confirmed, the identification of novel MALT1 cleavage sites in A20 demonstrates that the MALT1 active site is less selective than initially thought (**Fig. 16**).

Accordingly, it would be interesting to investigate whether we can manipulate the efficiency of substrate cleavage by individual point mutations of the cleavage site sequence. Like this, we may be able to convert a poor MALT1 substrate, like A20, into a strong substrate that is efficiently cleaved as soon as MALT1 is activated, which in turn could be of benefit to identify the role of individual substrate cleavage events. Additionally, this could assist in determining whether MALT1 substrate specificity is defined by the cleavage site sequence alone or whether an exosite within the substrates plays a role, as proposed by two different groups.[208,231]

**Figure 16: MALT1 consensus site sequence.** Sequence logo plot representing amino acid frequencies for P4-P1' amino acids from the cleavage site of all known MALT1 substrates. Basic amino acids are shown in blue, acidic amino acids in red, hydrophobic amino acids in black and polar amino acids in green. This figure was generated using WebLogo.

## 6.3.2 The role of MALT1-dependent A20 cleavage in T lymphocytes

To understand the role of MALT1-dependent A20 cleavage in T lymphocytes, the function of A20 in these cells needs to be determined. A20 is a well characterized negative regulator of NF-κB activity in different cells induced by diverse receptor signals. Additionally, a role of A20 in the determination of cell survival or cell death has been described for many cell types.[135] In T lymphocytes, A20 has been proposed to play roles in both, the regulation of NF-κB activity and cell death. Consequently, the MALT1-dependent cleavage of A20 could affect the two of them.

*The relevance of A20 cleavage in NF-κB activity*

Coornaert *et al.* demonstrated that MALT1-dependent A20 cleavage after R439 results in an N-terminal and a C-terminal cleavage fragment that completely or partially lost their NF-κB regulatory function. Furthermore, they showed that the partially active C-terminal fragment is rapidly degraded by the proteasome.[105] Our results confirmed that at all stable N-terminal cleavage fragments lost NF-κB regulatory function (**Fig. 13C**). Additionally, we have evidence that the two C-terminal cleavage fragments, resulting from cleavage at R439 and R479, but not the very small C-terminal fragments (cleavage at R596 and R706) partially retain some NF-κB regulatory functions (data not shown). However, if these C-terminal cleavage fragments remain stable in the cells and thereby still act on NF-κB activity could not be determined because of a lack of antibodies that specifically recognize the C-terminus of A20. In conclusion, our data together with previous findings suggest that MALT1-dependent cleavage of A20 impairs its NF-κB regulatory function.

In T lymphocytes, A20 was found to negatively regulate NF-κB by impairing K63-linked ubiquitination of MALT1. Although, the authors could not examine whether A20 directly cleaves the K63-linked ubiquitin chains from MALT1, they showed that the reduction of MALT1 polyubiquitination is dependent on the DUB catalytic activity.[101]

A20 thereby impairs the recruitment and activation of the IKK complex and negatively affects IκBα phosphorylation and degradation, NF-κB nuclear translocation and target gene expression like IL-2.[101] Consequently, cleavage of A20 by MALT1 was thought to promote TCR signal transduction to NF-κB activation.[105] However, the proteolytic activity of MALT1 was shown to be dispensable for TCR signal transduction to NF-κB activation.[94,97,101] Accordingly, A20 cleavage has no effect on MALT1 polyubiquitination and subsequent signal transduction to NF-κB nuclear translocation, nevertheless A20 cleavage might still affects T cell activation in another unknown manner.

Interestingly, although the proteolytic activity of MALT1 has no impact on initial NF-κB activation, it promotes NF-κB transcriptional activity and IL-2 production.[94,101] MALT1-dependent cleavage and inactivation of RelB as well as its auto-processing promotes NF-κB transcriptional activity and further, cleavage of CYLD, which promotes AP-1 activation, contributes to optimal IL-2 production.[103,104,107,117] Additionally, cleavage and subsequent degradation of the RNAse, Regnase-1, stabilizes immunoregulatory target transcripts, like IL-2 and strengthens T cell immune response.[109] Our findings and the one of Coornaert *et al.* that A20 cleavage fragments are unable to regulate NF-κB transcriptional activity and IL-2 production suggest that MALT1-dependent A20 cleavage might contribute to T cell activation.[105] However, according to the low abundance of A20 cleavage fragments, which might be due to the fact that none of the cleavage sites within A20 seems to be an optimal cleavage site to MALT1, the contribution of A20 cleavage to lymphocyte activation might be rather small. Indeed, reconstitution of A20-KO Jurkat cells with A20 WT or non-cleavable A20 showed no significant difference in dampening IL-2 production (**Fig. 13B**). Nevertheless, this result has to be taken with caution, because the expression levels of reconstituted A20 constructs were higher than endogenous A20, which might disguise minor effects between the different A20 constructs. Thus, the relevance of A20 cleavage in lymphocyte activation remains to be further explored.

Finally, our data indicate that the NF-κB regulatory function of A20 in lymphocytes relies on its very last two ZnF domains, since the A20p70 fragment, which lacks ZnF6 and ZnF7, was not able to dampen IL-2 production of A20-silenced Jurkat cells (**Fig. 13C**). This correlates with the results from Coornaert *et al.*, in which the N-terminal A20p50 (here A20p42) completely lost its NF-κB regulatory capability but the C-terminal A20p37 fragment retained some function. Taken together, these findings suggest that the C-terminal ZnFs, especially ZnF6 and ZnF7, rather than the N-terminal OTU domain with the deubiquitinating activity, are critical for A20s NF-κB

regulatory function in T cells. Thus, it would be interesting to compare the interactome of A20 full length with A20p70 in T cells, to further investigate A20's mechanism of T cell regulation and the role of MALT1-dependent A20 cleavage.

*The relevance of A20 cleavage in cell death*

In addition to its role in the regulation of NF-κB signaling, A20 was also identified as an inhibitor of cell death in T cells as well as in many other cell types. A20-deficient T lymphocytes are more susceptible to TCR stimulation-induced cell death.[153,154] Although in our hands, Jurkat T cells silenced for A20 were growing normally in culture, we cannot make any statement about cell survival upon T cell activation, since we stimulated cells for only a short time period (up to 16h) and effects on T cell survival were seen at the earliest 48h after cell stimulation.[153,154] However, we assume that long-term stimulation and activation of A20-deficient Jurkat cells may indeed result in decreased cell survival. Thus, it would be additionally of interest to investigate how MALT1-dependent A20 cleavage affects the cell death-regulating function of A20.

The study from Matsuzawa *et al.* confirmed that A20 promotes survival of CD4^{+} T cells by restricting mammalian target of rapamycin (mTOR) and thereby promoting autophagy.[155] Indeed, they demonstrated that A20 physically interacts with mTOR upon T cell stimulation and most probably dampens mTOR K63-linked polyubiquitination that was previously found to be an mTOR activating signal mediated by TRAF6.[155,232] Further, TRAF6 mediates the translocation of mTORC1 to lysosomes.[232] Interestingly, Li *et al.* showed that a fraction of endogenous A20 is localized to a lysosome-associated compartment.[233] Thus, lysosome-associated A20 might negatively regulate mTORC1 by impairing its ubiquitination and thereby promote autophagy and survival in T cells. Strikingly, A20 translocation to the lysosomal compartment was dependent on its C-terminal zinc fingers[233] and MALT1-dependent cleavage of A20 after R439 induced the cytosolic release of the N-terminal A20p42 (A20p50) fragment.[226] Hence, MALT1-dependent A20 cleavage may promote mTORC1 activity by dissecting the OTU domain from the ubiquitin-binding C-terminal zinc fingers. Intriguingly, MALT1 protease activity was found to be crucial for TCR-stimulated activation of mTORC1, however the responsible MALT1 substrate remained unknown.[234] Accordingly, it would be interesting to determine TCR stimulation-induced activation of mTORC1 in cells that express non-cleavable A20 or in cells overexpressing the C-terminal A20 cleavage fragment(s).

Furthermore, another group demonstrated that mTOR is a major player in determining T cell activation or T cell anergy. In this context, mTOR activity was indispensable for T cell activation, whereas inhibition of mTOR with rapamycin led to

T cell anergy upon T cell stimulation.[235]  Thus, the proteolytic function of MALT1, by cleaving A20 and activating mTOR, might prevent T cell anergy.

Overall, MALT1-dependent cleavage of A20 in T lymphocytes might be relevant for T cell activation via a still unknown mechanism but also could have broader meanings in regulating cell survival in an NF-κB-independent manner.

## 6.3.3 A20 cleavage in other cell types

Like MALT1, A20 is expressed in several different tissues. Consequently, MALT1-dependent A20 cleavage can occur in all kinds of cell types. Apart from T cells, A20 cleavage has been observed in B lymphocytes upon BCR triggering and in keratinocytes upon a Dectin-1 signal.[16,209]  However the consequence of A20 cleavage in these cells remains unclear.

*The role of A20 and its cleavage in B cells*

*In vivo* studies using B cell-specific A20-KO mice revealed the physiological role of A20 in B cells. First of all, A20 is required for normal differentiation and development of marginal zone and B1 B cells. Moreover, in mature B cells A20 restricts the response to stimuli downstream of different receptors like TLRs, BCR and CD40.[236-238]  Thereby the A20 expression is strongly induced by a CD40 signal.[236]  However, the molecular mechanism of the regulation of B cell activation by A20 is not known. Furthermore, A20 seems to sensitize activated B cells to Fas-mediated cell death, which is most probably due to a decrease in NF-κB-dependent expression of anti-apoptotic proteins, such as Bcl-x.[236]  Overall, mice with B cell-specific ablation of A20 develop an autoimmune phenotype upon aging, indicating an important function of A20 in B cell homeostasis.[236-238]

Here we showed that, similar as in primary T cells, A20 is cleaved in human primary B cells upon an antigen receptor signal (**Fig. 10F**). Convincingly, B cell lines derived from ABC DLBCL patients, which are characterized and dependent on constitutive NF-κB activity, exhibit A20 cleavage at steady-state (**Fig. 10D**), which was already shown previously.[209]  Interestingly, the survival of these cells relies strongly on constitutive MALT1 protease activity, thus the cleavage of A20 and potentially the cleavage of other MALT1 substrates promote B cell survival.[209]  Indeed, somatic loss-of-function mutations in A20 are frequently observed in DLBCL and other B cell lymphomas, such as MALT lymphoma, MCL, FL and Hodgkin's lymphoma, in which loss of A20 expression enhances NF-κB activity and cell proliferation, defining

A20 as a tumor suppressor.[167,239-242] Thus, B cell lymphomas have a survival and growth advantage by decreased A20 expression and/or increased A20 cleavage.

*The role of A20 and its cleavage in keratinocytes*

Several groups identified A20 gene polymorphisms associated with the inflammatory skin disorder psoriasis.[243-246] Interestingly, A20 expression, which is normally present in all layers of the epidermis, is strongly decreased in psoriatic skin lesions.[247,248] Psoriasis is characterized by epidermal hyperplasia and inflammation with altered keratinocyte differentiation and hyperproliferation.[189] Conclusively, this indicates an important function of A20 in keratinocyte homeostasis.

A20 deletion in keratinocytes of mice does not cause spontaneous psoriatic skin inflammations, however it was shown to sensitize keratinocytes to psoriasis-like inflammation in an experimentally induced psoriasis mouse model.[248,249] Thus, the absence of A20 alone cannot drive the development of psoriasis but it contributes to disease severity and/or develops as a consequence of chronic inflammation of the epidermis.

Remarkably, CARMA2 mutations have been recently found associated with the development of psoriatic skin diseases and gain-of-function mutations of CARMA2 were shown to constitutively drive CBM complex formation and NF-κB activity in keratinocytes.[190,250] Moreover, gain-of-function mutations of CARMA2 alone are sufficient to induce a psoriatic phenotype in mice.[250] Intriguingly, in a cell-based system, constitutively active CARMA2 mutants are able to activate MALT1 protease function in a similar way as oncogenic CARMA1 mutants.[15,250] Thus, MALT1 proteolytic activity and especially the cleavage of A20 might contribute to the development and severity of CARMA2-driven psoriasis.

Under physiological conditions the MALT1 protease activity in keratinocytes can be activated upon keratinocyte stimulation with the yeast cell wall glucan zymosan, which is detected by the surface receptor Dectin-1. Furthermore, MALT1 activation was dependent on the endogenous expression of wild-type CARMA2 and BCL10. Like zymosan, also gram-positive *Staphylococcus aureus* activates MALT1 protease function via another, yet unknown receptor.[16] Taken together, this indicates a crucial function of the CARMA2-CBM complex and MALT1 protease activity in the innate immunity of keratinocytes, in which A20 acts as a potent negative regulator.[247] However, the precise role of MALT1 protease activity and A20 cleavage in keratinocyte activation and psoriatic skin inflammation remains to be determined in future studies.

### 6.3.4 MALT1-dependent cleavage of murine A20

To study the role of MALT1-dependent A20 cleavage in T cells but also in other cells, it would be advantageous to generate mice expressing non-cleavable A20 and compare their phenotype with the one of MALT1-PD mice. However, whether A20 is cleaved by MALT1 in mice was never investigated. By stimulation of splenocytes from mice expressing wild-type MALT1 or MALT1-PD we revealed that murine A20 is cleaved in a MALT1-dependent manner (**Fig. 14B**). Unfortunately, the antibody used here, which was generated against human A20, yielded a lot of non-specific bands in immunoblots of lysates of mouse splenocytes. Thus, a specific antibody against murine A20 is needed to precisely visualize murine A20 cleavage fragments. Potentially, the isolation of T cells from the splenocyte population could also reduce the background staining of the existing antibody. Although the first cleavage site in A20 is not conserved in mice, Coornaert *et al.* demonstrated that murine A20 is indeed cleaved by MALT1 in a HEK293T overexpression system and, in view of the molecular weight of the N-terminal cleavage fragment, they claimed that the cleavage site is localized between the third and the fourth ZnF.[105] The here newly identified cleavage sites of human A20 are well conserved in the mouse and other species (**Fig. 14A**) and the counterpart of the human A20p60-generating residue R596, R581 in mouse A20, would match the size of the murine A20 cleavage fragment detected by Coornaert *et al.* In our hands, cleavage of murine A20 in HEK293T cells resulted in three N-terminal cleavage fragments of a similar molecular weight as the human A20p48, A20p60 and A20p70 fragments (**Fig. 14C**). However, only the p48 and the p70 fragments disappeared upon mutation of the corresponding P1 arginine residues (R471, R581 and R691) in murine A20 (**Fig. 14D**). Thus, murine A20 can be cleaved by human MALT1 after R471 and R691, suggesting a relevance of these two novel cleavage sites within different species. However, whether murine A20 is indeed cleaved by murine MALT1 at these two sites in mouse cells remains to be determined.

The formation of the murine A20 cleavage fragment of 60 kDa needs further investigation, nevertheless we demonstrated that it is dependent on MALT1 proteolytic activity, as it was not inducible by a catalytically inactive MALT1 mutant (**Fig. 14C**). This indicates that murine A20 is either cleaved by MALT1 at another neighboring arginine or by another protease that is dependent on MALT1 proteolytic activity. To investigate the first hypothesis, individual point mutations of arginine residues around R581 and the assessment of the cleavage of these mutants in HEK293Ts would be conclusive. However, comparison of the amino acid sequence from human and murine A20 showed no major differences in the area of R581, which could suggest the

existence of another cleavage site in murine A20 that is not present in human A20. A second possibility is that murine A20 is cleaved around R581 by another protease, whose activity is dependent on MALT1 proteolytic activity. Such a MALT1-dependent protease has not been identified so far. Nevertheless, MALT1 has been shown to activate Caspase 8 upon T cell activation in a MALT1 protease domain-dependent but MALT1 proteolytic activity-independent manner.[251] Thus, it is in principle conceivable that MALT1, as a protease, activates other proteases, in a manner that would be similar to the activation of effector caspases by initiator caspases.

# 7 Conclusion and perspectives

In this study, we identified the Ig3 domain of MALT1 as a novel ubiquitin-binding domain, responsible for MALT1 monoubiquitination and subsequent MALT1 proteolytic activity and lymphocyte activation. Furthermore, we revealed an allosteric, intramolecular signal transduction from the monoubiquitination site through the protease-Ig3 interaction surface to the catalytic active site of the protease domain. Overall, our results provide fundamentally new insights into the mechanism of MALT1 activation and might help for the development and identification of new MALT1 protease activity-modulating substances that will be useful in the treatment of different pathologies.

However, remaining questions have to be addressed in future studies. Firstly, it is still unclear how MALT1 becomes monoubiquitinated. Our data suggest that MALT1 might become monoubiquitinated in an E3 ubiquitin ligase-independent manner as it was shown for other ubiquitin-binding proteins.[228] However, we cannot exclude the involvement of a still unknown E3 ubiquitin ligase in this process, whose identification would be of interest as a new therapeutic target of pathologies with the involvement of MALT1 proteolytic activity, in case MALT1 inhibitors fail the approval. Secondly, this study suggests that the covalently linked ubiquitin on the Ig3 domain activates the proteolytic function of MALT1 by a direct interaction with a second, still unknown and potentially cryptic ubiquitin-binding site of MALT1. Future work has to uncover this second ubiquitin-binding site that is possibly formed upon substrate-binding or MALT1 dimerization. This information could uncover a new allosteric site that could be targeted and might help to develop more specific allosteric MALT1 inhibitors.

In the second project of this study, we determined that MALT1 cleaves A20 at a total of four distinct sites in activated lymphocytes and further identified the three novel cleavage sites that are conserved in the mouse and other species, but have sequence features that are distinct from previously identified substrates. This opens the question how MALT1 maintains substrate specificity. Furthermore, the functional relevance of A20 cleavage will be the target of future investigations. We showed that the cleavage fragments lost their capacity to regulate activation-induced IL-2 production, however it remains elusive whether MALT1-dependent cleavage of A20 contributes to it. In case it does, the underlying mechanism of A20-mediated regulation of the activation-induced IL-2 production should be investigated in future studies, since the known and established mechanism could not explain this effect. As the A20 cleavage fragments are stable within the cell, we suggest that MALT1-

dependent A20 cleavage has roles that might go beyond the NF-κB-dependent enhancement of lymphocyte activity. This and the relevance of A20 cleavage in other cell-types should be the target of impending investigations. For all of these purposes, animal models expressing non-cleavable A20 would be advantageous. Thus, the cleavage of murine A20 should be further investigated to elucidate its physiological role *in vivo* and to better understand the outcome of potential MALT1-targeting therapies.

# 8 References

1      Morgan, J. A. *et al.* Breakpoints of the t(11;18)(q21;q21) in mucosa-associated lymphoid tissue (MALT) lymphoma lie within or near the previously undescribed gene MALT1 in chromosome 18. *Cancer Res* **59**, 6205-6213 (1999).

2      Akagi, T. *et al.* A novel gene, MALT1 at 18q21, is involved in t(11;18) (q21;q21) found in low-grade B-cell lymphoma of mucosa-associated lymphoid tissue. *Oncogene* **18**, 5785-5794, doi:10.1038/sj.onc.1203018 (1999).

3      Dierlamm, J. *et al.* The apoptosis inhibitor gene API2 and a novel 18q gene, MLT, are recurrently rearranged in the t(11;18)(q21;q21) associated with mucosa-associated lymphoid tissue lymphomas. *Blood* **93**, 3601-3609 (1999).

4      Uren, A. G. *et al.* Identification of paracaspases and metacaspases: two ancient families of caspase-like proteins, one of which plays a key role in MALT lymphoma. *Mol Cell* **6**, 961-967, doi:10.1016/s1097-2765(00)00094-0 (2000).

5      Hulpiau, P., Driege, Y., Staal, J. & Beyaert, R. MALT1 is not alone after all: identification of novel paracaspases. *Cell Mol Life Sci* **73**, 1103-1116, doi:10.1007/s00018-015-2041-9 (2016).

6      Rosebeck, S., Rehman, A. O., Lucas, P. C. & McAllister-Lucas, L. M. From MALT lymphoma to the CBM signalosome: three decades of discovery. *Cell Cycle* **10**, 2485-2496, doi:10.4161/cc.10.15.16923 (2011).

7      Willis, T. G. *et al.* Bcl10 is involved in t(1;14)(p22;q32) of MALT B cell lymphoma and mutated in multiple tumor types. *Cell* **96**, 35-45, doi:10.1016/s0092-8674(00)80957-5 (1999).

8      Zhang, Q. *et al.* Inactivating mutations and overexpression of BCL10, a caspase recruitment domain-containing gene, in MALT lymphoma with t(1;14)(p22;q32). *Nat Genet* **22**, 63-68, doi:10.1038/8767 (1999).

9      Zhou, H., Du, M. Q. & Dixit, V. M. Constitutive NF-kappaB activation by the t(11;18)(q21;q21) product in MALT lymphoma is linked to deregulated ubiquitin ligase activity. *Cancer Cell* **7**, 425-431, doi:10.1016/j.ccr.2005.04.012 (2005).

10     Schlauderer, F. *et al.* Molecular architecture and regulation of BCL10-MALT1 filaments. *Nat Commun* **9**, 4041, doi:10.1038/s41467-018-06573-8 (2018).

11     Gaide, O. *et al.* Carma1, a CARD-containing binding partner of Bcl10, induces Bcl10 phosphorylation and NF-kappaB activation. *FEBS Lett* **496**, 121-127, doi:10.1016/s0014-5793(01)02414-0 (2001).

12     Che, T. *et al.* MALT1/paracaspase is a signaling component downstream of CARMA1 and mediates T cell receptor-induced NF-kappaB activation. *J Biol Chem* **279**, 15870-15876, doi:10.1074/jbc.M310599200 (2004).

13     Gross, O. *et al.* Card9 controls a non-TLR signalling pathway for innate anti-fungal immunity. *Nature* **442**, 651-656, doi:10.1038/nature04926 (2006).

14     McAllister-Lucas, L. M. *et al.* CARMA3/Bcl10/MALT1-dependent NF-kappaB activation mediates angiotensin II-responsive inflammatory signaling in nonimmune cells. *Proc Natl Acad Sci U S A* **104**, 139-144, doi:10.1073/pnas.0601947103 (2007).

15     Afonina, I. S. *et al.* The paracaspase MALT1 mediates CARD14-induced signaling in keratinocytes. *EMBO Rep* **17**, 914-927, doi:10.15252/embr.201642109 (2016).

16 Schmitt, A. *et al.* MALT1 Protease Activity Controls the Expression of Inflammatory Genes in Keratinocytes upon Zymosan Stimulation. *J Invest Dermatol* **136**, 788-797, doi:10.1016/j.jid.2015.12.027 (2016).

17 Howes, A. *et al.* Psoriasis mutations disrupt CARD14 autoinhibition promoting BCL10-MALT1-dependent NF-kappaB activation. *Biochem J* **473**, 1759-1768, doi:10.1042/BCJ20160270 (2016).

18 Staal, J. *et al.* Ancient Origin of the CARD-Coiled Coil/Bcl10/MALT1-Like Paracaspase Signaling Complex Indicates Unknown Critical Functions. *Front Immunol* **9**, 1136, doi:10.3389/fimmu.2018.01136 (2018).

19 Hara, H. *et al.* The adaptor protein CARD9 is essential for the activation of myeloid cells through ITAM-associated and Toll-like receptors. *Nat Immunol* **8**, 619-629, doi:10.1038/ni1466 (2007).

20 Roth, S. & Ruland, J. Caspase recruitment domain-containing protein 9 signaling in innate immunity and inflammation. *Trends Immunol* **34**, 243-250, doi:10.1016/j.it.2013.02.006 (2013).

21 Bi, L. *et al.* CARD9 mediates dectin-2-induced IkappaBalpha kinase ubiquitination leading to activation of NF-kappaB in response to stimulation by the hyphal form of Candida albicans. *J Biol Chem* **285**, 25969-25977, doi:10.1074/jbc.M110.131300 (2010).

22 Shenderov, K. *et al.* Cord factor and peptidoglycan recapitulate the Th17-promoting adjuvant activity of mycobacteria through mincle/CARD9 signaling and the inflammasome. *J Immunol* **190**, 5722-5730, doi:10.4049/jimmunol.1203343 (2013).

23 Poeck, H. *et al.* Recognition of RNA virus by RIG-I results in activation of CARD9 and inflammasome signaling for interleukin 1 beta production. *Nat Immunol* **11**, 63-69, doi:10.1038/ni.1824 (2010).

24 Roth, S. *et al.* Rad50-CARD9 interactions link cytosolic DNA sensing to IL-1beta production. *Nat Immunol* **15**, 538-545, doi:10.1038/ni.2888 (2014).

25 Hsu, Y. M. *et al.* The adaptor protein CARD9 is required for innate immune responses to intracellular pathogens. *Nat Immunol* **8**, 198-205, doi:10.1038/ni1426 (2007).

26 Gaide, O. *et al.* CARMA1 is a critical lipid raft-associated regulator of TCR-induced NF-kappa B activation. *Nat Immunol* **3**, 836-843, doi:10.1038/ni830 (2002).

27 Wang, D. *et al.* A requirement for CARMA1 in TCR-induced NF-kappa B activation. *Nat Immunol* **3**, 830-835, doi:10.1038/ni824 (2002).

28 Hara, H. *et al.* The MAGUK family protein CARD11 is essential for lymphocyte activation. *Immunity* **18**, 763-775, doi:10.1016/s1074-7613(03)00148-1 (2003).

29 Jun, J. E. *et al.* Identifying the MAGUK protein Carma-1 as a central regulator of humoral immune responses and atopy by genome-wide mouse mutagenesis. *Immunity* **18**, 751-762, doi:10.1016/s1074-7613(03)00141-9 (2003).

30 Malarkannan, S. *et al.* Bcl10 plays a divergent role in NK cell-mediated cytotoxicity and cytokine generation. *J Immunol* **179**, 3752-3762, doi:10.4049/jimmunol.179.6.3752 (2007).

31 Gross, O. *et al.* Multiple ITAM-coupled NK-cell receptors engage the Bcl10/Malt1 complex via Carma1 for NF-kappaB and MAPK activation to selectively control cytokine production. *Blood* **112**, 2421-2428, doi:10.1182/blood-2007-11-123513 (2008).

32 Klemm, S. *et al.* The Bcl10-Malt1 complex segregates Fc epsilon RI-mediated nuclear factor kappa B activation and cytokine production from mast cell degranulation. *J Exp Med* **203**, 337-347, doi:10.1084/jem.20051982 (2006).

33 Blonska, M. *et al.* The CARMA1-Bcl10 signaling complex selectively regulates JNK2 kinase in the T cell receptor-signaling pathway. *Immunity* **26**, 55-66, doi:10.1016/j.immuni.2006.11.008 (2007).

34 Wang, M. *et al.* Gain-of-Function Mutation of Card14 Leads to Spontaneous Psoriasis-like Skin Inflammation through Enhanced Keratinocyte Response to IL-17A. *Immunity* **49**, 66-79 e65, doi:10.1016/j.immuni.2018.05.012 (2018).

35 Blonska, M. & Lin, X. NF-kappaB signaling pathways regulated by CARMA family of scaffold proteins. *Cell Res* **21**, 55-70, doi:10.1038/cr.2010.182 (2011).

36 Grabiner, B. C. *et al.* CARMA3 deficiency abrogates G protein-coupled receptor-induced NF-{kappa}B activation. *Genes Dev* **21**, 984-996, doi:10.1101/gad.1502507 (2007).

37 Van Beek, M. *et al.* Bcl10 links saturated fat overnutrition with hepatocellular NF-kB activation and insulin resistance. *Cell Rep* **1**, 444-452, doi:10.1016/j.celrep.2012.04.006 (2012).

38 Jiang, T. *et al.* CARMA3 is crucial for EGFR-Induced activation of NF-kappaB and tumor progression. *Cancer Res* **71**, 2183-2192, doi:10.1158/0008-5472.CAN-10-3626 (2011).

39 Pan, D. *et al.* MALT1 is required for EGFR-induced NF-kappaB activation and contributes to EGFR-driven lung cancer progression. *Oncogene* **35**, 919-928, doi:10.1038/onc.2015.146 (2016).

40 Ekambaram, P. *et al.* The CARMA3-Bcl10-MALT1 Signalosome Drives NFkappaB Activation and Promotes Aggressiveness in Angiotensin II Receptor-Positive Breast Cancer. *Cancer Res* **78**, 1225-1240, doi:10.1158/0008-5472.CAN-17-1089 (2018).

41 Ruefli-Brasse, A. A., French, D. M. & Dixit, V. M. Regulation of NF-kappaB-dependent lymphocyte activation and development by paracaspase. *Science* **302**, 1581-1584, doi:10.1126/science.1090769 (2003).

42 Ruland, J., Duncan, G. S., Wakeham, A. & Mak, T. W. Differential requirement for Malt1 in T and B cell antigen receptor signaling. *Immunity* **19**, 749-758, doi:10.1016/s1074-7613(03)00293-0 (2003).

43 Ruland, J. *et al.* Bcl10 is a positive regulator of antigen receptor-induced activation of NF-kappaB and neural tube closure. *Cell* **104**, 33-42, doi:10.1016/s0092-8674(01)00189-1 (2001).

44 Demeyer, A. *et al.* MALT1-Deficient Mice Develop Atopic-Like Dermatitis Upon Aging. *Front Immunol* **10**, 2330, doi:10.3389/fimmu.2019.02330 (2019).

45 Jabara, H. H. *et al.* A homozygous mucosa-associated lymphoid tissue 1 (MALT1) mutation in a family with combined immunodeficiency. *J Allergy Clin Immunol* **132**, 151-158, doi:10.1016/j.jaci.2013.04.047 (2013).

46 McKinnon, M. L. *et al.* Combined immunodeficiency associated with homozygous MALT1 mutations. *J Allergy Clin Immunol* **133**, 1458-1462, 1462 e1451-1457, doi:10.1016/j.jaci.2013.10.045 (2014).

47 Punwani, D. *et al.* Combined immunodeficiency due to MALT1 mutations, treated by hematopoietic cell transplantation. *J Clin Immunol* **35**, 135-146, doi:10.1007/s10875-014-0125-1 (2015).

48 Frizinsky, S. *et al.* Novel MALT1 Mutation Linked to Immunodeficiency, Immune Dysregulation, and an Abnormal T Cell Receptor Repertoire. *J Clin Immunol* **39**, 401-413, doi:10.1007/s10875-019-00629-0 (2019).

49    Charbit-Henrion, F. *et al.* Deficiency in Mucosa-associated Lymphoid Tissue Lymphoma Translocation 1: A Novel Cause of IPEX-Like Syndrome. *J Pediatr Gastroenterol Nutr* **64**, 378-384, doi:10.1097/MPG.0000000000001262 (2017).

50    Verbsky, J. W. & Chatila, T. A. Immune dysregulation, polyendocrinopathy, enteropathy, X-linked (IPEX) and IPEX-related disorders: an evolving web of heritable autoimmune diseases. *Curr Opin Pediatr* **25**, 708-714, doi:10.1097/MOP.0000000000000029 (2013).

51    Schatz, D. G., Oettinger, M. A. & Schlissel, M. S. V(D)J recombination: molecular biology and regulation. *Annu Rev Immunol* **10**, 359-383, doi:10.1146/annurev.iy.10.040192.002043 (1992).

52    Medzhitov, R. Recognition of microorganisms and activation of the immune response. *Nature* **449**, 819-826, doi:10.1038/nature06246 (2007).

53    Krogsgaard, M. & Davis, M. M. How T cells 'see' antigen. *Nat Immunol* **6**, 239-245, doi:10.1038/ni1173 (2005).

54    Xiong, N. & Raulet, D. H. Development and selection of gammadelta T cells. *Immunol Rev* **215**, 15-31, doi:10.1111/j.1600-065X.2006.00478.x (2007).

55    Abram, C. L. & Lowell, C. A. The expanding role for ITAM-based signaling pathways in immune cells. *Sci STKE* **2007**, re2, doi:10.1126/stke.3772007re2 (2007).

56    Salmond, R. J., Filby, A., Qureshi, I., Caserta, S. & Zamoyska, R. T-cell receptor proximal signaling via the Src-family kinases, Lck and Fyn, influences T-cell activation, differentiation, and tolerance. *Immunol Rev* **228**, 9-22, doi:10.1111/j.1600-065X.2008.00745.x (2009).

57    Wang, H. *et al.* ZAP-70: an essential kinase in T-cell signaling. *Cold Spring Harb Perspect Biol* **2**, a002279, doi:10.1101/cshperspect.a002279 (2010).

58    Cantrell, D. Signaling in lymphocyte activation. *Cold Spring Harb Perspect Biol* **7**, doi:10.1101/cshperspect.a018788 (2015).

59    Kurosaki, T. & Hikida, M. Tyrosine kinases and their substrates in B lymphocytes. *Immunol Rev* **228**, 132-148, doi:10.1111/j.1600-065X.2008.00748.x (2009).

60    Su, T. T. *et al.* PKC-beta controls I kappa B kinase lipid raft recruitment and activation in response to BCR signaling. *Nat Immunol* **3**, 780-786, doi:10.1038/ni823 (2002).

61    Jattani, R. P., Tritapoe, J. M. & Pomerantz, J. L. Intramolecular Interactions and Regulation of Cofactor Binding by the Four Repressive Elements in the Caspase Recruitment Domain-containing Protein 11 (CARD11) Inhibitory Domain. *J Biol Chem* **291**, 8338-8348, doi:10.1074/jbc.M116.717322 (2016).

62    Holliday, M. J. *et al.* Structures of autoinhibited and polymerized forms of CARD9 reveal mechanisms of CARD9 and CARD11 activation. *Nat Commun* **10**, 3070, doi:10.1038/s41467-019-10953-z (2019).

63    Matsumoto, R. *et al.* Phosphorylation of CARMA1 plays a critical role in T Cell receptor-mediated NF-kappaB activation. *Immunity* **23**, 575-585, doi:10.1016/j.immuni.2005.10.007 (2005).

64    Sommer, K. *et al.* Phosphorylation of the CARMA1 linker controls NF-kappaB activation. *Immunity* **23**, 561-574, doi:10.1016/j.immuni.2005.09.014 (2005).

65    Rueda, D. & Thome, M. Phosphorylation of CARMA1: the link(er) to NF-kappaB activation. *Immunity* **23**, 551-553, doi:10.1016/j.immuni.2005.11.007 (2005).

66    Shinohara, H., Maeda, S., Watarai, H. & Kurosaki, T. IkappaB kinase beta-induced phosphorylation of CARMA1 contributes to CARMA1 Bcl10 MALT1 complex formation in B cells. *J Exp Med* **204**, 3285-3293, doi:10.1084/jem.20070379 (2007).

67     Cheng, J., Hamilton, K. S. & Kane, L. P. Phosphorylation of Carma1, but not Bcl10, by Akt regulates TCR/CD28-mediated NF-kappaB induction and cytokine production. *Mol Immunol* **59**, 110-116, doi:10.1016/j.molimm.2014.01.011 (2014).

68     Ishiguro, K. *et al.* Ca2+/calmodulin-dependent protein kinase II is a modulator of CARMA1-mediated NF-kappaB activation. *Mol Cell Biol* **26**, 5497-5508, doi:10.1128/MCB.02469-05 (2006).

69     Qiao, Q. *et al.* Structural architecture of the CARMA1/Bcl10/MALT1 signalosome: nucleation-induced filamentous assembly. *Mol Cell* **51**, 766-779, doi:10.1016/j.molcel.2013.08.032 (2013).

70     David, L. *et al.* Assembly mechanism of the CARMA1-BCL10-MALT1-TRAF6 signalosome. *Proc Natl Acad Sci U S A* **115**, 1499-1504, doi:10.1073/pnas.1721967115 (2018).

71     Sun, L., Deng, L., Ea, C. K., Xia, Z. P. & Chen, Z. J. The TRAF6 ubiquitin ligase and TAK1 kinase mediate IKK activation by BCL10 and MALT1 in T lymphocytes. *Mol Cell* **14**, 289-301, doi:10.1016/s1097-2765(04)00236-9 (2004).

72     Baens, M. *et al.* Selective expansion of marginal zone B cells in Emicro-API2-MALT1 mice is linked to enhanced IkappaB kinase gamma polyubiquitination. *Cancer Res* **66**, 5270-5277, doi:10.1158/0008-5472.CAN-05-4590 (2006).

73     Noels, H. *et al.* A Novel TRAF6 binding site in MALT1 defines distinct mechanisms of NF-kappaB activation by API2middle dotMALT1 fusions. *J Biol Chem* **282**, 10180-10189, doi:10.1074/jbc.M611038200 (2007).

74     Oeckinghaus, A. *et al.* Malt1 ubiquitination triggers NF-kappaB signaling upon T-cell activation. *EMBO J* **26**, 4634-4645, doi:10.1038/sj.emboj.7601897 (2007).

75     Meininger, I. *et al.* Alternative splicing of MALT1 controls signalling and activation of CD4(+) T cells. *Nat Commun* **7**, 11292, doi:10.1038/ncomms11292 (2016).

76     Wu, C. J. & Ashwell, J. D. NEMO recognition of ubiquitinated Bcl10 is required for T cell receptor-mediated NF-kappaB activation. *Proc Natl Acad Sci U S A* **105**, 3023-3028, doi:10.1073/pnas.0712313105 (2008).

77     Yang, Y. *et al.* Targeting Non-proteolytic Protein Ubiquitination for the Treatment of Diffuse Large B Cell Lymphoma. *Cancer Cell* **29**, 494-507, doi:10.1016/j.ccell.2016.03.006 (2016).

78     Yang, Y. K. *et al.* Molecular Determinants of Scaffold-induced Linear Ubiquitinylation of B Cell Lymphoma/Leukemia 10 (Bcl10) during T Cell Receptor and Oncogenic Caspase Recruitment Domain-containing Protein 11 (CARD11) Signaling. *J Biol Chem* **291**, 25921-25936, doi:10.1074/jbc.M116.754028 (2016).

79     Dubois, S. M. *et al.* A catalytic-independent role for the LUBAC in NF-kappaB activation upon antigen receptor engagement and in lymphoma cells. *Blood* **123**, 2199-2203, doi:10.1182/blood-2013-05-504019 (2014).

80     Rahighi, S. *et al.* Specific recognition of linear ubiquitin chains by NEMO is important for NF-kappaB activation. *Cell* **136**, 1098-1109, doi:10.1016/j.cell.2009.03.007 (2009).

81     Zhou, H. *et al.* Bcl10 activates the NF-kappaB pathway through ubiquitination of NEMO. *Nature* **427**, 167-171, doi:10.1038/nature02273 (2004).

82     Karin, M. & Ben-Neriah, Y. Phosphorylation meets ubiquitination: the control of NF-[kappa]B activity. *Annu Rev Immunol* **18**, 621-663, doi:10.1146/annurev.immunol.18.1.621 (2000).

83     Winston, J. T. *et al.* The SCFbeta-TRCP-ubiquitin ligase complex associates specifically with phosphorylated destruction motifs in IkappaBalpha and beta-catenin and

stimulates IkappaBalpha ubiquitination in vitro. *Genes Dev* **13**, 270-283, doi:10.1101/gad.13.3.270 (1999).

84      Liu, T., Zhang, L., Joo, D. & Sun, S. C. NF-kappaB signaling in inflammation. *Signal Transduct Target Ther* **2**, doi:10.1038/sigtrans.2017.23 (2017).

85      Oeckinghaus, A. & Ghosh, S. The NF-kappaB family of transcription factors and its regulation. *Cold Spring Harb Perspect Biol* **1**, a000034, doi:10.1101/cshperspect.a000034 (2009).

86      Sun, S. C., Chang, J. H. & Jin, J. Regulation of nuclear factor-kappaB in autoimmunity. *Trends Immunol* **34**, 282-289, doi:10.1016/j.it.2013.01.004 (2013).

87      Ghosh, S., May, M. J. & Kopp, E. B. NF-kappa B and Rel proteins: evolutionarily conserved mediators of immune responses. *Annu Rev Immunol* **16**, 225-260, doi:10.1146/annurev.immunol.16.1.225 (1998).

88      Hayden, M. S. & Ghosh, S. NF-kappaB, the first quarter-century: remarkable progress and outstanding questions. *Genes Dev* **26**, 203-234, doi:10.1101/gad.183434.111 (2012).

89      Blonska, M. *et al.* Jun-regulated genes promote interaction of diffuse large B-cell lymphoma with the microenvironment. *Blood* **125**, 981-991, doi:10.1182/blood-2014-04-568188 (2015).

90      Juilland, M. *et al.* CARMA1- and MyD88-dependent activation of Jun/ATF-type AP-1 complexes is a hallmark of ABC diffuse large B-cell lymphomas. *Blood* **127**, 1780-1789, doi:10.1182/blood-2015-07-655647 (2016).

91      Yu, J. W., Jeffrey, P. D., Ha, J. Y., Yang, X. & Shi, Y. Crystal structure of the mucosa-associated lymphoid tissue lymphoma translocation 1 (MALT1) paracaspase region. *Proc Natl Acad Sci U S A* **108**, 21004-21009, doi:10.1073/pnas.1111708108 (2011).

92      Wiesmann, C. *et al.* Structural determinants of MALT1 protease activity. *J Mol Biol* **419**, 4-21, doi:10.1016/j.jmb.2012.02.018 (2012).

93      Cabalzar, K. *et al.* Monoubiquitination and activity of the paracaspase MALT1 requires glutamate 549 in the dimerization interface. *PLoS One* **8**, e72051, doi:10.1371/journal.pone.0072051 (2013).

94      Rebeaud, F. *et al.* The proteolytic activity of the paracaspase MALT1 is key in T cell activation. *Nat Immunol* **9**, 272-281, doi:10.1038/ni1568 (2008).

95      Pelzer, C. *et al.* The protease activity of the paracaspase MALT1 is controlled by monoubiquitination. *Nat Immunol* **14**, 337-345, doi:10.1038/ni.2540 (2013).

96      Qiu, L. & Dhe-Paganon, S. Oligomeric structure of the MALT1 tandem Ig-like domains. *PLoS One* **6**, e23220, doi:10.1371/journal.pone.0023220 (2011).

97      Jaworski, M. *et al.* Malt1 protease inactivation efficiently dampens immune responses but causes spontaneous autoimmunity. *EMBO J* **33**, 2765-2781, doi:10.15252/embj.201488987 (2014).

98      Gewies, A. *et al.* Uncoupling Malt1 threshold function from paracaspase activity results in destructive autoimmune inflammation. *Cell Rep* **9**, 1292-1305, doi:10.1016/j.celrep.2014.10.044 (2014).

99      Bornancin, F. *et al.* Deficiency of MALT1 paracaspase activity results in unbalanced regulatory and effector T and B cell responses leading to multiorgan inflammation. *J Immunol* **194**, 3723-3734, doi:10.4049/jimmunol.1402254 (2015).

100     Yu, J. W. *et al.* MALT1 Protease Activity Is Required for Innate and Adaptive Immune Responses. *PLoS One* **10**, e0127083, doi:10.1371/journal.pone.0127083 (2015).

101  Duwel, M. *et al.* A20 negatively regulates T cell receptor signaling to NF-kappaB by cleaving Malt1 ubiquitin chains. *J Immunol* **182**, 7718-7728, doi:10.4049/jimmunol.0803313 (2009).

102  Demeyer, A. *et al.* MALT1 Proteolytic Activity Suppresses Autoimmunity in a T Cell Intrinsic Manner. *Front Immunol* **10**, 1898, doi:10.3389/fimmu.2019.01898 (2019).

103  Baens, M. *et al.* MALT1 auto-proteolysis is essential for NF-kappaB-dependent gene transcription in activated lymphocytes. *PLoS One* **9**, e103774, doi:10.1371/journal.pone.0103774 (2014).

104  Ginster, S. *et al.* Two Antagonistic MALT1 Auto-Cleavage Mechanisms Reveal a Role for TRAF6 to Unleash MALT1 Activation. *PLoS One* **12**, e0169026, doi:10.1371/journal.pone.0169026 (2017).

105  Coornaert, B. *et al.* T cell antigen receptor stimulation induces MALT1 paracaspase-mediated cleavage of the NF-kappaB inhibitor A20. *Nat Immunol* **9**, 263-271, doi:10.1038/ni1561 (2008).

106  Klei, L. R. *et al.* MALT1 Protease Activation Triggers Acute Disruption of Endothelial Barrier Integrity via CYLD Cleavage. *Cell Rep* **17**, 221-232, doi:10.1016/j.celrep.2016.08.080 (2016).

107  Hailfinger, S. *et al.* Malt1-dependent RelB cleavage promotes canonical NF-kappaB activation in lymphocytes and lymphoma cell lines. *Proc Natl Acad Sci U S A* **108**, 14596-14601, doi:10.1073/pnas.1105020108 (2011).

108  Klein, T. *et al.* The paracaspase MALT1 cleaves HOIL1 reducing linear ubiquitination by LUBAC to dampen lymphocyte NF-kappaB signalling. *Nat Commun* **6**, 8777, doi:10.1038/ncomms9777 (2015).

109  Uehata, T. *et al.* Malt1-induced cleavage of regnase-1 in CD4(+) helper T cells regulates immune activation. *Cell* **153**, 1036-1049, doi:10.1016/j.cell.2013.04.034 (2013).

110  Jeltsch, K. M. *et al.* Cleavage of roquin and regnase-1 by the paracaspase MALT1 releases their cooperatively repressed targets to promote T(H)17 differentiation. *Nat Immunol* **15**, 1079-1089, doi:10.1038/ni.3008 (2014).

111  Yamasoba, D. *et al.* N4BP1 restricts HIV-1 and its inactivation by MALT1 promotes viral reactivation. *Nat Microbiol* **4**, 1532-1544, doi:10.1038/s41564-019-0460-3 (2019).

112  Vercammen, D. *et al.* Type II metacaspases Atmc4 and Atmc9 of Arabidopsis thaliana cleave substrates after arginine and lysine. *J Biol Chem* **279**, 45329-45336, doi:10.1074/jbc.M406329200 (2004).

113  Juilland, M. & Thome, M. Holding All the CARDs: How MALT1 Controls CARMA/CARD-Dependent Signaling. *Front Immunol* **9**, 1927, doi:10.3389/fimmu.2018.01927 (2018).

114  Baens, M. *et al.* Malt1 self-cleavage is critical for regulatory T cell homeostasis and anti-tumor immunity in mice. *Eur J Immunol* **48**, 1728-1738, doi:10.1002/eji.201847597 (2018).

115  Reiley, W., Zhang, M. & Sun, S. C. Negative regulation of JNK signaling by the tumor suppressor CYLD. *J Biol Chem* **279**, 55161-55167, doi:10.1074/jbc.M411049200 (2004).

116  Reiley, W. W. *et al.* Deubiquitinating enzyme CYLD negatively regulates the ubiquitin-dependent kinase Tak1 and prevents abnormal T cell responses. *J Exp Med* **204**, 1475-1485, doi:10.1084/jem.20062694 (2007).

117  Staal, J. *et al.* T-cell receptor-induced JNK activation requires proteolytic inactivation of CYLD by MALT1. *EMBO J* **30**, 1742-1752, doi:10.1038/emboj.2011.85 (2011).

118     Lim, K. H., Yang, Y. & Staudt, L. M. Pathogenetic importance and therapeutic implications of NF-kappaB in lymphoid malignancies. *Immunol Rev* **246**, 359-378, doi:10.1111/j.1600-065X.2012.01105.x (2012).

119     Ruben, S. M. *et al.* I-Rel: a novel rel-related protein that inhibits NF-kappa B transcriptional activity. *Genes Dev* **6**, 745-760, doi:10.1101/gad.6.5.745 (1992).

120     Weih, F. *et al.* Multiorgan inflammation and hematopoietic abnormalities in mice with a targeted disruption of RelB, a member of the NF-kappa B/Rel family. *Cell* **80**, 331-340, doi:10.1016/0092-8674(95)90416-6 (1995).

121     Ishimaru, N., Kishimoto, H., Hayashi, Y. & Sprent, J. Regulation of naive T cell function by the NF-kappaB2 pathway. *Nat Immunol* **7**, 763-772, doi:10.1038/ni1351 (2006).

122     Elton, L. *et al.* MALT1 cleaves the E3 ubiquitin ligase HOIL-1 in activated T cells, generating a dominant negative inhibitor of LUBAC-induced NF-kappaB signaling. *FEBS J* **283**, 403-412, doi:10.1111/febs.13597 (2016).

123     Douanne, T., Gavard, J. & Bidere, N. The paracaspase MALT1 cleaves the LUBAC subunit HOIL1 during antigen receptor signaling. *J Cell Sci* **129**, 1775-1780, doi:10.1242/jcs.185025 (2016).

124     Hailfinger, S., Schmitt, A. & Schulze-Osthoff, K. The paracaspase MALT1 dampens NF-kappaB signalling by cleaving the LUBAC subunit HOIL-1. *FEBS J* **283**, 400-402, doi:10.1111/febs.13639 (2016).

125     Matsushita, K. *et al.* Zc3h12a is an RNase essential for controlling immune responses by regulating mRNA decay. *Nature* **458**, 1185-1190, doi:10.1038/nature07924 (2009).

126     Leppek, K. *et al.* Roquin promotes constitutive mRNA decay via a conserved class of stem-loop recognition motifs. *Cell* **153**, 869-881, doi:10.1016/j.cell.2013.04.016 (2013).

127     Glasmacher, E. *et al.* Roquin binds inducible costimulator mRNA and effectors of mRNA decay to induce microRNA-independent post-transcriptional repression. *Nat Immunol* **11**, 725-733, doi:10.1038/ni.1902 (2010).

128     Korn, T. *et al.* IL-6 controls Th17 immunity in vivo by inhibiting the conversion of conventional T cells into Foxp3+ regulatory T cells. *Proc Natl Acad Sci U S A* **105**, 18460-18465, doi:10.1073/pnas.0809850105 (2008).

129     Brustle, A. *et al.* The development of inflammatory T(H)-17 cells requires interferon-regulatory factor 4. *Nat Immunol* **8**, 958-966, doi:10.1038/ni1500 (2007).

130     Chen, G. *et al.* The NF-kappaB transcription factor c-Rel is required for Th17 effector cell development in experimental autoimmune encephalomyelitis. *J Immunol* **187**, 4483-4491, doi:10.4049/jimmunol.1101757 (2011).

131     Okamoto, K. *et al.* IkappaBzeta regulates T(H)17 development by cooperating with ROR nuclear receptors. *Nature* **464**, 1381-1385, doi:10.1038/nature08922 (2010).

132     Bauquet, A. T. *et al.* The costimulatory molecule ICOS regulates the expression of c-Maf and IL-21 in the development of follicular T helper cells and TH-17 cells. *Nat Immunol* **10**, 167-175, doi:10.1038/ni.1690 (2009).

133     Oberst, A. *et al.* The Nedd4-binding partner 1 (N4BP1) protein is an inhibitor of the E3 ligase Itch. *Proc Natl Acad Sci U S A* **104**, 11280-11285, doi:10.1073/pnas.0701773104 (2007).

134     Spel, L. *et al.* Nedd4-Binding Protein 1 and TNFAIP3-Interacting Protein 1 Control MHC-1 Display in Neuroblastoma. *Cancer Res* **78**, 6621-6631, doi:10.1158/0008-5472.CAN-18-0545 (2018).

135     Martens, A. & van Loo, G. A20 at the Crossroads of Cell Death, Inflammation, and Autoimmunity. *Cold Spring Harb Perspect Biol* **12**, doi:10.1101/cshperspect.a036418 (2020).

136     Lee, E. G. *et al.* Failure to regulate TNF-induced NF-kappaB and cell death responses in A20-deficient mice. *Science* **289**, 2350-2354, doi:10.1126/science.289.5488.2350 (2000).

137     Evans, P. C. *et al.* Zinc-finger protein A20, a regulator of inflammation and cell survival, has de-ubiquitinating activity. *Biochem J* **378**, 727-734, doi:10.1042/BJ20031377 (2004).

138     Wertz, I. E. *et al.* De-ubiquitination and ubiquitin ligase domains of A20 downregulate NF-kappaB signalling. *Nature* **430**, 694-699, doi:10.1038/nature02794 (2004).

139     Mauro, C. *et al.* ABIN-1 binds to NEMO/IKKgamma and co-operates with A20 in inhibiting NF-kappaB. *J Biol Chem* **281**, 18482-18488, doi:10.1074/jbc.M601502200 (2006).

140     Wertz, I. E. *et al.* Phosphorylation and linear ubiquitin direct A20 inhibition of inflammation. *Nature* **528**, 370-375, doi:10.1038/nature16165 (2015).

141     Shembade, N., Ma, A. & Harhaj, E. W. Inhibition of NF-kappaB signaling by A20 through disruption of ubiquitin enzyme complexes. *Science* **327**, 1135-1139, doi:10.1126/science.1182364 (2010).

142     Lu, T. T. *et al.* Dimerization and ubiquitin mediated recruitment of A20, a complex deubiquitinating enzyme. *Immunity* **38**, 896-905, doi:10.1016/j.immuni.2013.03.008 (2013).

143     De, A., Dainichi, T., Rathinam, C. V. & Ghosh, S. The deubiquitinase activity of A20 is dispensable for NF-kappaB signaling. *EMBO Rep* **15**, 775-783, doi:10.15252/embr.201338305 (2014).

144     Bosanac, I. *et al.* Ubiquitin binding to A20 ZnF4 is required for modulation of NF-kappaB signaling. *Mol Cell* **40**, 548-557, doi:10.1016/j.molcel.2010.10.009 (2010).

145     Skaug, B. *et al.* Direct, noncatalytic mechanism of IKK inhibition by A20. *Mol Cell* **44**, 559-571, doi:10.1016/j.molcel.2011.09.015 (2011).

146     Tokunaga, F. *et al.* Specific recognition of linear polyubiquitin by A20 zinc finger 7 is involved in NF-kappaB regulation. *EMBO J* **31**, 3856-3870, doi:10.1038/emboj.2012.241 (2012).

147     Verhelst, K. *et al.* A20 inhibits LUBAC-mediated NF-kappaB activation by binding linear polyubiquitin chains via its zinc finger 7. *EMBO J* **31**, 3845-3855, doi:10.1038/emboj.2012.240 (2012).

148     Polykratis, A. *et al.* A20 prevents inflammasome-dependent arthritis by inhibiting macrophage necroptosis through its ZnF7 ubiquitin-binding domain. *Nat Cell Biol* **21**, 731-742, doi:10.1038/s41556-019-0324-3 (2019).

149     Martens, A. *et al.* Two distinct ubiquitin-binding motifs in A20 mediate its anti-inflammatory and cell-protective activities. *Nat Immunol* **21**, 381-387, doi:10.1038/s41590-020-0621-9 (2020).

150     Razani, B. *et al.* Non-catalytic ubiquitin binding by A20 prevents psoriatic arthritis-like disease and inflammation. *Nat Immunol* **21**, 422-433, doi:10.1038/s41590-020-0634-4 (2020).

151     Krikos, A., Laherty, C. D. & Dixit, V. M. Transcriptional activation of the tumor necrosis factor alpha-inducible zinc finger protein, A20, is mediated by kappa B elements. *J Biol Chem* **267**, 17971-17976 (1992).

152 Tewari, M. *et al.* Lymphoid expression and regulation of A20, an inhibitor of programmed cell death. *J Immunol* **154**, 1699-1706 (1995).

153 Onizawa, M. *et al.* The ubiquitin-modifying enzyme A20 restricts ubiquitination of the kinase RIPK3 and protects cells from necroptosis. *Nat Immunol* **16**, 618-627, doi:10.1038/ni.3172 (2015).

154 Just, S. *et al.* A20 Curtails Primary but Augments Secondary CD8(+) T Cell Responses in Intracellular Bacterial Infection. *Sci Rep* **6**, 39796, doi:10.1038/srep39796 (2016).

155 Matsuzawa, Y. *et al.* TNFAIP3 promotes survival of CD4 T cells by restricting MTOR and promoting autophagy. *Autophagy* **11**, 1052-1062, doi:10.1080/15548627.2015.1055439 (2015).

156 Roth, S. *et al.* Vav Proteins Are Key Regulators of Card9 Signaling for Innate Antifungal Immunity. *Cell Rep* **17**, 2572-2583, doi:10.1016/j.celrep.2016.11.018 (2016).

157 Nakamura, Y., Yokoyama, K., Igaki, K. & Tsuchimori, N. Role of Malt1 protease activity in pathogenesis of inflammatory disorders mediated by FcgammaR signaling. *Int Immunopharmacol* **56**, 193-196, doi:10.1016/j.intimp.2018.01.028 (2018).

158 Jaworski, M. & Thome, M. The paracaspase MALT1: biological function and potential for therapeutic inhibition. *Cell Mol Life Sci* **73**, 459-473, doi:10.1007/s00018-015-2059-z (2016).

159 Fontan, L. *et al.* MALT1 small molecule inhibitors specifically suppress ABC-DLBCL in vitro and in vivo. *Cancer Cell* **22**, 812-824, doi:10.1016/j.ccr.2012.11.003 (2012).

160 Nagel, D. *et al.* Pharmacologic inhibition of MALT1 protease by phenothiazines as a therapeutic approach for the treatment of aggressive ABC-DLBCL. *Cancer Cell* **22**, 825-837, doi:10.1016/j.ccr.2012.11.002 (2012).

161 Lim, S. M. *et al.* Identification of beta-Lapachone Analogs as Novel MALT1 Inhibitors To Treat an Aggressive Subtype of Diffuse Large B-Cell Lymphoma. *J Med Chem* **58**, 8491-8502, doi:10.1021/acs.jmedchem.5b01415 (2015).

162 Schlapbach, A. *et al.* N-aryl-piperidine-4-carboxamides as a novel class of potent inhibitors of MALT1 proteolytic activity. *Bioorg Med Chem Lett* **28**, 2153-2158, doi:10.1016/j.bmcl.2018.05.017 (2018).

163 Juilland, M. & Thome, M. Role of the CARMA1/BCL10/MALT1 complex in lymphoid malignancies. *Curr Opin Hematol* **23**, 402-409, doi:10.1097/MOH.0000000000000257 (2016).

164 Pasqualucci, L. *et al.* Genetics of follicular lymphoma transformation. *Cell Rep* **6**, 130-140, doi:10.1016/j.celrep.2013.12.027 (2014).

165 Koehrer, S. & Burger, J. A. B-cell receptor signaling in chronic lymphocytic leukemia and other B-cell malignancies. *Clin Adv Hematol Oncol* **14**, 55-65 (2016).

166 Lenz, G. *et al.* Oncogenic CARD11 mutations in human diffuse large B cell lymphoma. *Science* **319**, 1676-1679, doi:10.1126/science.1153629 (2008).

167 Compagno, M. *et al.* Mutations of multiple genes cause deregulation of NF-kappaB in diffuse large B-cell lymphoma. *Nature* **459**, 717-721, doi:10.1038/nature07968 (2009).

168 Davis, R. E. *et al.* Chronic active B-cell-receptor signalling in diffuse large B-cell lymphoma. *Nature* **463**, 88-92, doi:10.1038/nature08638 (2010).

169 Snow, A. L. *et al.* Congenital B cell lymphocytosis explained by novel germline CARD11 mutations. *J Exp Med* **209**, 2247-2261, doi:10.1084/jem.20120831 (2012).

170    Brohl, A. S. *et al.* Germline CARD11 Mutation in a Patient with Severe Congenital B Cell Lymphocytosis. *J Clin Immunol* **35**, 32-46, doi:10.1007/s10875-014-0106-4 (2015).

171    Buchbinder, D. *et al.* Mild B-cell lymphocytosis in patients with a CARD11 C49Y mutation. *J Allergy Clin Immunol* **136**, 819-821 e811, doi:10.1016/j.jaci.2015.03.008 (2015).

172    Lamason, R. L., McCully, R. R., Lew, S. M. & Pomerantz, J. L. Oncogenic CARD11 mutations induce hyperactive signaling by disrupting autoinhibition by the PKC-responsive inhibitory domain. *Biochemistry* **49**, 8240-8250, doi:10.1021/bi101052d (2010).

173    Isaacson, P. G. & Du, M. Q. MALT lymphoma: from morphology to molecules. *Nat Rev Cancer* **4**, 644-653, doi:10.1038/nrc1409 (2004).

174    Du, M. Q. MALT lymphoma : recent advances in aetiology and molecular genetics. *J Clin Exp Hematop* **47**, 31-42, doi:10.3960/jslrt.47.31 (2007).

175    Murga Penas, E. M. *et al.* Translocations t(11;18)(q21;q21) and t(14;18)(q32;q21) are the main chromosomal abnormalities involving MLT/MALT1 in MALT lymphomas. *Leukemia* **17**, 2225-2229, doi:10.1038/sj.leu.2403122 (2003).

176    Rosebeck, S. *et al.* Cleavage of NIK by the API2-MALT1 fusion oncoprotein leads to noncanonical NF-kappaB activation. *Science* **331**, 468-472, doi:10.1126/science.1198946 (2011).

177    Nie, Z. *et al.* Conversion of the LIMA1 tumour suppressor into an oncogenic LMO-like protein by API2-MALT1 in MALT lymphoma. *Nat Commun* **6**, 5908, doi:10.1038/ncomms6908 (2015).

178    Streubel, B. *et al.* T(14;18)(q32;q21) involving IGH and MALT1 is a frequent chromosomal aberration in MALT lymphoma. *Blood* **101**, 2335-2339, doi:10.1182/blood-2002-09-2963 (2003).

179    Chuang, S. S. *et al.* Pulmonary mucosa-associated lymphoid tissue lymphoma with strong nuclear B-cell CLL/lymphoma 10 (BCL10) expression and novel translocation t(1;2)(p22;p12)/immunoglobulin kappa chain-BCL10. *J Clin Pathol* **60**, 727-728, doi:10.1136/jcp.2006.041012 (2007).

180    de Oliveira, D. E., Ballon, G. & Cesarman, E. NF-kappaB signaling modulation by EBV and KSHV. *Trends Microbiol* **18**, 248-257, doi:10.1016/j.tim.2010.04.001 (2010).

181    Bonsignore, L. *et al.* A role for MALT1 activity in Kaposi's sarcoma-associated herpes virus latency and growth of primary effusion lymphoma. *Leukemia* **31**, 614-624, doi:10.1038/leu.2016.239 (2017).

182    Kataoka, K. *et al.* Integrated molecular analysis of adult T cell leukemia/lymphoma. *Nat Genet* **47**, 1304-1315, doi:10.1038/ng.3415 (2015).

183    Vallois, D. *et al.* Activating mutations in genes related to TCR signaling in angioimmunoblastic and other follicular helper T-cell-derived lymphomas. *Blood* **128**, 1490-1502, doi:10.1182/blood-2016-02-698977 (2016).

184    Wang, L. *et al.* Genomic profiling of Sezary syndrome identifies alterations of key T cell signaling and differentiation genes. *Nat Genet* **47**, 1426-1434, doi:10.1038/ng.3444 (2015).

185    da Silva Almeida, A. C. *et al.* The mutational landscape of cutaneous T cell lymphoma and Sezary syndrome. *Nat Genet* **47**, 1465-1470, doi:10.1038/ng.3442 (2015).

186    Demeyer, A., Staal, J. & Beyaert, R. Targeting MALT1 Proteolytic Activity in Immunity, Inflammation and Disease: Good or Bad? *Trends Mol Med* **22**, 135-150, doi:10.1016/j.molmed.2015.12.004 (2016).

187    Brustle, A. *et al.* The NF-kappaB regulator MALT1 determines the encephalitogenic potential of Th17 cells. *J Clin Invest* **122**, 4698-4709, doi:10.1172/JCI63528 (2012).

188    Mc Guire, C. *et al.* Paracaspase MALT1 deficiency protects mice from autoimmune-mediated demyelination. *J Immunol* **190**, 2896-2903, doi:10.4049/jimmunol.1201351 (2013).

189    Lowes, M. A., Suarez-Farinas, M. & Krueger, J. G. Immunology of psoriasis. *Annu Rev Immunol* **32**, 227-255, doi:10.1146/annurev-immunol-032713-120225 (2014).

190    Israel, L. & Mellett, M. Clinical and Genetic Heterogeneity of CARD14 Mutations in Psoriatic Skin Disease. *Front Immunol* **9**, 2239, doi:10.3389/fimmu.2018.02239 (2018).

191    Ruland, J. & Hartjes, L. CARD-BCL-10-MALT1 signalling in protective and pathological immunity. *Nat Rev Immunol* **19**, 118-134, doi:10.1038/s41577-018-0087-2 (2019).

192    Van Nuffel, E. *et al.* CARD14-Mediated Activation of Paracaspase MALT1 in Keratinocytes: Implications for Psoriasis. *J Invest Dermatol* **137**, 569-575, doi:10.1016/j.jid.2016.09.031 (2017).

193    McAuley, J. R., Freeman, T. J., Ekambaram, P., Lucas, P. C. & McAllister-Lucas, L. M. CARMA3 Is a Critical Mediator of G Protein-Coupled Receptor and Receptor Tyrosine Kinase-Driven Solid Tumor Pathogenesis. *Front Immunol* **9**, 1887, doi:10.3389/fimmu.2018.01887 (2018).

194    Cheng, L., Deng, N., Yang, N., Zhao, X. & Lin, X. Malt1 Protease Is Critical in Maintaining Function of Regulatory T Cells and May Be a Therapeutic Target for Antitumor Immunity. *J Immunol* **202**, 3008-3019, doi:10.4049/jimmunol.1801614 (2019).

195    Wang, Y. *et al.* MALT1 promotes melanoma progression through JNK/c-Jun signaling. *Oncogenesis* **6**, e365, doi:10.1038/oncsis.2017.68 (2017).

196    Yang, F. *et al.* miR-181d/MALT1 regulatory axis attenuates mesenchymal phenotype through NF-kappaB pathways in glioblastoma. *Cancer Lett* **396**, 1-9, doi:10.1016/j.canlet.2017.03.002 (2017).

197    Zhang, S., Pan, D., Jia, X. M., Lin, X. & Zhao, X. The CARMA3-BCL10-MALT1 (CBM) complex contributes to DNA damage-induced NF-kappaB activation and cell survival. *Protein Cell* **8**, 856-860, doi:10.1007/s13238-017-0441-3 (2017).

198    Wang, W., Mani, A. M. & Wu, Z. H. DNA damage-induced nuclear factor-kappa B activation and its roles in cancer progression. *J Cancer Metastasis Treat* **3**, 45-59, doi:10.20517/2394-4722.2017.03 (2017).

199    Pan, D. *et al.* The CBM Complex Underwrites NF-kappaB Activation to Promote HER2-Associated Tumor Malignancy. *Mol Cancer Res* **14**, 93-102, doi:10.1158/1541-7786.MCR-15-0229-T (2016).

200    Rehman, A. O. & Wang, C. Y. CXCL12/SDF-1 alpha activates NF-kappaB and promotes oral cancer invasion through the Carma3/Bcl10/Malt1 complex. *Int J Oral Sci* **1**, 105-118, doi:10.4248/IJOS.09059 (2009).

201    Mahanivong, C. *et al.* Protein kinase C alpha-CARMA3 signaling axis links Ras to NF-kappa B for lysophosphatidic acid-induced urokinase plasminogen activator expression in ovarian cancer cells. *Oncogene* **27**, 1273-1280, doi:10.1038/sj.onc.1210746 (2008).

202    McAuley, J. R. *et al.* MALT1 is a critical mediator of PAR1-driven NF-kappaB activation and metastasis in multiple tumor types. *Oncogene* **38**, 7384-7398, doi:10.1038/s41388-019-0958-4 (2019).

203    Delekta, P. C. *et al.* Thrombin-dependent NF-{kappa}B activation and monocyte/endothelial adhesion are mediated by the CARMA3.Bcl10.MALT1 signalosome. *J Biol Chem* **285**, 41432-41442, doi:10.1074/jbc.M110.158949 (2010).

204    Savage, P. A., Leventhal, D. S. & Malchow, S. Shaping the repertoire of tumor-infiltrating effector and regulatory T cells. *Immunol Rev* **259**, 245-258, doi:10.1111/imr.12166 (2014).

205    Di Pilato, M. *et al.* Targeting the CBM complex causes Treg cells to prime tumours for immune checkpoint therapy. *Nature* **570**, 112-116, doi:10.1038/s41586-019-1215-2 (2019).

206    Rosenbaum, M. *et al.* Bcl10-controlled Malt1 paracaspase activity is key for the immune suppressive function of regulatory T cells. *Nat Commun* **10**, 2352, doi:10.1038/s41467-019-10203-2 (2019).

207    Powers, J. C., Asgian, J. L., Ekici, O. D. & James, K. E. Irreversible inhibitors of serine, cysteine, and threonine proteases. *Chem Rev* **102**, 4639-4750, doi:10.1021/cr010182v (2002).

208    Hachmann, J. *et al.* Mechanism and specificity of the human paracaspase MALT1. *Biochem J* **443**, 287-295, doi:10.1042/BJ20120035 (2012).

209    Hailfinger, S. *et al.* Essential role of MALT1 protease activity in activated B cell-like diffuse large B-cell lymphoma. *Proc Natl Acad Sci U S A* **106**, 19946-19951, doi:10.1073/pnas.0907511106 (2009).

210    Ferch, U. *et al.* Inhibition of MALT1 protease activity is selectively toxic for activated B cell-like diffuse large B cell lymphoma cells. *J Exp Med* **206**, 2313-2320, doi:10.1084/jem.20091167 (2009).

211    Dai, B. *et al.* B-cell receptor-driven MALT1 activity regulates MYC signaling in mantle cell lymphoma. *Blood* **129**, 333-346, doi:10.1182/blood-2016-05-718775 (2017).

212    Xin, B. T. *et al.* Development of new Malt1 inhibitors and probes. *Bioorg Med Chem* **24**, 3312-3329, doi:10.1016/j.bmc.2016.03.035 (2016).

213    Wu, G. *et al.* Synthesis and structure-activity relationship studies of MI-2 analogues as MALT1 inhibitors. *Bioorg Med Chem* **26**, 3321-3344, doi:10.1016/j.bmc.2018.04.059 (2018).

214    Neumayer, V. E., Riederer, P., Danielczyk, W. & Seemann, D. [Biochemical findings in the brain in endogenous depression]. *Wien Med Wochenschr* **125**, 344-349 (1975).

215    Sachlos, E. *et al.* Identification of drugs including a dopamine receptor antagonist that selectively target cancer stem cells. *Cell* **149**, 1284-1297, doi:10.1016/j.cell.2012.03.049 (2012).

216    Schlauderer, F. *et al.* Structural analysis of phenothiazine derivatives as allosteric inhibitors of the MALT1 paracaspase. *Angew Chem Int Ed Engl* **52**, 10384-10387, doi:10.1002/anie.201304290 (2013).

217    Saba, N. S. *et al.* MALT1 Inhibition Is Efficacious in Both Naive and Ibrutinib-Resistant Chronic Lymphocytic Leukemia. *Cancer Res* **77**, 7038-7048, doi:10.1158/0008-5472.CAN-17-2485 (2017).

218    Nagel, D. *et al.* Combinatorial BTK and MALT1 inhibition augments killing of CD79 mutant diffuse large B cell lymphoma. *Oncotarget* **6**, 42232-42242, doi:10.18632/oncotarget.6273 (2015).

219    Li, Y. *et al.* Central role of myeloid MCPIP1 in protecting against LPS-induced inflammation and lung injury. *Signal Transduct Target Ther* **2**, 17066, doi:10.1038/sigtrans.2017.66 (2017).

220     Lee, C. H., Bae, S. J. & Kim, M. Mucosa-associated lymphoid tissue lymphoma translocation 1 as a novel therapeutic target for rheumatoid arthritis. *Sci Rep* **7**, 11889, doi:10.1038/s41598-017-12349-9 (2017).

221     Liu, W. *et al.* MALT1 inhibitors prevent the development of DSS-induced experimental colitis in mice via inhibiting NF-kappaB and NLRP3 inflammasome activation. *Oncotarget* **7**, 30536-30549, doi:10.18632/oncotarget.8867 (2016).

222     Lee, K. W., Kim, M. & Lee, C. H. Treatment of Dextran Sulfate Sodium-Induced Colitis with Mucosa-Associated Lymphoid Tissue Lymphoma Translocation 1 Inhibitor MI-2 Is Associated with Restoration of Gut Immune Function and the Microbiota. *Infect Immun* **86**, doi:10.1128/IAI.00091-18 (2018).

223     Mc Guire, C. *et al.* Pharmacological inhibition of MALT1 protease activity protects mice in a mouse model of multiple sclerosis. *J Neuroinflammation* **11**, 124, doi:10.1186/1742-2094-11-124 (2014).

224     Bardet, M. *et al.* The T-cell fingerprint of MALT1 paracaspase revealed by selective inhibition. *Immunol Cell Biol* **96**, 81-99, doi:10.1111/imcb.1018 (2018).

225     Meloni, L. *et al.* Mepazine Inhibits RANK-Induced Osteoclastogenesis Independent of Its MALT1 Inhibitory Function. *Molecules* **23**, doi:10.3390/molecules23123144 (2018).

226     Malinverni, C. *et al.* Cleavage by MALT1 induces cytosolic release of A20. *Biochem Biophys Res Commun* **400**, 543-547, doi:10.1016/j.bbrc.2010.08.091 (2010).

227     Hicke, L., Schubert, H. L. & Hill, C. P. Ubiquitin-binding domains. *Nat Rev Mol Cell Biol* **6**, 610-621, doi:10.1038/nrm1701 (2005).

228     Hoeller, D. *et al.* E3-independent monoubiquitination of ubiquitin-binding proteins. *Mol Cell* **26**, 891-898, doi:10.1016/j.molcel.2007.05.014 (2007).

229     Cho, J. J. *et al.* Hectd3 promotes pathogenic Th17 lineage through Stat3 activation and Malt1 signaling in neuroinflammation. *Nat Commun* **10**, 701, doi:10.1038/s41467-019-08605-3 (2019).

230     Li, Y. *et al.* The HECTD3 E3 ubiquitin ligase suppresses cisplatin-induced apoptosis via stabilizing MALT1. *Neoplasia* **15**, 39-48, doi:10.1593/neo.121362 (2013).

231     Staal, J. & Beyaert, R. A two-step activation mechanism of MALT1 paracaspase. *J Mol Biol* **419**, 1-3, doi:10.1016/j.jmb.2012.03.006 (2012).

232     Linares, J. F. *et al.* K63 polyubiquitination and activation of mTOR by the p62-TRAF6 complex in nutrient-activated cells. *Mol Cell* **51**, 283-296, doi:10.1016/j.molcel.2013.06.020 (2013).

233     Li, L. *et al.* Localization of A20 to a lysosome-associated compartment and its role in NFkappaB signaling. *Biochim Biophys Acta* **1783**, 1140-1149, doi:10.1016/j.bbamcr.2008.01.029 (2008).

234     Nakaya, M. *et al.* Inflammatory T cell responses rely on amino acid transporter ASCT2 facilitation of glutamine uptake and mTORC1 kinase activation. *Immunity* **40**, 692-705, doi:10.1016/j.immuni.2014.04.007 (2014).

235     Zheng, Y. *et al.* A role for mammalian target of rapamycin in regulating T cell activation versus anergy. *J Immunol* **178**, 2163-2170, doi:10.4049/jimmunol.178.4.2163 (2007).

236     Tavares, R. M. *et al.* The ubiquitin modifying enzyme A20 restricts B cell survival and prevents autoimmunity. *Immunity* **33**, 181-191, doi:10.1016/j.immuni.2010.07.017 (2010).

237    Chu, Y. *et al.* B cells lacking the tumor suppressor TNFAIP3/A20 display impaired differentiation and hyperactivation and cause inflammation and autoimmunity in aged mice. *Blood* **117**, 2227-2236, doi:10.1182/blood-2010-09-306019 (2011).

238    Hovelmeyer, N. *et al.* A20 deficiency in B cells enhances B-cell proliferation and results in the development of autoantibodies. *Eur J Immunol* **41**, 595-601, doi:10.1002/eji.201041313 (2011).

239    Honma, K. *et al.* TNFAIP3/A20 functions as a novel tumor suppressor gene in several subtypes of non-Hodgkin lymphomas. *Blood* **114**, 2467-2475, doi:10.1182/blood-2008-12-194852 (2009).

240    Kato, M. *et al.* Frequent inactivation of A20 in B-cell lymphomas. *Nature* **459**, 712-716, doi:10.1038/nature07969 (2009).

241    Schmitz, R. *et al.* TNFAIP3 (A20) is a tumor suppressor gene in Hodgkin lymphoma and primary mediastinal B cell lymphoma. *J Exp Med* **206**, 981-989, doi:10.1084/jem.20090528 (2009).

242    Okosun, J. *et al.* Integrated genomic analysis identifies recurrent mutations and evolution patterns driving the initiation and progression of follicular lymphoma. *Nat Genet* **46**, 176-181, doi:10.1038/ng.2856 (2014).

243    Haase, O. *et al.* TNFAIP3 and IL12B gene polymorphisms associated with psoriasis vulgaris in an Egyptian cohort. *J Eur Acad Dermatol Venereol* **29**, 1297-1301, doi:10.1111/jdv.12799 (2015).

244    Indhumathi, S. *et al.* TNFAIP3 and TNIP1 polymorphisms confer psoriasis risk in South Indian Tamils. *Br J Biomed Sci* **72**, 168-173, doi:10.1080/09674845.2015.11665748 (2015).

245    Li, X. L., Yu, H. & Wu, G. S. Investigating the genetic association of HCP5, SPATA2, TNIP1, TNFAIP3 and COG6 with psoriasis in Chinese population. *Int J Immunogenet* **41**, 503-507, doi:10.1111/iji.12150 (2014).

246    Nair, R. P. *et al.* Genome-wide scan reveals association of psoriasis with IL-23 and NF-kappaB pathways. *Nat Genet* **41**, 199-204, doi:10.1038/ng.311 (2009).

247    Sohn, K. C. *et al.* The inhibitory effect of A20 on the inflammatory reaction of epidermal keratinocytes. *Int J Mol Med* **37**, 1099-1104, doi:10.3892/ijmm.2016.2514 (2016).

248    Devos, M. *et al.* Keratinocyte Expression of A20/TNFAIP3 Controls Skin Inflammation Associated with Atopic Dermatitis and Psoriasis. *J Invest Dermatol* **139**, 135-145, doi:10.1016/j.jid.2018.06.191 (2019).

249    Lippens, S. *et al.* Keratinocyte-specific ablation of the NF-kappaB regulatory protein A20 (TNFAIP3) reveals a role in the control of epidermal homeostasis. *Cell Death Differ* **18**, 1845-1853, doi:10.1038/cdd.2011.55 (2011).

250    Mellett, M. *et al.* CARD14 Gain-of-Function Mutation Alone Is Sufficient to Drive IL-23/IL-17-Mediated Psoriasiform Skin Inflammation In Vivo. *J Invest Dermatol* **138**, 2010-2023, doi:10.1016/j.jid.2018.03.1525 (2018).

251    Kawadler, H., Gantz, M. A., Riley, J. L. & Yang, X. The paracaspase MALT1 controls caspase-8 activation during lymphocyte proliferation. *Mol Cell* **31**, 415-421, doi:10.1016/j.molcel.2008.06.008 (2008).

# Annex I – Publication of Project 1

# Allosteric activation of MALT1 by its ubiquitin-binding Ig3 domain

Rebekka Schairer[a,1], Gareth Hall[b,c,1], Ming Zhang[a,1,2], Richard Cowan[b,c], Roberta Baravalle[b,c], Frederick W. Muskett[b,c], Peter J. Coombs[d], Chido Mpamhanga[d], Lisa R. Hale[d], Barbara Saxty[d], Justyna Iwaszkiewicz[e], Chantal Décaillet[a], Mai Perroud[a], Mark D. Carr[b,c,3], and Margot Thome[a,3]

[a]Department of Biochemistry, University of Lausanne, 1066 Epalinges, Switzerland; [b]Department of Molecular and Cell Biology, University of Leicester, LE1 7RH Leicester, United Kingdom; [c]Leicester Institute of Structural and Chemical Biology, University of Leicester, LE1 7RH Leicester, United Kingdom; [d]LifeArc, Accelerator Building, Open Innovation Campus, SG1 2FX Stevenage, United Kingdom; and [e]Swiss Institute of Bioinformatics, 1015 Lausanne, Switzerland

The catalytic activity of the protease MALT1 is required for adaptive immune responses and regulatory T (Treg)-cell development, while dysregulated MALT1 activity can lead to lymphoma. MALT1 activation requires its monoubiquitination on lysine 644 (K644) within the Ig3 domain, localized adjacent to the protease domain. The molecular requirements for MALT1 monoubiquitination and the mechanism by which monoubiquitination activates MALT1 had remained elusive. Here, we show that the Ig3 domain interacts directly with ubiquitin and that an intact Ig3-ubiquitin interaction surface is required for the conjugation of ubiquitin to K644. Moreover, by generating constitutively active MALT1 mutants that overcome the need for monoubiquitination, we reveal an allosteric communication between the ubiquitination site K644, the Ig3-protease interaction surface, and the active site of the protease domain. Finally, we show that MALT1 mutants that alter the Ig3-ubiquitin interface impact the biological response of T cells. Thus, ubiquitin binding by the Ig3 domain promotes MALT1 activation by an allosteric mechanism that is essential for its biological function.

protease | structure | ubiquitin | signaling | T cell

The paracaspase MALT1 is a proteolytic enzyme whose function is essential for adaptive immune responses and the development of particular lymphocyte subsets, such as Treg cells, marginal zone, and B1 B cells (1–6). MALT1 is activated upon triggering of the B- or T cell antigen receptors and other immunoreceptors, such as activating natural killer cell (NK) receptors or Fc receptors (7). A variety of G protein coupled receptors and certain tyrosine receptor kinases have also been reported to signal via MALT1 (7). A common feature of MALT1-activating receptors is their capacity to induce the formation of so-called CARMA-BCL10-MALT1 (CBM) complexes, comprising a CARD-containing scaffold protein, the adaptor protein BCL10, and MALT1 (8).

Based on structural studies on in vitro reconstituted CBM signalosomes from lymphocytes, which contain the scaffold protein CARMA1 (also known as CARD11), it has been proposed that the CBM complex adopts a helical filamentous structure in which CARMA1 nucleates the polymerization of BCL10 into filaments that can incorporate MALT1 (9, 10). MALT1 contains an N-terminal death domain (DD) that binds to the core of the BCL10 filament by interacting with the BCL10 CARD motif (9). The MALT1 DD is followed by two Ig-like domains, the protease domain, a third Ig-like domain, and an unstructured C-terminal extension (11, 12). The C-terminal part of MALT1 that comprises the protease domain is thought to protrude from the filamentous core (9), but the exact conformation and activation status of MALT1 within the BCL10/MALT1 fibers remain unknown. The crystallographic analysis of highly purified constructs of MALT1 containing the protease and the adjacent Ig3 domain has revealed that the protease domain can dimerize (13, 14). The dimer crystals additionally show that the protease and Ig3 domains physically interact and undergo a rotational movement upon binding of a substrate analog (13, 14).

Using biochemical approaches, we have previously shown that MALT1 activation requires its monoubiquitination on K644, a lysine residue situated at the surface of the Ig3 domain (15). Moreover, we demonstrated an interaction of ubiquitin with an unknown binding site within the C-terminal half of MALT1, which comprises the protease domain, the Ig3 domain, and a nonstructured C-terminal extension (15). However, the precise location of the ubiquitin-binding site and the way by which ubiquitin binding contributes to MALT1 activation have remained unknown.

Here, we present experimental evidence that suggests that ubiquitin binding to the Ig3 domain is required for MALT1 monoubiquitination, which, in turn, perturbs an inhibitory interaction of the Ig3 domain with the protease domain and induces conformational changes within the catalytic domain that lead to enhanced activity.

## Results

**Monomeric Ubiquitin Binds to the Ig3 Domain of MALT1.** We had previously shown that ubiquitin can interact physically with a C-terminal portion of MALT1 that comprises its protease domain, the Ig3 domain, and a nonstructured C-terminal extension (15).

IMMUNOLOGY AND INFLAMMATION

To identify key ubiquitin residues involved in the binding to MALT1, we monitored differences in the $^{15}$N/$^1$H HSQC spectrum of uniformly labeled ubiquitin (1–76) induced by the addition of MALT1 (Fig. 1$A$). The observed minimal shifts in backbone amide signals of ubiquitin upon MALT1 addition clearly identified a contiguous interaction surface showing significant shifts for 10 residues, including I13, G47, K6, K48, H68, Q49, L69, V70, L71, and R72, centered around I44 (Fig. 1$A$ and *SI Appendix*, Fig. S1$A$). These residues are predominantly localized to the β3–β5 strands collectively forming a continuous patch of ~172 Å$^2$ on the surface of ubiquitin (Fig. 1$B$). This surface patch comprises several positively charged amino acids, including K6, K48, H68, and R72, which together form a striking positively charged region on ubiquitin (Fig. 1$C$). To identify the

MALT1 residues involved in the interaction with ubiquitin, we then generated a soluble monomeric MALT1 construct comprising the protease and Ig3 domain (residues 339–719) and monitored changes in the $^{15}$N/$^1$H TROSY spectrum of uniformly labeled MALT1 induced by the addition of ubiquitin. Upon addition of increasing concentrations of free ubiquitin, we observed significant shifts in the backbone amide signals of several residues of MALT1, including E624, I625, Y692, L695, E696, D697, and T698 (Fig. 1$D$ and *SI Appendix*, Fig. S1$B$). These residues are mainly located within the β3/β4 and β6/β7 loops at the surface of the MALT1 Ig3 domain on the side opposing the Ig3-protease domain interaction surface (Fig. 1$E$), which combine to form a negatively charged area of ~246 Å$^2$ on the surface of MALT1 (Fig. 1$F$). To provide additional evidence for the
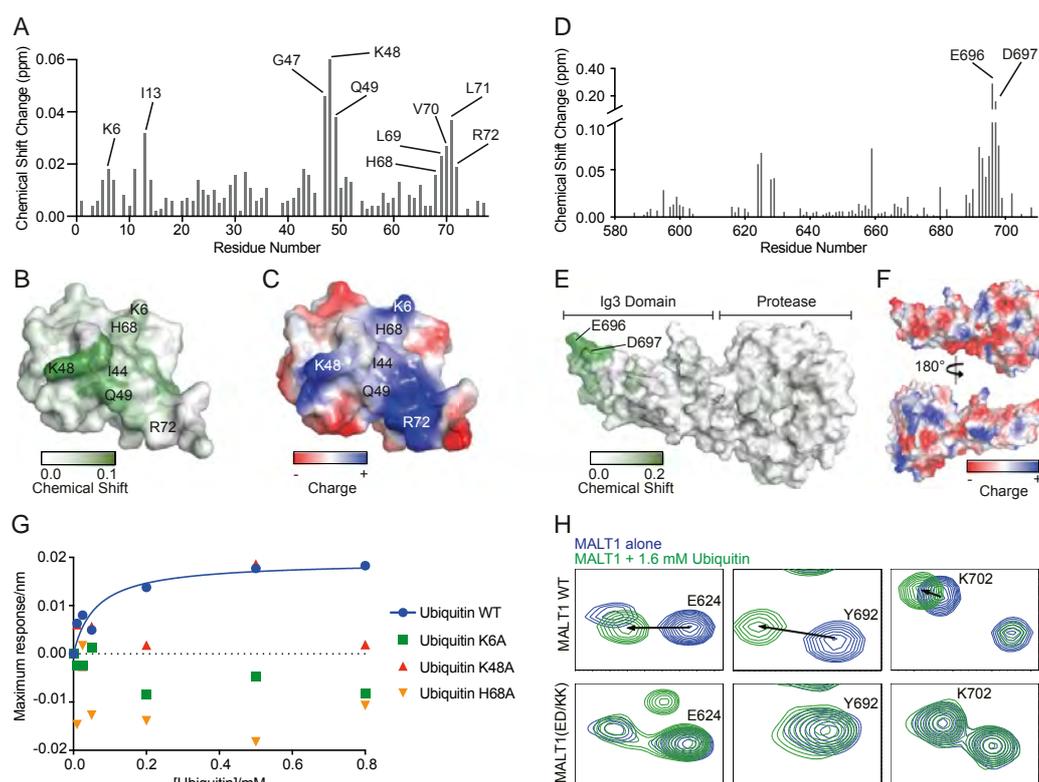


**Fig. 1.** Monomeric ubiquitin binds to the Ig3 domain of MALT1. (*A*) Backbone amide minimal shifts seen for $^{15}$N-labeled human ubiquitin (residues 1–76) upon mixing with an over fivefold molar excess of purified MALT1 (residues 339–719). (*B*) Mapping of the minimal shift backbone amide NMR data onto a surface representation of ubiquitin with significantly perturbed residues (shift >0.01 ppm) colored with a gradient from white to green. Residues for which no minimal shift data were obtained are also shown in white. (*C*) An electrostatic surface representation of ubiquitin shown in the same orientation as *B* with areas of significant positive charge indicated in blue, and areas with negative charge indicated in red. Images in *B* and *C* were prepared using PyMOL. (*D* and *E*) As in *A* and *B*, showing backbone amide shifts seen for $^{15}$N-labeled human MALT1 (residues 339–719) upon addition of an over 10-fold molar excess of human ubiquitin (residues 1–76). Data in *D* are only shown for amino acids constituting the Ig3 domain (580–709) as no significant changes were seen for backbone amide signals from residues in the MALT1 protease domain. (*F*) Surface charge representation of the MALT1 Ig3 and protease domains (positive charges are indicated in blue, and negative charges are indicated in red), highlighting the negatively charged surface around the region affected by ubiquitin binding. (*G*) MALT1 (residues 339–719) maximum binding response as a function of increasing concentrations of ubiquitin (residues 1–76) WT (blue filled circles), K6A (green filled squares), K48A (red filled upward triangles), and H68A (orange filled downward triangles). MALT1 WT binds to ubiquitin WT according to a one-site saturation-binding model with a dissociation constant ($K_D$) of ~62.0 μM. No binding is detected between MALT1 WT and ubiquitin variants K6A, K48A, and H68A. (*H*) Highlighted backbone amide peaks from the $^{15}$N-$^1$H TROSY spectra for E624, Y692, and K702, which show substantial shifts in MALT1 WT but not in MALT1(ED/KK) upon addition of ubiquitin.

binding of ubiquitin to the MALT1 Ig3 domain and gain insight into the underlying binding affinity, we used the Octet system (FortéBio) which measures interactions between purified proteins based on changes in light reflection from a protein-coated biosensor tip exposed to a protein-binding partner in solution. Under these conditions, ubiquitin bound to the MALT1 construct comprising the protease and Ig3 domains (residues 339–719), although with low affinity ($\sim$ 62 μM). Binding was lost upon mutation of residues within the positively charged surface patch of ubiquitin (K6A, K48A, or H68A) (Fig. 1*G*). Vice versa, wild-type (WT) ubiquitin was no longer able to induce changes in the $^{15}$N/$^1$H TROSY spectrum of MALT1 when the negatively charged Ig3 residues E696 and D697 were mutated into lysine (MALT1(ED/KK)). Indeed, we observed a loss of ubiquitin-induced shifts in the backbone amide signals of several surrounding Ig3 residues, including E624, Y692, and K702 (Fig. 1*H* and *SI Appendix*, Fig. S1*C*). Collectively, these findings suggest that the surface residues E696 and D697 within the ubiquitin-interacting surface patch of the Ig3 domain physically interact with the positively charged surface area surrounding isoleucine 44 (I44) in ubiquitin.

**The Ig3-Ubiquitin Interaction Is Required for Monoubiquitination-Dependent MALT1 Activation.** We then mutated several of the Ig3 MALT1 residues identified by 2D-NMR to be involved in ubiquitin binding into alanine and assessed the effect of these point mutations on the catalytic activity of MALT1. For this, we used a previously described cellular MALT1 activity assay in which MALT1 is activated by coexpression of an oncogenic, constitutively active mutant of CARMA1, G116S (16), and protease activity is assessed using a previously described fluorescence resonance energy transfer (FRET)-based reporter assay (15). This assay is based on the MALT1-dependent cleavage of an eYFP-linker-eCFP construct containing the linker sequence LVSR, which is derived from the MALT1 substrate RelB (17). Cleavage of the linker causes a loss of FRET and gain in CFP fluorescence that can be quantified by flow cytometry (15). Using this assay, we found that mutation of I625 into alanine (I625A) led to an almost complete loss of activity (*SI Appendix*, Fig. S2*A*) that was comparable to the defect of a previously described monoubiquitination-deficient mutant K644R (15). However, when comparable plasmid concentrations were used for transfection, the I625A expression construct consistently showed reduced expression and solubility. The position of I625, which points toward the inside of the Ig3 domain, suggests that its mutation may lead to misfolding of the domain as the aliphatic side chain sits within a hydrophobic pocket formed by residues V598, Y692, P622, and Y690; we, therefore, excluded it from further analysis. Individual mutation of D595, E624, T698, and K702 into alanine did not reduce MALT1 activity, but mutation of Y692 or of both E696 and D697 into alanine (ED/AA) led to a partial or strong reduction, respectively, of MALT1 activity (Fig. 2*A* and *SI Appendix*, Fig. S2*A*). This reduction of activity was even more pronounced when the two negatively charged surface residues were mutated into lysine (ED/KK) (Fig. 2*A*).

Next, we assessed the functional consequences of the above-described perturbations of the ubiquitin-MALT1 interaction on the protease function of MALT1 in living cells. We first monitored the capacity of the ED/AA and ED/KK mutants to cleave RelB and CYLD, two known MALT1 substrates with inhibitory roles in the NF-κB and AP-1 transcriptional pathways, respectively (17, 18). Cleavage of RelB and CYLD was easily induced upon their coexpression with oncogenic CARMA1 and WT MALT1 in 293T cells (Fig. 2*B* and *SI Appendix*, Fig. S2*B*). The cleavage of these substrates was entirely or strongly impaired when using catalytically inactive (C464A) or monoubiquitination-deficient (K644R) MALT1 mutants, respectively (Fig. 2*B* and *SI Appendix*, Fig. S2*B*). Mutation of the E696/D697 residues into AA or KK

led to a partial or strong reduction of substrate cleavage, respectively (Fig. 2*B* and *SI Appendix*, Fig. S2*B*).

To gain insight into the reasons underlying the reduced catalytic activity of the ED/KK mutant of MALT1, we next assessed its status of monoubiquitination, which we had previously identified as an important hallmark of MALT1 activation. In 293T cells, MALT1 monoubiquitination can be induced by coexpression of MALT1 with its binding partner BCL10 (15). In this system, the ubiquitin-binding-deficient ED/KK mutant showed a dramatically decreased capacity to become monoubiquitinated (Fig. 2*C*). To test whether mutation of the ED motif affected MALT1 monoubiquitination in T cells, we stably expressed various MALT1 constructs in a MALT1-deficient Jurkat T cell line. In these cells, MALT1 becomes monoubiquitinated on K644 as a consequence of cellular stimulation with phorbol myristate acetate (PMA) and the calcium ionophore ionomycin (mimicking strong T cell activation) (15). In stimulated cells, monoubiquitination was, indeed, detectable for WT and catalytically inactive (C464A) MALT1 but absent for the monoubiquitination-deficient K644R mutant as reported (15) (Fig. 2*D*). The ubiquitin-binding deficient ED/AA and ED/KK mutants showed impaired monoubiquitination (Fig. 2*D*). This suggests that ubiquitin binding by the Ig3 domain is required for MALT1 monoubiquitination, possibly in a manner that is similar to what has been shown for other ubiquitin-binding proteins (19, 20). Thus, via the ubiquitin-binding Ig3 domain, MALT1 may promote its own monoubiquitination by recruiting a ubiquitin-charged E2 or E3 enzyme that remains to be identified.

**The Ig3-Ubiquitin Interaction Is Required for MALT1-Dependent T Cell Activation.** To explore the biological consequences of perturbing the Ig3-ubiquitin interactions, we analyzed the effect of corresponding MALT1 mutants on T cell activation. For this purpose, we first silenced endogenous expression of MALT1 by CRISPR-mediated gene targeting in Jurkat T cells and then reconstituted the cells with various MALT1 mutants (Fig. 2*E* and *SI Appendix*, Fig. S2*C*). We then assessed diverse readouts of MALT1-dependent T cell activation upon stimulation of the Jurkat T cells with PMA and ionomycin. To assess MALT1 protease activity, we monitored the stimulation-induced cleavage of the MALT1 substrates CYLD and Roquin-1. As expected, we saw a complete or strong reduction of substrate cleavage for the cells reconstituted with the catalytically inactive (C464A) or monoubiquitination-deficient (K644R) mutants. The E696 and D697 mutants, ED/AA and ED/KK, showed a partial reduction of substrate cleavage (Fig. 2*E*). Stimulation-induced phosphorylation of the NF-κB inhibitor IκBα and activation of the c-Jun N-terminal kinase (JNK) pathway, which can be assessed by monitoring JNK phosphorylation, depends only on the scaffold function of MALT1 (3, 4, 6, 17, 21). Neither phosphorylation of IκBα nor activation of JNK was affected by ED/AA or ED/KK mutation (Fig. 2 *D* and *E*). This indicates that the identified ubiquitin-binding domain of MALT1 is necessary for its protease function but not for its scaffold function. The scaffold function of MALT1 requires its interaction with the ubiquitin ligase TRAF6, which mediates the recruitment and activation of the IκB kinase (IKK) complex to promote the phosphorylation and subsequent degradation of the NF-κB inhibitor IκBα (22–24). Consistent with an unaltered capacity to support IκBα and JNK phosphorylation, the MALT1 mutants ED/AA, ED/KK, and the ubiquitination-deficient MALT1 mutant K644R were still able to interact with TRAF6 upon coexpression in 293T cells (*SI Appendix*, Fig. S2*D*), in contrast to a MALT1 construct (E3A) mutated in three previously reported TRAF6-binding sites (22, 23). Thus, disrupting the region mediating the ubiquitin-MALT1 interaction impaired MALT1-dependent substrate cleavage in vivo but did not affect the scaffold function of MALT1.

Finally, we monitored the effect of MALT1 ED/AA and ED/KK mutants on the stimulation-induced transcription and
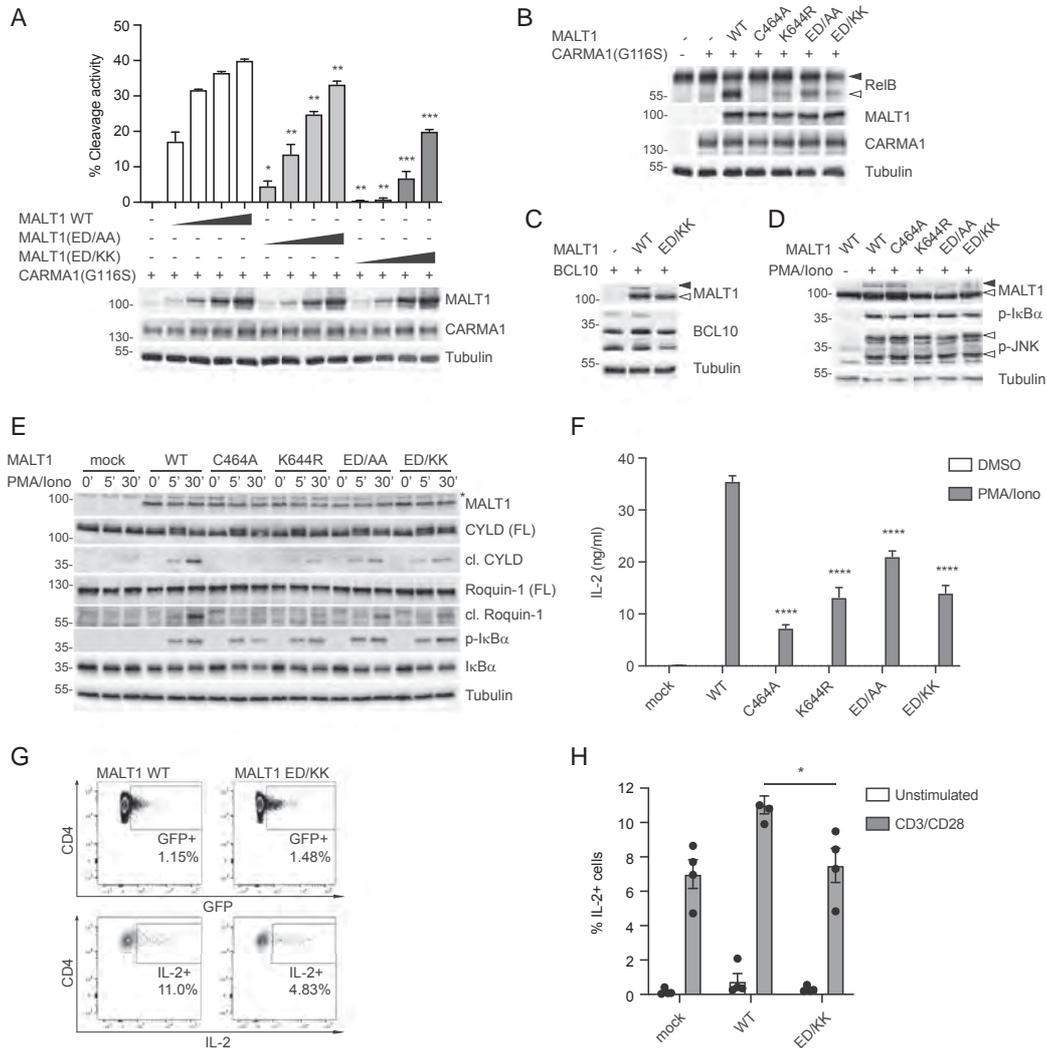
**Fig. 2.** The Ig3-ubiquitin interaction is required for monoubiquitination-dependent MALT1 activation and T cell function. (*A* and *B*) Assessment of MALT1-dependent FRET reporter cleavage (*A*) or RelB cleavage (*B*) in 293T cells. The reporter or RelB were coexpressed with oncogenic CARMA1(G116S) and WT MALT1 or the indicated MALT1 mutants of E696 and D697 (ED/AA or ED/KK). FRET reporter cleavage was assessed by flow cytometry (*A*) and protein expression, and RelB cleavage was assessed by Western blot as indicated (*A* and *B*). Positions of uncleaved (black arrowhead) and cleaved (open arrowhead) RelB are indicated. (*C*) HEK 293T cells were transfected with the indicated expression constructs for MALT1 and BCL10 and analyzed for MALT1 monoubiquitination by Western blot as indicated. Positions of monoubiquitinated MALT1 (black arrowhead) and unmodified MALT1 (open arrowhead) are indicated. Multiple bands in the BCL10 blot correspond to previously described phosphorylation isoforms (39). (*D*) MALT1-deficient Jurkat T cells were reconstituted with the indicated MALT1 constructs and incubated for 1 h with the MALT1 active site inhibitor z-LVSR-fmk before stimulation with PMA and ionomycin for 1 h. MALT1 monoubiquitination, phosphorylation of IκBα, and phosphorylation of JNK were analyzed by Western blot. (*E*) MALT1-deficient Jurkat T cells reconstituted with the indicated empty vector (mock) or MALT1 constructs were stimulated with PMA and ionomycin for 0, 5, or 30 min. Substrate cleavage (CYLD and Roquin-1) and phosphorylation of IκBα were analyzed by Western blot. Tubulin was used as a loading control, and positions of molecular weight markers (in kDa) are indicated (*A*–*E*). (*F*) IL-2 secretion of MALT1-deficient Jurkat T cells reconstituted with the indicated MALT1 constructs, stimulated for 16 h with PMA and ionomycin or solvent alone. (*G* and *H*) Analysis of intracellular IL-2 in isolated primary CD4$^+$ T cells from four healthy donors, lentivirally transduced with mock, MALT1 WT, or MALT1(ED/KK) constructs and stimulated with anti-CD3, anti-CD28, and a cross-linking antibody in the presence of brefeldin A. The percentage of IL-2$^+$ cells among infected GFP$^+$ cells was determined by flow cytometry. (*G*) Gating strategy for one donor for MALT1 WT and MALT1(ED/KK) transduced cells. (*H*) Combined analysis of four donors. Bars represent means ± SD (*A* and *F*) or means ± SEM (*H*); *$P < 0.05$, **$P < 0.01$, ***$P < 0.001$, and ****$P < 0.0001$. Data are representative of three (*A*–*D*), two (*E*), and four (*F* and *H*) experiments.

secretion of the cytokine IL-2, a major NF-κB target, in Jurkat T cells and primary human T cells. Similar to the catalytically inactive form of MALT1 (C464A), the monoubiquitination-deficient (K644R) or ubiquitin-binding-deficient (ED/KK) MALT1 mutants showed a strong impairment of their capacity to support the transcription and secretion of IL-2 in Jurkat T cells, an effect that was less pronounced for the ED/AA mutant (Fig. 2*F* and *SI Appendix*, Fig. S2*E*). The residual transcription and secretion of IL-2 observed with the catalytically inactive mutants in these assays are due to their remaining scaffold functions (15, 25). Finally, we transduced purified primary human CD4 T cells with lentiviral expression vectors for MALT1 and GFP and assessed the capacity of the transduced GFP-positive T cells to produce IL-2 by flow cytometry. In transduced T cells from four independent healthy donors, we observed that the ED/KK mutant was significantly impaired in its capacity to support stimulation-induced IL-2 production compared to WT MALT1 (Fig. 2 *G* and *H*). Thus, the intact ubiquitin-interaction surface of the Ig3 domain is required for optimal MALT1-dependent T cell activation.

**The Ubiquitin-Binding Deficient Ig3 Mutants Can Still Be Activated by Functional Ubiquitin.** So far, our data suggested that the Ig3 domain binds ubiquitin for the purpose of its conjugation to MALT1, but

it remained unclear whether the ubiquitin-binding site in the Ig3 domain was also required to mediate the activating effect of MALT1 monoubiquitination. We have previously shown that MALT1 can be artificially activated by the generation of a MALT1-ubiquitin (MALT1-Ub) fusion protein that mimics monoubiquitination by covalent attachment of ubiquitin to the MALT1 C terminus and that this fusion overcomes the catalytic defect of the ubiquitination-deficient K644R mutant (15). Therefore, we next assessed whether introduction of the ubiquitin-binding-deficient Ig3 mutations would affect the activity of the MALT1(K644R)-Ub constructs. Indeed, neither the ED/AA nor the ED/KK mutations affected the activity of the MALT1(K644R)-Ub, suggesting that monoubiquitin, once covalently attached to MALT1, promotes MALT1 activation in a manner that is independent of the ubiquitin-binding site in the Ig3 domain (Fig. 3*A*). Next, we assessed the capacity of ubiquitin to induce MALT1 activation in a different in vitro setting in which MALT1 activity is monitored by the fluorogenic cleavage of the optimal tetrapeptide substrate LVSR-amc (25, 26). We observed that purified recombinant ubiquitin can activate purified recombinant MALT1 (aa 199–824) in a dose-dependent manner (*SI Appendix*, Fig. S3*A*) and that this required the presence of the hydrophobic ubiquitin surface residue I44 (*SI Appendix*, Fig. S3*B*) (27).
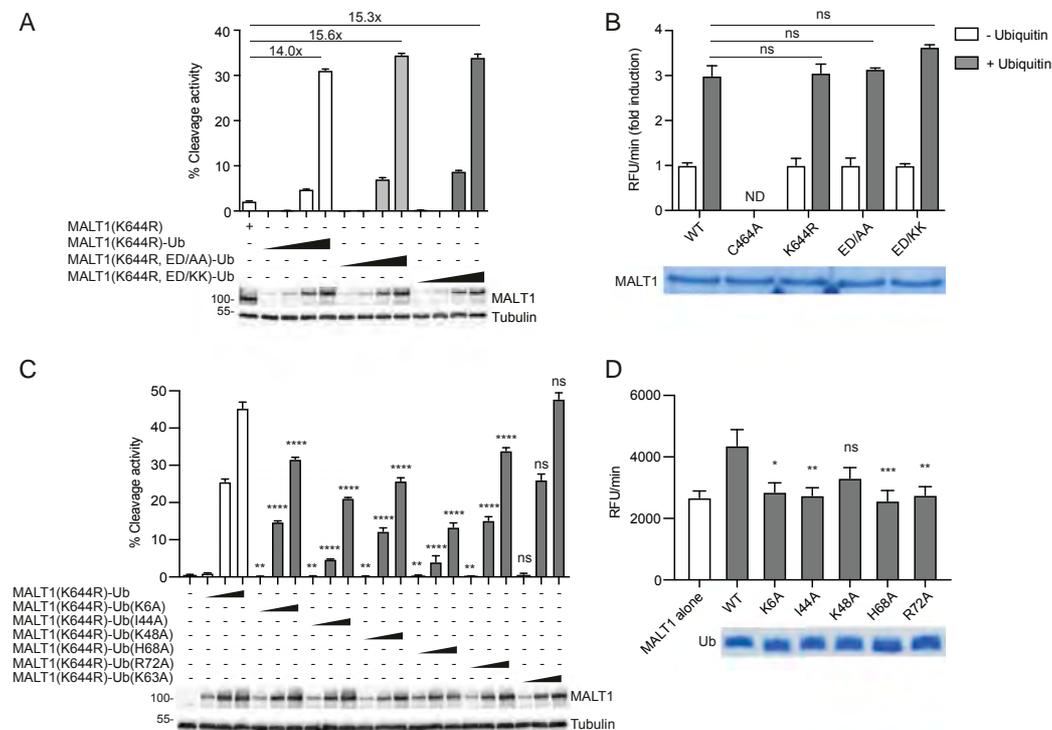


**Fig. 3.** The ubiquitin-binding deficient Ig3 mutants can still be activated by functional ubiquitin. (*A* and *C*) Flow cytometric assessment of MALT1-dependent FRET reporter cleavage in 293T cells. The reporter was coexpressed with the indicated MALT1-ubiquitin fusion constructs. Protein expression was controlled by Western blotting as indicated. Positions of molecular weight markers (in kDa) are indicated. (*B* and *D*) In vitro cleavage activity of indicated recombinant purified MALT1 constructs (residues 199–824, 0.6 μM) in the absence or presence of recombinant purified ubiquitin constructs (0.1 mM). Protein amount was controlled by Coomassie-blue staining as indicated. Data are representative of two experiments (*A–D*). Bars represent means ± SD; ns, nonsignificant, *$P < 0.05$, **$P < 0.01$, ***$P < 0.001$, and ****$P < 0.0001$.

Schairer et al.

IMMUNOLOGY AND INFLAMMATION

Importantly, in this system, ubiquitin cannot be covalently linked to K644 of MALT1, so to reach detectable MALT1 cleavage activity, high concentrations of free monoubiquitin have to be added. To test whether ubiquitin could still activate the ubiquitin-binding-deficient MALT1 Ig3 mutants, we generated these in recombinant purified form and tested their activity in the absence and presence of recombinant monoubiquitin. Under these conditions, and similar to our previous observations in the in vivo system, we found that addition of free ubiquitin was still able to activate both the ubiquitin conjugation- and the ubiquitin-binding-deficient MALT1 mutants (Fig. 3B). Thus, binding of the Ig3 domain to ubiquitin serves to promote monoubiquitination, but upon its covalent attachment in vivo (Fig. 3A) or addition in excess in vitro (Fig. 3B and *SI Appendix*, Fig. S3A), ubiquitin promotes MALT1 activation by additional means.

We next assessed whether mutations of four positively charged ubiquitin residues, K6, K48, H68, and R72, which are located close to I44, affected the capacity of ubiquitin to activate MALT1 upon their fusion to the C terminus of MALT1. At comparable levels of expression, we observed that mutation of I44, but also of the positively charged surface residues K6, K48, H68, and R72, reduced the capacity of the C-terminally fused ubiquitin to promote MALT1-dependent FRET reporter cleavage in 293T cells (Fig. 3C). In contrast, mutation of K63 to alanine, which is not located on the positively charged surface surrounding I44, had no effect on the cleavage activity of the MALT1-Ub fusion protein (Fig. 3C). Next, we monitored the capacity of recombinant purified ubiquitin constructs with these mutations to activate recombinant purified MALT1 in vitro. This revealed that mutation of I44 or of the four surrounding positively charged residues, K6, K48, H68, and R72 also impaired the capacity of free ubiquitin to activate MALT1 (Fig. 3D). Together with the results obtained in Fig. 1, these findings suggest that the positively charged ubiquitin surface surrounding I44, incorporating residues K6, K48, H68, and R72, is important for both its recruitment by the Ig3 domain and subsequent conjugation to K644 and for the subsequent monoubiquitin-dependent activation of MALT1.

**Mutation of Y657 Induces Coordinated Conformational Changes in the Loop Connecting K644 to Y657 and the Active Site.** The comparison of MALT1 crystal structures in the absence (PDB: 3V55) and presence (PDB: 3UO8) of a peptide inhibitor and substrate analog z-VRPR-fmk suggests that substrate binding induces a rotational movement of the protease domain with respect to the Ig3 domain (13). In the peptide-bound conformation, Y657 on the Ig3 domain forms a hydrogen bond with E368 and hydrophobic interactions with Y367 and L506, located on the surface of the protease domain (14) (Fig. 4A). Whether these interactions are relevant to the activation of MALT1 by monoubiquitination remains unknown. In our hands, addition of free ubiquitin did not show noticeable effects on backbone amide signals in this region (Fig. 1D and *SI Appendix*, Fig. S1B). However, the NMR approach relied on the use of monomeric MALT1 and free (not K644-attached) ubiquitin. Since the active form of MALT1 has been proposed to be a dimer (13, 14, 28), our approach is likely to miss additional conformational changes that could be induced by interactions of ubiquitin with MALT1 dimers as well as pulling or pushing forces that might be exerted by ubiquitin on the Ig3 domain as a result of its covalent attachment to K644. We reasoned that the latter may structurally alter the loop extending from K644 to Y657 and thereby potentially affect the previously reported hydrophobic interactions between residues Y657 on the Ig3 domain and L506 and Y367 in the protease domain, which are dramatically altered upon binding of the substrate analog z-VRPR-fmk (14) (Fig. 4A).

To test the proposed model, we next assessed the activity and structure of a Y657A MALT1 mutant in vitro. In the absence of ubiquitin, the Y657A mutant was hyperactive compared to WT

MALT1. Addition of ubiquitin led to a significant increase in the activity of WT MALT1 but had no significant impact on the activity of the hyperactive Y657A mutant (Fig. 4B). Thus, a mutational disruption of the Ig3-protease interaction rendered this mutant independent of ubiquitin-mediated activation. Consistent with this idea, the MALT1 Y657A mutant also no longer depended on ubiquitination-dependent activation through oncogenic CARMA1 in vivo (Fig. 4C and *SI Appendix*, Fig. S4A). To further probe the conformational effect of the Y657A mutation on MALT1 and to potentially understand how attachment of ubiquitin at K644 might be coupled to conformational changes at the Ig3-protease interface leading to the activation of the protease, a $^{15}N/^1H$ TROSY spectrum of uniformly labeled MALT1 Y657A (339–719) was collected and compared with the spectrum of the WT form of MALT1 (*SI Appendix*, Fig. S4 B and C). It should be noted that, due to the overlapped nature of peaks within the $^{15}N/^1H$ TROSY spectrum of MALT1, which contains backbone amide signals from over 365 residues, the minimal shift analysis presented here is a conservative method for determining residues that have undergone significant chemical shift perturbations due to the Y657A substitution, so some of the affected residues may not be identified. Comparing the $^{15}N/^1H$ TROSY spectra of WT MALT1 with MALT1 Y657A revealed that this single point mutation led to a significant number of chemical shift perturbations within both the Ig3 and the protease domains (Fig. 4 D and E and *SI Appendix*, Fig. S4 C and D), which extended beyond the region immediately surrounding the mutated residue. In particular, several of the residues in the loop region linking Y657 to K644 had chemical shift perturbations greater than 0.05 ppm (Fig. 4E), including D645, N647, K648, T650, E652, T654, and S656, suggesting the possibility of signal transfer between K664 and Y657 upon ubiquitin attachment. A number of residues within the protease domain also experienced very significant chemical shift perturbations (Fig. 4 D and E and *SI Appendix*, Fig. S4D), including L363, V364, Y367, and E368, located in the α1-helix of the protease domain directly adjacent to Y657A. More interestingly, some of the residues that line the substrate binding groove within the protease domain were also affected, including A413, H415, C464, and E497 (Fig. 4D and *SI Appendix*, Fig. S4D). These findings suggest that the Y657A mutation impacts on the conformation of residues surrounding the active site. Thus, ubiquitin conjugation to K644 likely drives a conformational change in the loop containing Y657, which leads to protease activation by changing the conformation and/or mobility of residues surrounding the hydrophobic Ig3-protease interface and active site region. The dramatic hyperactivation of the protease produced by the Y657A mutation and its uncoupling of activation from ubiquitin modification of K644 clearly highlights Y657 as a key mediator of signaling between the Ig3 and the protease domains of MALT1 through a series of concerted conformational changes.

**Mutants That Disturb the Ig3-Protease Interaction Activate MALT1 and Overcome Defects in Ubiquitin-Dependent MALT1 Activation.** To probe the idea that mutational disruption of the hydrophobic Ig3-protease interaction surface was a key determinant in MALT1 activation, we mutated several additional amino acids involved in these interactions, namely, L506, N508, and Y367 (13, 14). Mutation of these residues into alanine showed a dramatic activation of MALT1 in the absence of ubiquitination-promoting expression of oncogenic CARMA1 (Fig. 4F). For L506, the hyperactivation was even more dramatic when L506 was mutated into glycine (L506G) or lysine (L506K). Almost no activating effect was observed upon mutation of Y657 into phenylalanine (Y657F), which should maintain the possibility of hydrophobic interactions (Fig. 4F) but destroys the possibility of a hydrogen bond between Y657 and E368, suggested by the MALT1 crystal structure (14). Thus, disruption of a group of hydrophobic Ig3-protease interactions led to constitutive activation of MALT1. The activity of WT MALT1 and the Y657F mutant could be
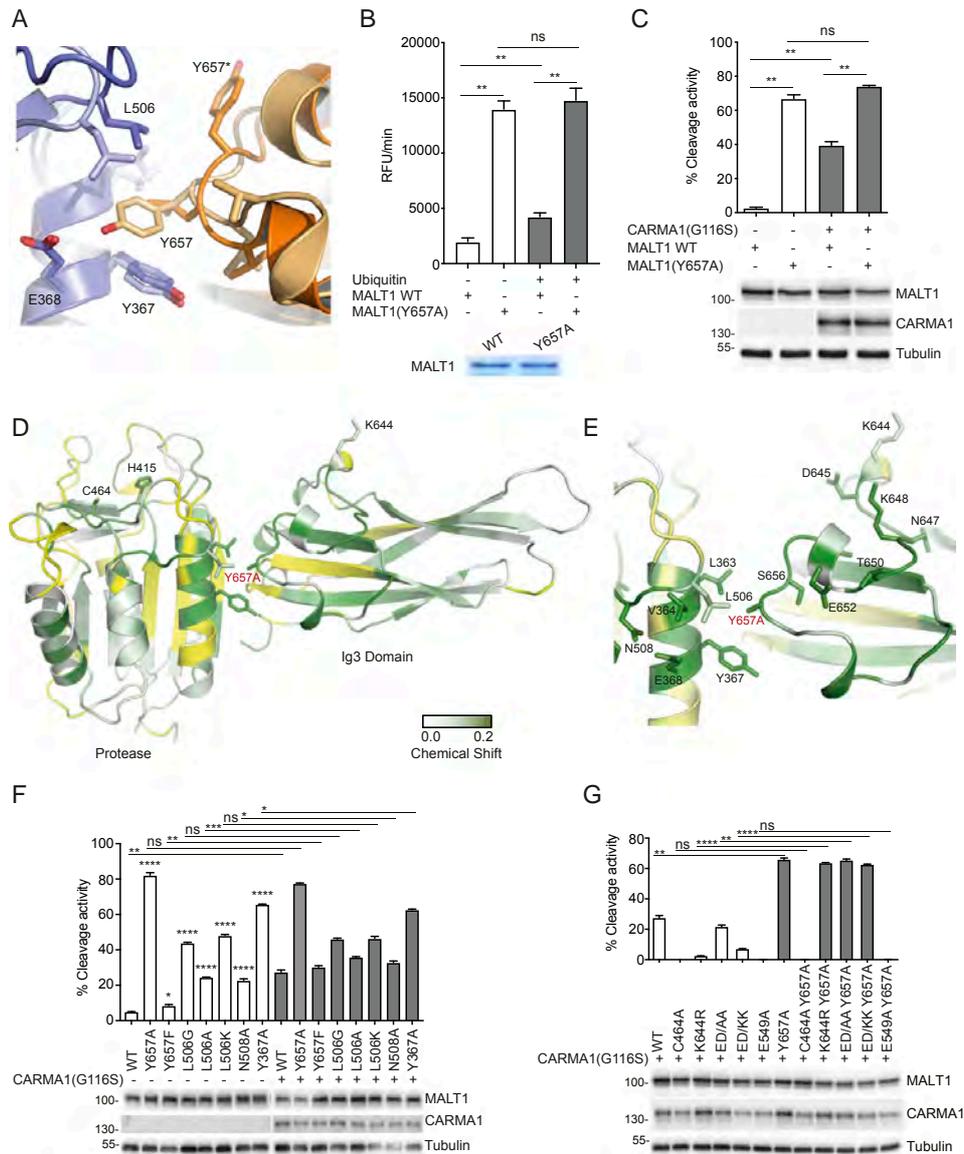
Schairer et al.

92

**Fig. 4.** Mutation of Y657 induces coordinated conformational changes in the loop connecting K644 to Y657 and the active site. (*A*) Overlay of the MALT1 Ig3-protease interface from reported crystal structures, which shows a major conformational switch of Y657 in the presence (light orange/light blue [PDB: 3UO8]) and the absence (dark orange/dark blue [PDB: 3V55]) of the active site peptide inhibitor z-VRPR-fmk. Blue and orange colors represent the protease and Ig3 domains, respectively. (*B*) In vitro cleavage assay comparing the capacity of ubiquitin (0.1 mM) to activate WT MALT1 or a MALT1 Y657A mutant (residues 199–824, 0.6 μM). Protein amount was controlled by Coomassie-blue staining as indicated. (*C*) Flow cytometric assessment of MALT1-dependent FRET reporter cleavage in 293T cells. The reporter was coexpressed with the indicated MALT1 constructs together with oncogenic CARMA1(G116S). Protein expression was controlled by Western blotting as indicated, and positions of molecular weight markers (in kDa) are indicated (*C*). (*D* and *E*) Backbone amide chemical shift changes induced by the Y657A mutation in MALT1 and mapped onto the reported structure of the Ig3-protease domains. Residues with significantly perturbed NMR signals (shift > 0.01 ppm) are colored with a gradient from white to green. Residues for which no minimal shift data were obtained are shown in yellow. Figure prepared using PyMOL. Residues with clearly shifted signals located at the Ig3-protease interface are highlighted (*E*). (*F* and *G*) Cleavage activity of the indicated MALT1 constructs was assessed as in *C*. Data are representative of two (*C*, *F*, and *G*) or three (*B*) experiments. Bars represent means ± SD; ns, nonsignificant, *P < 0.05, **P < 0.01, ***P < 0.001, and ****P < 0.0001.

further boosted by ubiquitination-promoting coexpression of oncogenic CARMA1. In contrast, oncogenic CARMA1 had no or little effect on the activity of the hyperactive L506A, L506G, L506K, N508A, and Y367A mutants, suggesting that their activity was no longer dependent on ubiquitination (Fig. 4*F*). Importantly, the Y657A mutation was also able to fully rescue the catalytic defect of the ubiquitination-deficient K644R mutant but not of the catalytically inactive C464A mutant (Fig. 4*G* and *SI Appendix*, Fig. S5). Similarly, introduction of the Y657A mutation into the functionally impaired ED/AA or ED/KK mutants fully restored their catalytic activity (Fig. 4*G*). Of note, the Y657A mutant was unable to restore the activity of a previously described dimerization-deficient MALT1 mutant in which E549 in the protease–protease interface has been mutated into alanine (E549A) (28) (Fig. 4*G*). Collectively, these findings suggest that ubiquitin attachment to K644 promotes a perturbation of the Ig3-protease interface, which is communicated to the active site through subtle conformational changes to promote MALT1 activation.

## Discussion

Here, we identify the Ig3 domain of MALT1 as a novel ubiquitin-binding motif that is essential for MALT1 activation through an allosteric mechanism. Our data support a model in which the Ig3 domain recruits ubiquitin to promote MALT1 monoubiquitination, which, in turn, leads to disruption of the hydrophobic Ig3-protease interface and induces conformational changes in the protease domain that increase MALT1 activity (Fig. 5). Using a combination of heteronuclear NMR studies, mutational, and biochemical approaches, we show that ubiquitin binds the Ig3 domain via a negatively charged surface patch including E696 and D697 that is located on the side opposing the Ig3-protease domain interaction surface. We also provide relevant insight into how ubiquitin promotes MALT1 activation. MALT1-binding induced shifts in ubiquitin backbone amide signals for a total of 13 amino acids forming a continuous positively charged patch on the surface of ubiquitin. These residues are likely to be important for ubiquitin recruitment by the Ig3 domain, but also for the capacity of ubiquitin to activate MALT1 upon its covalent conjugation to MALT1. In support of this, we found that mutation of several of the positively charged ubiquitin residues important for MALT1 binding were impaired in their capacity to promote MALT1 activation in vitro or in the context of a MALT1-Ub fusion protein. Thus, the same positively charged ubiquitin surface surrounding I44 is likely to be required for both Ig3-dependent ubiquitin binding/conjugation and for the subsequent MALT1 activation by K644-conjugated ubiquitin, which likely depends on an interaction of ubiquitin with a MALT1 surface that was not accessible in the in vitro NMR system used here. Indeed, for the 2D-NMR analysis, recombinant MALT1 needs to be monomeric in solution, and, under these conditions, free ubiquitin did not show noticeable effects on backbone amide signals in the protease domain or the protease-Ig3 interface. However, under the conditions of the assay used for monitoring its activity and in vivo, MALT1 is most likely active as a dimer or oligomer and/or adapts a different conformation. We, therefore, suspect that MALT1 contains a second cryptic ubiquitin-binding site that may be exposed only upon a specific conformational change or dimerization of MALT1. Consistent with the latter idea, we found that a Y657A mutation, which overcomes the need for monoubiquitination-dependent activation, was unable to activate a dimerization-deficient MALT1 mutant (E549A). Future studies will be targeted at elucidating how K644-conjugated ubiquitin activates dimeric MALT1.

We reasoned that, independent of the exact MALT1-binding site of K644-conjugated ubiquitin, such a binding could exert a mechanical force on K644 that might structurally order the loop extending from K644 to Y657. This could, in turn, disrupt the previously reported hydrophobic interaction between L506 and Y657 (14) and thereby affect the position of the A491–A507 loop
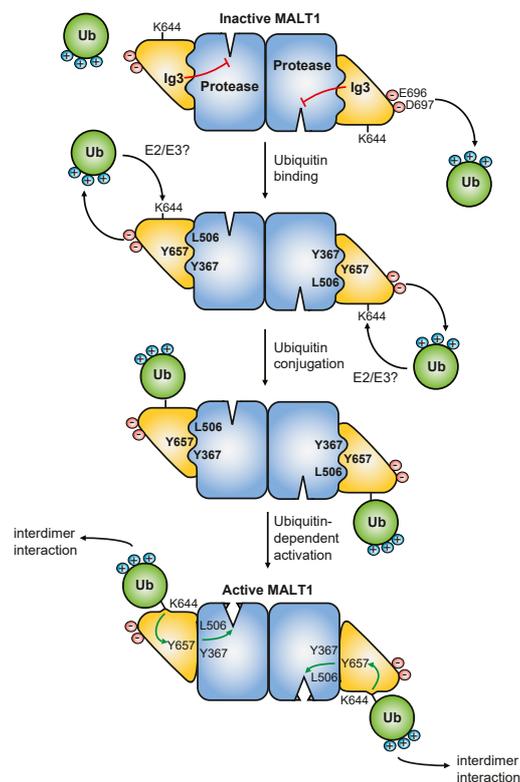


**Fig. 5.** Hypothetical model for allosteric MALT1 activation. In the inactive form, the Ig3 domain interacts with the protease domain via a hydrophobic interaction comprising Y657 on the surface of the Ig3 domain and L506 and Y367 on the surface of the protease domain. The negatively charged residues E696 and D697 of the Ig3 domain are necessary for the recruitment and conjugation of ubiquitin to K644 of the Ig3 domain via unknown E2/E3 enzymes. Upon conjugation to K644, ubiquitin likely interacts with an additional unknown ubiquitin-binding site of an adjacent MALT1 dimer. This induces a conformational change in the Ig3 domain that perturbs the hydrophobic Ig3-protease interaction thereby allowing the adoption of a catalytically active conformation.

within the protease domain. In support of this hypothesis, mutation of tyrosine 657 into alanine (Y657A) led to the creation of a hyperactive MALT1 mutant, which no longer depended on ubiquitination and the Ig3-ubiquitin interaction for its activation. Moreover, our 2D-NMR analysis revealed that the Y657A mutation, indeed, caused major chemical shift perturbations, both in the loop extending from Y657 to K644 and in the protease domain, including the active site residues H415 and C464. This supports the idea that the ubiquitin-conjugation site K644 and the Y657-surrounding Ig3-protease interaction sites communicate. Based on these findings, we propose that the interaction of K644-conjugated ubiquitin with an unknown ubiquitin-binding site on an adjacent MALT1 dimer activates the protease domain of the monoubiquitinated subunit by inducing a Y657-dependent change in the interaction of the Ig3 and protease domains, which lock MALT1 in its active conformation (Fig. 5).

Several studies have reported the development of MALT1 inhibitors with efficacy as immunomodulating or anticancer drugs in

Schairer et al.

94

mouse models of autoimmunity and lymphomas (29–31). Inhibition of MALT1 function preferentially in Treg cells, on the other hand, may reprogram these cells to become proinflammatory effectors (32–34) that sensitize tumors to the PD-1 blockade in mouse tumor models (32). Whether these approaches work similarly in humans and in mice remains unknown and requires further investigation. MALT1 inhibitors are either irreversible inhibitors that target the active site (30, 35, 36) or compounds that bind to an allosteric site located near W580 between the Ig3 and the protease domains and thereby prevent the conformational change required to form the active conformation (29, 37, 38). Our findings suggest that it should be possible to induce MALT1 activity in a reversible manner using drugs that interfere with the Ig3-protease interaction in the hydrophobic region surrounding Y657. Such drugs could be desirable to treat certain forms of severe immunodeficiencies or to strengthen antitumor immune responses, for example, by pretreatment of chimeric antigen receptor-T cells or other immune cells to be used for adoptive cancer immunotherapies.

## Materials and Methods

**Antibodies and Plasmids.** Details about antibodies and plasmids are provided in the *SI Appendix*.

**Transfection and Transduction of Cells.** Transient transfection of HEK293T cells and lentiviral transduction of Jurkat T cells have been previously described (25). To silence MALT1 expression, cells were stably transduced with a MALT1-specific single guide RNA (sgRNA) (5′-GCTGTTGGGGGACCCGCTAC-3′) or control sgRNA (5′-CTTCGAAATGTCCGTTCGGT-3′) and selected using puromycin. Cells were subsequently transduced to constitutively express GFP together with WT or mutant MALT1 constructs that were rendered CRISPR/Cas9 resistant by a silent point mutation. Transduced cells were sorted for live GFP+ cells using flow cytometry.

**Cell Culture, Cell Stimulation, and IL-2 Luciferase Reporter Assays.** HEK293T cells and Jurkat T cells were cultured in DMEM or in Roswell Park Memorial Institute (RPMI)-1640 medium supplemented with 10% fetal calf serum (FCS) (Biowest), respectively. Lentivirus-transduced Jurkat T cells were kept under puromycin selection (1 μg/mL; Alexis) for 14 d. For stimulation of T cells, a mixture of PMA (phorbol 12-myristate 13-acetate; 20 ng/mL; Alexis) and ionomycin (1 μM; Calbiochem) was used. In some experiments, cells were preincubated with z-LVSR-fmk (2 μM; Bachem) for 30–60 min before stimulation of Jurkat T cells or treated for 16 h after transfection of HEK293T cells. IL-2 luciferase reporter assay was performed as previously described (17, 25).

**Lysis, Immunoprecipitation, and Immunoblot Analysis.** Cells were lysed in lysis buffer containing 50 mM 4-(2-hydroxyethyl)-1-piperazineethanesulfonic acid (Hepes) pH 7.5, 150 mM NaCl, 1% Triton-X-100, protease inhibitors (Complete; Roche), and phosphatase inhibitors (NaF, Na$_4$P$_2$O$_7$, and Na$_3$VO$_4$). For optimal detection of MALT1 monoubiquitination, the lysis buffer was supplemented with *N*-Ethylmaleimide (10 mM). After preclearing the lysates with Sepharose beads for 20 min, StrepTactin Sepharose beads (IBA Lifesciences) were added, and samples were incubated for 1 h at 4 °C. The samples were then washed three times with lysis buffer. Samples were boiled in a reducing sodium dodecyl sulfate (SDS) sample buffer, separated by SDS/polyacrylamide gel electrophoresis, and analyzed by immunoblot as described (25).

**CD4+ T Cell Isolation from Blood Samples and Intracellular IL-2 Staining.** Blood samples from healthy, informed and consenting donors were obtained from the Interregional Blood Transfusion SRC Ltd. Peripheral blood mononuclear cells were isolated by density centrifugation with Lymphoprep. CD4+ T cells were obtained using CD4 MicroBeads from Miltenyi and cultivated in RPMI-1640 medium supplemented with 10% FCS (Biowest), 1% penicillin/streptomycin, and IL-2 (100 U/mL). One day before lentiviral transduction, cells were primed with anti-CD3, anti-CD28 (Biolegend) and a cross-linking

antibody (Jackson Immunoresearch) (1 μg/mL of each). Lentiviral transduction was performed in the presence of 6 μg/mL polybrene and a centrifugation of the cell-virus mix for 90 min at 800 g at 32 °C. After 2.5 d, cells were washed three times with fresh medium and cultivated in the presence of IL-2 for 1 wk. Further on, cells were restimulated with anti-CD3, anti-CD28 (0.5 μg/mL of each), and a cross-linking antibody (1 μg/mL) for 6 h in the presence of brefeldin A (eBioscience). All cells were stained for CD4 using an APC anti-human CD4 (SK3) antibody from BioLegend. Dead cells were stained with eBioscience Fixable Viability Dye eFlour 506 (Invitrogen). After fixation in 4% paraformaldehyde and permeabilization in 0.1% Saponin, intracellular IL-2 was stained by PE-CF594 Mouse Anti-Human IL-2 (5344.111) from BD Biosciences. The percentage of IL-2-positive cells was determined using a LSRIIb flow cytometer from BD Biosciences.

**Protein Purification and In Vitro Protease Activity Assay.** Recombinant glutathione *S*-transferase proteins containing the MALT1 Ig2, protease, Ig3 domains, and the C-terminal extension (aa 199–824, 0.6 μM), or monomeric ubiquitin, were generated and purified as previously described (25). To measure protease activity in vitro in the presence of purified monomeric ubiquitin, samples containing purified MALT1 constructs were incubated in cleavage buffer (20 mM Hepes, 10 mM KCl, 1.5 mM MgCl$_2$, 1 mM ethylenediaminetetraacetic acid, 1 mM dithiothreitol, 0.01% Triton X-100, and 10% glycerol, pH 7.5) containing 200 μM of the fluorescent substrate Ac-LVSR-amc (Peptides International) for 4 h at 30 °C, and the protease activity of MALT1 was monitored using a microplate reader (Molecular Devices).

**Minimal Shift Analysis Using NMR Spectroscopy.** Recombinant MALT1 (residues 339–719), MALT1 E696K/D697K, MALT1 Y657A, and ubiquitin (residues 1–76) were expressed and purified as described in the *SI Appendix*. All NMR data were acquired on a Bruker Avance III 800 MHz spectrometer equipped with a 5 mm HCN cryoprobe. Experimental parameters and data acquisition times for each experiment are described in the *SI Appendix*. All NMR data were processed and analyzed using TopSpin and SPARKY (University of California, San Francisco) software.

**Ubiquitin-MALT1-Binding Determination by Biolayer Interferometry.** The dissociation constant (K$_D$) for MALT1 binding to ubiquitin was determined by biolayer interferometry on a two-channel Octet RED384 system (FortéBio). Protein samples were diluted in 1× HBS-EP+ buffer (GE Healthcare), and experiments were carried out at 25 °C and 1,000 rpm constant shaking. Ni-NTA biosensors (FortéBio) were preequilibrated in buffer before coating with C-terminal hexahistidine MALT1 (339–719) at 375 nM for 600 s. MALT1 was titrated with increasing concentrations (0.0, 0.01, 0.025, 0.05, 0.2, 0.5, 0.8, and 1.2 mM) of untagged ubiquitin (Sigma-Aldrich, U6253) for a total time of 180 s association followed by a 300 s dissociation step. Experiments described above were run for the following ligand–analyte couples: MALT1 WT-ubiquitin WT, MALT1 WT-ubiquitin K6A, MALT1 WT-ubiquitin K48A, and MALT1 WT-ubiquitin H68A. Raw data were corrected by double referencing and analyzed using Prism7 software (GraphPad).

**Statistical Analysis.** Parametric two-tailed Student's *t* test or one-way ANOVA with Dunnett correction were used for statistical analysis; *P* values ≤ 0.05 were considered statistically significant.

**Data Availability Statement.** All data supporting the findings of this paper are available upon request from the corresponding authors (M.T. and M.D.C.).

1. J. Ruland, G. S. Duncan, A. Wakeham, T. W. Mak, Differential requirement for Malt1 in T and B cell antigen receptor signaling. *Immunity* **19**, 749–758 (2003).
2. A. A. Ruefli-Brasse, D. M. French, V. M. Dixit, Regulation of NF-kappaB-dependent lymphocyte activation and development by paracaspase. *Science* **302**, 1581–1584 (2003).
3. M. Jaworski *et al.*, Malt1 protease inactivation efficiently dampens immune responses but causes spontaneous autoimmunity. *EMBO J.* **33**, 2765–2781 (2014).
4. A. Gewies *et al.*, Uncoupling Malt1 threshold function from paracaspase activity results in destructive autoimmune inflammation. *Cell Rep.* **9**, 1292–1305 (2014).
5. J. W. Yu *et al.*, MALT1 protease activity is required for innate and adaptive immune responses. *PLoS One* **10**, e0127083 (2015).
6. F. Bornancin *et al.*, Deficiency of MALT1 paracaspase activity results in unbalanced regulatory and effector T and B cell responses leading to multiorgan inflammation. *J. Immunol.* **194**, 3723–3734 (2015).
7. S. Rosebeck, A. O. Rehman, P. C. Lucas, L. M. McAllister-Lucas, From MALT lymphoma to the CBM signalosome: Three decades of discovery. *Cell Cycle* **10**, 2485–2496 (2011).

Schairer et al.

8. J. Ruland, L. Hartjes, CARD-BCL-10-MALT1 signalling in protective and pathological immunity. *Nat. Rev. Immunol.* **19**, 118–134 (2019).

9. F. Schlauderer *et al.*, Molecular architecture and regulation of BCL10-MALT1 filaments. *Nat. Commun.* **9**, 4041 (2018).

10. Q. Qiao *et al.*, Structural architecture of the CARMA1/Bcl10/MALT1 signalosome: Nucleation-induced filamentous assembly. *Mol. Cell* **51**, 766–779 (2013).

11. A. G. Uren *et al.*, Identification of paracaspases and metacaspases: Two ancient families of caspase-like proteins, one of which plays a key role in MALT lymphoma. *Mol. Cell* **6**, 961–967 (2000).

12. H. Zhou, M. Q. Du, V. M. Dixit, Constitutive NF-kappaB activation by the t(11;18)(q21;q21) product in MALT lymphoma is linked to deregulated ubiquitin ligase activity. *Cancer Cell* **7**, 425–431 (2005).

13. C. Wiesmann *et al.*, Structural determinants of MALT1 protease activity. *J. Mol. Biol.* **419**, 4–21 (2012).

14. J. W. Yu, P. D. Jeffrey, J. Y. Ha, X. Yang, Y. Shi, Crystal structure of the mucosa-associated lymphoid tissue lymphoma translocation 1 (MALT1) paracaspase region. *Proc. Natl. Acad. Sci. U.S.A.* **108**, 21004–21009 (2011).

15. C. Pelzer *et al.*, MALT1 protease activity is controlled by monoubiquitination. *Nat. Immunol.* **14**, 337–345 (2013).

16. G. Lenz *et al.*, Oncogenic CARD11 mutations in human diffuse large B cell lymphoma. *Science* **319**, 1676–1679 (2008).

17. S. Hailfinger *et al.*, Malt1-dependent RelB cleavage promotes canonical NF-kappaB activation in lymphocytes and lymphoma cell lines. *Proc. Natl. Acad. Sci. U.S.A.* **108**, 14596–14601 (2011).

18. J. Staal *et al.*, T-cell receptor-induced JNK activation requires proteolytic inactivation of CYLD by MALT1. *EMBO J.* **30**, 1742–1752 (2011).

19. S. Polo *et al.*, A single motif responsible for ubiquitin recognition and mono-ubiquitination in endocytic proteins. *Nature* **416**, 451–455 (2002).

20. D. Hoeller *et al.*, E3-independent monoubiquitination of ubiquitin-binding proteins. *Mol. Cell* **26**, 891–898 (2007).

21. M. Düwel *et al.*, A20 negatively regulates T cell receptor signaling to NF-kappaB by cleaving Malt1 ubiquitin chains. *J. Immunol.* **182**, 7718–7728 (2009).

22. L. Sun, L. Deng, C. K. Ea, Z. P. Xia, Z. J. Chen, The TRAF6 ubiquitin ligase and TAK1 kinase mediate IKK activation by BCL10 and MALT1 in T lymphocytes. *Mol. Cell* **14**, 289–301 (2004).

23. H. Noels *et al.*, A novel TRAF6 binding site in MALT1 defines distinct mechanisms of NF-kappaB activation by API2middle dotMALT1 fusions. *J. Biol. Chem.* **282**, 10180–10189 (2007).

24. L. Deng *et al.*, Activation of the IkappaB kinase complex by TRAF6 requires a dimeric ubiquitin-conjugating enzyme complex and a unique polyubiquitin chain. *Cell* **103**, 351–361 (2000).

25. F. Rebeaud *et al.*, The proteolytic activity of the paracaspase MALT1 is key in T cell activation. *Nat. Immunol.* **9**, 272–281 (2008).

26. J. Hachmann *et al.*, Mechanism and specificity of the human paracaspase MALT1. *Biochem. J.* **443**, 287–295 (2012).

27. I. Dikic, S. Wakatsuki, K. J. Walters, Ubiquitin-binding domains–from structures to functions. *Nat. Rev. Mol. Cell Biol.* **10**, 659–671 (2009).

28. K. Cabalzar *et al.*, Monoubiquitination and activity of the paracaspase MALT1 requires glutamate 549 in the dimerization interface. *PLoS One* **8**, e72051 (2013).

29. D. Nagel *et al.*, Pharmacologic inhibition of MALT1 protease by phenothiazines as a therapeutic approach for the treatment of aggressive ABC-DLBCL. *Cancer Cell* **22**, 825–837 (2012).

30. L. Fontan *et al.*, MALT1 small molecule inhibitors specifically suppress ABC-DLBCL in vitro and in vivo. *Cancer Cell* **22**, 812–824 (2012).

31. C. Mc Guire *et al.*, Pharmacological inhibition of MALT1 protease activity protects mice in a mouse model of multiple sclerosis. *J. Neuroinflammation* **11**, 124 (2014).

32. M. Di Pilato *et al.*, Targeting the CBM complex causes T$_{reg}$ cells to prime tumours for immune checkpoint therapy. *Nature* **570**, 112–116 (2019).

33. M. Rosenbaum *et al.*, Bcl10-controlled Malt1 paracaspase activity is key for the immune suppressive function of regulatory T cells. *Nat. Commun.* **10**, 2352 (2019).

34. L. Cheng, N. Deng, N. Yang, X. Zhao, X. Lin, Malt1 protease is critical in maintaining function of regulatory T cells and may be a therapeutic target for antitumor immunity. *J. Immunol.* **202**, 3008–3019 (2019).

35. S. M. Lim *et al.*, Identification of β-lapachone analogs as novel MALT1 inhibitors to treat an aggressive subtype of diffuse large B-cell lymphoma. *J. Med. Chem.* **58**, 8491–8502 (2015).

36. B. T. Xin *et al.*, Development of new Malt1 inhibitors and probes. *Bioorg. Med. Chem.* **24**, 3312–3329 (2016).

37. J. Quancard *et al.*, An allosteric MALT1 inhibitor is a molecular corrector rescuing function in an immunodeficient patient. *Nat. Chem. Biol.* **15**, 304–313 (2019).

38. A. Schlapbach *et al.*, N-aryl-piperidine-4-carboxamides as a novel class of potent inhibitors of MALT1 proteolytic activity. *Bioorg. Med. Chem. Lett.* **28**, 2153–2158 (2018).

39. D. Rueda *et al.*, Bcl10 controls TCR- and FcgammaR-induced actin polymerization. *J. Immunol.* **178**, 4373–4384 (2007).

Schairer et al.

96

Supplementary Information for

**Allosteric activation of MALT1 by its ubiquitin-binding Ig3 domain**

Rebekka Schairer, Gareth Hall, Ming Zhang, Richard Cowan, Roberta Baravalle, Frederick W. Muskett, Peter J. Coombs, Chido Mpamhanga, Lisa R. Hale, Barbara Saxty, Justyna Iwaszkiewicz, Chantal Décaillet, Mai Perroud, Mark D. Carr, and Margot Thome

Corresponding authors: Margot Thome and Mark D. Carr
Email: *margot.thomemiazza@unil.ch* and *mdc12@leicester.ac.uk*

**This PDF file includes:**

> Supplementary text
> Figures S1 to S5
> SI References

1

**Supplementary Information Text**

**Materials and Methods**

**Antibodies**

Antibodies used include anti-Tubulin (B-5-1-2), anti-RelB (rabbit polyclonal), anti-phospho-I$\kappa$B$\alpha$ (Ser32/36) (5A5), anti-I$\kappa$B$\alpha$, anti-CARMA1 (CARD11) (1D12) and anti-CYLD (D1A10) from Cell Signaling, anti-BCL10 (331.3, Santa-Cruz), anti-FLAG (M2, Sigma), anti-HA (Covance), anti-JNK1&2 (pTpY183/185) (Biosource) and anti-Roquin-1 (Abcam). The affinity-purified rabbit anti-MALT1 antibody has been previously reported (1). Horseradish peroxidase–coupled goat anti-mouse or anti-rabbit were from Jackson Immunoresearch.

**Plasmids**

The eYFP-LVSR-eCFP reporter construct and the eukaryotic (pCR3-based) and bacterial (pGEX-based) MALT1 and Ubiquitin constructs have been previously described (2). For CRISPR/Cas9-mediated MALT1 silencing, we used the lentiCRISPRv2 vector from GeCKO. The reconstitution with MALT1 constructs was performed using pWPI vector from Addgene, which allows co-expression of MALT1 and GFP. MALT1 and ubiquitin point mutants were generated by quick-change PCR using Kapa high-fidelity DNA polymerase (Roche) and all mutations were verified by sequencing.

**Minimal shift analysis using NMR spectroscopy**

Recombinant MALT1 (residues 339-719) with a C-terminal hexahistidine tag was expressed as a soluble product using a pET21a (Novagen) vector transformed into the *E.coli* strain NiCo-21 (NEB). Uniformly $^{13}$C/$^{15}$N- and $^{15}$N- labelled MALT1 were prepared by growing at 37°C in modified Spizizen minimal medium (3) containing $^{15}$NH$_4$SO$_4$ (4 g L$^{-1}$) and/or $^{13}$C$_6$-glucose (2 g L$^{-1}$), as required. The protein was purified to homogeneity by chromatography on affinity (Ni-NTA column, Qiagen) and gel filtration (Superdex 75 16/60, GE healthcare) columns, into a final buffer of 20 mM Tris-HCl buffer, pH 7.5, containing 150 mM NaCl and 1 mM TCEP.

Recombinant ubiquitin (residues 1-76) with an N-terminal TEV cleavable hexa-histidine tag was expressed using a pET9a (Novagen) vector transformed into the *E.coli* strain BL-21 (DE3) (NEB). Uniformly $^{15}$N- labelled ubiquitin was prepared by growing overnight at 18 °C in modified Spizizen minimal medium (3) containing $^{15}$NH$_4$SO$_4$ (4 g L$^{-1}$). The protein was purified to homogeneity by chromatography on affinity (Ni-NTA column, Qiagen) and gel filtration (Superdex 75 16/60, GE healthcare) columns, into a final buffer of 25 mM HEPES buffer, pH 7.5, 50 mM NaCl and 1 mM TCEP.

All NMR data were acquired on a Bruker Avance III 800 MHz spectrometer equipped with a 5mm HCN cryoprobe. For the ubiquitin binding to MALT1 experiments both the MALT1 (339-

2

719) at 150 $\mu$M and ubiquitin (Sigma, U6253) NMR samples were prepared in 20 mM Tris-HCl buffer, pH 7.5, containing 150 mM NaCl and 1 mM TCEP in 90% $H_2O$/10% $D_2O$. The 2D $^{15}$N-$^1$H TROSY spectra of MALT1 were obtained at 25°C, in the absence or presence of 0.4 mM, 0.8 mM, 1.2 mM and 1.6 mM ubiquitin. Typical acquisition times for the 2D-NMR experiments were 50 ms in $F_2$ ($^1$H) and 40 ms in $F_1$ ($^{15}$N), with the spectra collected over approximately 4 hours. Backbone amide chemical shifts for free MALT1 were consistent with those reported previously and assigned accordingly (6). All NMR data were processed and analysed using TopSpin and SPARKY (University of California, San Francisco) software. The chemical shift changes in assigned backbone amide signals of MALT1 induced by ubiquitin-binding were used to identify MALT1 residues involved in ubiquitin binding. Backbone amide chemical shift changes were obtained from the combined chemical shift change in $^{15}$N and $^1$H for each assigned peak in the $^{15}$N/$^1$H TROSY spectrum of the free $^{15}$N-labelled MALT1, when compared to the equivalent peak in the $^{15}$N/$^1$H TROSY spectrum of the $^{15}$N-labelled MALT1 sample containing varying concentrations of ubiquitin (4, 5).

The MALT1 E696K/D697K mutant (339-719) at 100 $\mu$M and ubiquitin (Sigma, U6253) NMR samples were prepared in 20 mM Tris-HCl buffer, pH 7.5, 150 mM NaCl and 1 mM TCEP, in 90% $H_2O$/10% $D_2O$. The 2D $^{15}$N/$^1$H TROSY spectra of MALT1 E696K/D697K were obtained at 25ºC, in the absence or presence of 1.6 mM ubiquitin. Typical acquisition times for the NMR experiments were 50 ms in $F_2$ ($^1$H) and 40 ms in $F_1$ ($^{15}$N).

For the MALT1 addition to ubiquitin experiment, both the ubiquitin (1-76) at 50 $\mu$M and MALT1 (339-719) NMR samples were prepared in 25 mM HEPES buffer, pH 7.5, containing 50 mM NaCl and 1 mM TCEP in 90% $H_2O$/10% $D_2O$. The 2D $^{15}$N-$^1$H TROSY spectra of ubiquitin were obtained at 25°C in the absence or presence of 264 $\mu$M MALT1. Typical acquisition times for the double resonance experiments for ubiquitin were 83 ms in $F_2$ ($^1$H) and 89 ms in $F_1$ ($^{15}$N), with the spectra collected over approximately 10 hours. Backbone amide chemical shifts for free ubiquitin were consistent with those reported previously and assignments confirmed with a TOCSY-HSQC spectra. The minimal shift approach was used to identify ubiquitin residues involved in MALT1 binding. Backbone amide minimal shift values were obtained from the combined chemical shift change in $^{15}$N and $^1$H for each assigned peak in the $^{15}$N/$^1$H TROSY spectrum of the free $^{15}$N-labelled ubiquitin, when compared with all peaks observed in the $^{15}$N/$^1$H TROSY spectrum of the $^{15}$N-labelled ubiquitin sample containing 264 $\mu$M MALT1.

The $^{15}$N-labelled MALT1 Y657A (339-719) NMR sample was prepared in 25 mM HEPES buffer, pH 7.5, containing 50 mM NaCl and 1 mM TCEP in 90% $H_2O$/10% $D_2O$. Acquisition times for the $^{15}$N/$^1$H TROSY experiments were 50 ms in $F_2$ ($^1$H) and 40 ms in $F_1$ ($^{15}$N), with the spectra collected over approximately 4 h. Backbone amide minimal shifts for the MALT1 Y657A mutant were calculated by comparing the $^{15}$N/$^1$H TROSY spectra from MALT1 Y675A with all peaks observed in the $^{15}$N/$^1$H TROSY spectrum of the $^{15}$N-labelled wild-type MALT1 sample.
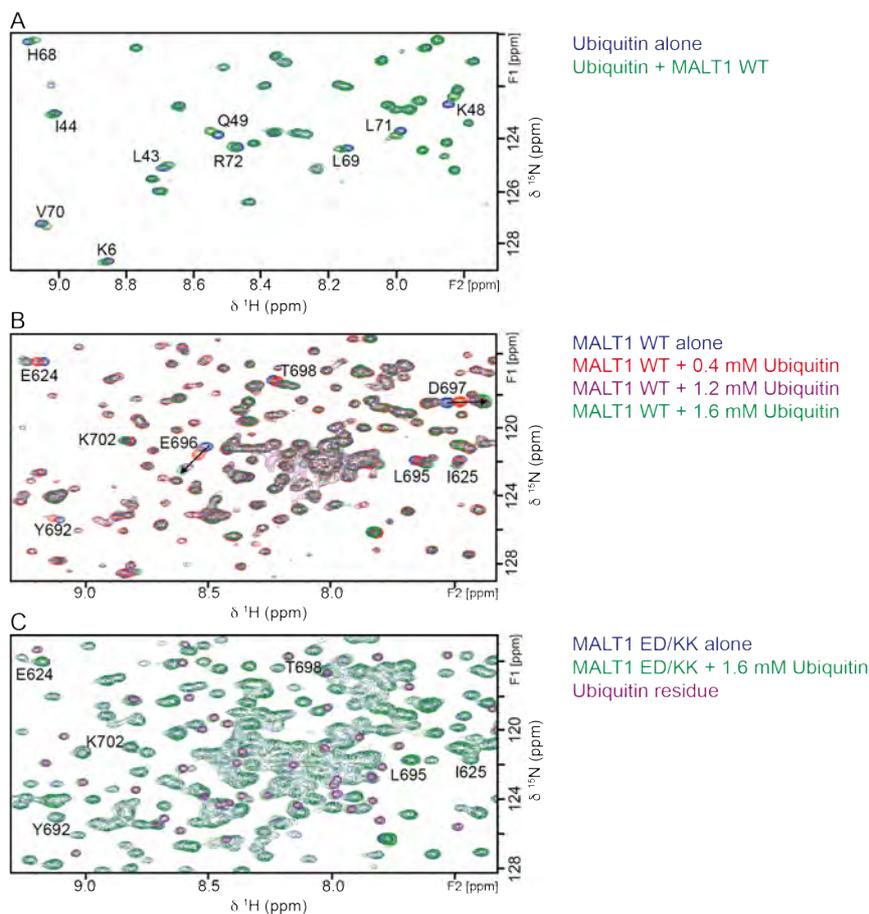
3

**Fig. S1. Ubiquitin interacts with the Ig3 domain *in vitro*.** (**A**) A selected region from the $^{15}$N-$^1$H TROSY spectra of $^{15}$N-labelled ubiquitin alone (blue) and following mixing with MALT1 (green), with the assignments for ubiquitin indicated. It is clear that the backbone amide peaks for K6, L43, I44, K48, Q49, H68, L69, V70, L71 and R72 show reasonable shifts. Images were prepared using Topspin (Bruker Biospin Ltd.). (**B**) A selected region from the $^{15}$N-$^1$H TROSY spectra of $^{15}$N-labelled MALT1 (0.15 mM) alone (blue) and following the addition of increasing concentrations of human ubiquitin 0.4 mM (red), 0.8 mM (not shown), 1.2 mM (purple) and 1.6 mM (green). The assignments for selected backbone amide signals of MALT1 are indicated. The backbone amide peaks for E696 and D697 show very substantial shifts upon ubiquitin-binding, with significant but somewhat smaller shifts seen for E624, I625, Y692, L695, T698 and K702. (**C**) A selected region from the $^{15}$N-$^1$H TROSY spectra of $^{15}$N-labelled MALT1 (ED/KK) (0.1 mM) alone (blue) and following the addition of human ubiquitin 1.6 mM (green). Peaks corresponding to natural abundance $^{15}$N-ubiquitin are also highlighted (purple). The backbone amide peaks for MALT1(ED/KK) show very little difference following ubiquitin addition.

4
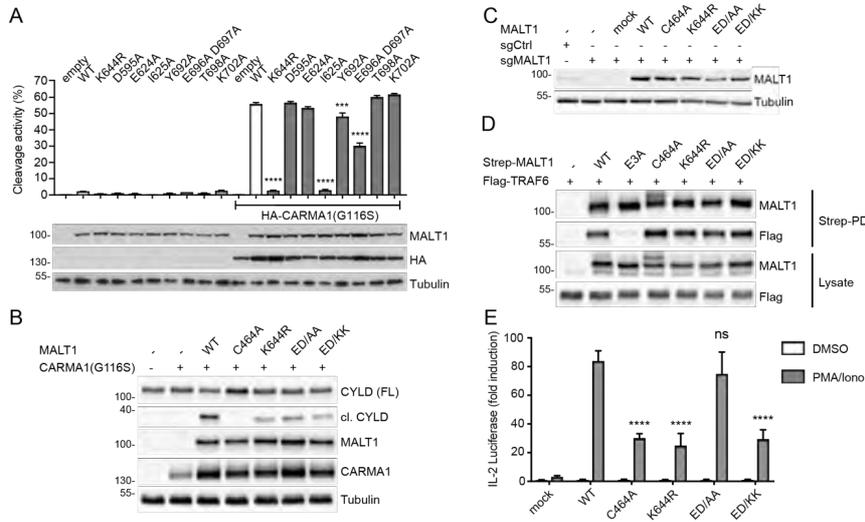
**Fig. S2. The Ig3-ubiquitin interaction is necessary for substrate cleavage but dispensable for the scaffold function of MALT1.** (**A**) Flow cytometric assessment of MALT1-dependent FRET reporter cleavage in 293T cells. The reporter was co-expressed with the indicated MALT1 constructs and oncogenic CARMA1(G116S). (**B**) 293T cells were transfected with the indicated expression constructs for MALT1, oncogenic CARMA1(G116S) and the MALT1 substrate CYLD and analyzed for substrate cleavage by Western blot as indicated. Positions of full length (FL) and cleaved (cl.) CYLD are indicated. (**C**) Jurkat cells were lentivirally transduced with MALT1-specific or control sgRNAs, as indicated, and MALT1-deficient cells were then transduced with a mock vector or the indicated MALT1 expression constructs. (**D**) 293T cells were transfected with the indicated expression constructs for Strep-tagged MALT1 and Flag-tagged TRAF6, and the capacity of MALT1 to bind to TRAF6 was assessed by Streptactin pull-down (Strep-PD) and Western blot. MALT1 constructs comprise the wild-type (WT) and mutants that are TRAF6 binding-deficient (E3A, mutating E316, E653 and E806 into A), catalytically inactive (C464A), monoubiquitination-deficient (K644R), and mutants of E696 and D697 (ED/AA or ED/KK). (**E**) Luciferase reporter assay of MALT1-deficient Jurkat T cells reconstituted with the indicated constructs of MALT1 and expressing an IL-2 luciferase reporter. Results are presented relative to those of unstimulated cells reconstituted with a mock vector. Positions of molecular weight markers (in kDa) are indicated. Tubulin was used as a loading control (**A, B, C**). Data are representative of two (**A, E**) and three (**B, D**) experiments. Bars represent means $\pm$ SD; $^*P < 0.05$, $^{**}P < 0.01$, $^{***}P < 0.001$, $^{****}P < 0.0001$.

5

A



B
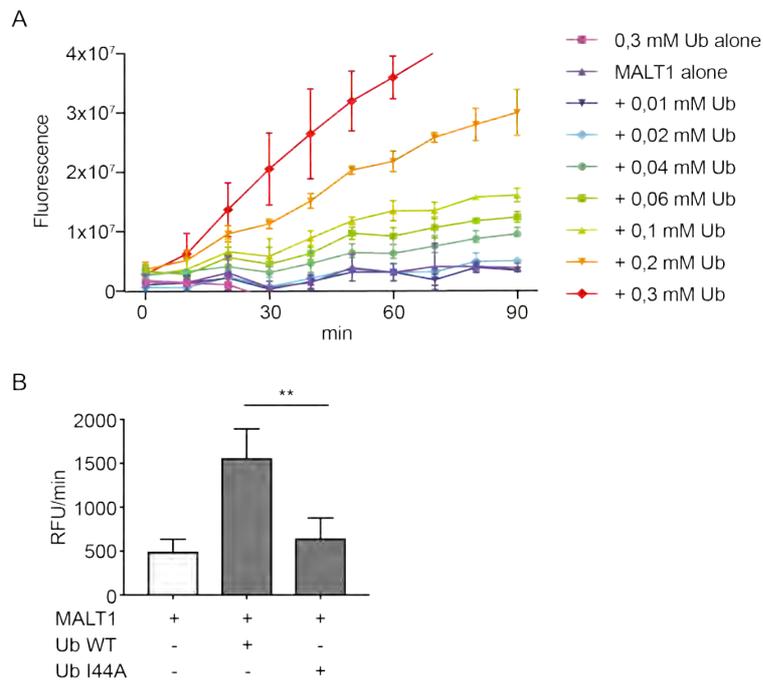


**Fig. S3. Monomeric ubiquitin promotes MALT1 protease activity *in vitro*.** (**A**) *In vitro* cleavage activity of recombinant purified MALT1 (residues 199-824, 0.6 µM) in presence of the indicated concentrations of recombinant purified ubiquitin. (**B**) *In vitro* cleavage assay comparing the capacity of wild-type ubiquitin and its I44A mutant (both used at 0.1 mM) to activate MALT1.

Data are representative of two (**A**) and three (**B**) experiments. Bars represent means $\pm$ SD; **$P$ < 0.01.

6

A



B



C



D
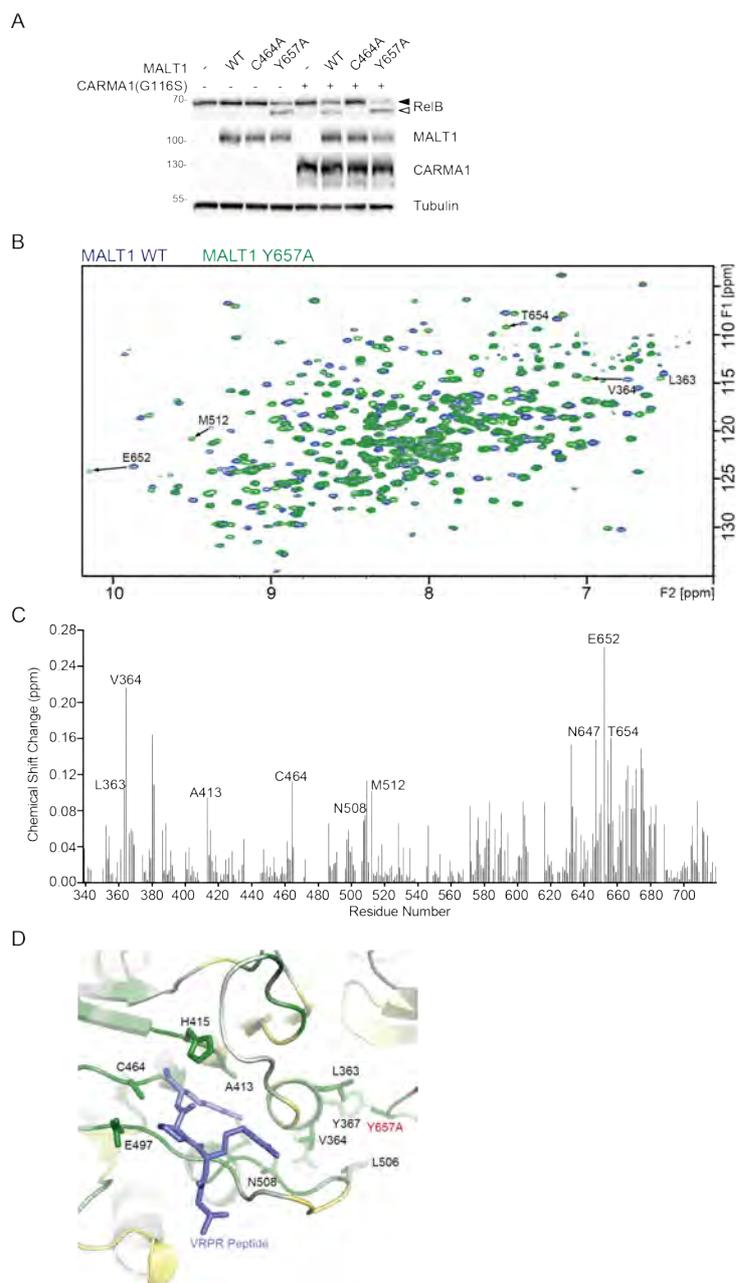


7

**Fig. S4. A hydrophobic cluster of residues around Y657 at the Ig3-protease interface mediates activation of MALT1.** (**A**) 293T cells were transfected with the indicated expression constructs for MALT1, oncogenic CARMA1(G116S) and the MALT1 substrate RelB and analyzed for substrate cleavage by Western blot as indicated. Tubulin was used as a loading control. Positions of uncleaved (black arrowhead) and cleaved (open arrowhead) RelB are indicated. The CARMA1-independent RelB cleavage by the Y657A mutation in MALT1 is clearly seen. Data are representative of two experiments. (**B**) A comparison of $^{15}$N-$^{1}$H TROSY spectra obtained for wild-type $^{15}$N-labelled MALT1 (residues 339-719, blue) with $^{15}$N-labelled MALT1 Y657A (green). Selected residues observed to show very significant shifts in their backbone amide NMR signals are highlighted. (**C**) Histogram revealing the backbone amide minimal shifts seen for $^{15}$N-labelled human MALT1 Y675A (residues 339-719) compared to wild-type MALT1. Selected residues observed to show very significant shifts in their backbone amide NMR signals are highlighted. (**D**) Backbone amide chemical shift changes induced by the Y657A mutation in MALT1, mapped onto the reported structure of the Ig3-protease domains. Residues with clearly shifted signals surrounding the active site are highlighted. Residues with significantly perturbed NMR signals (shift > 0.01 ppm) are colored with a gradient from white to green. Residues for which no minimal shift data were obtained are shown in yellow. The expected position of a VRPR substrate peptide bound in the active site of the protease domain is shown as violet sticks. Image was prepared using PyMOL.

8
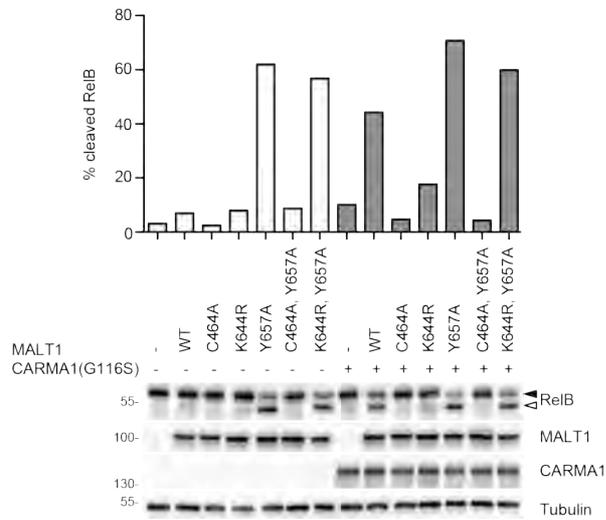
**Fig. S5. The MALT1 Y657A mutation overcomes the catalytic defect of the ubiquitination-deficient K644R mutant.**
293T cells were transfected with the indicated expression constructs for MALT1, oncogenic CARMA1(G116S) and the MALT1 substrate RelB and analyzed for substrate cleavage by Western blot as indicated. Tubulin was used as a loading control. Positions of uncleaved (black arrowhead) and cleaved (open arrowhead) RelB are indicated. The bar graph shows the quantification of RelB cleavage from the Western blot. Data are representative of a single experiment.

9

**SI References**

1.   F. Rebeaud *et al.*, The proteolytic activity of the paracaspase MALT1 is key in T cell activation. *Nature Immunol.* **9**, 272-281 (2008).
2.   C. Pelzer *et al.*, MALT1 protease activity is controlled by monoubiquitination. *Nature Immunol.* **14**, 337-345 (2013).
3.   J. Spizizen, Transformation of Biochemically Deficient Strains of Bacillus Subtilis by Deoxyribonucleate. *Proc Natl Acad Sci U S A* **44**, 1072-1078 (1958).
4.   R. A. Williamson, M. D. Carr, T. A. Frenkiel, J. Feeney, R. B. Freedman, Mapping the binding site for matrix metalloproteinase on the N-terminal domain of the tissue inhibitor of metalloproteinases-2 by NMR chemical shift perturbation. *Biochemistry* **36**, 13882-13889 (1997).
5.   V. Veverka *et al.*, Structural characterization of the interaction of mTOR with phosphatidic acid and a novel class of inhibitor: compelling evidence for a central role of the FRB domain in small molecule-mediated regulation of mTOR. *Oncogene* **27**, 585-595 (2008).
6.   S. Unnerstaale *et al.*, Backbone assignment of the MALT1 paracaspase by solution NMR. *PLoS One* **11**, e0146496 (2016).

10

# Annex II – Contribution to Publication – Mellett *et al.*

## CARD14 gain-of-function mutation alone is sufficient to drive IL-23/IL-17 – mediated psoriasiform skin inflammation in vivo.

Mark Mellett, Barbara Meier, Deepa Mohanan, Rebekka Schairer, Phil Cheng, Takashi K. Satoh, Betina Kiefer, Caroline Ospelt, Stephan Nobbe, Margot Thome, Emmanuel Contassot and Lars E. French

Published in *Journal of Investigative Dermatology*, Volume 138, Issue 9, September 2018, Pages 2010-2023

Psoriasis is a common chronic auto-inflammatory disease, which is driven by the infiltration of immune cells into the skin and their interaction with keratinocytes. Gain-of-function mutations of the CARMA1 homolog, CARD14, which is mainly expressed in the placenta and in keratinocytes, are associated with psoriasis. This study investigates the physiological impact of CARD14 gain-of-function mutations. By generating mice with heterozygous *Card14ΔE138* mutation, the authors show that hyperactivation of CARD14 alone drives T helper type 17-mediated psoriasis skin disease, resulting in keratinocyte hyperproliferation and immune cell infiltration in skin lesions of the mice. The IL-23/IL-17 axis was the driving force of the disease.

For this study, I performed FRET-based MALT1 cleavage assays in HEK293T cells to identify the effect of different CARD14 mutations on MALT1 proteolytic activity. The result of these experiments is shown in **Figure 1e**. For the supplementary Materials, I wrote the paragraph "FRET assay".

# CARD14 Gain-of-Function Mutation Alone Is Sufficient to Drive IL-23/IL-17—Mediated Psoriasiform Skin Inflammation In Vivo

Mark Mellett[1,4], Barbara Meier[1], Deepa Mohanan[1], Rebekka Schairer[2], Phil Cheng[1], Takashi K. Satoh[1], Betina Kiefer[1], Caroline Ospelt[3], Stephan Nobbe[1], Margot Thome[2], Emmanuel Contassot[1] and Lars E. French[1,4]

Rare autosomal dominant mutations in the gene encoding the keratinocyte signaling molecule CARD14, have been associated with an increased susceptibility to psoriasis, but the physiological impact of CARD14 gain-of-function mutations remains to be fully determined in vivo. Here, we report that heterozygous mice harboring a CARD14 gain-of-function mutation (*Card14ΔE138*) spontaneously develop a chronic psoriatic phenotype with characteristic scaling skin lesions, epidermal thickening, keratinocyte hyperproliferation, hyperkeratosis, and immune cell infiltration. Affected skin of these mice is characterized by elevated expression of anti-microbial peptides, chemokines, and cytokines (including T helper type 17 cell-signature cytokines) and an immune infiltrate rich in neutrophils, myeloid cells, and T cells, reminiscent of human psoriatic skin. Disease pathogenesis was driven by the IL-23/IL-17 axis, and neutralization of IL-23p19, the key cytokine in maintaining T helper type 17 cell polarization, significantly reduced skin lesions and the expression of antimicrobial peptides and proinflammatory cytokines. Therefore, hyperactivation of CARD14 alone is sufficient to orchestrate the complex immunopathogenesis that drives T helper type 17-mediated psoriasis skin disease in vivo.

## INTRODUCTION

Psoriasis is a common chronic inflammatory disease of the skin that is estimated to affect approximately 2% of the global population and is equally prevalent in males and females (Christophers, 2001; Gudjonsson and Elder, 2007). Psoriasis is characterized by scaly erythematous plaques on the skin, which, given its chronic course, significantly impairs the quality of life of affected individuals. The most common form of psoriasis is psoriasis vulgaris (plaque psoriasis), but other forms exist with distinct clinical features, including guttate psoriasis, pustular psoriasis, and palmoplantar psoriasis (Griffiths and Barker, 2007). Overall, 20—30% of plaque psoriasis cases are associated with debilitating psoriatic arthritis, and psoriasis patients can suffer from comorbidities including cardiovascular disease, diabetes, and obesity (Griffiths and Barker, 2007; Mease et al., 2013). Histological hallmarks of psoriasis include epidermal acanthosis, keratinocyte hyperproliferation, hyperkeratosis, cutaneous immune

cell infiltration, and angiogenesis. Disease symptoms arise from a complex interaction between keratinocytes and infiltrating immune cells (Bos and De Rie, 1999; Boyman et al., 2007; Sano et al., 2005; Valdimarsson et al., 1995). However, the early triggers that lead to full-blown disease are not well understood, confounded by the wide range of genetic factors that contribute to an elevated risk of developing psoriasis, including genes controlling epidermal barrier integrity (e.g., *LCE3B*, *LCE3D*) and antigen presentation (e.g., *HLA-Cw\*0602*, *ERAP1*) and genes of the innate (e.g., *NFKBIA*) and adaptive immune systems (e.g., *IL12B*, *IL23R*) (Tsoi et al., 2012). Although genome-wide association studies have shown that approximately more than 80 genes in Caucasian and Han Chinese populations are associated with an increased susceptibility to psoriasis, very few genetic variants have actually been studied in vivo (Sheng et al., 2014; Tsoi et al., 2017).

Rare autosomal dominant mutations in the gene encoding a keratinocyte scaffold molecule, CARD14 (which maps to the *PSORS2* locus) have been associated with a number of psoriatic phenotypes including plaque psoriasis and psoriatic arthritis, generalized pustular psoriasis, and palmoplantar pustular psoriasis, in addition to familial and sporadic cases of the clinically related but rare disease pityriasis rubra pilaris (PRP) (Fuchs-Telem et al., 2012; Has et al., 2016; Hong et al., 2014; Jordan et al., 2012a, 2012b; Li et al., 2015; Mossner et al., 2015; Sugiura et al., 2014; Takeichi et al., 2017a, 2017b). CARD14 is a proinflammatory signaling molecule whose expression is predominantly restricted to the placenta and keratinocytes of the skin, although CARD14 expression was also reported on CD31-positive endothelial cells (Fuchs-Telem, 2012; Harden et al., 2014). CARD14 is the second

member of the CARD/MAGUK domain (CARMA) protein family (Bertin et al., 2001; Scudiero et al., 2014). CARMA proteins contain CARD, coiled-coil, SH3, and guanylate kinase-like domains, and they exist in an auto-inhibitory state. In response to external stimuli, CARMA proteins are phosphorylated via protein kinase C isoforms (Scudiero et al., 2014). Subsequently, they undergo a conformational change, facilitating recruitment of the interacting partners Bcl10 (via CARD:CARD domain interactions) and Malt1 to form the CARMA:Bcl10:Malt1 (i.e., CBM) signaling complex, or "signalosome" (Bertin, 2001; Gaide et al., 2001; Howes et al., 2016; Jattani et al., 2016; McAllister-Lucas et al., 2001; Scudiero, 2014). CARD11 (CARMA1), expressed in lymphoid cells, is activated upon B- and T-cell receptor engagement, and gain-of-function (GoF) mutations in the genes encoding CARD11, Bcl10, and Malt1 have been associated with a number of lymphoid malignancies (Gaide, et al., 2002; Juilland and Thome, 2016; Pomerantz et al., 2002; Wang et al., 2002). Similarly, CARD10 (CARMA3), expressed in epithelial tissue and activated by G protein-coupled receptor stimulation, has been linked to the progression of various carcinomas (Du et al., 2014; Pan et al., 2016; Xia et al., 2016; Xie et al., 2014).

CARD14 was recently described to be activated in vitro in response to zymosan and *Staphylococcus aureus* pathogen-associated molecular pattern agonists (Schmitt et al., 2016; Scudiero et al., 2017). Therefore, CARD14 likely plays its main role in innate immune defense, which is supported by the genes activated downstream of CARD14, which typically encode for proinflammatory cytokines and chemokines, including IL-36γ, IL-8, and Ccl20 (Jordan, 2012a). The contribution of CARD14 GoF to psoriatic disease pathogenesis, however, remains unclear. CARD14 mutations are rare, and some polymorphisms (p.Arg820Trp, p.Arg547Ser) associated with PRP in a Taiwanese study were also shown to be present in the general population (Hong, 2014). Other polymorphisms (p.Gly117Ser) have shown phenotypes that vary considerably, with respect to age of onset and severity, raising the possibility that other genetic or environmental factors may be required (Jordan, 2012b).

Mutation or deletion of a single glutamic acid (E138) in the coiled-coil domain of CARD14 has been associated with both psoriasis and PRP (Fuchs-Telem, 2012; Has, 2016; Inoue et al., 2016; Jordan, 2012b). These variants resulted in severe phenotypes and add support to the relevance of CARD14 mutations to an increased risk of psoriatic skin disease. However, the contribution of CARD14 to psoriasis pathogenesis remains open, and therefore we sought to determine the functional impact of CARD14 E138 mutation in vivo.

## RESULTS

### CARD14 GoF mutation causes spontaneous signalosome formation in primary human keratinocytes, which is dependent on a functional CARD domain

Consistent with previous reports, CARD14 E138A and ΔE138 mutants both caused enhanced NF-κB and AP-1 activation in vitro in HEK293 cells compared with wild-type (WT) CARD14, with the E138A mutant showing a more potent response (see Supplementary Figure S1a online) (Afonina et al., 2016; Li et al., 2015). CARD14 E138A and CARD14

ΔE138 GoF mutants were also overexpressed in primary keratinocytes and HEK293 cells and were observed to interact with endogenous Bcl10 by co-immunoprecipitation (Figure 1a, and see Supplementary Figure S1b), whereas Bcl10 interaction with CARD14 WT was below detectable levels. Because this was contrary to previous findings (Afonina, 2016; Scudiero, 2011), we sought to assess other means of CARD14 activity. There was a reduction of Bcl10 expression observed in the presence of all three CARD14 constructs in HEK293 cells (see Supplementary Figure S1b) and a decrease of CARD14 mutant expression in primary keratinocytes (Figure 1a). Previously, it has been suggested that CARD14 mutants associated with psoriasis are less soluble than WT CARD14 (Berki et al., 2015). Additionally, it has been previously described that Bcl10 forms oligomeric structures that can be nucleated by CARD11 (Qiao et al., 2013). It was therefore of interest to determine whether interaction of CARD14 with Bcl10 can induce nucleation and insolubility of the latter. First, we assessed whether mutation of the CARD14 CARD domain could diminish downstream effects. The CARD14 R38 residue has been previously described to be at the Bcl10-interacting interface, and substitution of arginine R38 with cysteine in the CARD domain was previously reported to lack the ability to activate NF-κB (Jordan, 2012b; Qiao, 2013); therefore, it was anticipated that the R38C mutation would abolish CARD:CARD interactions. Indeed, mutation of the R38 residue in the CARD14 E138A construct completely abrogates the ability of the E138A mutant to interact with Bcl10 (see Figure 1b, Supplementary Figure S1c) and to potently activate NF-κB and AP-1 in HEK293 cells (see Supplementary Figure S1d). R38C mutation also diminished the ability of CARD14 E138A to drive IL-8 production in primary keratinocytes (see Supplementary Figure S1e).

To assess nucleation of Bcl10 in the presence of CARD14 GoF mutants, primary keratinocytes were transfected with CARD14 WT, CARD14 E138A, and CARD14 R38C/E138A. Cells were lysed in Triton X-100–containing buffer (Sigma Aldrich, St. Louis, MI), and Triton-insoluble and soluble fractions were assessed by SDS-PAGE. As expected, mutant CARD14 variants were found at higher levels in the insoluble fraction than WT CARD14. Moreover, levels of Bcl10 were more highly increased in the insoluble fraction in the presence of CARD14 E138A compared with CARD14 WT, and this was dependent on a functional CARD domain (Figure 1c), also consistent with a previous report (Bertin et al., 2001).

Insoluble mutant CARD14 E138A and CARD14 ΔE138/Bcl10 complexes or "signalosomes" are visible by confocal microscopy in primary keratinocytes (Figure 1d), whereas CARD14 WT was more widely expressed throughout the cytoplasm, consistent with its weak interaction with Bcl10 in co-immunoprecipitation studies. CARD14 R38C/E138A retained the ability to form insoluble oligomers (Figure 1c and d), but it failed to recruit Bcl10 to these complexes in primary keratinocytes (Figure 1d).

Spontaneous signalosome formation induced by CARD14 E138A and CARD14 ΔE138 resulted in enhanced Malt1 para-caspase activity in HEK293 cells, as measured using a previously described fluorescence resonance energy transfer-
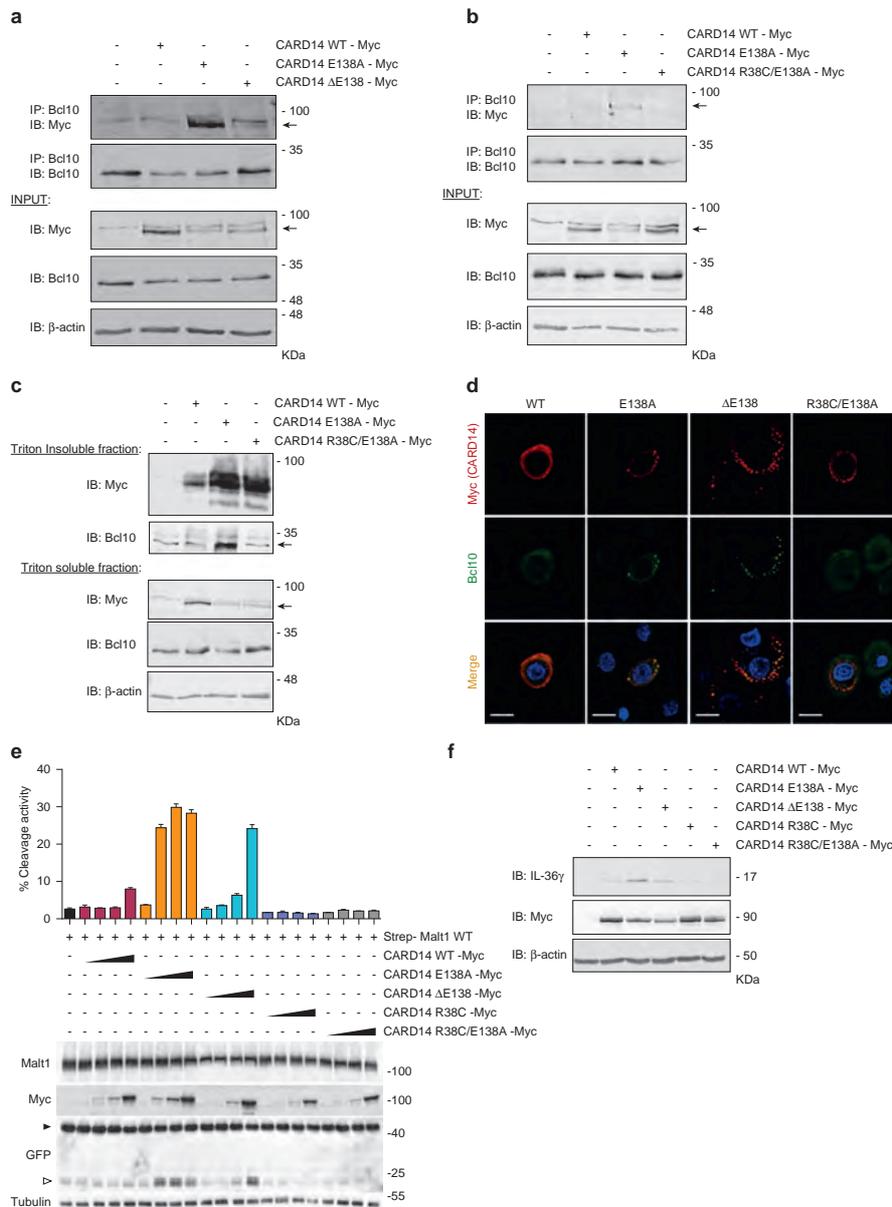
**Figure 1. Mutation of *Card14 E138* causes spontaneous signalosome assembly in primary keratinocytes and is dependent on a functional CARD domain.** (**a, b**) Primary keratinocytes were transfected with Myc-tagged CARD14 WT, CARD14 E138A, and (**a**) CARD14 ΔE138 or (**b**) CARD14 R38C/E138A for 24 hours. Cell lysates were immunoprecipitated with an anti-Bcl10 antibody, followed by immunoblotting with indicated antibodies. (**c**) Human primary keratinocytes were transfected for 24 hours with Myc-tagged CARD14 WT, CARD14 E138A, or CARD14 R38C/E138A. Cells were lysed in Triton X-100−containing buffer, and soluble and insoluble fractions were subject to SDS-PAGE followed by immunoblotting with indicated antibodies. (**d**) Human primary keratinocytes were transfected for 24 hours with Myc-tagged CARD14 WT, CARD14 E138A, CARD14 ΔE138, or CARD14 R38C/E138A and visualized for expression and localization by confocal microscopy using specific anti-Myc and anti-Bcl10 antibodies. Nuclei were stained with DAPI. Scale bar = 15 μm. (**e**) Flow cytometry analysis and immunoblot analysis of HEK293T cells transfected with increasing amounts of Myc-tagged CARD14 constructs with Strep-tagged Malt1 and the

**a**


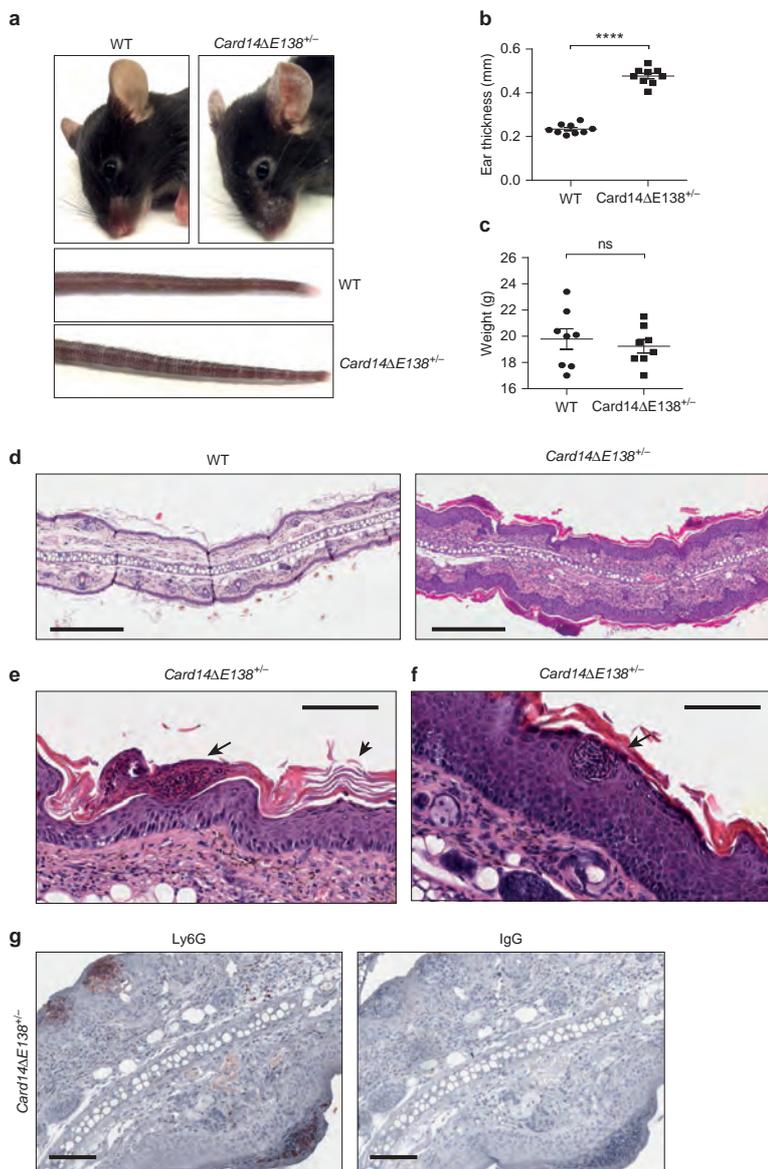
**b**



**c**



**d**



**e**



**f**



**g**



**Figure 2. *Card14ΔE138*⁺ᐟ⁻ heterozygous mice develop a spontaneous psoriatic phenotype.** (**a**) 8-week-old *Card14ΔE138*⁺ᐟ⁻ heterozygous mice develop dry skin around the eyes and whiskers and dry flaky skin on the ears and tail. (**b**) Ear thickness (mm) of *Card14ΔE138*⁺ᐟ⁻ and wild-type littermates measured with microcalipers (n = 9 per group). (**c**) *Card14ΔE138*⁺ᐟ⁻ mice and wild-type littermates were weighed at 8 weeks old (n = 8 per group). (**d–f, h**) Hematoxylin and eosin staining of ear sections from 8-week-old *Card14ΔE138*⁺ᐟ⁻ and wild-type mice. Arrows show (**e**) parakeratosis (arrow) and orthokeratosis (arrowhead), (**f**) microabscess, and (**h**) blood vessels. Scale bar = 300 μm in **d** or 100 μm in **e**, **f**, and **h**. (**g**) Ear sections from 8-week-old *Card14ΔE138*⁺ᐟ⁻ mice stained with a specific anti-Ly6G antibody or isotype control. Scale bar = 100 μm. (**i**) Ear sections from 8-week-old *Card14ΔE138*⁺ᐟ⁻ and wild-type littermates were stained with specific antibodies against Ki67, keratin-14, and keratin-1. Images (**a**) are representative of all *Card14ΔE138*⁺ᐟ⁻ heterozygous mice observed or (**d–i**) are representative of 8 individual mice per group, or (**b, c**) each data point represents an individual mouse and was subjected to a two-tailed unpaired Student $t$ test, ****$P < 0.0001$. ns, nonsignificant; WT, wild type.

based assay (Pelzer et al., 2013) (Figure 1e), consistent with previous reports (Afonina, 2016; Howes, 2016). Malt1 displayed augmented catalytic activity in the presence of CARD14 E138A and CARD14 ΔE138 mutants compared with WT (Figure 1e). However, CARD14 R38C/E138A lost the ability to stimulate Malt1 activity beyond basal levels. In primary keratinocytes, CARD14 E138A and CARD14 ΔE138 mutants drive production of IL-36γ; however, again

EYFP-LVSR-eCFP reporter plasmid for 24 hours. (**f**) Human primary keratinocytes were transfected for 24 hours with Myc-tagged CARD14 constructs. Cell lysates were subject to immunoblotting with anti-Myc, anti-IL-36γ, and anti-β-actin antibodies. Data in **a–f** are representative of three independent experiments. IB, immunoblot; IP, immunoprecipitation; WT, wild type.

**Figure 2.** Continued

h



i
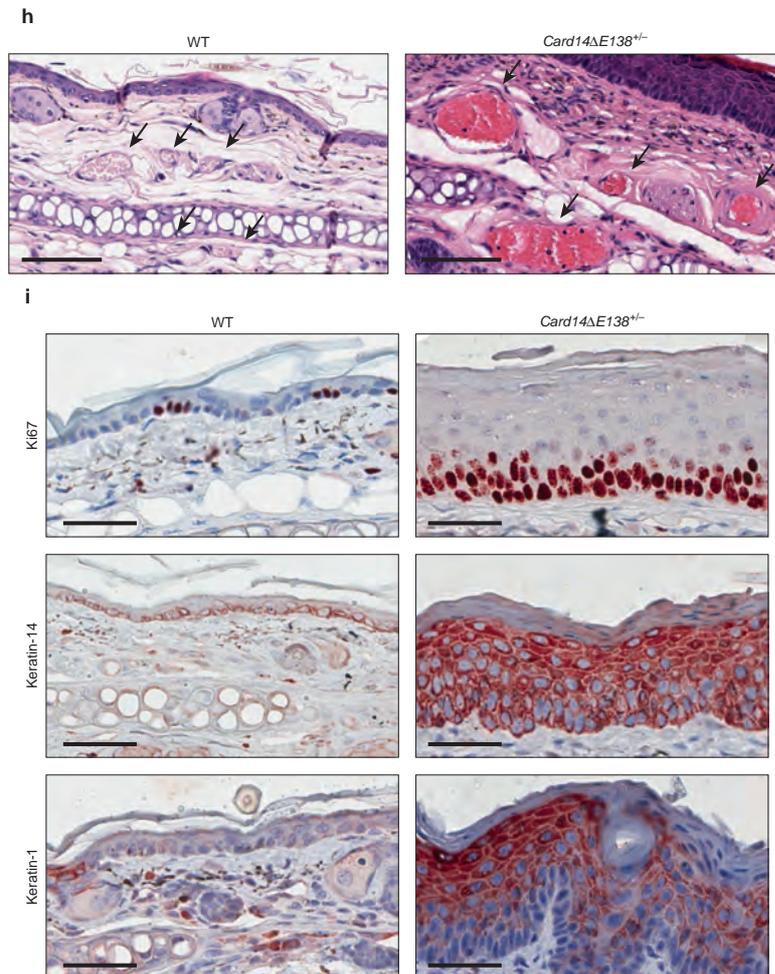


disruption of the CARD domain abolishes this effect (Figure 1f).

**Mutation of Card14 E138 causes spontaneous psoriasiform disease in mice**

To define the physiological impact of CARD14 E138 GoF mutation in potentially driving psoriasis pathogenesis, a transgenic mouse incorporating deletion of the E138 residue of CARD14 was generated using CRISPR/Cas9 technology (see Supplementary Figure S2a and b). The Card14ΔE138 mutation was chosen because it displayed less potent activation of NF-κB, and it was speculated that these mice might be less likely to suffer unwanted defects due to hyperactive NF-κB activity. Card14ΔE138 heterozygous mice appeared indistinguishable from WT littermates at birth (see Supplementary Figure S2c) but developed dry flaky skin

patches on the back at 5 days of age, which began to disappear at 7 days. However, this progressed to the development of thickened squamous skin on the tail (between 2 and 3 weeks) and, finally, the ears (at 4−5 weeks), reminiscent of human psoriasis skin lesions (see Supplementary Figure S2d and e). Adult mice showed a chronic psoriatic phenotype with thickened squamous skin of the ears and tail and dry skin around the eyes and whiskers, affecting 100% of heterozygous male and female mice (Figure 2a). Ear thickness was significantly increased in *Card14ΔE138*^{+/−} mice compared with WT littermates (Figure 2b). There was no significant difference in weight in *Card14ΔE138*^{+/−} adult mice compared with WT littermates (Figure 2c).

Hematoxylin and eosin staining of ear tissue from *Card14ΔE138*^{+/−} mice showed acanthosis due to keratinocyte hyperproliferation and immune cell infiltration of the

skin (Figure 2d), areas of hyperkeratosis (Figure 2e), including parakeratosis (arrow) and orthokeratosis (arrowhead), and keratotic follicular plugging (see Supplementary Figure S3a online), all hallmarks of human psoriatic skin disease. Similarly, tail skin showed marked hyperplasia (see Supplementary Figure S3b) with increased thickening of the epidermis and immune cell infiltration. In addition to a clear increase in infiltrate of immune cells, the presence of microabscesses was also observed in the epidermis of *Card14ΔE138*$^{+/-}$ mice (Figure 2f). Positive staining with the neutrophil marker Ly6G indicated that neutrophils make up the composition of these microabscesses (Figure 2g). An increased number of enlarged CD31-positive blood vessels were also histologically observed in the dermis, indicating an increase in the dermal vasculature in psoriatic tissue from *Card14ΔE138*$^{+/-}$ mice (Figure 2h, and see Supplementary Figure S3c). In *Card14ΔE138*$^{+/-}$mice, basal keratinocytes showed strong and abundant expression of the proliferation marker Ki67, indicating hyperproliferation of keratinocytes in the basal layer (Figure 2i, and see Supplementary Figure S3d). Similarly, keratin-14 expression, a marker for the proliferative basal layer of the epidermis, was no longer restricted to basal keratinocytes, as in WT mice, but also present in suprabasal layers, typical of human psoriasis. Expression of keratin-1 (an indicator of early keratinocyte differentiation), which was localized in the suprabasal layer of WT mice, is increased and expressed throughout the epidermis in *Card14ΔE138*$^{+/-}$ mouse skin. *Card14ΔE138* homozygous mice displayed development abnormalities (see Supplementary Figure S4a online) and increased mortality. Surviving neonates were runts (see Supplementary Figure S4b) and died after a few days, typically with a very marked psoriatic phenotype (see Supplementary Figure S4c and d). Toluidine blue staining was performed to determine whether neonates had a skin barrier defect and an increase in skin permeability. Toluidine blue dye failed to stain the epidermis, indicating that neither homozygous nor heterozygous pups had an epidermal barrier defect (see Supplementary Figure S4e).

**CARD14 GoF mutation in vivo results in a transcriptomic gene profile similar to human plaque psoriasis**
To obtain a comprehensive overview of the transcriptional signature of the inflammatory milieu driving disease pathogenesis in *Card14ΔE138*$^{+/-}$ mice, RNA was extracted from ear tissue of 8-week-old mice and subjected to RNA sequencing analysis (Figure 3a−c). Differentially expressed genes from the psoriatic tissue of *Card14ΔE138*$^{+/-}$ mice included up-regulated hyperproliferative keratins (*Krt6a, Krt6b, Krt16*); antimicrobial peptides including β-defensins (*Defb3, Defb4, Defb14*), S100 proteins (*S100a7, S100a8, S100a9*), and lipocalin-2 (*Lcn2*); and mRNA-encoding cytokines of the innate (IL-1α, IL-1β, IL-36α, IL-36β, IL-36γ, IL-6, and IL-17C) and adaptive (IL-20, IL-22, IL-23p19, and IL-17F) immune systems. IL-20 family member IL-19, a cytokine previously shown to be up-regulated in serum and tissue of psoriasis patients and a key component of the IL-23/IL-17A axis, was one of the most highly up-regulated cytokines. IL-19 was shown previously to be specifically expressed by keratinocytes and acts in an autocrine manner in synergy with IL-17A to further enhance induction of anti-bacterial

S100 proteins (Romer et al., 2003; Witte et al., 2014). Up-regulation of chemokines was also evident, including *Ccl20* and the neutrophil chemoattractants *Cxcl1, Cxcl2, Cxcl3,* and *Cxcl5*. This transcriptional signature likely also reflects secondary changes in dermal endothelial cells and infiltrating immune cells. IL-1 family cytokines, including receptor antagonists, NOD2, caspase-1, caspase-4, and NLRP3, are all up-regulated in *Card14ΔE138*$^{+/-}$ psoriatic tissue, indicating that this phenotype is very much dependent on auto-inflammatory and autoimmunity networks.

Psoriatic tissue from *Card14ΔE138*$^{+/-}$ mice also showed high expression of early cornified envelope proteins including involucrin (*Ivl*) and IL-17A−induced small proline rich proteins (*Sprr2b* and *Sprr2d*). The S100-interacting protein Fabp5 is also increased. Late cornified envelope proteins including *Lce3b* and *Lce3d* show high expression, and the serine protease inhibitors *Sepinb3a, Sepinb3c, Sepina9* are also highly up-regulated. Down-regulated differentially expressed genes include keratin-2 and -24, serpin3b, and serpin12. Filaggrin-2 was also down-regulated, inversely correlating with filaggrin-1 expression in this model. IL-38 (*Ilf10*), an anti-inflammatory cytokine that specifically inhibits IL-36 cytokines, was also down-regulated in *Card14ΔE138*$^{+/-}$ psoriatic tissue, suggesting that in psoriatic skin disease, increased activity of IL-36 cytokines is likely additionally enhanced by decreased expression of this endogenous inhibitor.

We performed pathway analysis and found that k*eratinization*, f*ormation of the cornified envelope, signaling by interleukins*, and a*ntimicrobial peptides* were enriched functions among up-regulated genes (Figure 3c). Comparing transcriptome analysis from *Card14ΔE138*$^{+/-}$ mice with that of human plaque psoriasis available from the publications of Li et al. (2014) (GSE54456) and Keermann et al. (2015) (GSE6651), there is positive enrichment of up-regulated genes with both human studies and negative enrichment of down-regulated genes (Figure 3d). This correlation shows that the transcriptional landscape induced by CARD14 GoF mutation in vivo is typical of human plaque psoriasis.

To further confirm transcriptomic data and to analyze the expression of proinflammatory genes at the onset of macroscopic skin changes in *Card14ΔE138*$^{+/-}$ mice, RNA was extracted from ear tissue of 5-week-old *Card14ΔE138*$^{+/-}$ mice and analyzed by quantitative PCR. Expression of mRNA encoding the proinflammatory cytokines IL-36γ, IL-1β, IL-17C, and IL-19 (Figure 3e) was significantly higher in ear tissue of *Card14ΔE138*$^{+/-}$ mice. Similar to human psoriatic skin, *Card14ΔE138*$^{+/-}$ murine tissue showed strong and significantly increased expression of genes encoding the S100 antimicrobial peptides *S100a7* and *S100a8* (Figure 3f); β-defensins *Defb3, Defb4,* and *Defb14* (Figure 3g); and the chemokines *Cxcl1, Cxcl2,* and *Ccl20* (Figure 3h). Expression of filaggrin-1 and filaggrin-2 was also assessed and confirmed RNA sequencing data, with an increase in filaggrin-1 (*Flg*) and a decrease in filaggrin-2 (*Flg2*) in psoriatic tissue (Figure 3i). Expression of caspase-14, which mediates pro-filaggrin processing to form the cornified envelope, is also increased in *Card14ΔE138*$^{+/-}$ psoriatic tissue (Figure 3a and b). Loss of filaggrin-1 expression is associated with an
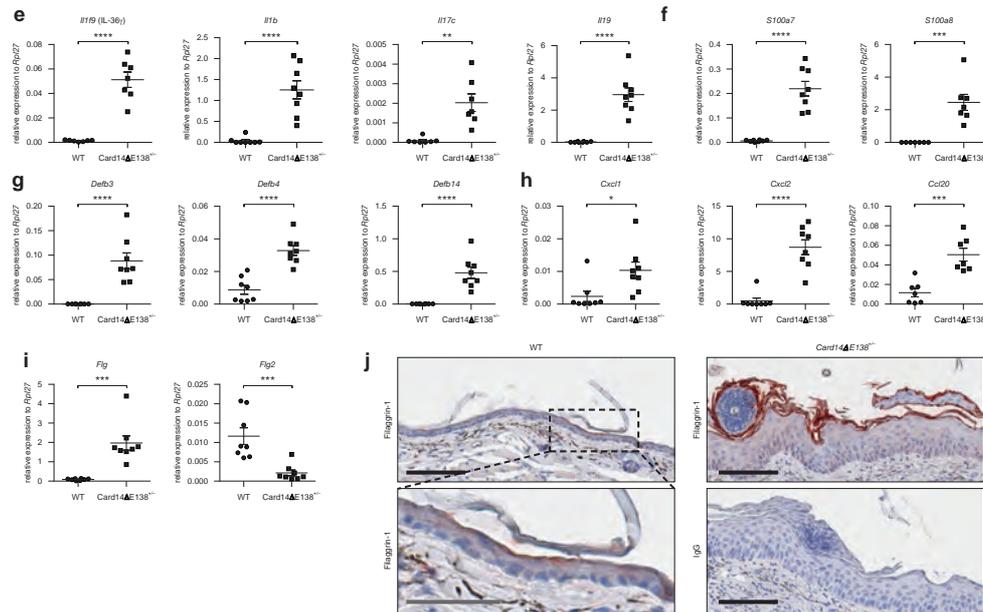
**M Mellett et al.**
CARD14 Mutation in Mice Drives Psoriasiform Disease



**Figure 3. Transcriptome analysis of psoriatic tissue from ears of *Card14ΔE138*^+/− mice shows a gene signature typical of human plaque psoriasis.** (**a**–**d**) RNA was extracted from 8-week-old *Card14ΔE138*^+/− heterozygous mice and wild-type littermates and subject to RNA sequencing analysis. (**a**) Heatmap showing the 542 genes DEGs between three replicates of *Card14ΔE138*^+/− heterozygous mice and wild-type littermates. (**b**) Volcano plot showing the threshold for significant genes from *Card14ΔE138*^+/− versus wild-type mice. A threshold of false discovery rate < 0.05 and log$_2$ ratio > 2 or < −2 was chosen. Differentially expressed genes of particular interest are labeled. (**c**) Dotplot showing the significantly enriched pathways from the Reactome. Each dot size represents the

**Figure 3.** Continued

epidermal barrier dysfunction, which grants microbes the means to invade the epidermis, as in atopic dermatitis (O'Regan et al., 2008). Robust expression of filaggrin-1 in psoriatic tissue of *Card14ΔE138*^{+/−} mice is consistent with the lack of any barrier defect in these mice (Figure 3j).

**The CARD14/Bcl10 signaling axis is hyperactive in primary keratinocytes from *Card14ΔE138*^{+/−} mice**
To determine whether the epidermal changes observed in *Card14ΔE138*^{+/−} mice were due to dysregulated CARD14 function, epidermal tissue from ear pinnae of WT and *Card14ΔE138*^{+/−} mice were stained for Bcl10 and CARD14 expression. Both molecules showed enhanced expression in the epidermis from *Card14ΔE138*^{+/−} mice compared with WT (Figure 4a). To further assess the CARD14/Bcl10 interaction in *Card14ΔE138*^{+/−} mice, primary keratinocytes were isolated from WT and *Card14ΔE138*^{+/−} mouse epidermis and cultured ex vivo. Murine keratinocytes were subject to lysis in Triton X-100−containing lysis buffer and soluble and insoluble fractions subject to SDS-PAGE (Figure 4b). CARD14 and Bcl10 showed increased expression in the insoluble fraction in *Card14ΔE138*^{+/−}-derived cells compared with WT control

cells, which correlated with decreased expression in the soluble fraction. Additionally, Bcl10 and CARD14 showed increased interaction as determined by co-immunoprecipitation (Figure 4c) and enhanced processing of Malt1 substrate protein RelB. Bcl10 expression was visualized by confocal microscopy, and in primary keratinocytes from WT mice, Bcl10 was expressed uniformly throughout the cytoplasm; however, in keratinocytes from *Card14ΔE138*^{+/−} mice Bcl10 was observed in discrete signalosome structures (Figure 4d). To assess the downstream effects of this increased interaction, transcript levels of pro-inflammatory molecules were assessed in keratinocytes isolated and cultured from WT and *Card14ΔE138*^{+/−} mouse epidermis by quantitative PCR. Levels of mRNA encoding S100A7, IL-17C, IL-19, and IL-36γ were significantly increased in *Card14ΔE138*^{+/−} keratinocytes compared with WT cells (Figure 4e).

**Neutralization of the T helper type 17-polarizing cytokine IL-23 p19 subunit attenuates disease symptoms**
We next characterized the immune infiltrate of the skin of *Card14ΔE138*^{+/−} mice. Psoriatic skin of *Card14ΔE138*^{+/−}
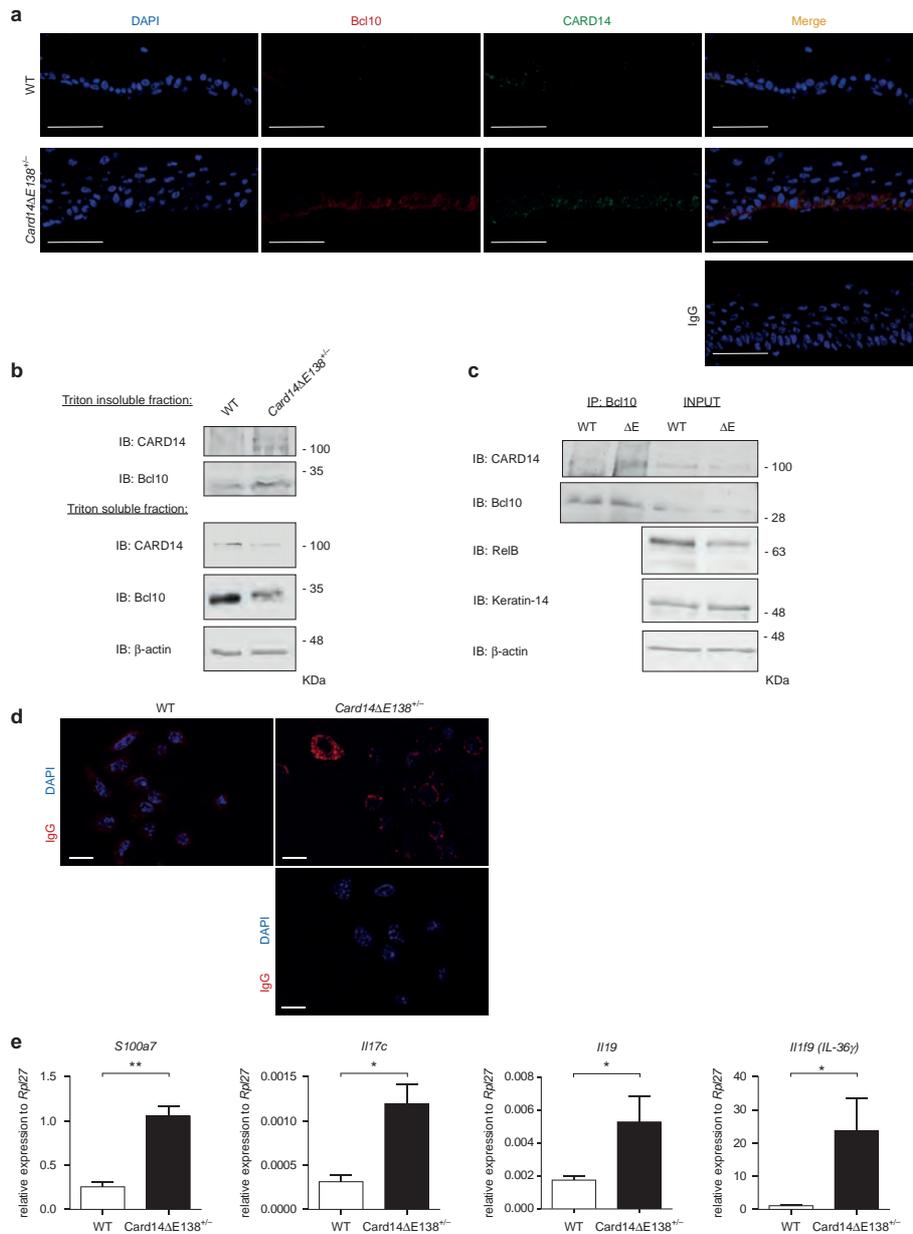
**Figure 4. Keratinocytes from *Card14ΔE138⁺/⁻* mice display enhanced CARD14/Bcl10 activity.** (**a**) Confocal microscopy analysis of epidermal tissue from ear pinnae from WT and *Card14ΔE138⁺/⁻* mice stained for specific anti-Bcl10, -CARD14, or isotype control antibodies. Nuclei were stained with DAPI. Scale bar = 50 μm. (**b–e**) Primary murine keratinocytes were isolated from WT and *Card14ΔE138⁺/⁻* tail epidermis and cultured ex vivo for 3−4 days. (**b**) Cells were lysed in Triton-X−containing buffer, and soluble and insoluble fractions were subject to SDS-PAGE followed by immunoblotting with indicated antibodies. (**c**) Cell lysates were immunoprecipitated with an anti-Bcl10 antibody, followed by immunoblotting with indicated antibodies. ΔE = keratinocytes from *Card14ΔE138⁺/⁻* mice. (**d**) Cells visualized for expression and localization of endogenous murine Bcl10 by confocal microscopy using a specific anti-Bcl10 antibody. Nuclei were stained with DAPI. Scale bar = 15 μm. (**e**) RNA was extracted from whole ear tissue of 5-week-old mice and subjected to quantitative PCR

mice harbors a pronounced infiltrate of CD45-positive leukocytes (Figure 5a). This immune infiltrate is composed of increased numbers of neutrophils, myeloid antigen-presenting cells, and γδ and αβ T cells compared with WT littermates (Figure 5b, and see Supplementary Figure S5 online). T helper (Th) 17 cells play a central role in psoriasis pathogenesis, and IL-23 maintains the differentiation of pathogenic Th17 cells, which secrete IL-17A and IL-22, two of the cytokines that mediate the inflammatory effects and hyperproliferation associated with human psoriasis (Cai et al., 2012). Indeed, protein levels of IL-17A and IL-22 were significantly increased in *Card14ΔE138*$^{+/-}$ ear tissue of adult mice (Figure 5c). IL-23p19, IL-17A, and IL-22–encoding transcripts were also seen at significantly higher levels in 5-week-old *Card14ΔE138*$^{+/-}$ mouse skin (Figure 5d). Similarly, the Th1 cytokines IFNγ and TNF-α were also significantly elevated in ear tissue of 5-week-old *Card14ΔE138*$^{+/-}$ mice (Figure 5e), contributing to an inflammatory milieu typical of human psoriasis.

To assess whether CARD14-induced psoriatic disease symptoms can be attenuated in vivo by targeted disruption of the IL-23/Th17 axis, *Card14ΔE138*$^{+/-}$ heterozygous mice were treated with a neutralizing antibody specific for the murine IL-23p19 subunit by intraperitoneal injection over the course of 15 days, and control mice were administered an IgG isotype antibody. Mice receiving anti-IL-23p19–neutralizing antibody showed a significantly decreased psoriatic phenotype on the ears and tail after 2 weeks of therapy (Figure 5f) and a significant reduction in ear thickness versus at the onset of treatment and versus IgG control animals (Figure 5g). Further reductions were evident after administration of IL-23p19 over 3 weeks (see Supplementary Figure S6a–c online). Histological features were assessed by the scoring system of Baker et al. (1992), and IL-23p19–treated mice showed a significant decrease in murine clinical score (Figure 5h and i). In vivo blockade of IL-23p19 also reduced expression of mRNA encoding β-defensins, S100 proteins, IL-36γ, and IL-19 (Figure 5j). These results indicate that disruption of the IL-23/Th17 immune signaling axis is sufficient to reverse the aberrant epidermal signaling networks induced by CARD14 GoF mutation. Thus, CARD14 GoF drives IL-23–mediated psoriatic skin disease, and targeting of IL-23p19 in this mouse model is a rapid and effective therapeutic option, consistent with reports from phase III clinical trials in patients with plaque-type psoriasis (Nakamura et al., 2017; Papp et al., 2017; Reich et al., 2017).

## DISCUSSION

Psoriasis is a common but complex inflammatory skin disease that arises from the interplay between stress or trauma within the epidermis and a dysregulated immune response. Genetic studies have shown a role for selected genes, particularly those of the innate and adaptive immune system and the IL-23/IL-17 signaling axis (Tsoi, 2012). Several genes encoding proteins in epithelial barrier function have also been linked to psoriasis susceptibility, and GoF mutations in

the gene encoding the keratinocyte signaling molecule, CARD14, have been associated with both psoriasis and PRP, although the extent to which CARD14 genetic variants contribute to disease susceptibility is currently unclear.

Here, we unequivocally show that CARD14 GoF alone is sufficient to drive disease pathogenesis in vivo and show that a single amino acid mutation of a key glutamic acid (E138) results in the complete immunological and clinical phenotype of plaque-type psoriasis in mice. The etiology of psoriasis has been elusive in the past, regarding the contribution of keratinocyte dysfunction versus altered immune function (Bos et al., 2005; Christophers, 1996). However, our data strongly suggest that dysregulated keratinocyte signaling pathways initiated by CARD14 contribute to drive the pathogenic IL-23/IL-17 axis in vivo. *Card14ΔE138* heterozygous mice spontaneously and rapidly developed a chronic psoriatic phenotype with scaling skin lesions, epidermal acanthosis, parakeratosis, and hyperkeratosis, keratinocyte hyperproliferation, and immune cell infiltration of lesional skin. In addition to *Card14ΔE138*$^{+/-}$ tissue recapitulating the histological features of psoriasis, transcriptome profiling from affected skin in these mice correlated with up-regulated and down-regulated gene signatures observed in human plaque psoriasis. In particular, high expression of antimicrobial peptides (β-defensins, S100 proteins), chemokines (*Cxcl2*, *Ccl20*), and cytokines (including IL-19, IL-36γ, IL-1β, and IL-23p19) were observed. Additionally, neutralization of IL-23p19 significantly reduced skin lesions and the expression of anti-microbial peptides and proinflammatory cytokines in the skin of *Card14ΔE138* mice.

Tanaka et al. (2018) recently showed that CARD14-deficient mice were protected from developing imiquimod-induced psoriasiform disease (Tanaka et al., 2018), which is consistent with our results that GoF mutation in CARD14 is sufficient to drive the complete immunopathogenesis of psoriatic disease in vivo. Tanaka's study shows a role for CARD14-positive hematopoietic cells in imiquimod-induced psoriasiform disease. In our study, keratinocytes harboring mutant CARD14 contribute to disease pathogenesis; however, it will be of interest to further tease out the interplay of these different cell types in disease pathogenesis. Taken together, these reports place CARD14 in a central role of mediating psoriatic skin disease pathogenesis, which warrants further clinical appraisal. The physiological relevance to human disease means that the *Card14ΔE138*$^{+/-}$ mouse model will become an invaluable tool for dissecting the complex signaling networks associated with psoriatic skin disease. This model will also be beneficial in the preclinical assessment of therapeutics aimed at specifically targeting molecular drivers of psoriasis and PRP in the future. These findings highlight the formation of the CARD14/Bcl10/Malt1 complex as a key cellular process to target in the development of future therapies for psoriatic disease. Malt1-specific inhibitors have been suggested as a potential therapeutic strategy that can be used for treating psoriatic skin disease, because inhibition of Malt1 function would have the benefit

analysis of mRNA expression of *S100a7*, *Il17c*, *Il19*, and *Il1f9* (IL-36γ). (**a**–**d**) Images are representative of three independent experiments or (**e**) data are presented as the mean ± standard error of the mean of three independent experiments and were subjected to a two-tailed unpaired Student *t* test. *$P < 0.05$, **$P < 0.01$. IB, immunoblot; WT, wild type.

*M Mellett* et al.
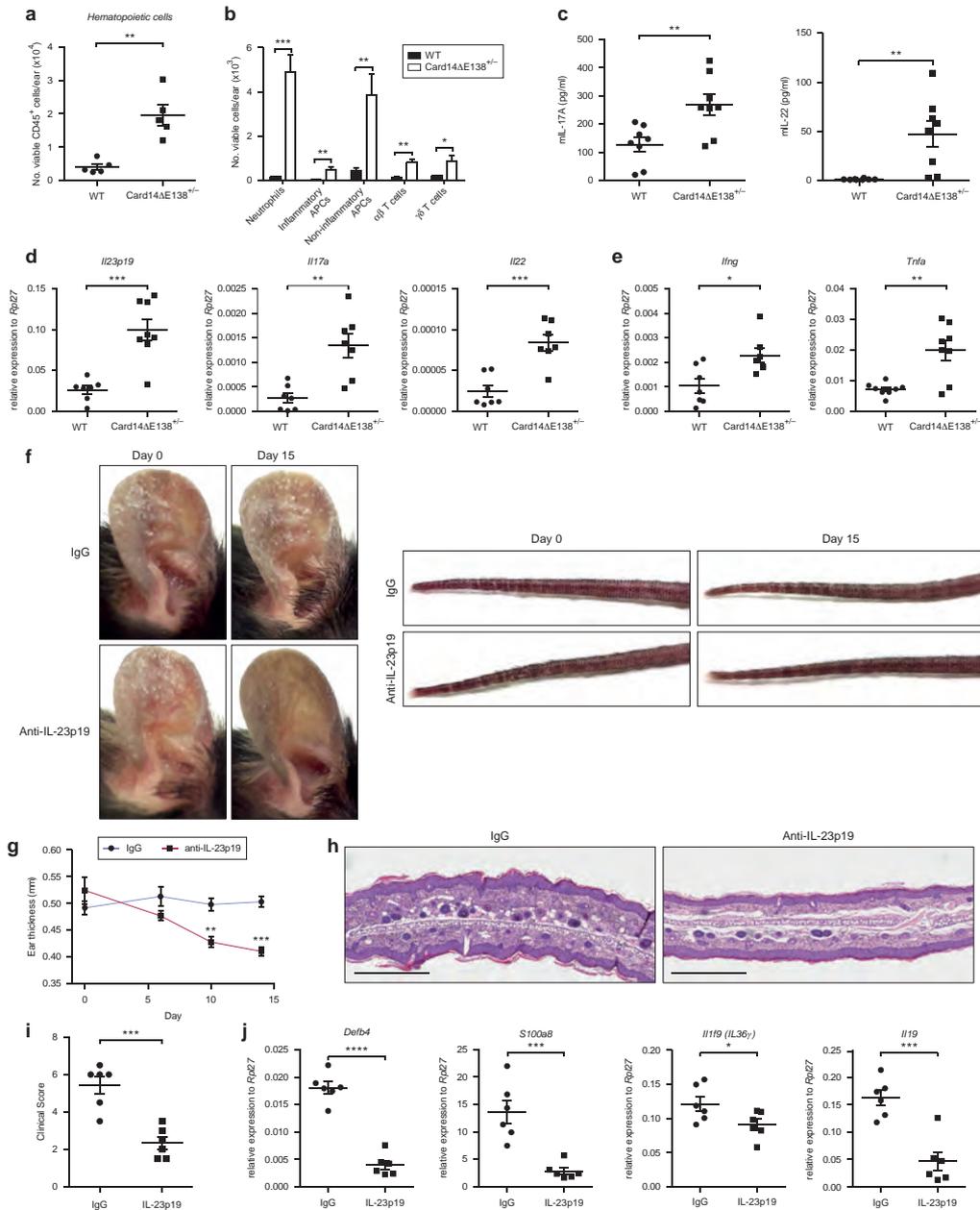CARD14 Mutation in Mice Drives Psoriasiform Disease



**Figure 5. Immune cell infiltrate shows a T helper type 17 signature, and IL-23p19 neutralization ameliorates the phenotype in *Card14ΔE138*^{+/−} mice. (a, b)** Flow cytometry analysis of single-cell suspension from ear tissue from age- and sex-matched adult *Card14ΔE138*^{+/−} mice and littermate controls. Shown are the number of (**a**) CD45^{+} hematopoietic cells and (**b**) neutrophils (CD11b^{+}Ly6G^{+}), inflammatory (CD11b^{+}Ly6G^{−}NK1.1^{−}MHCII^{hi}Ly6C^{hi}) and noninflammatory (CD11b^{+}Ly6G^{−}NK1.1^{−}MHCII^{hi}Ly6C^{−}) APCs, αβ T cells (CD3^{low}TCRβ^{+}), and γδ T cells (CD3^{low}TCRβ^{−}) per ear. (**c**) Whole ears from age- and sex-matched adult *Card14ΔE138*^{+/−} and wild-type mice were homogenized and analyzed for IL-17A and IL-22 protein levels by ELISA (n = 8). (**d, e**) RNA was extracted from whole ear tissue of 5-week-old mice and subjected to quantitative PCR analysis of (**d**) *Il23p19*, *Il17a,* and *Il22* or (**e**) *Ifng* (IFNγ) and *Tnfa* mRNA expression

of affecting T-cell and keratinocyte function (downstream of CARD11 and CARD14, respectively) (Van Nuffel et al., 2017). Targeting CARD14 directly, however, may permit the development of more specific therapies with decreased adverse effect profiles, and this merits further investigation into understanding CARD14 biology.

## MATERIALS AND METHODS
Details of the materials and methods are given in the Supplementary Materials online.

### Genetically modified mouse strains
To generate *Card14ΔE138* mice, C57BL/6J (JR 000664) oocytes were microinjected with Cas9 mRNA and donor DNA along with one of two guide RNA sequences. Two strains harboring the *Card14ΔE138* deletion were generated from separate founder animals, strains 28900 (C57BL/6J-Card14em9(delE138)Lutzy/J) and 28882 (C57BL/6J-Card14em5(delE138)Lutzy/J). Mouse strain 28900 was used for the experiments described in the article. All animal experiments were performed in accordance with the regulations and guidelines of and with ethical approval from the Cantonal Veterinary Office of Zürich, Switzerland.

### Cell culture
Human primary keratinocytes were cultured as previously described (Feldmeyer et al., 2007). Briefly, human primary foreskin keratinocytes were passaged in keratinocyte serum-free medium (Thermo Fisher Scientific, Waltham, MA), supplemented with epithelial growth factor and bovine pituitary extract (Thermo Fisher Scientific), and seeded for experiments after 3 passages. All cells were maintained at $37\,^{\circ}C$ in a humidified atmosphere of 5% $CO_2$.

### RNA sequencing transcriptome analysis
RNA was extracted from whole ear tissue from 8-week-old female WT and *Card14ΔE138*$^{+/-}$ mice. After library preparation, samples were analyzed with the Illumina HiSeq 4000 (Illumina, San Diego, CA), which was used to generate single end reads of length 125 nucleotides. For data processing, the raw reads were first cleaned by removing adapter sequences, trimming low-quality ends, and filtering reads with low quality (phred quality < 20) using Trimmomatic (Bolger et al., 2014). Sequence alignment of the resulting high-quality reads to the Mus musculus reference genome (build GRCm38) and quantification of gene level expression was carried out using RSEM, version 1.3.0 (Li and Dewey, 2011). Differential expression was computed using the generalized linear model implemented in the Bioconductor package EdgeR, version 3.20.1 (Robinson et al., 2010). The data was deposited in the European Nucleotide Archive (accession number PRJEB25394). Pathway analysis was performed using ReactomePA (Yu and He, 2016). The top significant pathways were plotted as a dotplot. Gene set enrichment analysis was performed using fgsea (Sergushichev, 2016), and datasets from GSE66511 and

GSE54456 were obtained from the National Center for Biotechnology Information Gene Expression Omnibus.

### CONFLICT OF INTEREST
The authors state no conflict of interest.

### AUTHOR CONTRIBUTIONS
MM conceived the study and mouse models, developed the concept, designed and performed experiments, analyzed the data, co-supervised the project and wrote the manuscript. BM designed and performed immunohistochemistry experiments and analysis. DM performed flow cytometry and analysis. RS performed the fluorescence resonance energy transfer assay and subsequent flow cytometry, immunoblotting and data analysis. PC analyzed the RNA sequencing transcriptomic data, BK performed immunohistochemistry experiments, TS and SN contributed critical analysis and experimental design. MT and EC designed experiments, provided critical analysis of data and the manuscript. LEF supervised the project, provided critical analysis of data and co-wrote the manuscript.

### SUPPLEMENTARY MATERIAL
Supplementary material is linked to the online version of the paper at www.jidonline.org, and at https://doi.org/10.1016/j.jid.2018.03.1525.

### REFERENCES
Afonina IS, Van Nuffel E, Baudelet G, Driege Y, Kreike M, Staal J, et al. The paracaspase MALT1 mediates CARD14-induced signaling in keratinocytes. EMBO Rep 2016;17:914−27.

Baker BS, Brent L, Valdimarsson H, Powles AV, al-Imara L, Walker M, et al. Is epidermal cell proliferation in psoriatic skin grafts on nude mice driven by T-cell derived cytokines? Br J Dermatol 1992;126:105−10.

Berki DM, Liu L, Choon SE, David Burden A, Griffiths CEM, Navarini AA, et al. Activating CARD14 mutations are associated with generalized pustular psoriasis but rarely account for familial recurrence in psoriasis vulgaris. J Invest Dermatol 2015;135:2964−70.

Bertin J, Wang L, Guo Y, Jacobson MD, Poyet JL, Srinivasula SM, et al. CARD11 and CARD14 are novel caspase recruitment domain (CARD)/membrane-associated guanylate kinase (MAGUK) family members that interact with BCL10 and activate NF-kappa B. J Biol Chem 2001;276:11877−82.

Bolger AM, Lohse M, Usadel B. Trimmomatic: a flexible trimmer for Illumina sequence data. Bioinformatics 2014;30:2114−20.

Bos JD, De Rie MA. The pathogenesis of psoriasis: immunological facts and speculations. Immunol Today 1999;20:40−6.

---

levels. (**f**) Macroscopic images of ears and tails of IgG- and IL-23p19−treated mice at the beginning and end (day 15) of the experiment. (**g**) Ear thickness of IL-23p19−treated animals and control animals at days 0, 6, 10, and 15 of the experiment. IL-23p19 group, n = 6; IgG group, n = 6. (**h**) Representative histological features shown by hematoxylin and eosin staining at day 15. Scale bar = 500 μm. (**i**) Clinical scoring of histological features of IgG- versus IL-23p19−treated mice. (**j**) quantitative PCR analysis of mRNA expression of *Defb4*, *S100a8*, *Il1f9* (IL-36γ), and *Il19* in ear tissue from IL-23p19−treated and IgG-treated mice. Data are representative of (**a, b**) three independent experiments, (**c**) one experiment with eight or nine mice per group, or (**d, e**) two independent experiments with seven or eight mice per group. Total n = 15. (**f**) Images are representative of IgG- and IL-23p19−treated mice (total n = 10 per group) or (**g−j**) data are presented as the mean ± standard error of the mean of six mice, representative of two independent experiments (total n = 10 per group) and were subjected to a two-tailed unpaired Student *t* test. *$P$ < 0.05, **$P$ < 0.01, ***$P$ < 0.001, ****$P$ < 0.0001. APC, antigen-presenting cell; WT, wild type.

**M Mellett et al.**
CARD14 Mutation in Mice Drives Psoriasiform Disease

Bos JD, de Rie MA, Teunissen MB, Piskin G. Psoriasis: dysregulation of innate immunity. Br J Dermatol 2005;152:1098−107.

Boyman O, Conrad C, Tonel G, Gilliet M, Nestle FO. The pathogenic role of tissue-resident immune cells in psoriasis. Trends Immunol 2007;28:51−7.

Cai Y, Fleming C, Yan J. New insights of T cells in the pathogenesis of psoriasis. Cell Mol Immunol 2012;9:302−9.

Christophers E. The immunopathology of psoriasis. Int Arch Allergy Immunol 1996;110:199−206.

Christophers E. Psoriasis—epidemiology and clinical spectrum. Clin Exp Dermatol 2001;26:314−20.

Du S, Jia L, Zhang Y, Fang L, Zhang X, Fan Y. CARMA3 is upregulated in human pancreatic carcinoma, and its depletion inhibits tumor proliferation, migration, and invasion. Tumour Biol 2014;35:5965−70.

Feldmeyer L, Keller M, Niklaus G, Hohl D, Werner S, Beer HD. The inflammasome mediates UVB-induced activation and secretion of interleukin-1beta by keratinocytes. Curr Biol 2007;17:1140−5.

Fuchs-Telem D, Sarig O, van Steensel MA, Isakov O, Israeli S, Nousbeck J, et al. Familial pityriasis rubra pilaris is caused by mutations in CARD14. Am J Hum Genet 2012;91:163−70.

Gaide O, Favier B, Legler DF, Bonnet D, Brissoni B, Valitutti S, et al. CARMA1 is a critical lipid raft-associated regulator of TCR-induced NF-kappa B activation. Nat Immunol 2002;3:836−43.

Gaide O, Martinon F, Micheau O, Bonnet D, Thome M, Tschopp J. Carma1, a CARD-containing binding partner of Bcl10, induces Bcl10 phosphorylation and NF-kappaB activation. FEBS Lett 2001;496(2-3):121−7.

Griffiths CE, Barker JN. Pathogenesis and clinical features of psoriasis. Lancet 2007;370(9583):263−71.

Gudjonsson JE, Elder JT. Psoriasis: epidemiology. Clin Dermatol 2007;25:535−46.

Harden JL, Lewis SM, Pierson KC, Suarez-Farinas M, Lentini T, Ortenzio FS, et al. CARD14 expression in dermal endothelial cells in psoriasis. PLoS One 2014;9(11):e111255.

Has C, Schwieger-Briel A, Schlipf N, Hausser I, Chmel N, Rosler B, et al. Target-sequence capture and high throughput sequencing identify a de novo CARD14 mutation in an infant with erythrodermic pityriasis rubra pilaris. Acta Derm Venereol 2016;96:989−90.

Hong JB, Chen PC, Chen YT, Tsai TF. Genetic analysis of CARD14 in non-familial pityriasis rubra pilaris: a case series. Acta Derm Venereol 2014;94:587−8.

Howes A, O'Sullivan PA, Breyer F, Ghose A, Cao L, Krappmann D, et al. Psoriasis mutations disrupt CARD14 autoinhibition promoting BCL10-MALT1-dependent NF-kappaB activation. Biochem J 2016;473:1759−68.

Inoue N, Dainichi T, Fujisawa A, Nakano H, Sawamura D, Kabashima K. CARD14 Glu138 mutation in familial pityriasis rubra pilaris does not warrant differentiation from familial psoriasis. J Dermatol 2016;43:187−9.

Jattani RP, Tritapoe JM, Pomerantz JL. Cooperative control of caspase recruitment domain-containing protein 11 (CARD11) signaling by an unusual array of redundant repressive elements. J Biol Chem 2016;291:8324−36.

Jordan CT, Cao L, Roberson ED, Duan S, Helms CA, Nair RP, et al. Rare and common variants in CARD14, encoding an epidermal regulator of NF-kappaB, in psoriasis. Am J Hum Genet 2012a;90:796−808.

Jordan CT, Cao L, Roberson ED, Pierson KC, Yang CF, Joyce CE, et al. PSORS2 is due to mutations in CARD14. Am J Hum Genet 2012b;90:784−95.

Juilland M, Thome M. Role of the CARMA1/BCL10/MALT1 complex in lymphoid malignancies. Curr Opin Hematol 2016;23:402−9.

Keermann M, Koks S, Reimann E, Prans E, Abram K, Kingo K. Transcriptional landscape of psoriasis identifies the involvement of IL36 and IL36RN. BMC Genomics 2015;16:322.

Li B, Dewey CN. RSEM: accurate transcript quantification from RNA-seq data with or without a reference genome. BMC Bioinformatics 2011;12:323.

Li B, Tsoi LC, Swindell WR, Gudjonsson JE, Tejasvi T, Johnston A, et al. Transcriptome analysis of psoriasis in a large case-control sample: RNA-seq provides insights into disease mechanisms. J Invest Dermatol 2014;134:1828−38.

Li Q, Jin Chung H, Ross N, Keller M, Andrews J, Kingman J, et al. Analysis of CARD14 polymorphisms in pityriasis rubra pilaris: activation of NF-kappaB. J Invest Dermatol 2015;135:1905−8.

McAllister-Lucas LM, Inohara N, Lucas PC, Ruland J, Benito A, Li Q, et al. Bimp1, a MAGUK family member linking protein kinase C activation to Bcl10-mediated NF-kappaB induction. J Biol Chem 2001;276:30589−97.

Mease PJ, Gladman DD, Papp KA, Khraishi MM, Thaci D, Behrens F, et al. Prevalence of rheumatologist-diagnosed psoriatic arthritis in patients with psoriasis in European/North American dermatology clinics. J Am Acad Dermatol 2013;69:729−35.

Mossner R, Frambach Y, Wilsmann-Theis D, Lohr S, Jacobi A, Weyergraf A, et al. Palmoplantar pustular psoriasis is associated with missense variants in CARD14, but not with loss-of-function mutations in IL36RN in European patients. J Invest Dermatol 2015;135:2538−41.

Nakamura M, Lee K, Jeon C, Sekhon S, Afifi L, Yan D, et al. Guselkumab for the treatment of psoriasis: a review of phase III trials. Dermatol Ther (Heidelb) 2017;7:281−92.

O'Regan GM, Sandilands A, McLean WH, Irvine AD. Filaggrin in atopic dermatitis. J Allergy Clin Immunol 2008;122:689−93.

Pan D, Zhu Y, Zhou Z, Wang T, You H, Jiang C, et al. The CBM complex underwrites NF-kappaB activation to promote HER2-associated tumor malignancy. Mol Cancer Res 2016;14:93−102.

Papp KA, Blauvelt A, Bukhalo M, Gooderham M, Krueger JG, Lacour JP, et al. Risankizumab versus ustekinumab for moderate-to-severe plaque psoriasis. N Engl J Med 2017;376:1551−60.

Pelzer C, Cabalzar K, Wolf A, Gonzalez M, Lenz G, Thome M. The protease activity of the paracaspase MALT1 is controlled by monoubiquitination. Nat Immunol 2013;14:337−45.

Pomerantz JL, Denny EM, Baltimore D. CARD11 mediates factor-specific activation of NF-kappaB by the T cell receptor complex. EMBO J 2002;21:5184−94.

Qiao Q, Yang C, Zheng C, Fontan L, David L, Yu X, et al. Structural architecture of the CARMA1/Bcl10/MALT1 signalosome: nucleation-induced filamentous assembly. Mol Cell 2013;51:766−79.

Reich K, Papp KA, Blauvelt A, Tyring SK, Sinclair R, Thaci D, et al. Tildrakizumab versus placebo or etanercept for chronic plaque psoriasis (reSURFACE 1 and reSURFACE 2): results from two randomised controlled, phase 3 trials. Lancet 2017;390(10091):276−88.

Robinson MD, McCarthy DJ, Smyth GK. edgeR: a Bioconductor package for differential expression analysis of digital gene expression data. Bioinformatics 2010;26:139−40.

Romer J, Hasselager E, Norby PL, Steiniche T, Thorn Clausen J, Kragballe K. Epidermal overexpression of interleukin-19 and -20 mRNA in psoriatic skin disappears after short-term treatment with cyclosporine a or calcipotriol. J Invest Dermatol 2003;121:1306−11.

Sano S, Chan KS, Carbajal S, Clifford J, Peavey M, Kiguchi K, et al. Stat3 links activated keratinocytes and immunocytes required for development of psoriasis in a novel transgenic mouse model. Nat Med 2005;11:43−9.

Schmitt A, Grondona P, Maier T, Brandle M, Schonfeld C, Jager G, et al. MALT1 protease activity controls the expression of inflammatory genes in keratinocytes upon zymosan stimulation. J Invest Dermatol 2016;136:788−97.

Scudiero I, Mazzone P, D'Andrea LE, Ferravante A, Zotti T, Telesio G, et al. CARMA2sh and ULK2 control pathogen-associated molecular patterns recognition in human keratinocytes: psoriasis-linked CARMA2sh mutants escape ULK2 censorship. Cell Death Dis 2017;8(2):e2627.

Scudiero I, Vito P, Stilo R. The three CARMA sisters: so different, so similar: a portrait of the three CARMA proteins and their involvement in human disorders. J Cell Physiol 2014;229:990−7.

Scudiero I, Zotti T, Ferravante A, Vessichelli M, Vito P, Stilo R. Alternative splicing of CARMA2/CARD14 transcripts generates protein variants with differential effect on NF-kappaB activation and endoplasmic reticulum stress-induced cell death. J Cell Physiol 2011;226:3121−31.

Sergushichev A. An algorithm for fast preranked gene set enrichment analysis using cumulative statistic calculation. bioRxiv 2016. https://doi.org/10.1101/060012. Accessed 28 May 2018.

Sheng Y, Jin X, Xu J, Gao J, Du X, Duan D, et al. Sequencing-based approach identified three new susceptibility loci for psoriasis. Nat Commun 2014;5:4331.

Sugiura K, Muto M, Akiyama M. CARD14 c.526G>C (p.Asp176His) is a significant risk factor for generalized pustular psoriasis with psoriasis vulgaris in the Japanese cohort. J Invest Dermatol 2014;134:1755−7.

Takeichi T, Kobayashi A, Ogawa E, Okuno Y, Kataoka S, Kono M, et al. Autosomal dominant familial generalized pustular psoriasis caused by a CARD14 mutation. Br J Dermatol 2017;177:e133−5.

Takeichi T, Sugiura K, Nomura T, Sakamoto T, Ogawa Y, Oiso N, et al. Pityriasis rubra pilaris type V as an autoinflammatory disease by CARD14 mutations. JAMA Dermatol 2017;153:66–70.

Tanaka M, Kobiyama K, Honda T, Uchio-Yamada K, Natsume-Kitatani Y, Mizuguchi K, et al. Essential role of CARD14 in murine experimental psoriasis. J Immunol 2018;200:71–81.

Tsoi LC, Spain SL, Knight J, Ellinghaus E, Stuart PE, Capon F, et al. Identification of 15 new psoriasis susceptibility loci highlights the role of innate immunity. Nat Genet 2012;44:1341–8.

Tsoi LC, Stuart PE, Tian C, Gudjonsson JE, Das S, Zawistowski M, et al. Large scale meta-analysis characterizes genetic architecture for common psoriasis associated variants. Nat Commun 2017;8:15382.

Valdimarsson H, Baker BS, Jonsdottir I, Powles A, Fry L. Psoriasis: a T-cell-mediated autoimmune disease induced by streptococcal superantigens? Immunol Today 1995;16:145–9.

Van Nuffel E, Schmitt A, Afonina IS, Schulze-Osthoff K, Beyaert R, Hailfinger S. CARD14-mediated activation of paracaspase MALT1 in keratinocytes: implications for psoriasis. J Invest Dermatol 2017;137:569–75.

Wang D, You Y, Case SM, McAllister-Lucas LM, Wang L, DiStefano PS, et al. A requirement for CARMA1 in TCR-induced NF-kappa B activation. Nat Immunol 2002;3:830–5.

Witte E, Kokolakis G, Witte K, Philipp S, Doecke WD, Babel N, et al. IL-19 is a component of the pathogenetic IL-23/IL-17 cascade in psoriasis. J Invest Dermatol 2014;134:2757–67.

Xia ZX, Li ZX, Zhang M, Sun LM, Zhang QF, Qiu XS. CARMA3 regulates the invasion, migration, and apoptosis of non-small cell lung cancer cells by activating NF-κB and suppressing the P38 MAPK signaling pathway. Exp Mol Pathol 2016;100:353–60.

Xie C, Han Y, Fu L, Li Q, Qiu X, Wang E. Overexpression of CARMA3 is associated with advanced tumor stage, cell cycle progression, and cisplatin resistance in human epithelial ovarian cancer. Tumour Biol 2014;35:7957–64.

Yu G, He QY. ReactomePA: an R/Bioconductor package for reactome pathway analysis and visualization. Mol Biosyst 2016;12:477–9.
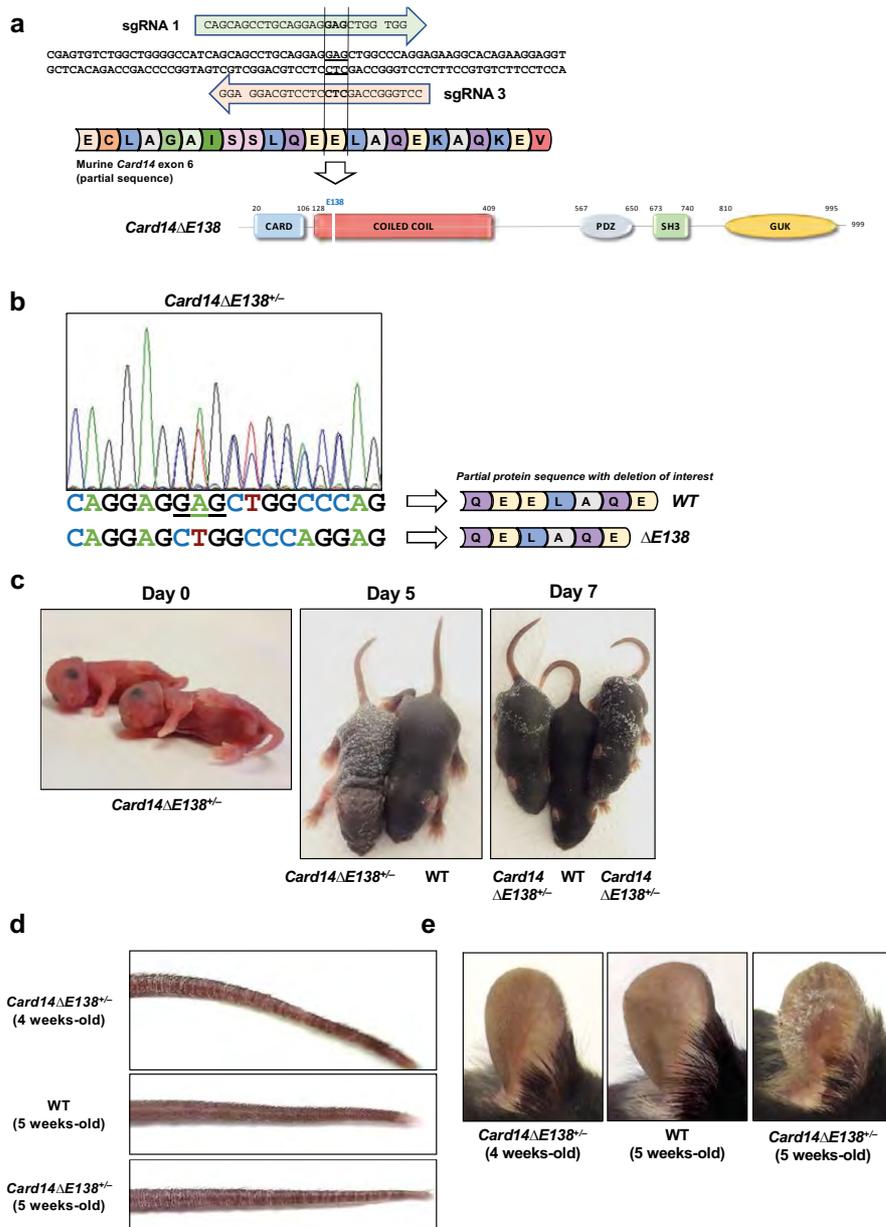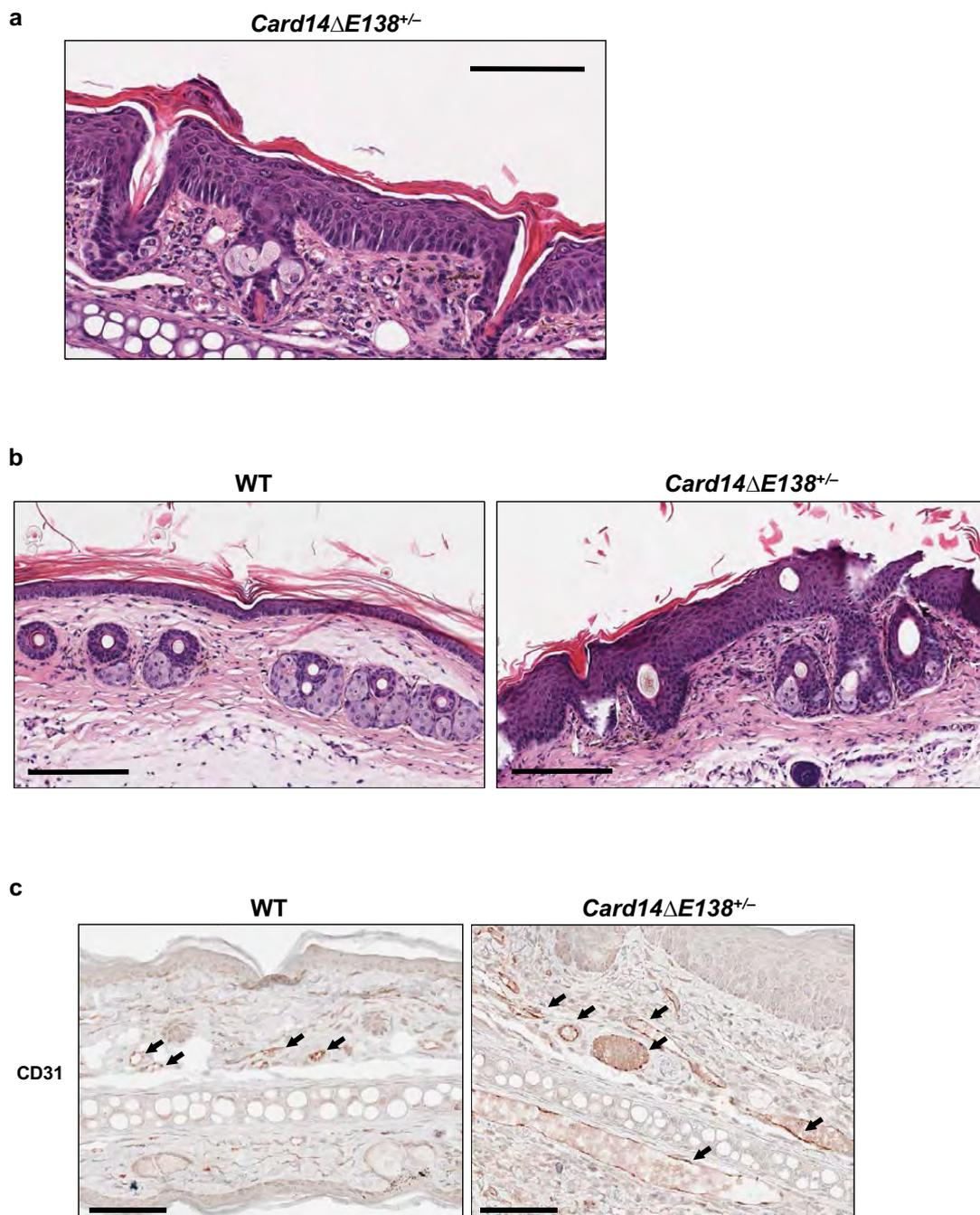
## Supplementary Figure S1
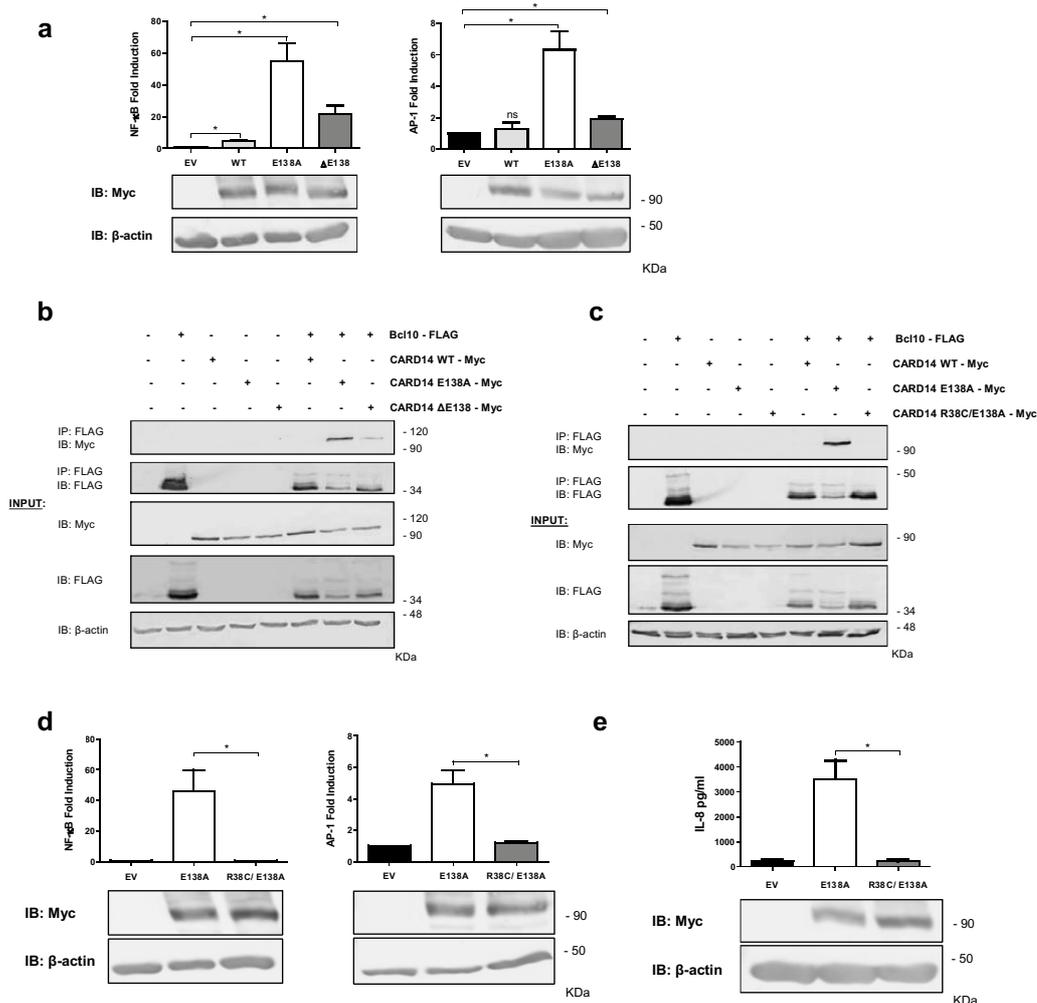


**Supplementary Figure S1 Mutation of the CARD domain of CARD14 disrupts interaction with Bcl10 and abrogates downstream effects.** (**a**) Assay of NF-κB- and AP-1-regulated luciferase reporter activity in HEK293 cells transfected with Myc-tagged CARD14 WT, CARD14 E138A and CARD14 ΔE138 or empty vector (EV, pcDNA3.1) with luciferase reporter plasmids. TK Renilla luciferase was measured to determine transfection efficiency. Immunoblotting shows expression of constructs. (**b, c**) HEK293 cells were transfected with FLAG-tagged Bcl10 and (**b**) Myc-tagged CARD14 WT, CARD14 E138A, CARD14 ΔE138 or (**c**) Myc-tagged CARD14 WT, CARD14 E138A and CARD14 R38C/E138A for 24 hours. Cell lysates were immunoprecipitated with an anti-FLAG antibody, followed by immunoblotting with indicated antibodies. (**d**) Assay of NF-κB and AP-1-regulated luciferase reporter activity in HEK293 cells transfected with CARD14 E138A, CARD14 R38C/E138A or empty vector with luciferase reporter plasmids. TK Renilla luciferase was measured to determine transfection efficiency. Immunoblotting shows expression of constructs. (**e**) Human primary keratinocytes were transfected with CARD14 E138A, CARD14 R38C/E138A or empty vector for 24 hours. Conditioned medium was collected and assayed for IL-8 secretion by ELISA. Immunoblotting shows expression of constructs. Data are (**b, c**) representative of three independent experiments or (**a, d, e**) are presented as the mean ±s.e.m of four independent experiments and were subjected to a two-tailed paired Student's t-test. *P<0.05. EV, empty vector; IB, immunoblotting; IP, immunoprecipitation; WT, wild-type.
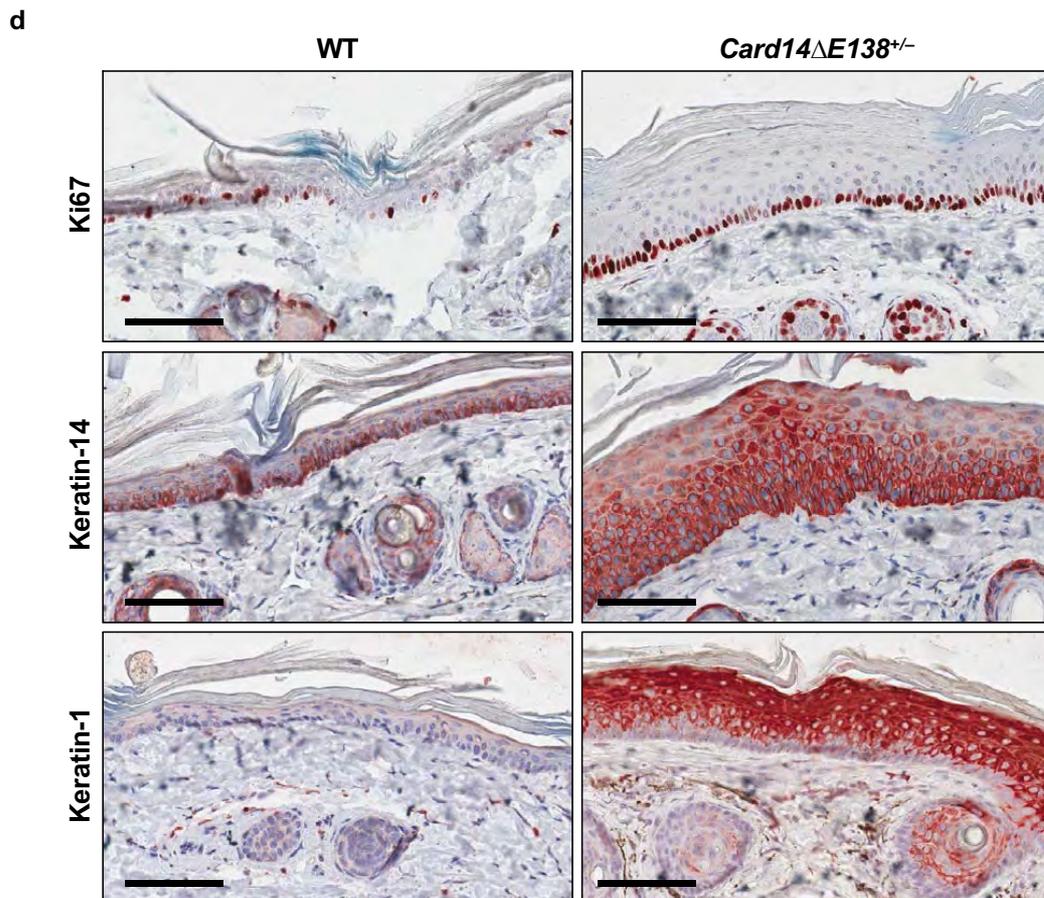
## Supplementary Figure S2



**Supplementary Figure S2 Temporal development of the *Card14ΔE138*^{+/−} psoriatic phenotype.** (**a**) Schematic of location of targeted amino acid using CRISPR/Cas9 technology. Depicted are sgRNAs (1 and 3), that resulted in two separate founder animals giving rise to JR strains 28900 and 28882 (Jackson Laboratories) (*CARD14 protein schematic adapted from Scudiero et al., 2014*). (**b**) Sanger sequencing showing heterozygous *Card14ΔE138*^{+/−} genotype. Depicted is targeted codon (underlined) and resulting partial WT and mutant allele sequences. (**c**) Temporal development of psoriatic phenotype in *Card14ΔE138*^{+/−} heterozygous neonates, shown at days 0, 5 and 7. (**d, e**) Development of psoriatic phenotype on the tail and ears of 4-week-old and 5-week-old mice. Pictures are representative of at least 8 heterozygous *Card14ΔE138*^{+/−} mice observed. WT, wild-type.
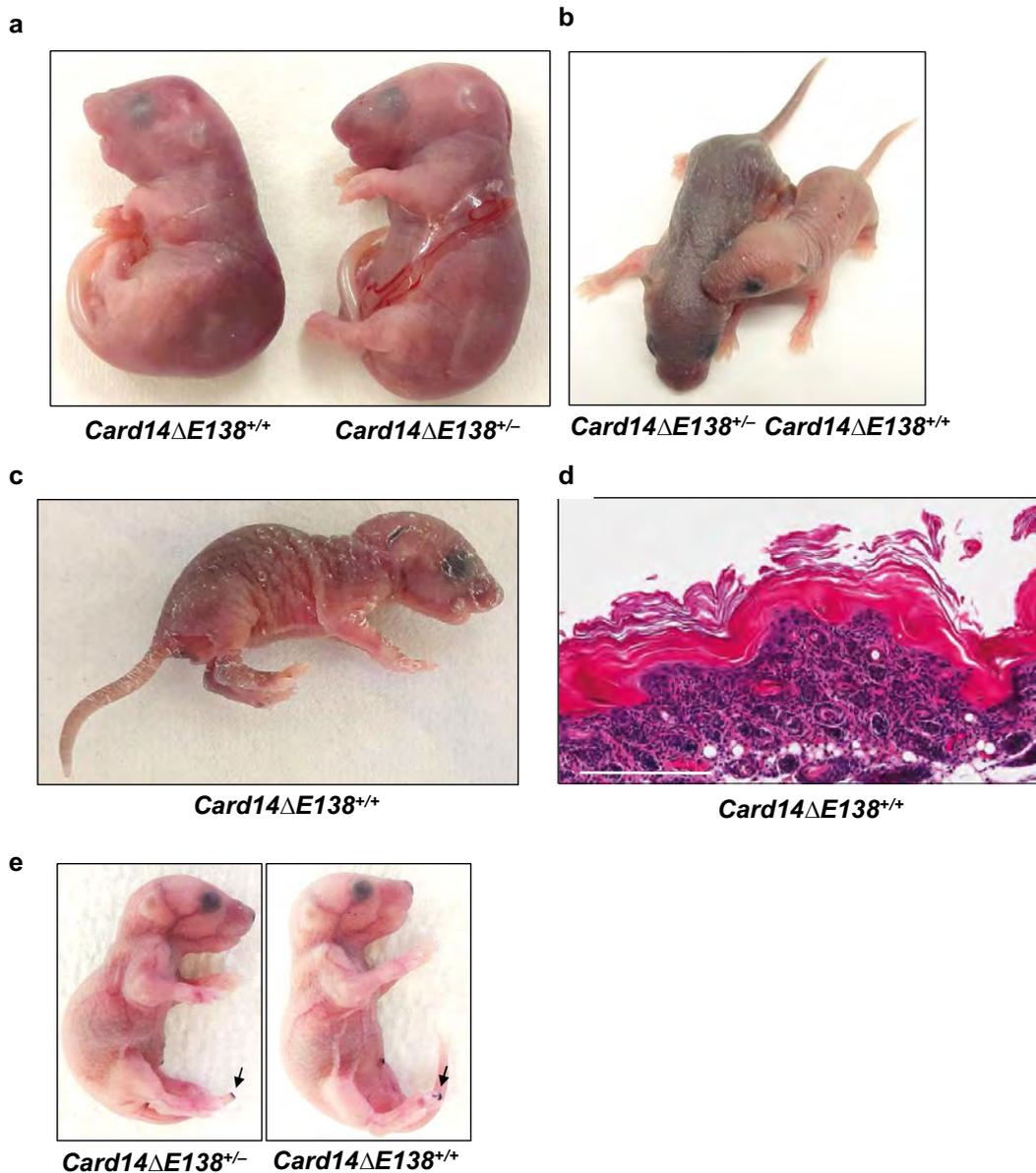
## Supplementary Figure S3

**a**

*Card14∆E138⁺/⁻*



**b**

WT                                    *Card14∆E138⁺/⁻*



**c**

WT                                    *Card14∆E138⁺/⁻*

CD31

**Supplementary Figure 3 ctd**

d



|  | WT | *Card14ΔE138⁺ᐟ⁻* |
| --- | --- | --- |

Ki67

Keratin-14

Keratin-1

**Supplementary Figure S3** *Card14ΔE138* **heterozygous mice display hallmarks of human psoriatic skin disease.** (**a**) Ear and (**b**) tail sections from 8 week-old *Card14ΔE138⁺ᐟ⁻* and wild-type littermates (n=8 per group) were stained with hematoxylin and eosin. Scale bar = (**a**) 100 µm or (**b**) 200 µm. (**c**) Ear sections from 8 week-old *Card14ΔE138⁺ᐟ⁻* mice were stained with a specific anti-CD31 antibody. Scale bar = 70 µm (**d**) Tail sections from 8-week-old *Card14ΔE138⁺ᐟ⁻* and wild-type littermates were stained with specific antibodies against Ki67, Keratin-14 and Keratin-1. Scale bar = 100 µm. Pictures are representative of 8 individual mice per group (**a – d**). WT, wild-type.

## Supplementary Figure S4

**a**



*Card14ΔE138⁺/⁺*      *Card14ΔE138⁺/⁻*

**b**



*Card14ΔE138⁺/⁻* *Card14ΔE138⁺/⁺*

**c**



*Card14ΔE138⁺/⁺*

**d**



*Card14ΔE138⁺/⁺*

**e**



*Card14ΔE138⁺/⁻*    *Card14ΔE138⁺/⁺*

**Supplementary Figure S4 *Card14ΔE138* homozygous mice suffer from neonatal mortality.** (**a**) Unborn homozygous *Card14ΔE138⁺/⁺* neonate display some developmental abnormalities compared to heterozygous littermates. (**b**) Surviving homozygous *Card14ΔE138⁺/⁺* pups are runts compared to heterozygous littermates (Day 4). (**c, d**) Homozygous *Card14ΔE138⁺/⁺* neonate displaying dry flaky skin on body as seen (**c**) macroscopically and by (**d**) Hemotoxylin and eosin staining. Scale bar = 200 μm (**e**) Barrier effects were determined using Toluidine staining of heterozygous and homozygous pups (Day 0). Arrows show positive staining of tail and toe clipping. Images are representative of 2-3 observed animals.

**Supplementary Figure S5**
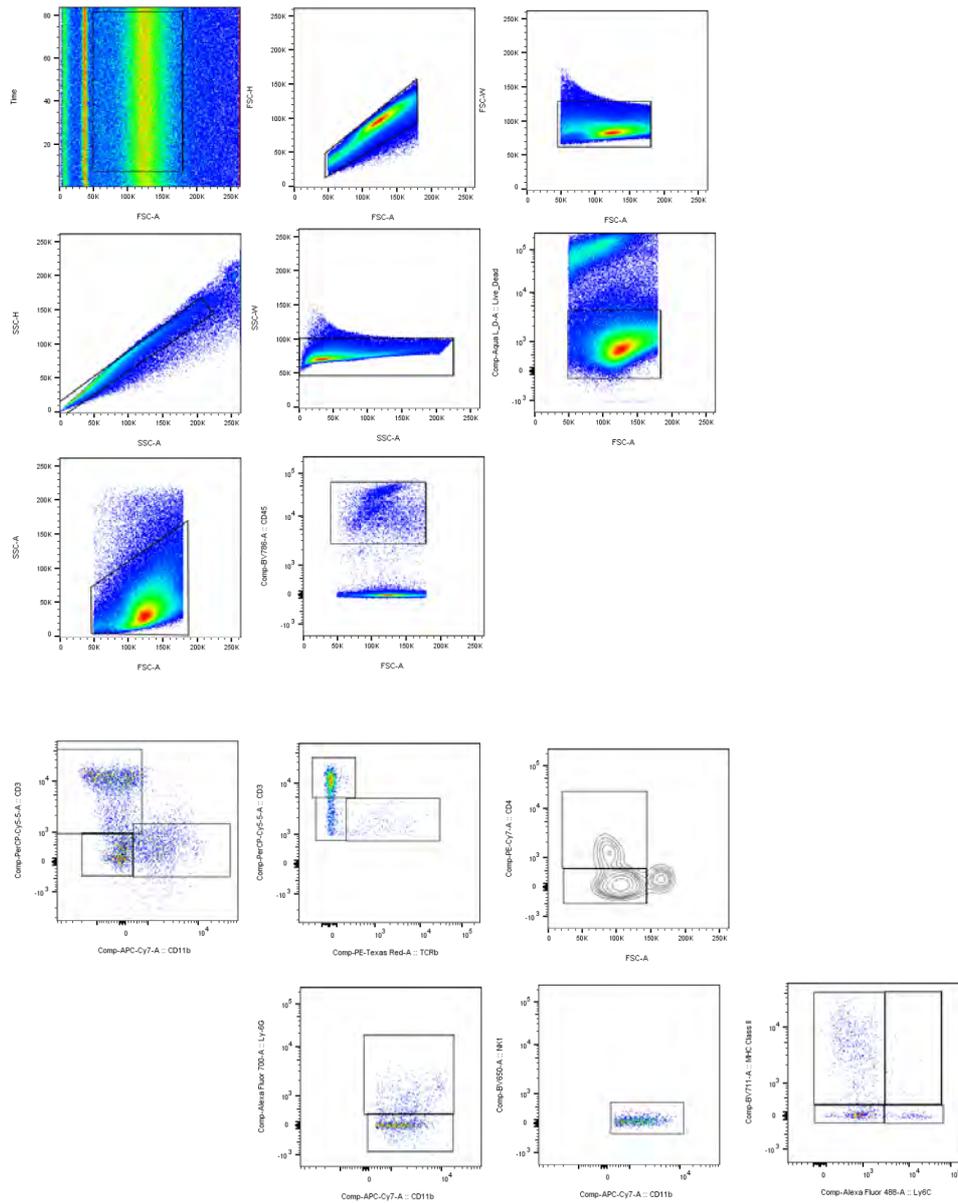


**Supplementary Figure S5 Gating strategy for immune cell infiltrate.** Representative plots of gating strategy for flow cytometry analysis of single cell suspension from ear tissue from age-matched and sex-matched adult *Card14ΔE138$^{+/-}$* mice and littermate controls. Irrelevant cells were removed by pre-gating (flow, exclusion of doublets and dead cells, and by size and granularity). Immune cells were identified by the expression of CD45. Lymphoid and myeloid cells were identified by their expression of CD3 and CD11b, respectively. Within the lymphoid gate, T cells were identified as Dendritic epidermal T cells (CD3$^{hi}$TCRβ$^{-}$), γδ T cells (CD3$^{low}$TCRβ$^{-}$), and αβ TCs (CD3$^{low}$TCRβ$^{+}$). The αβ T cells were further subdivided into CD4$^{+}$ T cells and CD8$^{+}$ T cells based on CD4 expression. Within the myeloid gate, neutrophils were identified by their expression of Ly6G. Ly6G$^{-}$ cells were further analysed for the expression of NK1.1. NK1.1$^{-}$ cells were identified as being non-inflammatory APCs (MHCII$^{hi}$Ly6C$^{-}$) and inflammatory APCs (MHCII$^{hi}$Ly6C$^{hi}$). Data are representative of three independent experiments with 5 mice per group (total n=15).

## Supplementary Figure S6

**a**



**b**



**c**
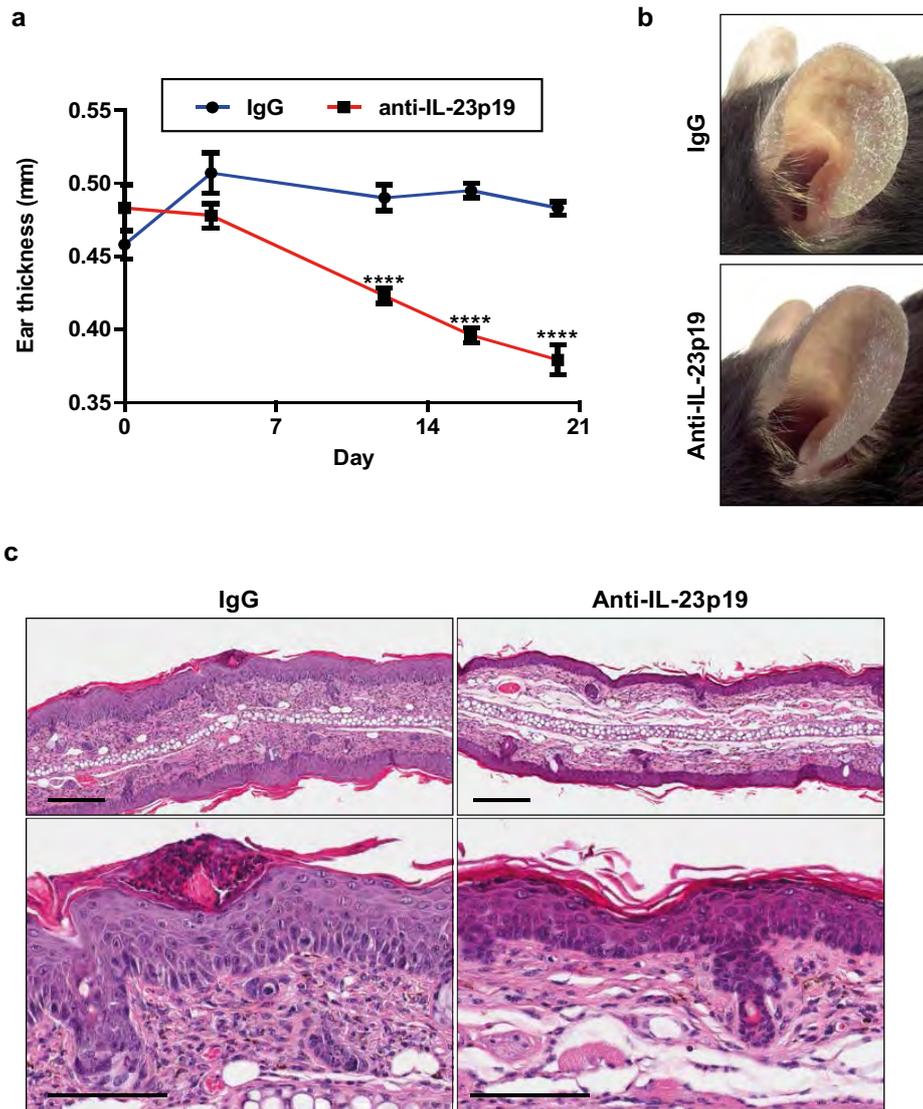


**Supplementary Figure S6 Prolonged IL-23p19 neutralization further ameliorates the phenotype in *Card14ΔE138+/−* mice.** (**a - c**) *Card14ΔE138+/−* mice were treated for 3 weeks with a IL-23p19-specific neutralizing antibody or an IgG isotype control antibody (n=5 per group). (**a**) Ear thickness of treated animals and control animals was measured at days 0, 4, 12, 15 and 20 of the experiment. (**b**) Macroscopic images of ears of IgG- and IL-23p19-treated mice at the end (day 21) of the experiment. (**c**) Representative histological features shown by hemotoxylin and eosin staining at Day 21. Scale bar = 200 μm (upper panel) or 100 μm (lower panel). Images are representative of IgG- and IL-23p19-treated mice (total n=5 per group) or (**a**) data are presented as the mean ±s.e.m of 5 mice and were subjected to a two-tailed unpaired Student's t-test. **** $P < 0.0001$.

SUPPLEMENTARY INFORMATION:

MATERIALS AND METHODS

**Plasmids and reagents:** The CARD14 short alternative spliced variant was generated by GenScript and sub-cloned into a pcDNA3.1 plasmid vector. Site-directed mutagenesis was performed using pfu Turbo (Thermo Scientific, Waltham, MA) as per manufacturer's instructions to generate point mutants, with respective primer pairs CARD14 E138A (forward 5'- GCAGCCTGCAGGAGGCGCTGAACC AGGAA – 3', reverse 5' – TTCCTGGTTCAGCGCCTCCTGCAGGCTGC – 3'), CARD14 ΔE138 (forward 5'-TCGGCAGCCTGCAGGAGCTGAAC – 3', reverse 5' – CCCTTTTCCTGGTTCA GCTCCTG – 3'), CARD14 R38C (forward 5'-CATCTGCCCCAGCTGCCTCACCCCCTACC – 3', reverse 5' – GGTAGGGGGTGAGGCAGCTGGGGCAGATG – 3') and CARD14 R38C/E138A. The NF-κB-luciferase, AP1-luciferase and TK *Renilla*-luciferase reporter constructs were gifts from Professor Paul Moynagh (Maynooth University, Ireland). FLAG-tagged Bcl10 and Strep-tagged Malt1 were described previously (Pelzer et al., 2013). Anti-Bcl10 antibodies were from Santa Cruz Biotechnology (Santa Cruz, CA). Anti-CARD14 antibodies were from Abcam (Cambridge, UK) and Proteintech (Rosemont, IL). The anti-myc antibody was from Clontech (Mountain View, CA). The anti-β-actin and anti-FLAG antibodies were supplied by Sigma-Aldrich (St. Louis, MI). Anti-RelB and Anti-Tubulin were from Cell Signaling Technology (Danvers, MA). Anti-GFP was from Enzo LifeSciences (Exeter, UK). The Ki67, Ly6G and CD31 antibodies were from Abcam (Cambridge, UK). The Filaggrin antibody was from LifeSpan BioSciences and the Keratin-14 and Keratin-1 antibodies were from BioLegend (San Diego, CA). 4', 6-diamidino-2-phenylindole (DAPI) was from Thermo Scientific (Watham, MA). The Malt1 antibody was described previously (Rebeaud et al., 2008).

***Card14* transgenic mice**: Card14ΔE138 mice were generated using CRISPR/Cas9 technology. Briefly, C57BL/6J (JR 000664) oocytes were microinjected with Cas9 mRNA and donor DNA along with one of two guide RNA sequences, sgRNA1 or sgRNA3, sequences 5'-CAGCAGCCTGCAGGAGGAGCTGGTGG -3' and 5'-CCTGGGCCAGCTCCTCCTGCAGGAGG -3', respectively. The 140 nt donor oligo sequence used was: 5'-CTGTGCAGGTCTCATGGAGACATCCAAGCTGACCGAGTGTCTGGCTGGGGCCATC AGCAGCCTGCAGGAG~~GAG~~CTGGCCCAGGAGAAGGCACAGAAGGAGGTTCTGCTC CGGAGATGCCAGCAGCTGAAGGAGCGCCTGGGCT -3' (minus the targeted GAG codon (strikethrough)). Founder mice, derived from transplantation of the microinjected oocytes into pseudopregant females, were screened for mutations in *Card14* by PCR amplification and DNA sequencing using primers spanning the targeted exon 6 (Forward: 5'-AGCAGAACTCTCGGGGAACT-3' and Reverse: 5'- GCCTGAGAAAAACTGGATCG -3'). Selected indel ΔE138 carrying mice were backcrossed twice to C57BL/6J mice prior to intercrossing and evaluation. Mice were backcrossed again with C57BL/6J wild-type mice and progeny bred to generate age- and sex-matched mice for experiments and colony maintenance. Two strains harboring the *Card14ΔE138* deletion were generated from separate founder animals, strain 28900 (C57BL/6J-Card14em9(delE138)Lutzy/J) and 28882 (C57BL/6J-Card14em5(delE138)Lutzy/J) using sgRNA1 and sgRNA3, respectively. Both strains

developed identical phenotypes with the same temporal profile. Mouse strain 28900 was used for the experiments described within the manuscript. To genotype *Card14* transgenic mice, toe-clippings were taken from 5 – 8 day old pups, tissue was lysed with Proteinase K (Qiagen) and genomic DNA was used as PCR template using the above primers. PCR products were subject to Sanger sequencing for the GAG deletion or nucleotide insertion using the same PCR primers. Mice were housed in individually ventilated cages with high-efficiency particulate air filters at the SPF-facility of the University Hospital Zürich. All animal experiments were performed in accordance with the regulations, guidelines and with ethical approval from the Cantonal Veterinary Office of Zürich, Switzerland.

**Cell culture:** HEK293 T cells were cultured in Dulbecco's modified Eagle's medium supplemented with 10% (v/v) fetal bovine serum (FBS), and Antibiotic-Antimycotic solution (100X, Gibco BRL, Paisley, Scotland). Human primary keratinocytes were cultured as previously described (Feldmeyer et al., 2007). Briefly, human primary foreskin keratinocytes were passaged in keratinocyte serum free medium (Gibco BRL), supplemented with EGF and BPE (Gibco BRL) and seeded for experiments after 3 passages. All cells were maintained at 37 °C in a humidified atmosphere of 5% $CO_2$. Murine primary keratinocytes were isolated from tail tissue of wild-type and *Card14ΔE138$^{+/-}$* mice using a previously described protocol (Lichti et al., 2008). Briefly, tail tissue was floated dermis down on trypsin (1%) for 1 h at 37 °C. Dermis and epidermis were separated and epidermis minced and incubated with Dnase for 30 min at 37 °C and filtered through a 70 μm strainer. Cells were centrfuged, washed with defined Keratinocyte medium (containing cholera toxin ($10^{-10}$ M), defined keratinocyte medium supplements, and Antibiotic-Antimycotic solution (100X)), respun and plated in same medium for 24 h at 37 °C. Medium was removed and replaced with fresh medium and cells were cultured for 3-4 days at 37 °C.

**Luciferase reporter assay:** HEK293 T cells were seeded ($1.5 \times 10^5$ cells ml$^{-1}$) in 96-well plates (200 μl per well) for overnight. When cells were 70 – 80% confluent were then transfected using Lipofectamine 2000 (Invitrogen), according to the manufacturer's instruction, with constructs encoding NF-κB- or AP1-regulated firefly luciferase reporter constructs (80 ng), constitutively expressed TK *Renilla*-luciferase reporter construct (phRL-TK) (40 ng), with CARD14 wild-type and mutants (50 ng) as indicated in figure legends. Total DNA was kept constant (200 ng per well) using empty vector, pcDNA3.1. Cell extracts were generated 24 h post transfection using Reporter Lysis Buffer (Promega, Fitchburg, WI) and extracts were assayed for firefly luciferase and *Renilla*-luciferase activity using the Luciferase Assay system (Promega) and coelenterazine (0.1 μg ml$^{-1}$, Sigma Aldrich), respectively. Conditioned medium was collected and stored for enzyme-linked immunosorbent assay (ELISA) analysis. Luminescence was monitored with the Cytation3 Imaging Reader (BioTek). Data are presented as fold stimulation of firefly luciferase expression relative to cells expressing EV.

**ELISA**: Primary keratinocytes were seeded at ($1 \times 10^5$ cells ml$^{-1}$; 1 ml) in 12-well plates and grown for 16 h. Cells were subsequently transfected with wild-type CARD14 and CARD14 mutant constructs as indicated in figure legends, or control vector pcDNA3.1 (250 ng) with TransIT-X2® Dynamic Delivery System (Mirus) as per manufacturer's instructions. Medium was changed 6 h post transfection and supernatants were collected 24 h later. Conditioned

media was measured for levels of human IL-8 (Biolegend antibodies, clones BH0814 and BH0840). Conditioned medium from HEK293 T cells from Luciferase assay experiments were collected and measured for levels of human IL-8 (Biolegend).

Ears from *Card14ΔE138$^{+/-}$* mice or wild-type littermates were snap-frozen in liquid nitrogen. Tissue was homogenized in T-PER™ Tissue Protein Extraction Reagent (Thermo Scientific) with protease and phosphatase inhibitor cocktails (Roche, Basel, Switzerland) using the TissueLyser II (Qiagen, Venlo, the Netherlands). Protein extracts were quantified using the Pierce BCA protein assay kit (Thermo Scientific) assayed for IL-17A and IL-22 (eBioscience).

**Co-immunoprecipitation analysis:** HEK293 T cells were seeded ($2 \times 10^5$ cells ml$^{-1}$; 3 ml) in six-well plates and transfected, using Lipofectamine 2000, with FLAG-tagged Bcl10 (1 µg) and myc-tagged CARD14 WT and mutant constructs (1 µg), or empty vector pcDNA3.1 as described in figure legends. 24 h after transfection cells were washed with pre-chilled PBS (1 ml) and then lysed with pre-chilled lysis buffer (300 µl) (50 mM Tris-Hcl, pH 7.5 containing 15 mM EDTA, 0.1% (v/v) Triton-X and 100 mM NaCl, and adding 1 mM Na$_3$VO$_4$, 1 mM DTT, 1 mM PMSF and complete protease and phosphatase cocktail inhibitors (Roche) for 30 min on a rocker at 4 °C. Cell lysates were centrifuged at 12,000 *g* for 10 min at 4 °C. Aliquots (50 µl) were retained for immunoblotting "Input" samples, while the remaining supernatants were removed to fresh pre-chilled tubes. Samples were incubated overnight with the appropriate antibody, anti-FLAG (1 µg) at 4 °C with rocking. This was followed by the addition of protein A/G agarose beads (30 µl per sample). Incubations were placed at 4 °C with rocking for 2 h. Immunoprecipitates were collected by centrifugation at 1,000 *g* for 5 min at 4 °C and the beads were then washed five times with lysis buffer (600 µl). The beads were resuspended in 2 X SDS–polyacrylamide gel electrophoresis (PAGE) sample buffer (60 µl) and incubated for 15 min at RT. Samples were centrifuged at 16,000 *g* for 1 min, subsequently boiled at 100 °C for 5 min and subjected to immunoblotting.

**Triton-X-100 insoluble fractionation of primary keratinocytes**: Human or mouse keratinocytes were lysed in a Triton X-100-containing buffer (0.5% Triton X-100 in 50 mM Tris/HCl, pH 7.6) as previously described (Fenini et al., 2017). After centrifugation at 8'000g for 30 min at 4 °C, supernatents (Triton-X-soluble fraction) were stored at -20°C and pellets (Triton X-100-insoluble fraction) were resuspended in 2 X SDS-sample buffer (60 µl), sonicated and boiled at 100 °C for 5 min and analyzed by SDS-PAGE and immunoblotting.

**RNA isolation and quantitative PCR:** 5-week old wild-type and *Card14ΔE138$^{+/-}$* mice were euthanized by CO$_2$ and ear tissue was taken and immediately placed in RNALater (Qiagen) and stored for 24 h at 4 °C and subsequently at -20 °C for longer periods. Before RNA extraction ear tissue was washed twice with ice-cold PBS before addition of 1 ml Tri-Reagent (Sigma). Tissue was homogenized for 5 min using the TissueLyser II (Qiagen) and RNA extracted according to the manufacturer's instructions. RNA was quantified using a Nanodrop (ACTGene, LabGene Scientific) and complementary DNA was generated from RNA using the RevertAid First Strand cDNA Synthesis Kit (Thermo Scientific). Quantitative real-time PCR was performed using a LightCycler®480 (Roche) with SYBR Green I Master mix (Roche). Real-time qPCR included an initial denaturation at 95°C for 10 min, followed by 45 cycles at

95°C for 10 s, 58°C for 10 s, 72°C for 20 s, and one cycle at 95°C for 10 min, 65°C for 60 s, 97°C for 30 s. *Rpl27* was used as a housekeeping gene.

The following primers were used for amplification of specific murine genes: Ccl20 forward GCC TCT CGT ACA TAC AGA CGC and reverse CCA GTT CTG CTT TGG ATC AGC; Cxcl1 forward AGA CCA TGG CTG GGA TTC AC and reverse CAA GGG AGC TTC AGG GTC AA; Cxcl2 forward CCA CCA ACC ACC AGG CTA CAG GGG C and reverse AGG CTC CTC CTT TCC AGG TCA GTT AGC; Defb3 forward CAT CTG CCT CCT TTC CTC AA and reverse CTT TGC ATT TCT CCT GGT GC; Defb4 forward GCA GCC TTT ACC CAA ATT ATC and reverse ACA ATT GCC AAT CTG TCG AA; Defb14 forward TCT TGT TCT TGG TGC CTG CT and reverse CGA CCG CTA TTA GAA CAT CGA C; Flg forward CTC CTT CAG CTG CAT TCG ATand reverse TGC CTG TAG TTG TCC TTC CA; Flg2 forward TGC GTC AGG CCT TAT CCT AC and reverse TCC TTC TCC AGC AGT TCC TT; Ifng forward AAG CGT CAT TGA ATC ACA CCT G and reverse TGA CCT CAA ACT TGG CAA TAC TC; Il1b forward AAA AAG CCT CGT GCT GTC GGA CC and reverse TGA GGC CCA AGG CCA CAG GTA; Il17a forward ATC CCT CAA AGC TCA GCG TGT C and reverse GGG TCT TCA TTG CGG TGG AGA G; Il17c forward CCTCTAGCTGGAACACAGTGC and reverse GCGGTTCTCATCTGTGTCG; Il19 forward GCC AAC TCT TTC CTC TGC GT and reverse GGT GGC TTC CTG ACT GCA GT; Il22 forward ATG AGT TTT TCC CTT ATG GGG AC and reverse GCT GGA AGT TGG ACA CCT CAA; Il23p19 forward TAT CCA GTG TGA AGA TGG TTG TG and reverse CAC TAA GGG CTC AGT CAG AGT TG; Il1f9 (IL-36γ) forward CAG GTG TGG ATC TTT CGT AAT CA and reverse CAT GGG AGG ATA GTC ACG CTG; Rpl27 forward AAA GCC GTC ATC GTG AAG AAC and reverse GCT GTC ACT TTC CGG GGA TAG; S100a7 forward GAG GAG TTG AAA GCT CTG CTC TTG and reverse GTG ATG TAG TAT GGC TGC CTG CGG; S100a8 forward AAA TCA CCA TGC CCT CTA CAA G and reverse CCC ACT TTT ATC ACC ATC GCA A; Tnfa forward TCC AGG CGG TGC CTA TGT and reverse CAC CCC GAA GTT CAG TAG ACA GA.

**Confocal microscopy of primary human and murine keratinocytes:** Primary human keratinocytes ($1 \times 10^5$ cells ml$^{-1}$) were seeded directly on coverslips and incubated overnight at 37 °C. Primary keratinocytes were transfected using TransIT-X2® Dynamic Delivery System (Mirus) as per manufacturer's instructions. Medium was changed 6 h post transfection and cells were incubated for 24 h at 37 °C. Murine keratinocytes were prepared as above and seeded on collagen-coated coverslips ($1 \times 10^6$ cells ml$^{-1}$) with defined Keratinocyte medium (containing cholera toxin ($10^{-10}$ M), defined keratinocyte medium supplements, and Antibiotic-Antimycotic solution (100X)) for 24 h at 37 °C. Medium was removed, and the cells were gently washed three times in PBS (500 μl). Cells were then fixed by the addition of 3% (v/v) paraformaldehyde with 2% sucrose (500 μl) for 30 min. Cells were again washed and then permeabilized for 2 min with 0.2% TritonX-100 (500 μl). Cells were washed and blocking was performed with 1% BSA in PBST for 30 min. Cells were then incubated with primary antibodies in 1% BSA as indicated in figure legends for 1 h at room temperature. Cells were washed thrice and subsequently incubated with anti-rabbit DyLight488 and anti-mouse DyLight650 (Abcam) secondary antibodies and DAPI in 1% BSA (1/500) for 1 h at room temperature. Cells were washed and coverslips were mounted with ProLong® Gold antifade reagent (Molecular Probes). Confocal

images were captured using the × 63 objective lens on the Leica TCS SP5 laser-scanning microscope equipped with the appropriate filter sets. Acquired images were analyzed using the Imaris x64 imaging software.

**Confocal microscopy of ear pinnae:** Ear pinnae were prepared as previously described (Linehan et al., 2018). Briefly, ear pinnae were split with forceps, sliced into longitudinal strips and fixed overnight at 4 °C, blocked for 4 hours in 1% BSA, 0.25% Triton-X blocking buffer at room temperature and incubated with specific anti-Bcl10 and anti-CARD14 or IgG isotype control antibodies overnight at 4 °C. Slides were washed four times with PBS-Tween and probed with DAPI and anti-rabbit DyLight488 and anti-mouse DyLight650 (Abcam) secondary antibodies in 1% BSA (1/500) for 2 h at room temperature. Tissue was washed four times and mounted with ProLong® Gold antifade reagent (Molecular Probes).

**Immunohistochemistry**: 8-week old female *Card14ΔE138$^{+/-}$* and wild-type littermates were euthanized and ears and tails taken and stored in Formalin (4% (g/v)) for at least 24 h. 5 µm of paraffin-embedded tissue sections were deparaffinized and rehydrated. Antigen demasking was performed using pressure cooker heating of the slides for 25 minutes in Target Retrieval solution (DAKO, Glostrup, Denmark). After permeabilization using 0.03% Triton X in PBS for 10 minutes, sections were blocked using 5% BSA in PBS for one hour at room temperature. After washing with PBS, sections were stained overnight at 4 °C with specific rabbit anti-CD31, Ly6G, Keratin-1, Keratin-14 and filaggrin-1 antibodies. A rabbit IgG isotype antibody (Abcam) at corresponding concentrations were used as controls. Slides were washed with PBS and a goat-anti-rabbit secondary antibody (Southern Biotech, Birmingham, USA) was added and incubated for 1 hour at room temperature. Slides were washed with PBS and mounted with an Avidin-Biotin-complex (Vector Laboratories, Peterborough, UK). After 45 minutes of incubation, slides were washed with PBS, and AEC (3-amino-9-ethylcarbazole) HRP substrate (Vector Laboratories) was added to produce a red reaction product. After washing, a counterstain with hematoxylin was performed. The sections were mounted in mounting medium (DAKO) and imaged by using an Aperio ScanScope (Leica Biosystems, Wetzlar, Germany).

**Flow cytometry**: Ears from age- and sex-matched *Card14ΔE138$^{+/-}$* and wild-type littermates were taken and dorsal and ventral sides of ears were separated and minced up. Tissue was digested for 60 min with shaking using Liberase TM (1.3U/ml, Roche) in RPMI and HEPES buffer as per manufacturer's instructions. Dispase was added for a further 30 min incubation. Digested tissue was strained through a 70 µm cell-strainer (BD Biosciences). For surface staining the following antibodies coupled to the appropriate fluorochromes were used: CD45, TCR☐CD11b, Ly6G, MHC II, Ly6C, NK1.1, CD3, CD4. After surface staining cells were fixed. Samples were run on the LSR Fortessa (BD Biosciences) benchtop flow cytometers at the USZ Flow Cytometry Facility. The instrument was compensated using UltraComp eBeads (Thermo Scientific). For each sample, 50,000 123count™ eBeads (Thermo Scientific) were collected. Data were analyzed using FlowJo version 10 (Treestar, Inc., Ashland, OR) and gating was established using fluorescent minus one (FMO) controls. Gating strategy is outlined in the relevant figure legend.

**FRET assay:** HEK293 T cells, seeded in 3.5 cm dishes (3.5 x $10^5$ cells/well), were transfected with Myc-tagged wild-type and mutant CARD14 constructs (1 – 40 ng) as indicated, Strep-tagged Malt1 (1 µg) together with an eYFP-LVSR-eCFP reporter construct (100 ng). 24 h after transfection, cells were collected, washed and resuspended in FACS-Buffer (2% FCS, 2mM EDTA pH 8 in PBS). The fluorescent signals of the cells were detected with a LSR II from BD Biosciences containing 405 and 488 nm lasers. For each probe, 10,000 highly eYFP+ cells were analyzed that were excited with a 488 nm laser and detected with a 530/30 filter. The FRET and eCFP signal of these cells was measured by using 405 nm laser and 585/42 or 450/50 filter, respectively. The data were analyzed with the FlowJo vX.0.7 software.

***In vivo* neutralization of IL-23p19:** 12 mg/Kg specific murine IL-23p19 antibody (Invitrogen) or control Rat IgG1 κ isotype (Biolegend) was administered 3 times by intraperitoneal injection into 8-week old female *Card14ΔE138$^{+/-}$* mice over the course of 15 days (or 21 days). Ear thickness of mice was measured using a microcalipers on days indicated in figure legends and a the end of experiment. At the end of experiment mice were euthanized and ears taken for immunohistochemistry and RNA analysis.

**Statistical analysis:** For luciferase assays data are expressed relative to empty vector and are the mean ±s.e.m. of triplicate determinations from 4 independent experiments (as indicated in figure legends). For comparison between two groups, Student's two-tailed paired *t*-test was used. For ELISA results were subjected to a two-tailed paired *t*-test. For comparison between serum and tissue samples from mice, Student's two-tailed unpaired *t*-test was used. In the *in vivo* IL-23p19 neutralization experiments ANOVA and Bonferroni post-tests were used as indicated in figure legends. Differences were considered significant when *$p<0.05$, ** $p<0.01$, *** $p<0.001$ and **** $p<0.0001$.

**REFERENCES**

Feldmeyer L, Keller M, Niklaus G, Hohl D, Werner S, Beer HD. The inflammasome mediates UVB-induced activation and secretion of interleukin-1beta by keratinocytes. Curr Biol. 2007;17(13):1140-5.

Fenini G, Grossi S, Gehrke S, Beer HD, Satoh TK, Contassot E, et al. The p38 Mitogen-Activated Protein Kinase Critically Regulates Human Keratinocyte Inflammasome Activation. J Invest Dermatol. 2017.

Lichti U, Anders J, Yuspa SH. Isolation and short-term culture of primary keratinocytes, hair follicle populations and dermal cells from newborn mice and keratinocytes from adult mice for in vitro analysis and for grafting to immunodeficient mice. Nat Protoc. 2008;3(5):799-810.

Linehan JL, Harrison OJ, Han SJ, Byrd AL, Vujkovic-Cvijin I, Villarino AV, et al. Non-classical Immunity Controls Microbiota Impact on Skin Immunity and Tissue Repair. Cell. 2018;172(4):784-96 e18.

Pelzer C, Cabalzar K, Wolf A, Gonzalez M, Lenz G, Thome M. The protease activity of the paracaspase MALT1 is controlled by monoubiquitination. Nat Immunol. 2013;14(4):337-45.

Rebeaud F, Hailfinger S, Posevitz-Fejfar A, Tapernoux M, Moser R, Rueda D, et al. The proteolytic activity of the paracaspase MALT1 is key in T cell activation. Nat Immunol. 2008;9(3):272-81.

# Annex III – Contribution to Publication – Cheng *et al.*

## GRK2 suppress lymphomagenesis by inhibiting the MALT1 proto-oncoprotein

Jing Cheng, Linda R. Klei, Nathaniel E. Hubel, Ming Zhang, Rebekka Schairer, Lisa M. Maurer, Hanna B. Klei, Heejae Kang, Vincent J. Concel, Phillip C. Delekta, Eric V. Dang, Michelle A. Mintz, Mathijs Baens, Jason G. Cyster, Narayanan Parameswaran, Margot Thome, Peter C. Lucas, and Linda M. McAllister-Lucas

G-protein-coupled receptor kinase 2 (GRK2) is a serine/threonine kinase known for phosphorylating GPCRs, resulting in receptor desensitization and internalization. Additionally, GRK2 has been found to regulate different signaling pathways in an kinase-independent manner. Several studies revealed the role of GRK2 in cell proliferation and cell survival in different malignancies. Among others, GRK2 is also expressed in lymphocytes but the function of GRK2 in lymphoid cells is not known. This publication demonstrates the interaction of GRK2 with MALT1 in lymphocytes. GRK2 binding to MALT1 inhibited its scaffold and protease function resulting in a negative regulation of the NF-κB signaling pathway upon an antigen receptor signal. Silencing of GRK2 enhanced tumor growth of ABC DLBCL that rely on MALT1 activity, *in vitro* and *in vivo*. Patients with ABC DLBCL with a low GRK2 expression have a worse outcome compared to patients with high GRK2 expression, indicating GRK2 as a tumor suppressor by inhibiting MALT1.

For this study, I performed FRET-based MALT1 cleavage assays in HEK293T cells to identify the effect of co-expression of different GRK2 constructs on MALT1 proteolytic activity. The result of these experiments is shown in **Figure 3C**.
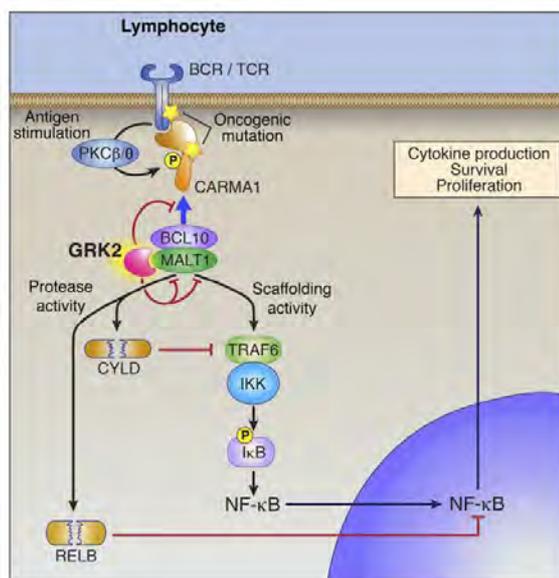
# GRK2 suppresses lymphomagenesis by inhibiting the MALT1 proto-oncoprotein

Jing Cheng, … , Peter C. Lucas, Linda M. McAllister-Lucas

**Research Article** | Immunology | Oncology

## Graphical abstract



**Find the latest version:**

https://jci.me/97040/pdf

**RESEARCH ARTICLE**

# GRK2 suppresses lymphomagenesis by inhibiting the MALT1 proto-oncoprotein

Jing Cheng,[1] Linda R. Klei,[1] Nathaniel E. Hubel,[1,2] Ming Zhang,[3] Rebekka Schairer,[3] Lisa M. Maurer,[1] Hanna B. Klei,[1] Heejae Kang,[2] Vincent J. Concel,[1] Phillip C. Delekta,[4] Eric V. Dang,[5] Michelle A. Mintz,[5] Mathijs Baens,[6,7] Jason G. Cyster,[5,8,9] Narayanan Parameswaran,[10] Margot Thome,[3] Peter C. Lucas,[2] and Linda M. McAllister-Lucas[1]

[1]Department of Pediatrics and [2]Department of Pathology, University of Pittsburgh School of Medicine and UPMC Hillman Cancer Center, Pittsburgh, Pennsylvania, USA. [3]Department of Biochemistry, Center of Immunity and Infection, University of Lausanne, Epalinges, Switzerland. [4]Department of Microbiology and Molecular Genetics, Michigan State University, East Lansing, Michigan, USA. [5]Department of Biophysics and Biochemistry, UCSF, San Francisco, California, USA. [6]Human Genome Laboratory, VIB Center for the Biology of Disease, and [7]Center for Human Genetics, Katholieke Universiteit Leuven, Leuven, Belgium. [8]Howard Hughes Medical Institute and [9]Department of Microbiology and Immunology, UCSF, San Francisco, California, USA. [10]Department of Physiology, Michigan State University, East Lansing, Michigan, USA.

Antigen receptor–dependent (AgR-dependent) stimulation of the NF-κB transcription factor in lymphocytes is a required event during adaptive immune response, but dysregulated activation of this signaling pathway can lead to lymphoma. AgR stimulation promotes assembly of the CARMA1-BCL10-MALT1 complex, wherein MALT1 acts as (a) a scaffold to recruit components of the canonical NF-κB machinery and (b) a protease to cleave and inactivate specific substrates, including negative regulators of NF-κB. In multiple lymphoma subtypes, malignant B cells hijack AgR signaling pathways to promote their own growth and survival, and inhibiting MALT1 reduces the viability and growth of these tumors. As such, MALT1 has emerged as a potential pharmacological target. Here, we identified G protein–coupled receptor kinase 2 (GRK2) as a new MALT1-interacting protein. We demonstrated that GRK2 binds the death domain of MALT1 and inhibits MALT1 scaffolding and proteolytic activities. We found that lower GRK2 levels in activated B cell–type diffuse large B cell lymphoma (ABC-DLBCL) are associated with reduced survival, and that GRK2 knockdown enhances ABC-DLBCL tumor growth in vitro and in vivo. Together, our findings suggest that GRK2 can function as a tumor suppressor by inhibiting MALT1 and provide a roadmap for developing new strategies to inhibit MALT1-dependent lymphomagenesis.

## Introduction

Diffuse large B cell lymphoma (DLBCL) is the most frequent subtype of non-Hodgkin lymphoma (NHL), accounting for 30%–40% of newly diagnosed cases (1). With more than 20,000 deaths from lymphoma occurring each year in the United States (2), new approaches to diagnosis, prognosis, and treatment are needed. Although the molecular and genetic features that drive aggressive behavior of B cell lymphomas are not fully defined, gene expression profiling studies have identified at least 2 distinct molecular subtypes of DLBCL, termed germinal center B cell (GCB) and activated B cell (ABC) (3). ABC-DLBCL exhibits an inferior outcome following standard R-CHOP chemotherapy, with a 3-year progression-free survival of approximately 40% compared with 75% for non-ABC cases, and is associated with constitutive canonical NF-κB activation (4, 5). A loss-of-function RNA interference screen revealed that the majority of ABC-DLBCL cell lines rely on components of the B cell receptor–dependent (BCR-dependent) NF-κB signaling pathway for growth and survival (6).

Stimulation of the B or T cell antigen receptor (AgR) results in assembly and activation of the CBM complex, which is composed of the scaffolding protein CARMA1 (also known as CARD11), the adaptor protein BCL10, and the protease MALT1 (7, 8). Loss of any component of this complex is toxic for ABC-DLBCL cells, indicating that it plays a critical role in the molecular pathogenesis of this tumor (6). MALT1 functions as the essential downstream effector molecule of the CBM complex by carrying out 2 important functions. First, MALT1 acts as a scaffold to recruit downstream signaling proteins, most notably the ubiquitin ligase TNF receptor–associated factor 6 (TRAF6). In turn, TRAF6 directs an array of polyubiquitinations that promote stimulation of the IκB kinase (IKK) complex (9–11). IKK then phosphorylates the inhibitor of NF-κB (IκB), thereby targeting it for proteasomal degradation and freeing NF-κB subunits to translocate into the nucleus and alter target gene expression (12). Second, MALT1 acts as protease to enzymatically cleave and inactivate multiple substrates, including several negative regulators of canonical NF-κB signaling (13, 14). Thus, MALT1 protease activity is thought to amplify and sustain NF-κB activation by clearing proteins that dampen this pathway. For example, activated MALT1 protease cleaves the NF-κB family member RELB (15). Since RELB is an inhibitor of canonical RELA-dependent transcriptional activity, MALT1-dependent cleavage of RELB results in enhanced expression of canonical NF-κB gene targets. MALT1 also cleaves several other substrates,

**RESEARCH ARTICLE**

including its binding partner BCL10 and the deubiquitinases A20 and cylindromatosis (CYLD) (15–19). Collectively, these cleavage events not only optimize NF-κB activation but also regulate cellular adhesion and enhance the related c-Jun N-terminal kinase (JNK) signaling pathway (20).

In ABC-DLBCL, mutations in the CD79A or CD79B subunits of BCR are present in approximately 23% of cases (21, 22), and gain-of-function mutations of CARMA1 occur in another 9% of cases (1, 22–24). These mutations mimic BCR signaling and consequently result in constitutive MALT1-mediated NF-κB activation. Blockade of MALT1 activity, by either genetic knockdown or chemical inhibition of protease activity, reduces viability and growth of ABC-DLBCL lines (25–29). In addition to ABC-DLBCL, inappropriate MALT1 activation also occurs in a variety of other NHL subtypes and is critical to tumor pathogenesis. Translocations t(1;14) and t(14;18) in MALT lymphoma position BCL10 and MALT1, respectively, adjacent to the Ig heavy chain enhancer, leading to BCL10 and MALT1 overexpression and NF-κB activation (12). The t(11;18) translocation, which occurs in 30% of MALT lymphomas, creates an oncogenic fusion protein that links the N-terminus of cellular inhibitor of apoptosis (API2) to the MALT1 C-terminus, and this results in constitutive MALT1 proteolytic activity (30–32). Furthermore, recent studies have suggested that a subset of mantle cell lymphomas, peripheral T cell lymphomas, and T cell leukemias may also require MALT1 proteolytic activity for survival (33–35). In light of these observations, MALT1 has emerged as a promising new target for pharmaceutical intervention in the treatment of multiple subtypes of lymphoid malignancy.

Here, we identify G protein–coupled receptor kinase 2 (GRK2) as a new MALT1-interacting protein and provide compelling evidence that GRK2 inhibits MALT1-mediated NF-κB activity in lymphoma cells, which leads to reduced tumor growth. GRK2 is 1 of 7 members of the GRK family, a group of proteins best known as serine/threonine kinases that phosphorylate activated G protein–coupled receptors, signaling receptor desensitization (36). Emerging evidence indicates that in addition to this canonical function, GRK2 binds to a variety of other cellular proteins involved in diverse aspects of signal transduction, and regulates the activity of these signaling proteins via kinase-independent mechanisms (37). While GRK2 has been reported to influence many of the processes involved in the hallmarks of cancer, such as cell proliferation, survival, motility metabolism, and others, the role of GRK2 in tumor formation and progression has only recently begun to be investigated (38). GRK2 is expressed in several cell types within the immune system, though relatively little is known about the function of GRK2 in either normal or malignant lymphocytes (39). Our findings suggest that GRK2 can act as a tumor suppressor by binding and inhibiting MALT1. This study provides important new insight into the molecular mechanisms that regulate the MALT1 proto-oncoprotein and represents a major step toward developing improved prognostication and targeted therapeutics for MALT1-dependent lymphomas.

## Results

*GRK2 binds to MALT1 in both T cells and B cells and dissociates from MALT1 after AgR stimulation.* Using coimmunoprecipitation (co-IP) coupled with liquid chromatography–mass spectrometry,

we identified GRK2 as a new MALT1-interacting protein (Supplemental Figure 1A; supplemental material available online with this article; https://doi.org/10.1172/JCI97040DS1). We validated this interaction by Western blot analysis, showing endogenous GRK2 and MALT1 co-IP in both Jurkat T cells and BJAB B cells (Figure 1A), as well as in HEK293T cells (Supplemental Figure 1B). We then used purified recombinant proteins to demonstrate a direct interaction between GRK2 and MALT1, but not between GRK2 and BCL10, another member of the CBM complex (Figure 1B and Supplemental Figure 1C). Next, we investigated whether AgR stimulation, which promotes both MALT1 scaffolding and proteolytic activities, impacts the GRK2-MALT1 interaction. We found that treatment with phorbol ester 12-myristate 13-acetate and the calcium ionophore ionomycin (PMA/Iono), which mimics AgR stimulation by promoting PKC-dependent phosphorylation of CARMA1 and subsequent activation of the CBM complex (40, 41), resulted in time-dependent dissociation of GRK2/MALT1 in Jurkat T cells (Figure 1, C and D). Notably, GRK2 dissociation from MALT1 occurred within the same general time course as CARMA1 association with BCL10/MALT1 and phosphorylation of IκB. Similar results were also observed in BJAB B cells (Supplemental Figure 1D). These findings could suggest that GRK2 binding to MALT1 inhibits CBM complex function, with dissociation of GRK2 somehow allowing full activation of MALT1 and downstream NF-κB pathway signaling following lymphocyte AgR stimulation.

*The GRK2 N-terminus interacts with MALT1 death domain and inhibits MALT1-dependent NF-κB activation.* As an initial approach to testing whether GRK2 binding to MALT1 plays an inhibitory role in lymphocyte signaling, we investigated the impact of overexpression of GRK2. We found that GRK2 overexpression inhibited the coimmunoprecipitation of BCL10 and MALT1 (Supplemental Figure 2A). In addition, using differentially epitope-tagged MALT1 monomers, we demonstrated that GRK2 overexpression inhibited BCL10-dependent MALT1 oligomerization (Supplemental Figure 2B). While these overexpression studies suggest that GRK2 might interfere with the BCL10-MALT1 interaction, we did not observe an increase in the association of BCL10 and MALT1 upon GRK2 dissociation after PMA/Iono treatment in lymphocytes (Figure 1C).

We next sought to identify the specific region of MALT1 that interacts with GRK2. MALT1 contains 2 Ig-like protein-protein interaction domains that are required for binding to BCL10 (refs. 42–44 and Figure 2A), and a central catalytic domain that shares homology with the proteolytic active site of the caspase family of serine proteases (43). MALT1 also contains an N-terminal death domain (DD), and recent studies suggest that this domain may interact with BCL10 (44). Interestingly, co-IP mapping studies revealed that GRK2 binds to this MALT1 DD (amino acids 1–139) (Figure 2A). Notably, a recent report demonstrated that MALT1 undergoes autoproteolysis in response to AgR stimulation, cleaving itself after arginine-149 (R149), thereby separating this DD from the remaining 76-kDa (p76) C-terminal portion of MALT1 (45). In contrast to full-length (FL) MALT1, the p76 cleavage fragment potently activates NF-κB independently of CARMA1/BCL10. These findings suggest that the DD may possess a negative regulatory function and serve to somehow restrain MALT1-dependent signaling.

Together, our findings that GRK2 dissociates from MALT1 in response to AgR stimulation and that GRK2 binds to the MALT1
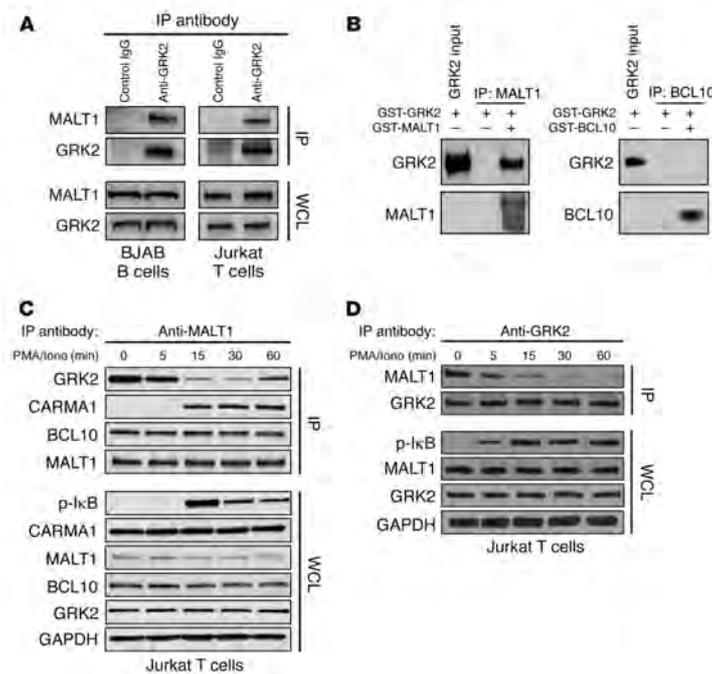
**Figure 1. GRK2 binds to MALT1 and dissociates from MALT1 after AgR stimulation.** (**A**) Endogenous MALT1 and GRK2 interact in BJAB B and Jurkat T cells. Coimmunoprecipitation (co-IP) of MALT1 with GRK2 was demonstrated by Western blot. (**B**) Co-IP analysis reveals that purified recombinant GRK2 interacts directly with MALT1 (left) but not BCL10 (right). (**C**) AgR stimulation leads to GRK2/MALT1 dissociation in the same general time course as CARMA1 association with BCL10/MALT1. Jurkat T cells were serum-starved and exposed to PMA (50 ng/mL)/ionomycin (1 μM) (PMA/Iono) for the indicated times. Cell lysates were subjected to immunoprecipitation (IP) with anti-MALT1, followed by immunoblotting with either anti-GRK2, anti-CARMA1, or anti-BCL10. (**D**) Reverse immunoprecipitation with anti-GRK2 also confirmed that AgR stimulation leads to GRK2/MALT1 dissociation in Jurkat T cells. Cells were treated as in **C**, and cell lysates were subjected to immunoprecipitation with anti-GRK2, followed by immunoblotting with anti-MALT1. All blots shown are representative of 3 separate experiments.

DD could suggest that GRK2 exerts an inhibitory effect on MALT1-dependent signaling, which is relieved after AgR stimulation. Indeed, we found that GRK2 inhibited BCL10/MALT1–dependent NF-κB activation (Figure 2B, left). Notably, the kinase-deficient K220R GRK2 mutant (GRK2 K220R) (46) was equally as effective as wild-type (WT) GRK2 at inhibiting BCL10/MALT1–dependent NF-κB activation, indicating that GRK2 kinase activity is not required for this effect. Importantly, GRK2 did not inhibit NF-κB signaling triggered by the API2-MALT1 fusion oncoprotein (Figure 2B, middle) or by the p76 MALT1 C-terminal autoproteolytic cleavage fragment (Figure 2B, right), both of which are constitutively active forms of MALT1 that lack the DD. These results are consistent with the notion that GRK2-dependent inhibition of MALT1 signaling requires the presence of the MALT1 DD.

Given the strong indications that interaction with GRK2 negatively impacts MALT1 activity, we sought to more precisely characterize how GRK2 interfaces with MALT1. As a first step, we identified the specific region within GRK2 that is responsible for MALT1 binding. Our analysis revealed that the site of MALT1 interaction is located within the N-terminal amino acids (aa 1–173) of GRK2 (Figure 2C). This GRK2 region is composed of the extreme N-terminal helix (referred to as αN) (aa 1–20) and the regulator of G protein signaling homology (RH) protein-protein interaction domain (aa 30–173). Notably, this GRK2 fragment (aa 1–173) alone inhibited BCL10/MALT1–dependent NF-κB activation in a concentration-dependent manner (Figure 2D) and was as effective as full-length GRK2 at blocking BCL10/MALT1 signaling (Supplemental Figure 2C). Similarly to full-length GRK2, expres-

sion of this GRK2(1–173) fragment also effectively inhibited the coimmunoprecipitation of BCL10 and MALT1 (Supplemental Figure 2D). Our results indicate that the other domains within GRK2, such as the kinase and pleckstrin homology (PH) domains, are not required for MALT1 inhibition.

*GRK2 inhibits MALT1 proteolytic activity.* In order to investigate whether GRK2 modulates MALT1 catalytic activity, we first analyzed whether expression of GRK2 in HEK293T cells impacts the proteolytic processing of CYLD or RELB, 2 known MALT1 substrates. We found that BCL10/MALT1–dependent cleavage of CYLD and RELB were both inhibited by expression of GRK2, while API2-MALT1–mediated cleavage of both substrates was not affected (Figure 3, A and B). This lack of effect on API2-MALT1 proteolytic activity is presumably due to the fact that the API2-MALT1 fusion does not retain the DD of MALT1 (31), and parallels the finding noted above that GRK2 does not block API2-MALT1–dependent NF-κB activation (Figure 2B). We also performed fluorescence resonance energy transfer (FRET) analysis, which demonstrated that both full-length GRK2 and the GRK2 αN/RH fragment (aa 1–173) inhibited BCL10/MALT1–mediated cleavage of the YFP-LVSR-CFP fluorescent MALT1 substrate in a concentration-dependent fashion (Figure 3C). This parallels our finding that the GRK2 αN/RH fragment (aa 1–173) is as effective as full-length GRK2 in blocking BCL10/MALT1–dependent NF-κB luciferase activation.

To complement our cell-based analyses, we also analyzed the cleavage of the LVSR-AMC fluorogenic MALT1 peptide substrate in a cell-free system. This peptide is based on the MALT1 cleavage site within RELB and is the most efficiently cleaved MALT1 pep-
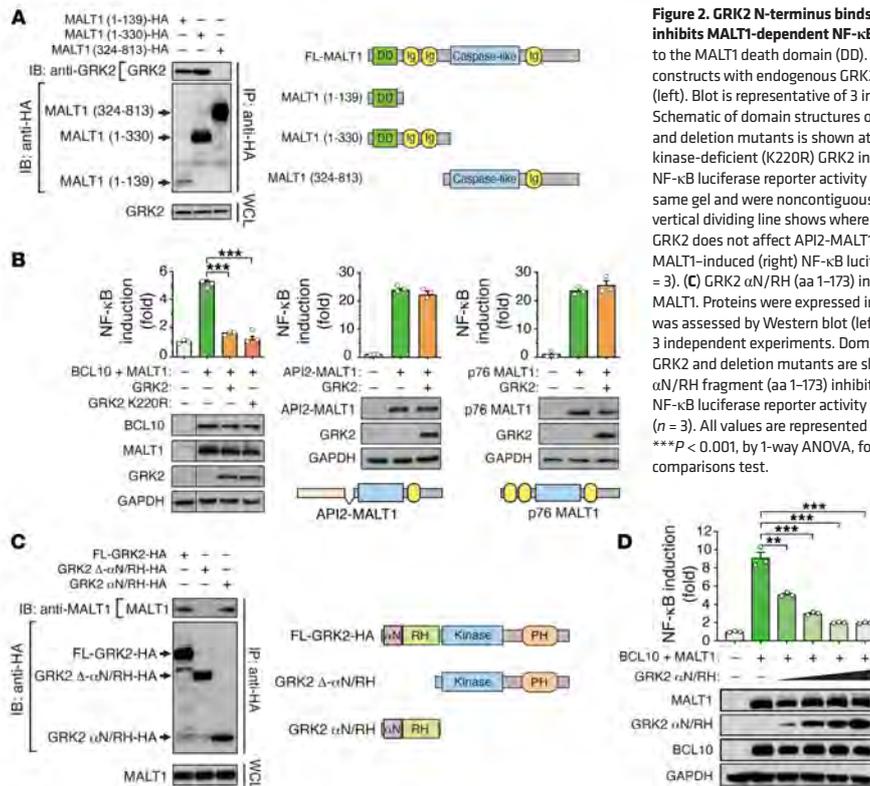
　　　　　**RESEARCH ARTICLE**



**Figure 2. GRK2 N-terminus binds to MALT1 death domain and inhibits MALT1-dependent NF-κB activation.** (**A**) GRK2 binds to the MALT1 death domain (DD). Co-IP of HA-tagged MALT1 constructs with endogenous GRK2 in HEK293T cells is shown (left). Blot is representative of 3 independent experiments. Schematic of domain structures of full-length (FL) MALT1 and deletion mutants is shown at right. (**B**) Both WT and kinase-deficient (K220R) GRK2 inhibit BCL10/MALT1–induced NF-κB luciferase reporter activity (left). Lanes were run on the same gel and were noncontiguous in the leftmost blot; the vertical dividing line shows where images are spliced together. GRK2 does not affect API2-MALT1–induced (middle) or p76 MALT1–induced (right) NF-κB luciferase reporter activity ($n$ = 3). (**C**) GRK2 αN/RH (aa 1–173) interacts with endogenous MALT1. Proteins were expressed in HEK293T cells, and co-IP was assessed by Western blot (left). Blot is representative of 3 independent experiments. Domain structures of full-length GRK2 and deletion mutants are shown at right. (**D**) The GRK2 αN/RH fragment (aa 1–173) inhibits BCL10/MALT1–induced NF-κB luciferase reporter activity in a dose-dependent manner ($n$ = 3). All values are represented as mean ± SEM. **$P < 0.01$, ***$P < 0.001$, by 1-way ANOVA, followed by Tukey's multiple-comparisons test.

tide substrate currently available (15). Using purified recombinant human proteins, we found that addition of GRK2 into the reaction reduced the cleavage of LVSR-AMC by MALT1 (Figure 3D). This analysis with recombinant purified MALT1 demonstrates that BCL10 does not need to be present for GRK2 to exert an inhibitory effect on MALT1 protease activity. Together, our data in both cell-based and cell-free systems provide convincing evidence that GRK2 inhibits MALT1 proteolytic activity.

*GRK2 attenuates MALT1 scaffolding and proteolytic activities, NF-κB induction, and IL-2 production in stimulated T cells.* To begin evaluating the impact of GRK2 on MALT1 activity in lymphocytes, we transiently transfected Jurkat T cells with either WT or kinase-deficient (K220R) GRK2 and then stimulated the cells with PMA/Iono. We found that increased expression of either WT GRK2 or K220R kinase-dead GRK2 mutant abrogated PMA/Iono–induced NF-κB activation (Figure 4A, top). In contrast, GRK2 had no effect on NF-κB induction by TNF, which is known to occur via a signaling pathway that is independent of MALT1 (Figure 4A, bottom, and ref. 47). To complement this analysis, we performed the converse experiment and stably knocked down GRK2 in Jurkat T cells using lentiviral shRNA. In order to rule out off-target effects of the shRNA, we used 3 distinct shRNAs targeting different regions of GRK2 (designated as shRNAs 1, 2, and 3). First, we examined

the impact of GRK2 depletion on AgR-induced CBM complex formation. While we did not observe a significant change in the interaction between MALT1 and BCL10, PMA/Iono–induced co-IP of CARMA1 with MALT1 was significantly enhanced after stable GRK2 knockdown, suggesting that GRK2 may inhibit overall CBM complex assembly (Figure 4B and Supplemental Figure 3A). Second, we also examined AgR-induced IκB phosphorylation, a signaling event that is dependent on MALT1 scaffolding activity but does not require MALT1 proteolytic activity (15, 17, 20). Strikingly, although our shRNA-mediated GRK2 knockdown was incomplete, cells responded to PMA/Iono or anti-CD3/CD28 with substantially more robust IκB phosphorylation when GRK2 levels were reduced (Figure 4B and Supplemental Figure 3, A and B). Consistent with our observation that enforced expression of GRK2 has no effect on TNF-α–dependent NF-κB transcriptional activation, we found that TNF-α–induced IκB phosphorylation remained unaffected after GRK2 knockdown. Third, we evaluated the effect of GRK2 knockdown on MALT1 proteolytic activity by comparing the ratios of cleaved CYLD and RELB fragment levels to full-length protein levels in control and GRK2-depleted T cells. We found that the relative levels of cleaved CYLD (Figure 4C) and cleaved RELB (Figure 4D and Supplemental Figure 3C) in response to PMA/Iono or CD3/CD28 stimulation in T cells were
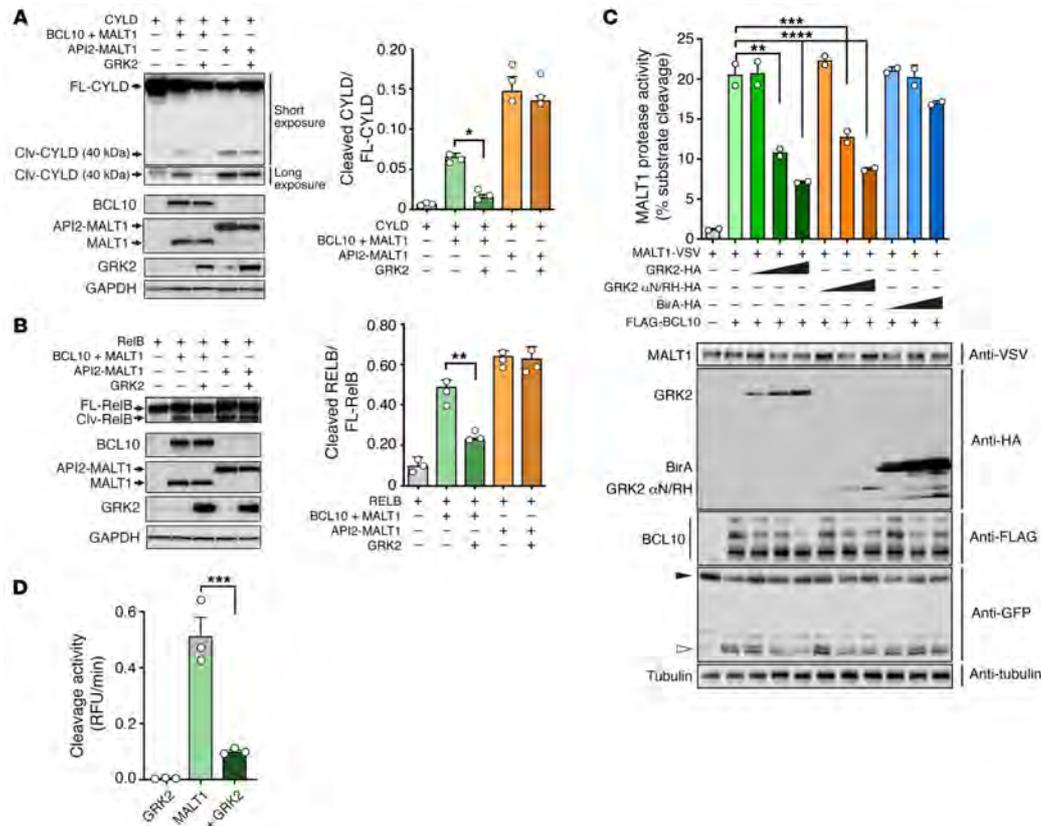
141

**Figure 3. GRK2 inhibits MALT1 proteolytic activity.** (**A** and **B**) GRK2 inhibits MALT1-mediated cleavage of CYLD and RELB. Recombinant proteins were expressed in HEK293T cells, and cleavage of CYLD (**A**) or RELB (**B**) was assessed by Western blot. Quantification of the cleavage is shown to the right of the blots. Densitometric analysis was performed using AlphaView software (ProteinSimple) ($n = 3$). (**C**) Both GRK2 and GRK2 αN/RH (aa 1–173) inhibit MALT1 protease activity in a dose-dependent manner. Indicated proteins were expressed in HEK293T cells together with the eYFP-Leu-Val-Arg-eCFP reporter construct. Cells were evaluated using flow cytometry 24 hours after transfection. Filled and open arrowheads indicate full-length and cleaved reporter, respectively, detected by GFP antibody ($n = 2$). (**D**) GRK2 inhibits in vitro MALT1 cleavage of the LVSR-AMC substrate in a cell-free system. Recombinant purified proteins were incubated with 50 μM Ac-LVSR-AMC. Cleavage activity of MALT1 was determined by the increase of AMC fluorescence measured with a Synergy microplate reader ($n = 3$). All values are represented as mean ± SEM. *$P < 0.05$, **$P < 0.01$, ***$P < 0.001$, ****$P < 0.0001$, by 1-way ANOVA, followed by Tukey's multiple-comparisons test.

significantly higher after GRK2 shRNA knockdown. In addition, we observed enhanced p65 nuclear translocation (Supplemental Figure 3D) and DNA binding (Supplemental Figure 3E) when GRK2 was stably knocked down. Together, our results indicate that GRK2 depletion in T lymphocytes results in enhanced MALT1 scaffolding and proteolytic activities, leading to enhanced activation of canonical NF-κB signaling.

Next, to determine the downstream impact of GRK2-mediated MALT1 inhibition on T cell activation, we used ELISA to compare the level of secreted IL-2 after PMA/Iono or CD3/CD28 stimulation in control and GRK2-deficient Jurkat T cells. We chose to focus on IL-2 because it is an NF-κB–inducible cytokine produced

in activated T cells after AgR stimulation that plays a pivotal role in the T cell immune response (48). We found that GRK2 shRNA knockdown resulted in significantly increased IL-2 secretion (Figure 4E and Supplemental Figure 3F).

Moreover, we also analyzed the impact of GRK2 deficiency using primary B cells isolated from the spleens of B cell–specific GRK2-knockout mice (Mb1-cre[+]GRK2^{fl/fl}) (49). We found that PMA/Iono–induced IκB phosphorylation was also enhanced in GRK2-deficient primary B cells when compared with control primary B cells (Mb1-cre[–]GRK2^{fl/+}) (Supplemental Figure 3G).

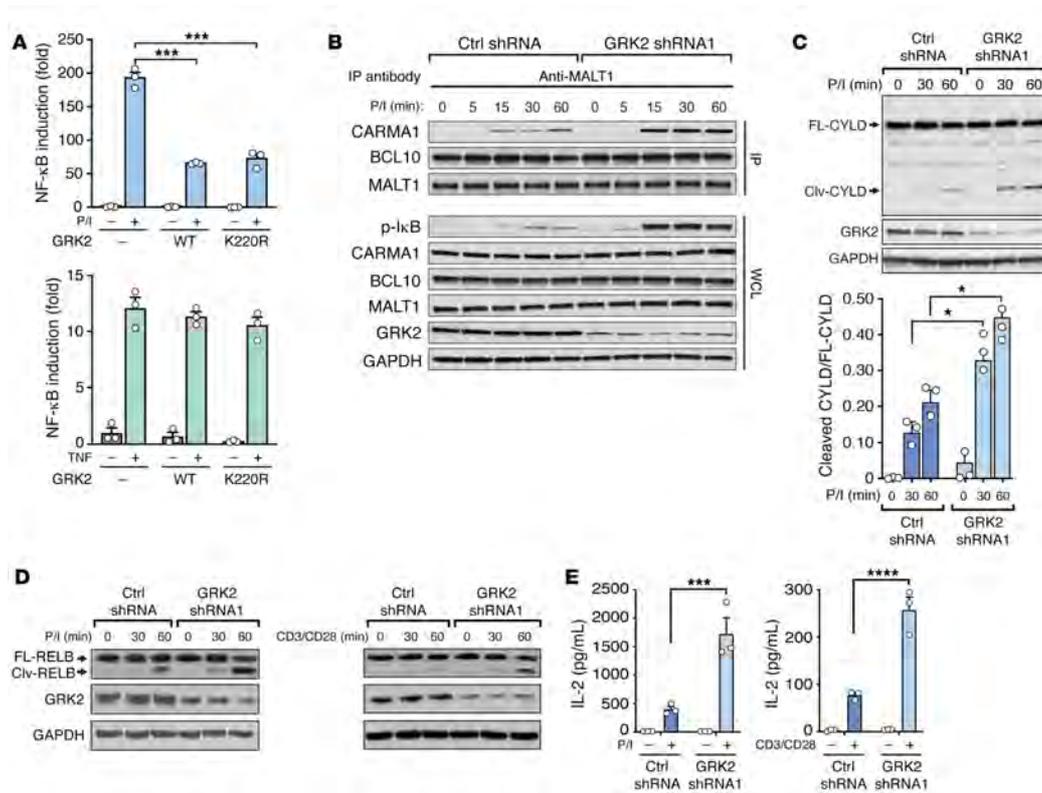To even further confirm the influence of GRK2 on MALT1 activity, we performed targeted deletion of GRK2 in Jurkat T

**Figure 4. GRK2 attenuates AgR stimulation–induced NF-κB activation, CBM complex formation, MALT1 activity, and IL-2 production in Jurkat T cells.**
(**A**) Expression of WT GRK2 or kinase-deficient (K220R) GRK2 mutant in Jurkat T cells inhibits PMA/ionomycin–induced (P/I-induced) (top) but not TNF-induced (bottom) NF-κB luciferase reporter activity (*n* = 3). (**B**) Knockdown of GRK2 in Jurkat T cells leads to enhanced P/I-induced CBM complex formation. Jurkat T cells were subjected to knockdown with either control or GRK2 shRNA lentivirus (GRK2 shRNA1) and then treated with or without P/I. Binding of BCL10 and CARMA1 to immunoprecipitated MALT1 and phosphorylation of IκB were examined. Blot is representative of 2 independent experiments. (**C**) GRK2 knockdown in Jurkat T cells leads to increased cleavage of CYLD in response to P/I stimulation. Quantification of the cleavage is shown below. Densitometric analysis was performed using AlphaView software (*n* = 3). (**D**) GRK2 knockdown in Jurkat T cells leads to increased cleavage of RELB in response to P/I (left) or anti-CD3/CD28 (right) stimulation. Blots are representative of 3 independent experiments. (**E**) GRK2 knockdown leads to enhanced IL-2 production in Jurkat T cells. Cells were treated with or without P/I (left) or anti-CD3/CD28 (right) for 24 hours, and IL-2 in supernatant was measured by ELISA (*n* = 3). All values are represented as mean ± SEM. *P* < 0.05, ****P* < 0.001, *****P* < 0.0001. Data from **A**, **C**, and **E** were analyzed by 2-way ANOVA, followed by Tukey's multiple-comparisons test.

cells using CRISPR/Cas9. Guide RNA (gRNA) with the highest cleavage efficiency was selected for use in the generation of the knockout cell lines (Supplemental Figure 4A). After selecting and expanding individual clones (designated as Jurkat T3, T14, and T26), we confirmed the targeted disruption of GRK2 using Sanger sequencing. TIDE (Tracking Indels by DEcompositon) analysis (50) was used to identify insertion or deletion (INDEL) on individual alleles (Supplemental Figure 4B). We also performed Western blot and confirmed that no detectable GRK2 was seen in the Jurkat GRK2-knockout clones (Figure 5A and Supplemental Figure 4, C and D). As expected based on our shRNA knockdown analysis, the GRK2-CRISPR-knockout Jurkat clones demonstrated enhanced IκB phosphorylation, RELB cleavage, and IL-2 production in response to PMA/Iono or CD3/CD28 stimulation (Figure 5, A–C,

and Supplemental Figure 4, C–E). Next, we rescued the homozygous GRK2-CRISPR-knockout Jurkat clone (T3) using lentivirus expressing WT GRK2. Western blot showed that the level of rescued GRK2 expression was comparable to the endogenous level of GRK2 in control Jurkat cells (Supplemental Figure 4F). We found that GRK2 rescue reversed the enhanced IκB phosphorylation, RELB cleavage, and IL-2 production caused by GRK2 knockout (Figure 5, D–F). Taken together, our results convincingly demonstrate that GRK2 inhibits both MALT1 scaffolding and proteolytic activity, thereby abrogating AgR-induced CBM-dependent NF-κB activation in Jurkat T cells.

*Lower GRK2 expression level is associated with reduced survival in ABC-DLBCL.* Since our data indicate that GRK2 binds and inhibits MALT1, we wondered whether GRK2 might play an important role
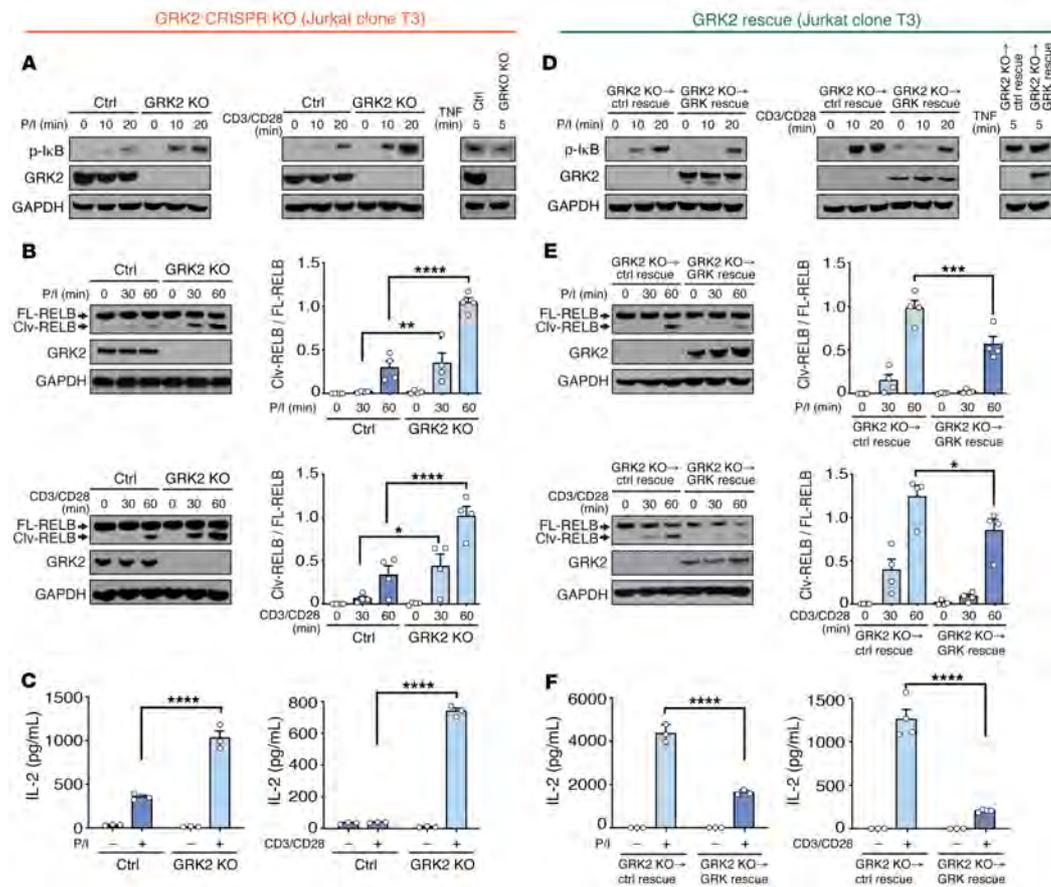
143

**Figure 5. GRK2 CRISPR/Cas9 knockout leads to enhanced MALT1-dependent activities in Jurkat T cells, and rescue of GRK2 reverses this phenotype. (A)** GRK2 knockout (KO) leads to increased IκB phosphorylation after P/I (left) or anti-CD3/CD28 (middle) but not after TNF (right) stimulation in Jurkat T cells. GRK2-KO Jurkat T cells were made using Cas9/gRNA. GRK2 knockout was confirmed by Western blot. Blots are representative of at least 3 experiments. (**B**) GRK2 KO in Jurkat T cells leads to increased cleavage of RELB after P/I (top) or anti-CD3/CD28 (bottom) stimulation. Blots shown are representative of *n* = 4. Clv, cleaved; FL, full-length. Quantification of cleavage is shown to the right of the blots. *\*P* < 0.05, \*\**P* < 0.01, \*\*\*\**P* < 0.0001. (**C**) GRK2 KO leads to increased IL-2 production in Jurkat T cells after P/I (left) or anti-CD3/CD28 (right) stimulation. IL-2 secretion was determined by ELISA (*n* = 3). \*\*\*\**P* < 0.0001. (**D**) GRK2 rescue in GRK2-KO Jurkat T cells reverses the enhanced IκB phosphorylation after P/I (left) or anti-CD3/CD28 (middle) but has no effect on the TNF response (right). GRK2-KO Jurkat T cells were rescued using lentivirus expressing WT GRK2, and stable cell lines were made by selection using puromycin. GRK2 rescue was confirmed by Western blot. Blots are representative of at least 3 experiments. (**E**) Rescue of GRK2 in GRK2-KO Jurkat T cells reverses the enhanced cleavage of RELB caused by GRK2 KO. Blots shown are representative of *n* = 4. Quantification of cleavage is shown to the right of the blots. *\*P* < 0.05, \*\*\**P* < 0.001. (**F**) GRK2 rescue leads to reduced IL-2 production in GRK2-KO Jurkat T cells. IL-2 secretion was determined by ELISA (*n* = 3–4). All values are represented as mean ± SEM. \*\*\*\**P* < 0.0001. Statistical significance for **B**, **C**, **E**, and **F** was evaluated by 2-way ANOVA, followed by Tukey's multiple-comparisons test.

in modulating the growth and survival of MALT1-dependent lymphomas. As a first step in evaluating such a role for GRK2 in these tumors, we used a published data set to compare mRNA levels of *GRK2* (also known as *ADRBK1*) in 44 DLBCL patient tumor samples versus 20 healthy B cell control samples (51). We found that *GRK2* mRNA levels are markedly lower in a subset of DLBCL cases compared with normal B cell controls (Figure 6A). We considered

the possibility that the observed decrease in *GRK2* could reflect gene expression changes during B cell differentiation rather than a lymphoma/cancer-associated effect, but our analyses of publicly available data sets suggest that *GRK2* mRNA levels remain relatively constant and high throughout B cell development (Figure 6B). Kaplan-Meier analysis of the publicly available Visco data set (GEO GSE31312) (52) showed that progression-free survival and overall
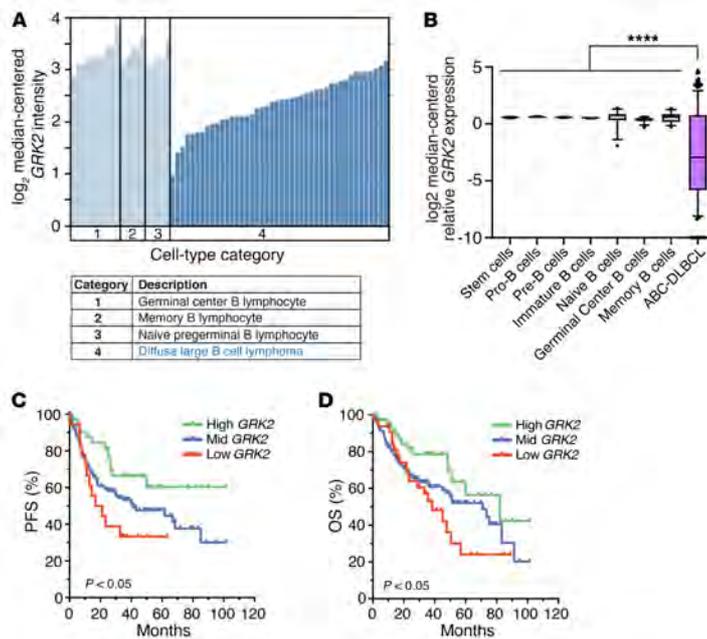
**Figure 6. Lower GRK2 expression level is associated with reduced survival in ABC-DL-BCL.** (**A**) *GRK2* mRNA levels are markedly lower in a subset of DLBCL tumor specimens (*n* = 44) compared with normal control B cells (*n* = 20). Data were accessed using www.oncomine.com (GSE12195). GRK2 expression values were median centered and expressed on $\log_2$ scale. (**B**) *GRK2* mRNA expression levels are relatively consistent throughout B cell development and significantly higher in normal B cells than what is seen in ABC-DL-BCL cells. Data were obtained from public repositories (GSE2350, GSE10846, GSE22886, and GSE45460) and analyzed using R (version 3.0.2) and GraphPad Prism (version 7.0.1). *P* value was calculated by 1-way ANO-VA, followed by Bonferroni post-test. ****$P$ < 0.0001. (**C** and **D**) Rates of progression-free survival (PFS) (**C**) and overall survival (OS) (**D**) of ABC-DLBCL patients are lower in patients with low GRK2 (bottom 25%) compared with high GRK2 (top 25%). Expression of GRK2 was stratified into high, mid, and low categories using data set–wide quartile cutoffs (low 25%, mid 50%, high 25%). Statistical significance was evaluated using log-rank test. Data for **C** and **D** were accessed from a public repository (GSE31312).

survival rates for ABC-DLBCL are significantly worse in patients with low *GRK2* levels (bottom 25%) as compared with high *GRK2* (top 25%) (Figure 6, C and D). We also performed multivariate Kaplan-Meier analysis for progression-free survival and overall survival, controlling for age, sex, stage, prognostic index, and chemotherapy response, and results indicated that lower *GRK2* level remains an independent predictor in ABC-DLBCL patients (representative graphs with correction for age and sex are shown in Supplemental Figure 5, A and B). The association of lower *GRK2* expression level with inferior survival in ABC-DLBCL was also further confirmed by analysis of a second independent data set (GSE4732) (ref. 53 and Supplemental Figure 5, C and D). In contrast to ABC-DLBCL, *GRK2*-low groups do not show reduced survival relative to *GRK2*-high groups for patients with GCB-DLBCL, a DLBCL subtype that is not dependent on MALT1 for growth and survival (ref. 7 and Supplemental Figure 5, E and F).

We also compared *GRK2* mRNA expression levels in ABC-DLBCL tumor specimens obtained from patients with localized disease with those from patients with advanced-stage disease. We found that lower *GRK2* expression level is associated with an increased degree of extranodal spread of lymphoma (GSE10846) (Supplemental Figure 5G and ref. 54). Together, our analyses indicate that lower *GRK2* level is associated with inferior survival in ABC-DLBCL.

*GRK2 restrains MALT1-dependent signaling and cellular proliferation in ABC-DLBCL.* Multiple studies have demonstrated that ABC-DLBCL cells are dependent on MALT1 proteolytic activity for growth and survival (27, 29). We queried publicly available cell line mRNA expression data sets and noted that most ABC-DLBCL cell

lines demonstrated lower *GRK2* mRNA expression as compared with non–MALT1-dependent GCB-DLBCL cell lines (Figure 7A and Supplemental Figure 6A). We next assessed GRK2 protein levels in several ABC-DLBCL cell lines, as well as in several GCB-DLBCL cell lines. Specifically, we evaluated HBL1, TMD8, and OCI-Ly10 cells, which harbor activating mutations in a BCR CD79 subunit, as well as OCI-Ly3 cells, which harbor an activating mutation in CARMA1 (ref. 21 and Figure 7B). Although a small cohort, we were intrigued to find that GRK2 protein level is quite low in a subset of ABC-DLBCL lines when compared with GCB-DLBCL lines, which is consistent with what we had observed above in cell line mRNA expression data sets. We evaluated the interaction of GRK2 and MALT1 in ABC-DLBCL cells and found that despite the relatively low GRK2 protein level and despite the presence of upstream activating mutations that drive constitutive CBM assembly and MALT1 activity, some degree of baseline interaction between GRK2 and MALT1 can still be detected by co-IP in both OCI-Ly3 and HBL1 cells (Supplemental Figure 6B). Intriguingly, the relative amount of GRK2 coimmunoprecipitated with MALT1 is notably higher in GCB cells (OCI-Ly1 and OCI-Ly7 cells: density ratios of GRK2/MALT1 with MALT1 co-IP are 1.36 and 1.90, respectively) than in ABC-DLBCL cells (OCI-Ly3 and HBL1: GRK2/MALT1 density ratios are 0.41 and 0.23, respectively) (Supplemental Figure 6C). We speculate that this relative difference in GRK2-MALT1 interaction could be the result of some degree of GRK2 dissociation from MALT1 induced by the upstream gain-of-function mutations that mimic AgR stimulation in the ABC-DLBCL cells.

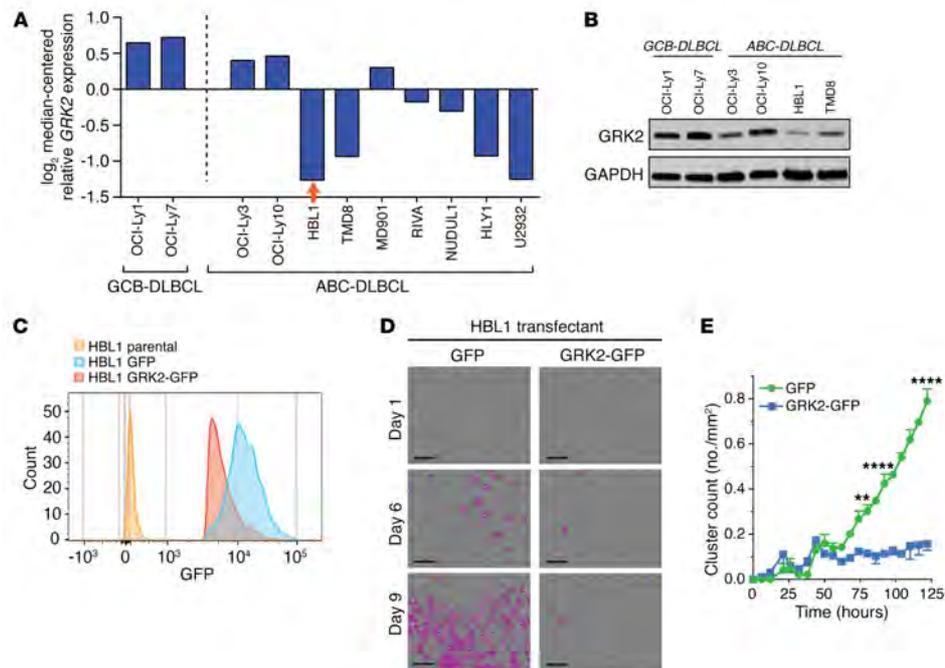We attempted to overexpress GRK2 in HBL1 cells, our ABC-DLBCL line with the lowest GRK2 mRNA and protein levels, using

**Figure 7. Overexpression of GRK2 inhibits ABC-DLBCL proliferation.** (**A**) HBL1 cells demonstrate relatively low *GRK2* mRNA expression. cDNA microarray data were retrieved from a public repository (ArrayExpress, E-GEOD-42203) and analyzed. DLBCL cell lines were grouped based on GCB or ABC subtype. (**B**) HBL-1 cells express the lowest level of GRK2 protein among all cell lines tested. GRK2 protein levels in a panel of GCB-DLBCL (OCI-Ly1, OCI-Ly7) and ABC-DLBCL (OCI-Ly3, OCI-Ly10, HBL1, and TMD8) cells were assessed by Western blot. Cell lysates were subjected to immunoblotting with antibodies as indicated. Blots are representative of 2 independent experiments. (**C**) GRK2-GFP is effectively expressed in HBL1 cells infected with lentivirus, as detected by flow cytometry. Data are representative of at least 5 independent experiments. (**D**) GRK2-GFP–positive cells fail to proliferate, while control GFP-only HBL1 cells proliferate efficiently. Proliferation of HBL1 cells was monitored using a cell clustering immune cell proliferation assay. Representative images of 3 independent experiments are shown. Phase-contrast images are overlaid with Incucyte Zoom (Essen Biosciences) confluence segmentation mask (magenta). Scale bars: 300 μm. (**E**) Cluster count quantification is shown with time as a continuous variable. HBL1 cell proliferation was measured at 5-hour intervals using Incucyte Zoom (*n* = 3). Two-way ANOVA and Šidák's multiple-comparisons test were performed to show growth difference between the GRK2-GFP and control GFP groups. **$P < 0.01$, ****$P < 0.0001$.

a lentiviral approach. Although we were able to isolate GFP-tagged GRK2-positive HBL1 cells by flow cytometry sorting (Figure 7C), these GRK2-overexpressing cells failed to proliferate, while control GFP-only–positive HBL1 cells proliferated efficiently (Figure 7, D and E). Similar to the situation with HBL1 cells, we were able to isolate GFP-tagged GRK2 positive OCI-Ly3 cells (Supplemental Figure 6D), and like the HBL1 cells expressing GFP-GRK2, these OCI-Ly3 cells expressing GFP-GRK2 did not survive. In contrast to these ABC-DLBCL cell lines, we were able to successfully generate GCB-DLBCL lines (OCI-Ly1 and OCI-Ly7) as well as Jurkat T cell lines that overexpress GFP-tagged GRK2 (Supplemental Figure 6E) using the same lentiviral system. These results are consistent with the notion that GRK2 can function as a tumor modulator/suppressor, and its downregulation in a subset of ABC-DLBCL cases is required for pathologic growth and survival. Restoration of GRK2 expression in this setting therefore inhibits cell growth and survival.

In light of these results, we took the converse approach, and analyzed the impact of GRK2 knockdown in OCI-Ly3 cells,

an ABC-DLBCL line with higher GRK2 level compared with HBL1 and others (Figure 7, A and B, and Supplemental Figure 6A). Using lentiviral shRNA, we generated multiple OCI-Ly3 clones with significantly reduced GRK2 levels, and these GRK2-deficient OCI-Ly3 clones all displayed significantly enhanced basal IκB phosphorylation as compared with control OCI-Ly3 clones (Figure 8A, left). We also performed targeted deletion of GRK2 in OCI-Ly3 cells using CRISPR/Cas9. After selecting and expanding individual clones (designated as T5, T39, and T47), we confirmed the targeted disruption of GRK2 using Sanger sequencing (TIDE analysis and chromatogram sequence alignment are shown in Supplemental Figure 7). Similar to our analysis of GRK2-shRNA-knockdown OCI-Ly3 clones, the GRK2-CRISPR-knockout OCI-Ly3 clones demonstrated higher levels of basal IκB phosphorylation (Figure 8A, middle, and Supplemental Figure 8A). We next attempted to rescue the homozygous GRK2-CRISPR-knockout clone T5 using lentivirus expressing WT GRK2. While we were successful in expressing GRK2 in
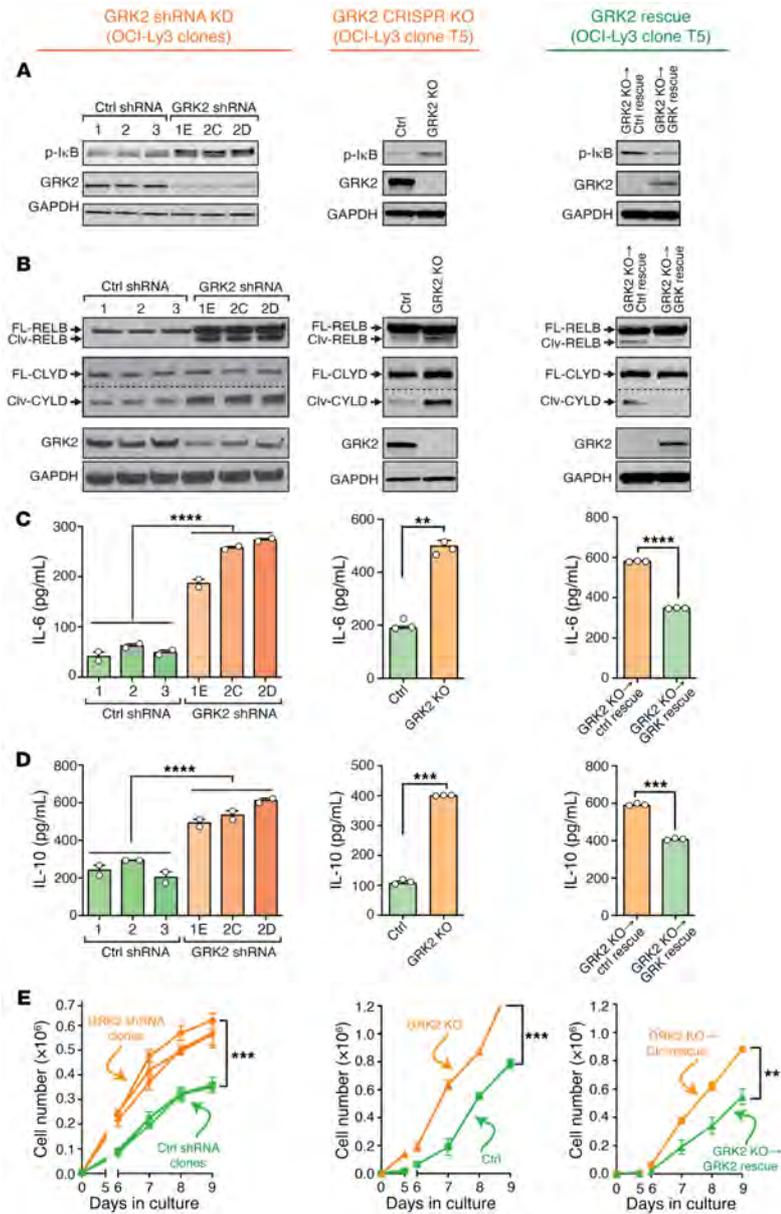
**Figure 8. shRNA knockdown or CRISPR/Cas9 knockout of GRK2 in ABC-DLBCL (OCI-Ly3) cells leads to enhanced MALT1-mediated IκB phosphorylation, RELB and CYLD cleavage, cytokine secretion, and cell proliferation, and GRK2 rescue reverses these effects.** (**A**) GRK2 knockdown (KD) (left) or knockout (KO) (middle) leads to increased basal IκB phosphorylation in ABC-DLBCL line OCI-Ly3. Stable OCI-Ly3 cells with GRK2 KD were made using specific shRNA lentivirus. GRK2 KOs were made using Cas9/gRNA. GRK2 KD or KO was confirmed by Western blot. Rescue of GRK2 in GRK2-KO cells reverses this phenotype (right). Blots are representative of at least 3 experiments. (**B**) GRK2 KD (left) or KO (middle) in OCI-Ly3 cells leads to increased cleavage of RELB and CYLD. Rescue of GRK2 in GRK2-KO cells reverses this phenotype (right). Blots shown are representative of 3 experiments. Clv, cleaved; FL, full-length. (**C** and **D**) GRK2 KD (left) leads to increased IL-6 and IL-10 production in OCI-Ly3 cells. Control clones (1, 2, and 3) and GRK2-KD clones (1E, 2C, and 2D) were analyzed separately (total of *n* = 6 for both control and GRK2 KD). GRK2 KO (middle) leads to increased IL-6 and IL-10 production in OCI-Ly3 cells (*n* = 3). Rescue of GRK2 in GRK2-KO cells (right) reverses this phenotype (*n* = 3). IL-6 and IL-10 secretion was determined by ELISA. All values are represented as mean ± SEM. **$P < 0.01$, ***$P < 0.001$, ****$P < 0.0001$, by unpaired, 2-tailed Student's *t* test. (**E**) GRK2 KD (left) or KO (middle) leads to increased proliferation of OCI-Ly3 cells. Rescue of GRK2 in GRK2-KO cells reverses this phenotype (right) (*n* = 3). Two-way ANOVA and Šidák's multiple-comparisons test were performed to show proliferation differences between the GRK2-KD or -KO and control groups (only significance for the end time points is shown). ***$P < 0.001$.

our GRK2-CRISPR-knockout cells, the level of GRK2 expression achieved in the rescued OCI-Ly3 cells was significantly lower than the endogenous GRK2 level in CRISPR control cells (Supplemental Figure 8B). Even with this relatively lower level of GRK2 expression, we found that GRK2 rescue reversed the enhanced IκB phosphorylation (Figure 8A, right).

Consistent with our previous analysis indicating that GRK2 inhibits MALT1 proteolytic activity (Figure 3), we found that the GRK2-shRNA-knockdown and GRK2-CRISPR-knockout OCI-Ly3 clones demonstrated enhanced MALT1-mediated cleavage of RELB and CYLD compared with controls (Figure 8B and Supplemental Figure 8, C and D). Notably, GRK2 knockdown/knockout
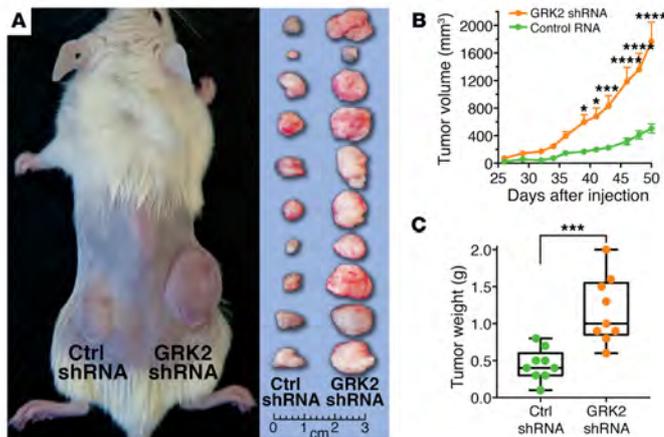
**Figure 9. Knockdown of GRK2 leads to enhanced tumor growth of ABC-DLBCL cells in vivo. (A–C)** GRK2 knockdown leads to increased tumor volume and weight in a xenograft model of DLBCL. NOD. Cg-Prkdc$^{scid}$ Il2rg$^{tm1Wjl}$/SzJ (NSG) mice were inoculated with OCI-Ly3 cells (2.5 × 10$^6$) stably expressing control shRNA or GRK2 shRNA. Tumors were measured 3 times weekly with calipers, and tumor weight was determined at week 7. A representative mouse and resected tumor pairs (*n* = 10) are shown in **A**. Two-way ANOVA and Šidák's multiple-comparisons test were performed to show growth differences between the GRK2 shRNA and control groups. Paired *t* test was performed for tumor weights. *$P < 0.05$, ***$P < 0.001$, ****$P < 0.0001$.

in ABC-DLBCL was associated with an increase in total RELB levels in these cells. It is possible that this occurs as a result of enhanced MALT1-dependent activation of the transcription of the *RELB* gene, a known NF-κB transcriptional target (15). Importantly, GRK2 rescue reversed the enhanced RELB and CYLD cleavage in GRK2-knockout OCI-Ly3 cells (Figure 8B, right).

IL-6 and IL-10 are cytokines present in the lymphoma tumor microenvironment that promote the proliferation and survival of the malignant B cells (55). In DLBCL, autocrine IL-6 production provides proliferative and antiapoptotic signals, and elevated IL-6 levels in patient serum correlate with adverse outcome (56). Previous studies have demonstrated that ABC-DLBCL cells, including OCI-Ly3, spontaneously secrete IL-6 and IL-10 (55), and that transcription and expression of these 2 cytokines depend on MALT protease activity (26). Again, consistent with a tumor-suppressing role for GRK2, we found that GRK2 shRNA knockdown or CRISPR knockout enhanced the secretion of these tumor-promoting cytokines (Figure 8, C and D, and Supplemental Figure 8, E and F), and GRK2 rescue reversed this enhanced cytokine secretion (Figure 8, C and D).

The GRK2-deficient OCI-Ly3 clones all displayed significantly enhanced proliferation in vitro as compared with control OCI-Ly3 clones (Figure 8E, left and middle, and Supplemental Figure 8G), and GRK2 rescue reversed this enhanced proliferation (Figure 8E, right). Notably, stable knockdown of GRK2 in another ABC-DLBCL cell line, HBL1, had similar effects, enhancing basal IκB phosphorylation, MALT1 cleavage activity, IL-10 secretion, and in vitro proliferation (Supplemental Figure 9, A–E). Intriguingly, we observed that GRK2 knockdown in ABC-DLBCL cells also resulted in increased cell aggregation and attachment (Supplemental Figure 8H). It has been reported that MALT1-dependent cleavage of BCL10 enhances β$_1$ integrin–dependent T cell adhesion (17). Our results in ABC-DLBCL cells could therefore be consistent with a model in which a decrease in GRK2 level results in an increase in MALT1-dependent cleavage of BCL10, leading to enhanced cell adhesion. Further studies are needed to more fully elucidate the molecular mechanisms mediating this observed increase in adhesion in the GRK2-deficient cells.

In light of our in vitro observations, we next examined the influence of GRK2 on lymphoma growth in vivo. To this end, we used our OCI-Ly3 ABC-DLBCL cell lines harboring either control shRNA or GRK2-targeting shRNA, and subcutaneously injected these lines into opposite flanks of 5-week-old NOD.Cg-Prkdc$^{scid}$ Il2rg$^{tm1Wjl}$/SzJ (NSG) mice. Xenograft growth was monitored over the ensuing ~2 months, revealing a dramatic increase in the growth of tumors with GRK2 knockdown (Figure 9, A–C). Thus, both our in vitro and in vivo studies provided evidence that GRK2 abrogates ABC-DLBCL tumor growth.

## Discussion

Our present study reveals a new mechanism by which MALT1, a proto-oncoprotein that plays a critical role in the pathogenesis of several subtypes of NHL, is regulated. The *MALT1* gene was originally identified in 1999 as a target for chromosomal translocation in the B cell malignancy MALT lymphoma (57–60). Since that time, accumulating evidence has revealed that the CBM complex plays an essential role in the normal adaptive immune response by bridging TCR or BCR upstream signaling to the canonical NF-κB pathway, thus promoting lymphocyte activation and proliferation in response to antigen (47, 61, 62). Deregulation of this CBM complex, with resultant constitutive MALT1 activity and unrestricted NF-κB signaling, has recently emerged as a common feature of multiple lymphoid malignancies (7). Here, we demonstrate that GRK2 binds to and inhibits MALT1, negatively impacting both MALT1 scaffolding and proteolytic activities and blocking downstream MALT1-mediated NF-κB activation.

Several groups have demonstrated that ABC-DLBCL, which can harbor gain-of-function mutations in CARMA1 or the upstream CD79A or CD79B subunit of BCR, relies on constitutive MALT1 activity for growth and survival (21, 23, 26, 28). We provide multiple lines of evidence indicating that GRK2 inhibits the growth of these MALT1-dependent tumors. More recently, Rahal et al. demonstrated that a subset of mantle cell lymphomas similarly depend on constitutive MALT1 signaling for growth and survival (34). In addition, a role for deregulated MALT1 signaling has

recently been extended beyond B cell lymphoma to include T cell malignancy. Activating mutations in CARMA1, and its upstream regulators PKCβ and PLCγ1, have been identified in both adult T cell leukemia/lymphoma and Sézary syndrome, a form of cutaneous T cell lymphoma, suggesting that these malignant T cells are also dependent on MALT1 for survival (63–65). This ever-expanding role for MALT1 in a spectrum of lymphoid malignancy suggests that inhibition of MALT by GRK2 likely impacts the pathogenesis of multiple subtypes of lymphoma beyond ABC-DLBCL. This concept underscores the potentially broad scope of influence of the GRK2-MALT1 interaction in lymphoid malignancy and warrants further study.

The discovery that in addition to scaffolding activity, MALT1 also possesses proteolytic activity, represented a major step in advancing our understanding of lymphocyte biology and the molecular pathogenesis of CBM-driven lymphomas (17, 18, 66). Thus far, 10 specific proteolytic substrates of MALT1 have been identified (20, 67), and we demonstrate that GRK2 inhibits its MALT1-mediated cleavage of 2 of these known substrates, RELB and CYLD. MALT1 protease activity is thought to sustain NF-κB activation and promote lymphomagenesis in part by cleaving RELB, an NF-κB subunit that forms transcriptionally inactive complexes with and thereby inhibits RELA and c-REL (15). While modulation of NF-κB activity is the most well-studied role of MALT1 protease activity, MALT1 cleaves several additional substrates that impact other aspects of lymphocyte biology. For example, MALT1-dependent cleavage of the deubiqitinase CYLD is essential for AgR-induced activation of JNK (19), and similarly to constitutive NF-κB activation, constitutive JNK activation is also a hallmark of ABC-DLBCL (68). In addition, recent studies demonstrate that MALT1 cleaves multiple substrates involved in regulating RNA stability in lymphocytes (69, 70). MALT1 is also able to cleave its binding partner BCL10, and this cleavage may promote lymphocyte adhesion (17). We expect that, in addition to inhibiting cleavage of CYLD and RELB, as shown here, GRK2 likely influences the processing of other diverse MALT1 proteolytic substrates. Precisely how GRK2 influences the overall balance of MALT1-driven NF-κB activity, JNK signaling, RNA stability, cellular adhesion, and/or other cellular functions impacted by MALT1 protease activity probably varies depending on cellular context, and the broad impact of GRK2 on these processes warrants further investigation. Our current study indicates that in MALT1-dependent ABC-DLBCL cells, a net effect of GRK2 is to inhibit cell aggregation and proliferation.

Our data show that AgR stimulation induces the dissociation of GRK2 and MALT1, and this occurs within the same general time course as AgR-induced CARMA1 association with BCL10/MALT1 and phosphorylation of IκB. We also find that GRK2 knockdown results in significantly enhanced AgR-induced CARMA1 association with BCL10/MALT1 and IκB phosphorylation. Together these results suggest that GRK2 inhibits overall CBM complex assembly. While we find that overexpression of either GRK2 or the GRK2 N-terminal fragment (αN/RH, aa 1–173) inhibits the coimmunoprecipitation of MALT1 and BCL10 as well as downstream BCL10/MALT1–dependent NF-κB activation, we do not observe an increase in BCL10-MALT1 interaction when GRK2 is knocked down in T cells. We do find that MALT1 scaffolding activity (mea-

sured by IκB phosphorylation) and MALT1 proteolytic activity (measured by substrate cleavage), as well as MALT1-dependent upregulation of IL-2, are all significantly increased in cells with GRK2 knockdown. Thus, based on our analysis thus far, it seems likely that the ability of GRK2 to inhibit BCL10/MALT1–dependent NF-κB signaling is not solely a result of direct competition between BCL10 and GRK2 for MALT1 binding. In fact, we find that GRK2 inhibits the proteolytic activity of purified MALT1 in vitro, which indicates that GRK2 can exert an inhibitory effect on MALT1 activity in the absence of either CARMA1 or BCL10. Detailed structural studies will be needed in the future in order to elucidate the precise molecular mechanism(s) by which GRK2 interaction with MALT1 results in the inhibition of MALT1 signaling activities. Importantly, while this current article was in preparation, a detailed cryo–electron microscopy structural analysis of the BCL10-MALT1 interaction was published by the Krappmann and Lammens laboratories (44). This new work, which revealed the interaction of BCL10 with the MALT1 DD, will be highly relevant to future structural analyses of the interaction of GRK2 with the MALT1 DD.

Inhibition of MALT1 proteolytic activity is selectively toxic to ABC-DLBCL human lymphoma cell lines in vitro and to ABC-DLBCL xenograft tumors in vivo (26, 27, 29). These findings have led to considerable interest in the development of inhibitors of MALT1 protease activity as therapeutic agents. Multiple distinct categories of small-molecule MALT1 protease inhibitors have been reported, including (a) phenothiazine derivatives (e.g., mepazine), which bind to an allosteric site located between the MALT1 Ig3 domain and catalytic domain, and reversibly inhibit MALT1 by preventing the rearrangement of the enzyme into an active conformation (29); (b) MI-2 and its derivatives, which are irreversible inhibitors thought to covalently modify the MALT1 active site cysteine (27, 71); (c) β-lapachone analogs, which are also irreversible inhibitors that form a covalent bond with the MALT1 catalytic cysteine (72); and (d) MLT-748 and MLT-747, which are closely related allosteric inhibitors that bind to the interface between the catalytic and Ig3 domains (73). Our current study suggests that GRK2 inhibits MALT1 proteolytic activity via a mechanism distinct from that of these MALT1 protease inhibitors, by interacting with the MALT1 DD. We have determined that the N-terminal region of GRK2, composed of a short helix (αN) (aa 1–20) followed by a regulator of G protein signaling homology (RH) protein-protein interaction domain (aa 30–173), mediates this interaction with MALT1. This region of GRK2 (aa 1–173), which excludes the kinase and PH domains, is both necessary and sufficient to inhibit MALT1-dependent signaling, indicating that GRK2 kinase activity is not required to inhibit MALT1. It will be of great interest to precisely define the structural features within GRK2 that are required for interaction with the MALT1 DD and inhibition of MALT1 activities. We anticipate that elucidation of these required features of GRK2 could provide a roadmap for developing a new category of MALT1 inhibitor that would abrogate both scaffolding and proteolytic activities via interaction with the MALT1 DD.

GRK2 is emerging as an important "oncomodulator," a protein that influences multiple cellular functions related to the hallmarks of cancer, such as cell proliferation, cell survival, cell motility, cell metabolism, and angiogenesis, via its impact on cancer-relevant signaling networks (38). Many recent studies show

that in addition to its canonical role of regulating G protein–coupled receptors via phosphorylation-dependent desensitization and internalization, GRK2 can also exert effects in a phosphorylation-independent manner by engaging in a diverse repertoire of protein-protein interactions (36, 74). GRK2 has been reported to influence tumor progression in several different cancers, and the specific mechanism by which GRK2 exerts its influence depends on the tumor cell type. For example, it has been reported that GRK2 promotes the growth of certain breast cancers via phosphorylation and activation of histone deacetylase 6 (HDAC6) (38, 75). As another example, 2 recent reports suggest that GRK2 is overexpressed in pancreatic cancer and may serve as an indicator of unfavorable prognosis (76, 77). In contrast to breast and pancreatic cancer, GRK2 appears to inhibit tumor growth in other cancers. For example, several studies suggest that GRK2 inhibits the proliferation of hepatocellular carcinoma (HCC) cells, and this is thought to occur via GRK2-mediated inhibition of insulin-like growth factor 1 (IGF-1) signaling (78, 79). In HCC, GRK2 kinase activity is required for GRK2 to suppress cell proliferation. Unlike this kinase-dependent mechanism by which GRK2 inhibits IGF-1 signaling and cell proliferation in HCC, our studies suggest that GRK2 inhibits MALT1-dependent tumor progression via a mechanism that is kinase-independent.

Our studies suggest that GRK2 functions as an oncomodulator/tumor suppressor in ABC-DLBCL. We demonstrate that lower *GRK2* mRNA expression in ABC-DLBCL, but not in GCB-DLBCL, is associated with worse overall survival and progression-free survival. Furthermore, our studies show that lowering GRK2 protein levels within ABC-DLBCL cells results in enhanced tumor growth in vitro and in vivo. These data lead us to propose that measuring *GRK2* mRNA and/or protein levels in ABC-DLBCL tumor specimens might become useful in guiding prognosis and treatment. Additionally, it will be of great interest to elucidate the molecular mechanisms responsible for regulating levels of *GRK2* mRNA and/or protein and the degree of GRK2-mediated MALT1 inhibition in these tumors. Thus far, we have not identified specific mutations in the *GRK2* gene that could account for the lower *GRK2* mRNA expression in a subset of ABC-DLBCL tumor specimens or the lower GRK2 protein expression in a subset of ABC-DLBCL cell lines. However, GRK2 protein expression and function are known to be regulated at multiple levels, including at the posttranscriptional and posttranslational levels (37, 80, 81). Future studies will be aimed at elucidating the mechanisms by which GRK2 expression and function are controlled in ABC-DLBCL and other MALT1-dependent tumors.

Taken together, our data identify GRK2 as a binding partner and negative modulator of MALT1. We found that GRK2 bound to the MALT1 DD, and, to our knowledge, GRK2 is the first protein demonstrated to inhibit MALT1 scaffolding and protease activities. Our molecular biological analyses of ABC-DLBCL cells and bioinformatic analyses of human patient tumor specimens are consistent with a tumor suppressor role for GRK2 in ABC-DLBCL, a cancer that requires active MALT1 for growth and survival. Since the MALT1 proto-oncoprotein is now emerging as a critical mediator of tumor growth and survival for an even wider variety of lymphoid neoplasms, elucidating the molecular mechanisms by which GRK2 inhibits MALT1 will be critical for understanding the overall land-scape of lymphoid neoplasia and for developing targeted therapies for the spectrum of MALT1-dependent malignancies.

## Methods

*Cell lines and reagents.* The DLBCL cell lines OCI-Ly1, OCI-Ly3, OCI-Ly7, and OCI-Ly10 were provided by Mark D. Minden (University Health Network, Toronto, Ontario, Canada). HBL1 and TMD8 were provided by Louis Staudt (National Cancer Institute, NIH). OCI-Ly1 and OCI-Ly7 cells were cultured in IMDM supplemented with 10% FBS and 100 U/mL penicillin/streptomycin. OCI-Ly3 cells were cultured in IMDM supplemented with 20% FBS and 100 U/mL penicillin/streptomycin. OCI-Ly10 cells were cultured in IMDM with 20% human serum (Valley Biomedical), penicillin/streptomycin, and 50 μM β-mercaptoethanol. HBL1, TMD8, Jurkat, and BJAB cells were cultured in RPMI 1640 medium with 10% FBS and 100 U/mL penicillin/streptomycin. Stimulation of Jurkat and BJAB cells was accomplished by addition of phorbol 12-myristate 13-acetate (PMA) (5 ng/mL; Sigma) and ionomycin (1 μM; Calbiochem). GST-GRK2, GST-MALT1, and GST-BCL10 recombinant proteins were purchased from Novus Biologicals. TRC lentiviral human GRK2/ADRBK1 shRNA (TRCN0000000557, TRCN0000000558, TRCN0000000559, TRCN0000000560, TRCN0000000561) (NC0765786) were purchased from Dharmacon. Lentiviral ORF cDNA clones for *GRK2/ADRBK1* (EX-A0311-Lv103 with N-eGFP) and empty vector control plasmid (EX-NEG-Lv103) were from GeneCopoeia. The proteasome inhibitor MG132 was purchased from Calbiochem. Pierce protein A/G-Agarose and Aminolink coupling resin were from Thermo Fisher Scientific. Plasmids expressing MALT1 and BCL10 have been described previously (43). pcDNAGRK2, pcDNAGRK2-K220R, pHA-GRK2, pHA-GRK2RH, and Flag-RelB plasmids were previously described (15, 82–84). FLAG-tagged CYLD expression plasmids were generated by cloning of CYLD cDNA, or fragments thereof, into the pEAK10 plasmid as previously described (85).

*Recombinant protease cleavage assay.* Recombinant GST-MALT1 was purified from *E. coli*. For measurement of protease activity in vitro, proteins were incubated for 3 hours at 30°C with 50 μM Ac-LVSR-AMC (MCA-3952-PI; Peptides International), and the protease activity of MALT1 was determined by measurement of the increase of AMC fluorescence with a Synergy microplate reader (BioTek) as previously reported (86).

*FRET-based assay of protease and flow cytometry.* HEK293T cells were transfected with the appropriate constructs together with the eYFP-Leu-Val-Ser-Arg-eCFP reporter construct. Twenty-four hours after transfection, cells were resuspended in flow cytometry buffer and analyzed with a BD LSR II flow cytometer (BD Biosciences) as previously reported (87).

*Xenograft model of DLBCL.* Tumors were engrafted into 5-week-old female NOD.Cg-Prkdc[scid] Il2rg[tm1Wjl]/SzJ (NSG) mice from The Jackson Laboratory (stock 005557) by subcutaneous injection of $2.5 \times 10^6$ OCI-Ly3 control or GRK2 shRNA cells resuspended in Matrigel (Cultrex Basement Membrane Extract, Type 3, PathClear; Trevigen). Control and GRK2-knockdown tumors were engrafted on opposite flanks of individual mice, with 10 mice in each group. Tumor sizes were measured 3 times weekly after visual appearance using a caliper and calculated using the formula: (smallest diameter$^2$ × largest diameter)/2. Mice were sacrificed when tumors reached 2500 mm$^3$.

*Study approval.* All experiments were performed in compliance with guidelines of the University of Pittsburgh and UCSF and according to the protocol approved by the IACUCs of these institutions.

**RESEARCH ARTICLE**

*Statistical analysis.* All values are represented as mean ± SEM. Data were analyzed and statistics calculated with GraphPad Prism software using Student's *t* test (for comparing 2 groups) and ANOVA (for comparing 3 or more groups). Figure legends contain details regarding *t* test and ANOVA analyses for individual experiments. In vitro and in vivo growth curves were evaluated using 2-way ANOVA and Šidák's multiple-comparisons tests. Survival analysis was performed using the Kaplan-Meier method, and differences were compared using a log-rank (Mantel-Cox) test. Multivariate Kaplan-Meier analysis was performed using IBM Statistics SPSS 19 software and the Cox proportional hazards regression model. *P* values of 0.05 or less were considered statistically significant.

*Additional methods.* Additional materials and methods are described in the Supplemental Methods.

## Author contributions
JC designed and performed the majority of experiments, wrote the first draft of the manuscript, and constructed figures. LRK designed and performed analysis of Jurkat T cells with shRNA-GRK2 knockdown and CRISPR/Cas9-GRK2 knockout. NEH performed bioinformatic analyses of human tumor specimens. MZ and RS designed and performed experiments demonstrating GRK2 inhibition of MALT1 proteolytic activity. LMM designed and performed co-IP analyzing the impact of GRK2(1–173) on BCL10-MALT1 interaction. HBK designed and performed ELISA analysis of cytokine secretion. HK designed and performed initial immunoprecipitation analyses to demonstrate GRK2-MALT1 interaction. VJC assisted with bioinformatic analysis and generation of GRK2-knockdown cell lines. PCD performed initial experiments demonstrating GRK2 inhibition of MALT1-mediated NF-κB activation. EVD and MAM performed analysis of GRK2-deficient primary murine B cells under the supervision of JGC. MB generated multiple critical reagents required to investigate the interaction of GRK2 with the MALT1 DD. JGC developed a mouse strain with GRK2-deficient B cells and supervised analysis of primary murine B cells. NP performed the initial immunoprecipitation/mass

spectrometry analysis that led to discovery of the GRK2-MALT1 interaction. MT developed methods for demonstrating GRK2-mediated inhibition of MALT1 protease activity, supervised those studies, and provided expert guidance for overall project development. PCL and LMML are the principal investigators of the laboratory where they supervised the development of this project in its entirety, procured funding to support the work, and led the construction of the manuscript. LMML is listed last because she serves as primary mentor for first author JC.

Address correspondence to: Linda M. McAllister-Lucas or Peter C. Lucas, Rangos Research Building, Children's Hospital of Pittsburgh, University of Pittsburgh School of Medicine, 4401 Penn Avenue, Pittsburgh, Pennsylvania 15224, USA. Phone: 412.692.7608; Email: linda.mcallister@chp.edu; lucaspc@upmc.edu.

1. Roschewski M, Staudt LM, Wilson WH. Diffuse large B-cell lymphoma-treatment approaches in the molecular era. *Nat Rev Clin Oncol*. 2014;11(1):12–23.
2. Surveillance, Epidemiology, and End Results Program; National Cancer Institute Web Site. https://seer.cancer.gov. Updated May 30, 2019. Accessed December 23, 2019.
3. Alizadeh AA, et al. Distinct types of diffuse large B-cell lymphoma identified by gene expression profiling. *Nature*. 2000;403(6769):503–511.
4. Davis RE, Brown KD, Siebenlist U, Staudt LM. Constitutive nuclear factor kappaB activity is required for survival of activated B cell–like diffuse large B cell lymphoma cells. *J Exp Med*. 2001;194(12):1861–1874.
5. Rosenwald A, et al. The use of molecular profiling to predict survival after chemotherapy for diffuse large-B-cell lymphoma. *N Engl J Med*. 2002;346(25):1937–1947.
6. Ngo VN, et al. A loss-of-function RNA interference screen for molecular targets in cancer. *Nature*. 2006;441(7089):106–110.

7. Juilland M, Thome M. Role of the CARMA1/BCL10/MALT1 complex in lymphoid malignancies. *Curr Opin Hematol*. 2016;23(4):402–409.
8. Yang C, David L, Qiao Q, Damko E, Wu H. The CBM signalosome: potential therapeutic target for aggressive lymphoma? *Cytokine Growth Factor Rev*. 2014;25(2):175–183.
9. Noels H, et al. A novel TRAF6 binding site in MALT1 defines distinct mechanisms of NF-κB activation by API2·MALT1 fusions. *J Biol Chem*. 2007;282(14):10180–10189.
10. Oeckinghaus A, et al. Malt1 ubiquitination triggers NF-kappaB signaling upon T-cell activation. *EMBO J*. 2007;26(22):4634–4645.
11. Sun L, Deng L, Ea CK, Xia ZP, Chen ZJ. The TRAF6 ubiquitin ligase and TAK1 kinase mediate IKK activation by BCL10 and MALT1 in T lymphocytes. *Mol Cell*. 2004;14(3):289–301.
12. Lucas PC, McAllister-Lucas LM, Nunez G. NF-kappaB signaling in lymphocytes: a new cast of characters. *J Cell Sci*. 2004;117(pt 1):31–39.
13. Afonina IS, Elton L, Carpentier I, Beyaert R. MALT1—a universal soldier: multiple strategies

to ensure NF-κB activation and target gene expression. *FEBS J*. 2015;282(17):3286–3297.
14. McAllister-Lucas LM, Baens M, Lucas PC. MALT1 protease: a new therapeutic target in B lymphoma and beyond? *Clin Cancer Res*. 2011;17(21):6623–6631.
15. Hailfinger S, et al. Malt1-dependent RelB cleavage promotes canonical NF-kappaB activation in lymphocytes and lymphoma cell lines. *Proc Natl Acad Sci U S A*. 2011;108(35):14596–14601.
16. Klei LR, et al. MALT1 Protease activation triggers acute disruption of endothelial barrier integrity via CYLD cleavage. *Cell Rep*. 2016;17(1):221–232.
17. Rebeaud F, et al. The proteolytic activity of the paracaspase MALT1 is key in T cell activation. *Nat Immunol*. 2008;9(3):272–281.
18. Coornaert B, et al. T cell antigen receptor stimulation induces MALT1 paracaspase-mediated cleavage of the NF-κB inhibitor A20. *Nat Immunol*. 2008;9(3):263–271.
19. Staal J, et al. T-cell receptor-induced JNK activation requires proteolytic inactivation of CYLD by MALT1. *EMBO J*. 2011;30(9):1742–1752.

RESEARCH ARTICLE

The Journal of Clinical Investigation

20. Jaworski M, Thome M. The paracaspase MALT1: biological function and potential for therapeutic inhibition. *Cell Mol Life Sci*. 2016;73(3):459–473.

21. Davis RE, et al. Chronic active B-cell-receptor signalling in diffuse large B-cell lymphoma. *Nature*. 2010;463(7277):88–92.

22. Shaffer AL, Young RM, Staudt LM. Pathogenesis of human B cell lymphomas. *Annu Rev Immunol*. 2012;30:565–610.

23. Lenz G, et al. Oncogenic CARD11 mutations in human diffuse large B cell lymphoma. *Science*. 2008;319(5870):1676–1679.

24. Lohr JG, et al. Discovery and prioritization of somatic mutations in diffuse large B-cell lymphoma (DLBCL) by whole-exome sequencing. *Proc Natl Acad Sci U S A*. 2012;109(10):3879–3884.

25. Hailfinger S, Lenz G, Thome M. Targeting B-cell lymphomas with inhibitors of the MALT1 paracaspase. *Curr Opin Chem Biol*. 2014;23:47–55.

26. Ferch U, et al. Inhibition of MALT1 protease activity is selectively toxic for activated B cell-like diffuse large B cell lymphoma cells. *J Exp Med*. 2009;206(11):2313–2320.

27. Fontan L, et al. MALT1 small molecule inhibitors specifically suppress ABC-DLBCL in vitro and in vivo. *Cancer Cell*. 2012;22(6):812–824.

28. Hailfinger S, et al. Essential role of MALT1 protease activity in activated B cell-like diffuse large B-cell lymphoma. *Proc Natl Acad Sci U S A*. 2009;106(47):19946–19951.

29. Nagel D, et al. Pharmacologic inhibition of MALT1 protease by phenothiazines as a therapeutic approach for the treatment of aggressive ABC-DLBCL. *Cancer Cell*. 2012;22(6):825–837.

30. Lucas PC, et al. A dual role for the API2 moiety in API2-MALT1-dependent NF-κB activation: heterotypic oligomerization and TRAF2 recruitment. *Oncogene*. 2007;26(38):5643–5654.

31. Rosebeck S, et al. Cleavage of NIK by the API2-MALT1 fusion oncoprotein leads to noncanonical NF-kappaB activation. *Science*. 2011;331(6016):468–472.

32. Rosebeck S, et al. The API2-MALT1 fusion exploits TNFR pathway-associated RIP1 ubiquitination to promote oncogenic NF-κB signaling. *Oncogene*. 2014;33(19):2520–2530.

33. Arora M, Kaul D, Varma N, Marwaha RK. Cellular proteolytic modification of tumor-suppressor CYLD is critical for the initiation of human T-cell acute lymphoblastic leukemia. *Blood Cells Mol Dis*. 2015;54(1):132–138.

34. Rahal R, et al. Pharmacological and genomic profiling identifies NF-κB-targeted treatment strategies for mantle cell lymphoma. *Nat Med*. 2014;20(1):87–92.

35. Vallois D, et al. Activating mutations in genes related to TCR signaling in angioimmunoblastic and other follicular helper T-cell-derived lymphomas. *Blood*. 2016;128(11):1490–1502.

36. Evron T, Daigle TL, Caron MG. GRK2: multiple roles beyond G protein-coupled receptor desensitization. *Trends Pharmacol Sci*. 2012;33(3):154–164.

37. Penela P, Murga C, Ribas C, Lafarga V, Mayor F. The complex G protein-coupled receptor kinase 2 (GRK2) interactome unveils new physiopathological targets. *Br J Pharmacol*. 2010;160(4):821–832.

38. Nogués L, Reglero C, Rivas V, Neves M, Penela P, Mayor F. G-protein-coupled receptor kinase 2 as

a potential modulator of the hallmarks of cancer. *Mol Pharmacol*. 2017;91(3):220–228.

39. Vroon A, Heijnen CJ, Kavelaars A. GRKs and arrestins: regulators of migration and inflammation. *J Leukoc Biol*. 2006;80(6):1214–1221.

40. Matsumoto R, et al. Phosphorylation of CARMA1 plays a critical role in T cell receptor-mediated NF-κB activation. *Immunity*. 2005;23(6):575–585.

41. Sommer K, et al. Phosphorylation of the CARMA1 linker controls NF-kappaB activation. *Immunity*. 2005;23(6):561–574.

42. Langel FD, Jain NA, Rossman JS, Kingeter LM, Kashyap AK, Schaefer BC. Multiple protein domains mediate interaction between Bcl10 and MALT1. *J Biol Chem*. 2008;283(47):32419–32431.

43. Lucas PC, et al. Bcl10 and MALT1, independent targets of chromosomal translocation in malt lymphoma, cooperate in a novel NF-κB signaling pathway. *J Biol Chem*. 2001;276(22):19012–19019.

44. Schlauderer F, et al. Molecular architecture and regulation of BCL10-MALT1 filaments. *Nat Commun*. 2018;9(1):4041.

45. Baens M, et al. MALT1 auto-proteolysis is essential for NF-κB-dependent gene transcription in activated lymphocytes. *PLoS One*. 2014;9(8):e103774.

46. Dale LB, et al. G protein-coupled receptor kinase-mediated desensitization of metabotropic glutamate receptor 1A protects against cell death. *J Biol Chem*. 2000;275(49):38213–38220.

47. Ruefli-Brasse AA, French DM, Dixit VM. Regulation of NF-κB-dependent lymphocyte activation and development by paracaspase. *Science*. 2003;302(5650):1581–1584.

48. Liao W, Lin JX, Leonard WJ. Interleukin-2 at the crossroads of effector responses, tolerance, and immunotherapy. *Immunity*. 2013;38(1):13–25.

49. Arnon TI, et al. GRK2-dependent S1PR1 desensitization is required for lymphocytes to overcome their attraction to blood. *Science*. 2011;333(6051):1898–1903.

50. Brinkman EK, Chen T, Amendola M, van Steensel B. Easy quantitative assessment of genome editing by sequence trace decomposition. *Nucleic Acids Res*. 2014;42(22):e168.

51. Compagno M, et al. Mutations of multiple genes cause deregulation of NF-κB in diffuse large B-cell lymphoma. *Nature*. 2009;459(7247):717–721.

52. Visco C, et al. Comprehensive gene expression profiling and immunohistochemical studies support application of immunophenotypic algorithm for molecular subtype classification in diffuse large B-cell lymphoma: a report from the International DLBCL Rituximab-CHOP Consortium Program Study. *Leukemia*. 2012;26(9):2103–2113.

53. Dave SS, et al. Molecular diagnosis of Burkitt's lymphoma. *N Engl J Med*. 2006;354(23):2431–2442.

54. Lenz G, et al. Stromal gene signatures in large-B-cell lymphomas. *N Engl J Med*. 2008;359(22):2313–2323.

55. Lam LT, et al. Cooperative signaling through the signal transducer and activator of transcription 3 and nuclear factor-κB pathways in subtypes of diffuse large B-cell lymphoma. *Blood*. 2008;111(7):3701–3713.

56. Nacinović-Duletić A, Stifter S, Dvornik S, Skunca Z, Jonjić N. Correlation of serum IL-6, IL-8 and IL-10 levels with clinicopathological features and

prognosis in patients with diffuse large B-cell lymphoma. *Int J Lab Hematol*. 2008;30(3):230–239.

57. Akagi T, et al. A novel gene, MALT1 at 18q21, is involved in t(11;18) (q21;q21) found in low-grade B-cell lymphoma of mucosa-associated lymphoid tissue. *Oncogene*. 1999;18(42):5785–5794.

58. Dierlamm J, et al. The apoptosis inhibitor gene API2 and a novel 18q gene, MLT, are recurrently rearranged in the t(11;18)(q21;q21) associated with mucosa-associated lymphoid tissue lymphomas. *Blood*. 1999;93(11):3601–3609.

59. Morgan JA, et al. Breakpoints of the t(11;18) (q21;q21) in mucosa-associated lymphoid tissue (MALT) lymphoma lie within or near the previously undescribed gene MALT1 in chromosome 18. *Cancer Res*. 1999;59(24):6205–6213.

60. Suzuki H, Motegi M, Akagi T, Hosokawa Y, Seto M. API1-MALT1-MLT is involved in mucosa-associated lymphoid tissue lymphoma with t(11;18) (q21;q21). *Blood*. 1999;94(9):3270–3271.

61. Hara H, et al. The MAGUK family protein CARD11 is essential for lymphocyte activation. *Immunity*. 2003;18(6):763–775.

62. Ruland J, et al. Bcl10 is a positive regulator of antigen receptor-induced activation of NF-κB and neural tube closure. *Cell*. 2001;104(1):33–42.

63. Kataoka K, et al. Integrated molecular analysis of adult T cell leukemia/lymphoma. *Nat Genet*. 2015;47(11):1304–1315.

64. Wang L, et al. Genomic profiling of Sézary syndrome identifies alterations of key T cell signaling and differentiation genes. *Nat Genet*. 2015;47(12):1426–1434.

65. da Silva Almeida AC, et al. The mutational landscape of cutaneous T cell lymphoma and Sézary syndrome. *Nat Genet*. 2015;47(12):1465–1470.

66. McAllister-Lucas LM, Lucas PC. Finally, MALT1 is a protease! *Nat Immunol*. 2008;9(3):231–233.

67. Yamasoba D, et al. N4BP1 restricts HIV-1 and its inactivation by MALT1 promotes viral reactivation. *Nat Microbiol*. 2019;4(9):1532–1544.

68. Knies N, et al. Lymphomagenic CARD11/ BCL10/MALT1 signaling drives malignant B-cell proliferation via cooperative NF-κB and JNK activation. *Proc Natl Acad Sci U S A*. 2015;112(52):E7230–E7238.

69. Uehata T, et al. Malt1-induced cleavage of regnase-1 in CD4(+) helper T cells regulates immune activation. *Cell*. 2013;153(5):1036–1049.

70. Jeltsch KM, et al. Cleavage of roquin and regnase-1 by the paracaspase MALT1 releases their cooperatively repressed targets to promote T(H)17 differentiation. *Nat Immunol*. 2014;15(11):1079–1089.

71. Xin BT, et al. Development of new Malt1 inhibitors and probes. *Bioorg Med Chem*. 2016;24(15):3312–3329.

72. Lim SM, et al. Identification of β-lapachone analogs as novel MALT1 inhibitors to treat an aggressive subtype of diffuse large B-cell lymphoma. *J Med Chem*. 2015;58(21):8491–8502.

73. Quancard J, et al. An allosteric MALT1 inhibitor is a molecular corrector rescuing function in an immunodeficient patient. *Nat Chem Biol*. 2019;15(3):304–313.

74. Watari K, Nakaya M, Kurose H. Multiple functions of G protein-coupled receptor kinases. *J Mol Signal*. 2014;9(1):1.

152

75. Nogués L, et al. G Protein-coupled receptor kinase 2 (GRK2) promotes breast tumorigenesis through a HDAC6-Pin1 axis. *EBioMedicine*. 2016;13:132–145.

76. Buchholz M, et al. A multistep high-content screening approach to identify novel functionally relevant target genes in pancreatic cancer. *PLoS One*. 2015;10(4):e0122946.

77. Zhou L, et al. G-protein-coupled receptor kinase 2 in pancreatic cancer: clinicopathologic and prognostic significance. *Hum Pathol*. 2016;56:171–177.

78. Wei Z, Hurtt R, Ciccarelli M, Koch WJ, Doria C. Growth inhibition of human hepatocellular carcinoma cells by overexpression of G-protein-coupled receptor kinase 2. *J Cell Physiol*. 2012;227(6):2371–2377.

79. Wei Z, Hurtt R, Gu T, Bodzin AS, Koch WJ, Doria

C. GRK2 negatively regulates IGF-1R signaling pathway and cyclins' expression in HepG2 cells. *J Cell Physiol*. 2013;228(9):1897–1901.

80. Ribas C, et al. The G protein-coupled receptor kinase (GRK) interactome: role of GRKs in GPCR regulation and signaling. *Biochim Biophys Acta*. 2007;1768(4):913–922.

81. Nogués L, et al. G protein-coupled receptor kinases (GRKs) in tumorigenesis and cancer progression: GPCR regulators and signaling hubs. *Semin Cancer Biol*. 2018;48:78–90.

82. Kong G, Penn R, Benovic JL. A β-adrenergic receptor kinase dominant negative mutant attenuates desensitization of the β2-adrenergic receptor. *J Biol Chem*. 1994;269(18):13084–13087.

83. Levay K, Satpaev DK, Pronin AN, Benovic JL, Slepak VZ. Localization of the sites for Ca²⁺-bind-

ing proteins on G protein-coupled receptor kinases. *Biochemistry*. 1998;37(39):13650–13659.

84. Patial S, Luo J, Porter KJ, Benovic JL, Parameswaran N. G-protein-coupled-receptor kinases mediate TNFα-induced NFκB signalling via direct interaction with and phosphorylation of IκBα. *Biochem J*. 2009;425(1):169–178.

85. O'Donnell MA, et al. Caspase 8 inhibits programmed necrosis by processing CYLD. *Nat Cell Biol*. 2011;13(12):1437–1442.

86. Hailfinger S, Pelzer C, Thome M. Detection and measurement of paracaspase MALT1 activity. *Methods Mol Biol*. 2014;1133:177–188.

87. Pelzer C, Cabalzar K, Wolf A, Gonzalez M, Lenz G, Thome M. The protease activity of the paracaspase MALT1 is controlled by monoubiquitination. *Nat Immunol*. 2013;14(4):337–345.

153

## Supplemental Materials and Methods

*Mass Spectrometry.* Raw264.7 cells were plated in 15 cm plates and grown to confluence. Cells were washed with cold PBS and lysed. After centrifugation, supernatants were used for immunoprecipitation. Lysates were first precleared using mouse IgG coupled resin (for 2h) and then incubated with GRK2 antibody-coupled resin or mouse IgG resin as control (overnight at 4° C). Resin was washed four times with lysis buffer to remove any non-specific proteins, and then acid eluted and neutralized with Tris (pH 9). Samples were separated on SDS-PAGE gels and proteins were visualized using Coomassie stain. Unique bands present in the GRK2 IPs but not present in the control IPs were excised and submitted to Michigan State University Proteomics Facility for trypsinization and subsequent LC-MS/MS analysis. Data were analyzed using Scaffold program (Proteome Software, Inc).

*Antibodies.* Anti-BCL10 (sc-5611), anti-MALT1 (H300) (sc-28246), anti-MALT1 (B-12) (sc-46677), and anti-GRK2(C-15) (SC-562) were purchased from Santa Cruz Biotechnology. Anti-RELB (C1E4) (Cat. No 4922), anti-GAPDH (D16H11) (Cat. No 5174), anti-phospho-IκB (5A5, Ser32/36) (Cat. No 9246), anti-p65 (Cat No 3987s), anti-HDAC1 (10E2, HRP conjugate, cat No 59581S) were purchased from Cell Signaling Technology. Anti-CYLD (733) (Cat.No 43-700) was purchased from Invitrogen. Anti-Myc (4A6) (Cat. No 05-724) was purchased from EMD Millipore. Anti-mouse, rabbit and rat secondary antibodies were from Promega. Anti-HA affinity Matrix (3F10, Cat. No 11 815 016 001) and Anti-HA high affinity antibody (3F10, Cat.No 11 867 423 001) were from Roche.

*Immunoprecipitation and immunoblotting.* For immunoprecipitation, cells were rinsed in PBS, and lysed in buffer (150mM NaCl, 2mM EDTA, 10% glycerol, 1% Nonidet P-40, 20mM, Tris HCl, pH 7.4) containing protease and phosphatase inhibitors. Supernatants were incubated with

1

specified antibody for 1 hour at 4 °C followed by 30ul protein A/G beads overnight at 4 ° C with gentle rotation. Beads were then pelleted at 1000 rpm for 2 min and washed 3 times. Antibody-protein conjugates were removed from beads by boiling (5 min) and samples were then subjected to SDS-PAGE and immunoblotting.

*MALT1-GRK2 binding.* Purified recombinant full-length human GST-MALT1 (1 µg) or GST-BCL10 (1 µg) was incubated with purified recombinant full-length human GST-GRK2 (1 µg) in buffer (150mM NaCl, 2mM EDTA, 10% glycerol, 1% Nonidet P-40, 20mM, Tris HCl, pH 7.4) containing protease inhibitors for 1h at 4°C. The reaction mix was subjected to immunoprecipitation with specified antibody.

*Lentivirus production and construction of stable cell lines.* All recombinant lentiviruses were produced by transient transfection of 293Ta cells (Lenti-Pac 293Ta, Cat. No. CLv-PK-01; GeneCopoeia). For GRK2 shRNA lentivirus, subconfluent 293Ta cells (10cm plate) were co-transfected with 10 µg GRK2 shRNA or control shRNA, 5 µg pRRE, 2.5 µg pRSV, and 3 µg pVSV using lipofectamine 3000 (Invitrogen). For GRK2 ORF cDNA lentivirus, subconfluent 293Ta cells (10cm plate) were co-transfected with 10 µg lentiviral ORF cDNA clones for *GRK2/ ADRBK1* (EX-A0311-Lv103) with N-eGFP or empty vector control plasmid (Ex-NEG-Lv103), together with 5 µg pRRE, 2.5 µg pRSV and 3 µg pVSV using lipofectamine 3000 (Invitrogen). Lentivirus-containing supernatants of transfected cells were collected at 48h, the solution was filtered at 0.45 µM and concentrated using the Lenti-Pac™ lentivirus concentration solution (GeneCopoeia). Stable transfection of cells was established by lentiviral infection. Transfection efficiency was determined by flow cytometry and western blot analysis. Lentivirus-transduced cells were kept under puromycin selection at the indicated concentrations: Jurkat T (5 µg/ml), OCI- Ly1 and Ly7 (2 µg/ml), OCI-Ly3 and HBL1 (1 µg/ml).

2

*GRK2 Knockout with CRISPR/Cas9 system.* The Jurkat and OCI-LY3 GRK2 knockout cell lines were custom-made by Genscript. gRNAs targeting the RGS region of GRK2 were designed using the CCTOP gRNA design tool (https://crispr.cos.uni-heidelberg.de/) along with CRISPRater which together determined the most efficient and specific guiding RNAs. Guide RNA sequence TCAGTGGCACTCTTCGAGAA with highest cleavage efficiency was used to generate gRNA-Cas9 plasmid or the gRNA-Cas9 ribonucleoprotein reagent. Jurkat cells were electroporated with gRNA-Cas9 plasmid and OCI-Ly3 cells were electroporated with gRNA-Cas9 RNP following Genscript user manual and monoclonal cell populations were generated by limiting dilution. Targeted disruption of GRK2 was confirmed by Sanger sequencing. Allelic analysis was carried out using Sanger sequencing and Tracking of Indels by decomposition (TIDE) (available at https://tide.nki.nl/).

*GRK2-deficient B cells.* To generate bone marrow chimeras, BM cells from Mb1cre- GRK2$^{fl/+}$ or Mb1cre+ GRK2$^{fl/fl}$ mice (provided by Dr. Jason Cyster, UCSF) were transferred into irradiated C57BL/6(B6) (NCI) recipients. Chimeras were analyzed at 8-12 weeks after reconstitution. Spleens and pLN were isolated from Mb1cre- GRK2$^{fl/+}$ or Mb1cre+ GRK2$^{fl/fl}$ mice and primary B cells were enriched with EasySep™ Mouse Pan-B Cell Isolation Kit (STEMCELL technologies).

*Cell proliferation assay.* Cell numbers were counted using Vi-cell cell counter (the trypan blue dye exclusion method) from Beckman Coulter.

*Luciferase assay.* HEK-293T cells were transfected with varying amounts of plasmid expressing the indicated proteins, in combination with an NF-κB-responsive luciferase reporter plasmid (pNF-κB-luciferase) (Stratagene, La Jolla, CA), and a *Renilla* plasmid (phRL-TK) (Promega, Madison, WI) was used to control for transfection efficiency. In each experiment, the total amount of DNA in each sample was kept constant by supplementation with the appropriate empty parental

3

expression vector. 24h post-transfection, the activities of Firefly and Renilla luciferase were measured using the Dual-luciferase reporter assay system (Promega), according to the manufacturer's instructions. The data represent relative Firefly luciferase activity normalized to Renilla luciferase activity and are representative of the independent experiments in triplicate. Data are presented as mean ±SEM. Jurkat T cells were transfected by electroporation using a Gene-Pulser (Bio-Rad) at 250 V and 960 μF and cultured overnight before stimulation.

*ELISA.* Cytokine concentrations in culture supernatants were measured by ELISA. Human IL-2 (431804), IL-6 (430504), Il-10 (430604) ELISAs (BioLegend) were performed according to the manufacturer's protocols.

*Nuclear protein extraction and NF-κB (p65) Transcription Factor Assay.* After experimental exposures, $7.5 \times 10^6$ cells were spun down, supernatant removed, and rinsed twice in PBS. Following centrifugation, the cell pellet was resuspended in 500ml buffer A (10mM HEPES, pH 7.9, 0.1mM EDTA, 0.1mM EGTA, 10mM KCL and protease inhibitors, 1.0mM DTT and 1% NP-40 added fresh) to lyse the cells. After a 20 minutes incubation on ice, the lysate was centrifuged at 13,000g for 5 min at 4°C to pellet the nuclei. The cytosolic supernatant was removed and saved while the nuclei pellet was washed 3x by adding 250ml of buffer A and centrifuged as previous. After washing, the nuclei pellet was resuspended in 15ml buffer C (20mM HEPES, pH 7.9, 0.42M NaCl, 1.0mM EDTA, 0.1mM EGTA, with DTT and protease inhibitors added fresh) and samples were vortexed and shaken at 4°C for 15 min. After a 10 min centrifugation at 13,000g, 4°C, the nuclear protein supernatant was removed and mixed with 22.5ml of buffer D (20mM HEPES, pH 7.9, 20% v/v glycerol, 0.1M KCl, 1.0mM EDTA, 0.1mM EGTA with 1% NP-40, DTT and protease inhibitors added fresh). Nuclear protein concentration was determined by Coomassie dye-based assay (Pierce, Rockford, Il) comparing samples to a BSA standard curve. 5 mg of

4

nuclear protein was used in NFkB (p65) ELISA Kit (Rockland Antibodies and Assays, Cat# KAA065). Duplicate technical reps of biological triplicates were assayed according to manufacturer's directions. Data was analyzed by 2way ANOVA with a Tukey's multiple comparison post-test (Graphpad Prism) and data is presented is one of 3 different experiments.

*Immune cell clustering and proliferation assay.* HBL1 cells with control GFP or GFP-GRK2 were seeded into 6-well plates in duplicate and placed into the IncuCyte ZOOM instrument (Essen Bioscience). IncuCyte ZOOM software was utilized to schedule repeat scanning every 2 hours. Immune cell proliferation was quantified by IncuCyte software using the confluence algorithm. To quantify immune cell clustering, size filters are applied to the confluence algorithm to identify aggregates with a minimal area of 1500 $\mu m^2$ and a maximal eccentricity of 0.95. Results are expressed as the number of clusters per square millimeter.

5
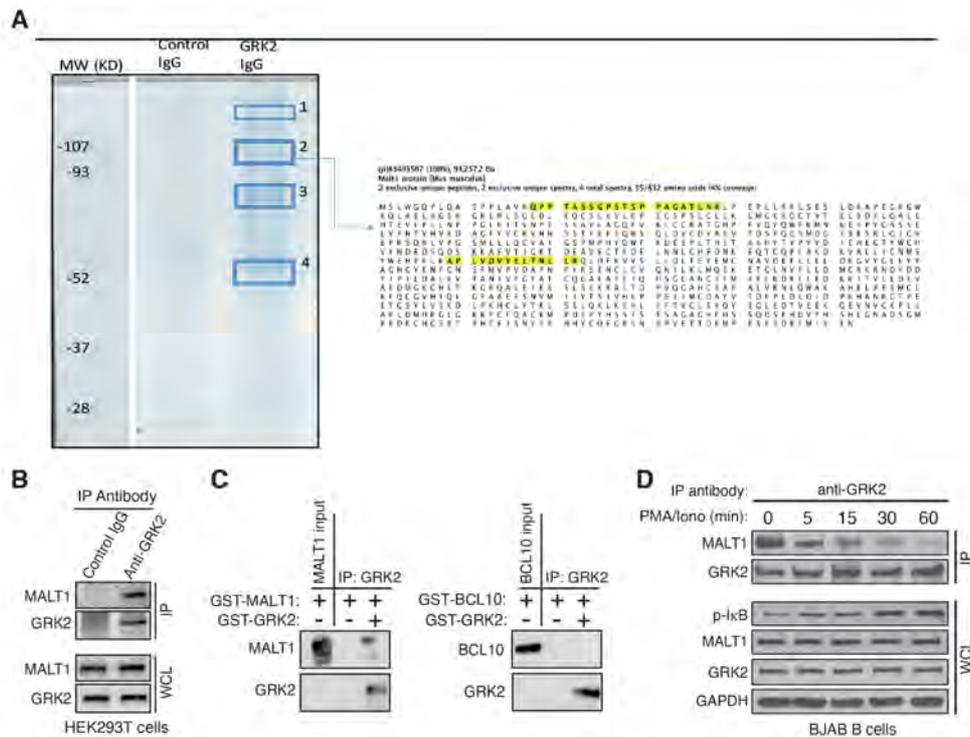
**Supplemental Figure 1. Identification of GRK2 as a novel MALT1 binding partner.** (**A**) GRK2 IP coupled with mass spectrometry identified MALT1 as a co-immunoprecipitated protein. Raw264.7 cell lysates were precleared with control-IgG-coupled aminolink resin for 2 hours, then immunoprecipitated with either GRK2 or control IgG antibody-coupled resin overnight. Eluted proteins were run on SDS-PAGE and visualized using coomassie stain. Unique bands from GRK2 IP were excised and submitted for trypsin digestion and mass spectrometry analysis (LS-MS-MS). Peptides identified by mass spectrometry, spanning the MALT1 protein, are shown highlighted in yellow. (**B**) Endogenous MALT1 and GRK2 interact in HEK 293T cells. Co-IP of MALT1 and GRK2 was demonstrated by western blot. (**C**) Reverse pull-down with purified recombinant proteins confirmed that GRK2 directly interacts with MALT1 but not BCL10. (**D**) AgR stimulation leads to GRK2/MALT1 dissociation in BJAB B-cells. All blots shown are representative of at least two seperate experiments.
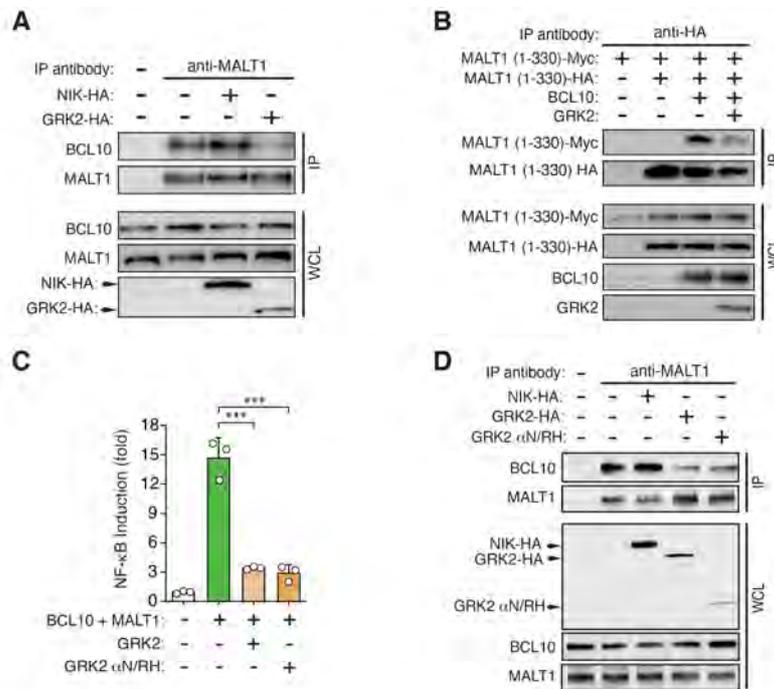
**Supplemental Figure 2. GRK2 inhibits MALT1 interaction with BCL10 and MALT1 oligomerization, and GRK2 αN/RH (AA 1-173) is as effective as full-length (FL) GRK2 in inhibiting NF-κB activation and MALT1/BCL10 interaction.** (A) GRK2 inhibits BCL10 interaction with MALT1. HA-tagged GRK2 or control protein, HA-NIK, were expressed in HEK293T cells and the Co-IP of endogenous BCL10 with MALT1 was assessed by western blot (n=3). GRK2 disrupts the BCL10/MALT1 interaction whereas the unrelated control protein, NIK, does not. (B) GRK2 inhibits MALT1 oligomerization. HA-tagged and Myc-tagged MALT1 (AA1-330) were transfected as indicated together with/without BCL10. The impact of GRK2 on BCL10 dependent MALT1 oligomerization was analyzed by western blot (n=3). (C) GRK2 αN/RH (AA 1-173) is as effective as FL GRK2 in inhibiting BCL10/MALT1-induced NF-κB luciferase reporter activity (n=3). ***P<0.001, by one-way ANOVA, followed by Tukey's multiple comparison test. (D) GRK2 αN/RH (AA 1-173) is as effective as FL GRK2 in inhibiting BCL10 interaction with MALT1. HA-tagged GRK2 (FL or GRK2 αN/RH) or control protein, HA-NIK, were expressed in HEK293T cells and the Co-IP of endogenous BCL10 with MALT1 was assessed by western blot (n=3).
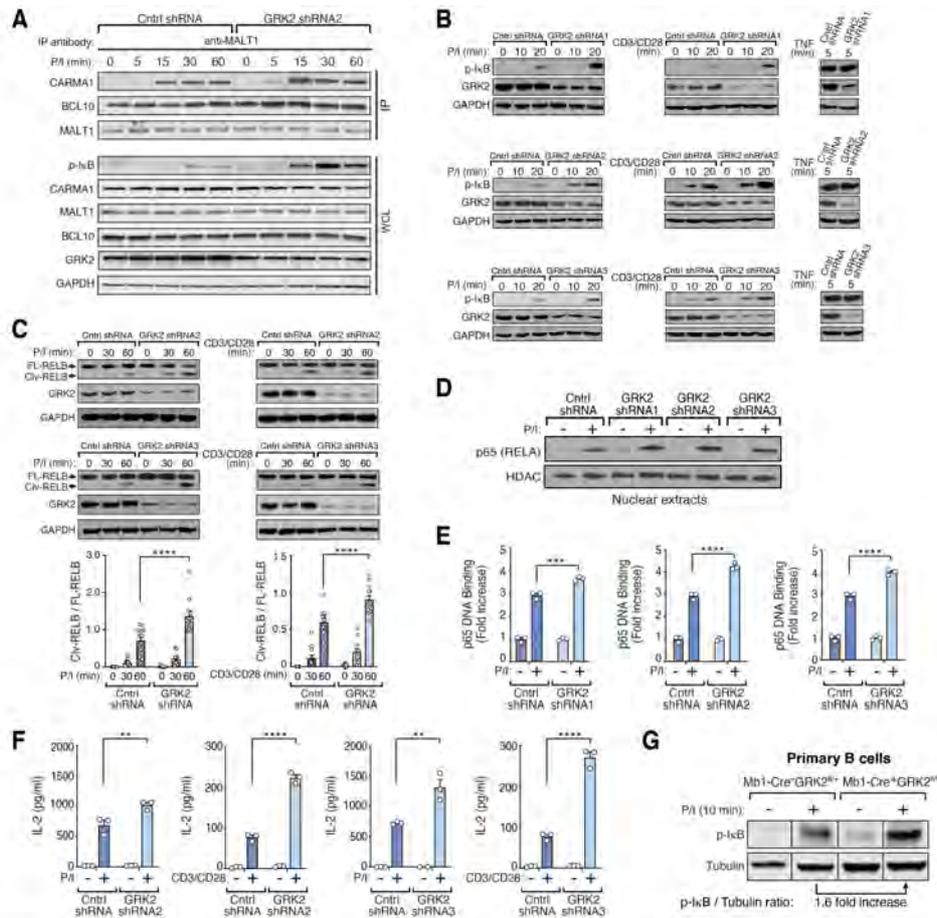
**Supplemental Figure 3. GRK2 attenuates AgR stimulation induced CBM complex formation, MALT1 protease activity, NF-κB activation, and IL-2 production.** (A) Knockdown (KD) of GRK2 in Jurkat T-cells enhances P/I-induced CBM complex formation in an additional Jurkat GRK2 KD clone infected by lentiviral GRK2 shRNA targeting a different region of GRK2 (GRK2 shRNA2). Jurkat T-cells were subjected to knockdown with either control or GRK2 shRNA lentivirus and then treated with/without P/I. Binding of BCL10 and CARMA1 to immunoprecipated MALT1 were examined (n=3). (B) GRK2 KD in Jurkat T-cells was performed using three distinct shRNAs targetting different regions of GRK2. In each case, knockdown of GRK2 leads to enhanced P/I (left panel) or anti-CD3/CD28 (middle panel) but not TNF(right panel) induced IκB phosphorylation. (C) GRK2 KD leads to increased cleavage of RELB in response to P/I (left panel) or anti-CD3/CD28 (right panel) stimulation in two additional Jurkat GRK2 KD clones (GRK2 shRNA2 and GRK2 shRNA3). Quantification is shown below (n=3-4 per shRNA clone x 3 individual shRNAs). ****P<0.0001. (D) GRK2 KD leads to enhanced p65 nuclear translocation after P/I stimulation. Nuclear extracts were made and analyzed by western blot. HDAC was used as a control for nuclear protein. (E) GRK2 KD leads to enhanced p65 DNA binding after P/I stimualtion. Nuclear extracts were made from P/I treated control and GRK2 KD cells and analyzed using non-radioactive EMSA kit (n=3). ***P<0.001, ****P<0.0001. (F) GRK2 KD leads to enhanced IL-2 production in Jurkat T- cells. Cells were treated as indicated for 24 hours and IL-2 in supernatants was measured by ELISA (n=3). *P<0.05, ***P<0.001,****P<0.0001. (G) GRK2 knockout in primary B cells enhances P/I-induced IκB phosphorylation. Bone marrow cells of Mb1-Cre-GRK2^fl/+ or Mb1-Cre+GRK2^fl/fl mice were transfered to irradiated C57BL/6 (B6) recipients. Chimeras were analyzed 8-12 weeks after reconstitution. Primary B cells were isolated from spleens and treated with P/I for indicated time (n=2). Vertical lines are included in the figure to indicate that lanes were run on the same gel but were non-contiguous. Statistical significance for panels C, E, and F was evaluated by two-way ANOVA, followed by Tukey's multiple comparison test.
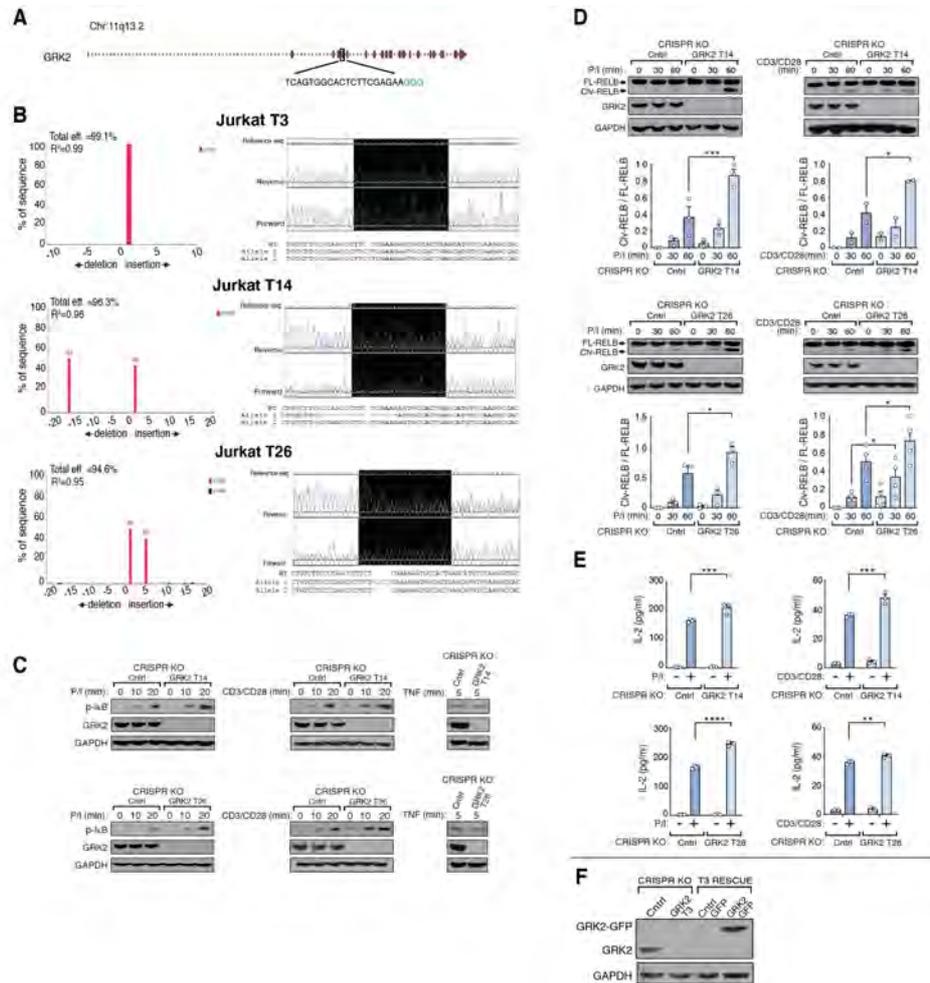
**Supplemental Figure 4. Targeted knockout (KO) of GRK2 leads to enhanced MALT1-dependent activities in Jurkat T-cells** (**A**) Overview schematic of the Cas9/gRNA target site. Genomic coordinates are shown on the left. The gRNA-targeting sequence is shown, and the PAM sequence is labeled in green. (**B**) TIDE analysis (left), chromatogram sequence alignment and allelic analysis of the gene editing activity (right), around the GRK2 target site of the clonally expanded populations (T3, T14 and T26) are shown. Sanger sequencing of both the forward and reverse strand is shown. (**C**) GRK2 KO leads to increased P/I-(left panels) or anti-CD3/CD28-(middle panels) but not TNF-(right panels) induced IκB phosphorylation in additional Jurkat T-cell clones (T14 and T26). GRK2 KO was confirmed by western blot. Blots are representative of at least 3 experiments. (**D**) Cleavage of RELB induced by P/I (left panel) or anti-CD3/CD28 (right panel) was enhanced in additional GRK2 KO Jurkat T-cell clones (T14 and T26). Densitometric quantification was performed using Alphaview software (n=2-4). Clv, cleaved; FL, full-length. *P<0.05, ***P<0.001. (**E**) IL-2 production was enhanced in additional GRK2 KO Jurkat T-cell clones (T14 and T26). Cells were treated with/without P/I or anti-CD3/CD28 for 24 hours and IL-2 in the supernatant was measured by ELISA. Results are expressed as the mean ± SEM (n=3-4). **P<0.01, ***P<0.001, ****P<0.0001. (**F**) GRK2 rescue in GRK2 KO Jurkat T-cell clone T3 was achieved using lentiviral WT GRK2-GFP. Statistical significance for panels D and E was evaluated by two-way ANOVA, followed by Tukey's multiple comparison test.
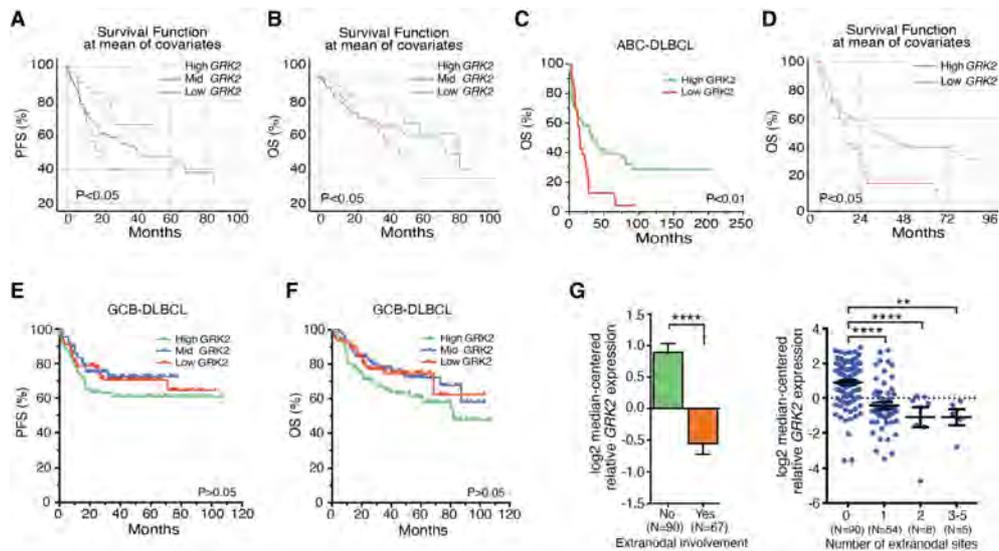
**Supplemental Figure 5. Additional bioinformatic analyses related to *GRK2* expression in human DLBCL.** (A,B) Kaplan-Meier plots for PFS (**A**) and OS (**B**) at the mean of sampled covariates show that *GRK2* is an independent risk factor for mortality. Data for panels A and B were accessed from same public repository (GSE31312) as in **Figure 6C** and **D** and then analyzed by multivariate Kaplan Meier analysis, controlling for age and gender. (**C**) OS rates of ABC-DLBCL patients are significantly lower in patients with low *GRK2* as compared to high *GRK2*. Overall survival curves were stratified by high and low *GRK2* expression values from an additional dataset (GSE4732). Statistical significance was evaluated using Log-rank test. (**D**) The Kaplan Meier plots of dataset (GSE4732) at the mean of sampled covariates confirms that *GRK2* is a independent predictor of OS (P<0.05) in ABC-DLBCL patients. Data were analyzed by multivariate Kaplan Meier analysis as in (A) and (B). (**E,F**) Rates of PFS (**E**) and OS (**F**) of GCB-DLBCL patients are not different between GRK2 high and low groups. Expression of GRK2 was stratified into high, mid and low ranges using dataset-wide quartile cutoffs (high 25%, mid 50%, low 25%). Statistical significance was evaluated using Log-rank test. Data were accessed from the same repository as in **Figure 6C** and **D** (GSE31312). (**G**) Low *GRK2* expression in ABC-DLBCL is associated with extranodal spread (left panel). Further, the number of extranodal sites involved correlates with increasingly lower *GRK2* levels (right panel). *GRK2* expression levels were obtained from microarray data available in public repository GSE10846. **P<0.01, ****P<0.0001, by MANOVA.
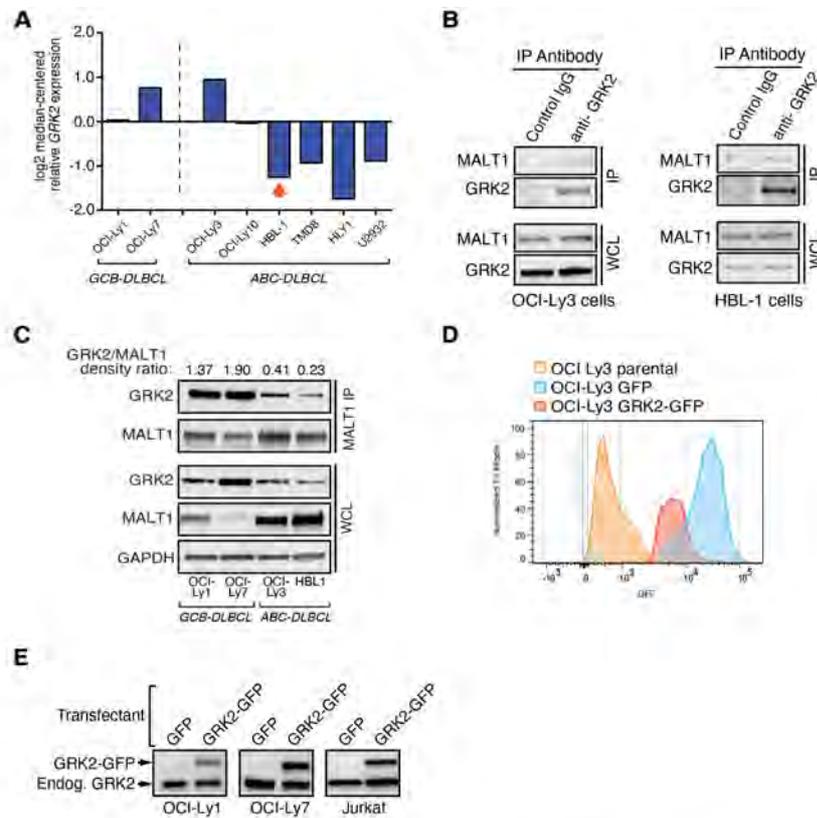
Supplemental Figure 6. GRK2 expression and endogenous MALT1 and GRK2 interaction in GCB and ABC-DLBCL lines. (A) An independent dataset was used to confirm the markedly low GRK2 mRNA level in HBL1 cells. cDNA microarray data were retrieved from the public repository (GSE57083) and analyzed. (B) Endogenous MALT1 and GRK2 interact in OCI-Ly3 and HBL1 cells. Co-IP of MALT1 with GRK2 was demonstrated by western blotting. Blots are representative of 3 separate experiments. (C) Relatively less binding of GRK2 to MALT1 was found in ABC-DLBCL as compared to GCB-DLBCL cell lines. CO-IP of MALT1 and GRK2 was demonstrated by western blot (n=3). The amount of GRK2 associated with immuno-precipited MALT1 was quantified (numbers shown above the blots). (D) GRK2-GFP was effectively expressed in OCI-Ly3 cells infected with lentivirus, as detected by flow cytometry. Data are representative of 3 independent experiments. (E) GRK2-GFP was efficiently expressed in two GCB-DLBCL lines (OCI-Ly1 and OCI-Ly7) and in Jurkat T-cells (n=3). Stable cell lines were made using the same lentivirus as was used in ABC-DLBCL cells.
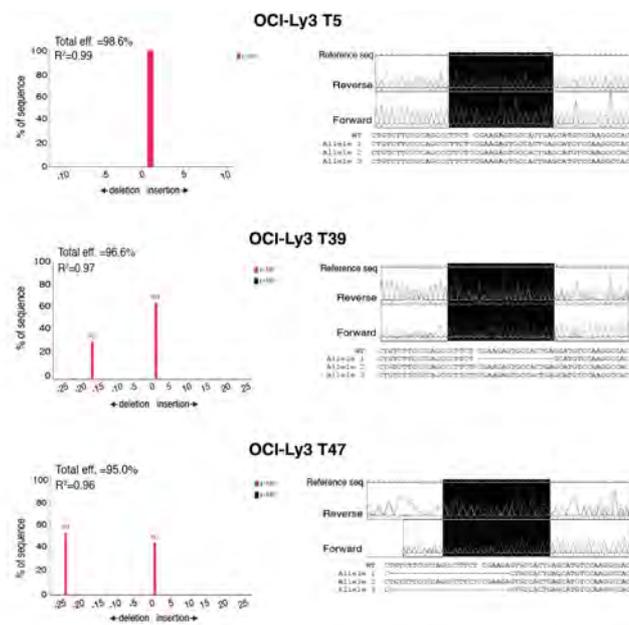
**Supplemental Figure 7.** TIDE analysis (left), chromatogram sequence alignment and allelic analysis of the gene editing activity (right), around the GRK2 target site of the clonally expanded populations (T5, T39 and T47) of OCI-Ly3 cells are shown. Sanger sequencing of both the forward and reverse strand is shown.
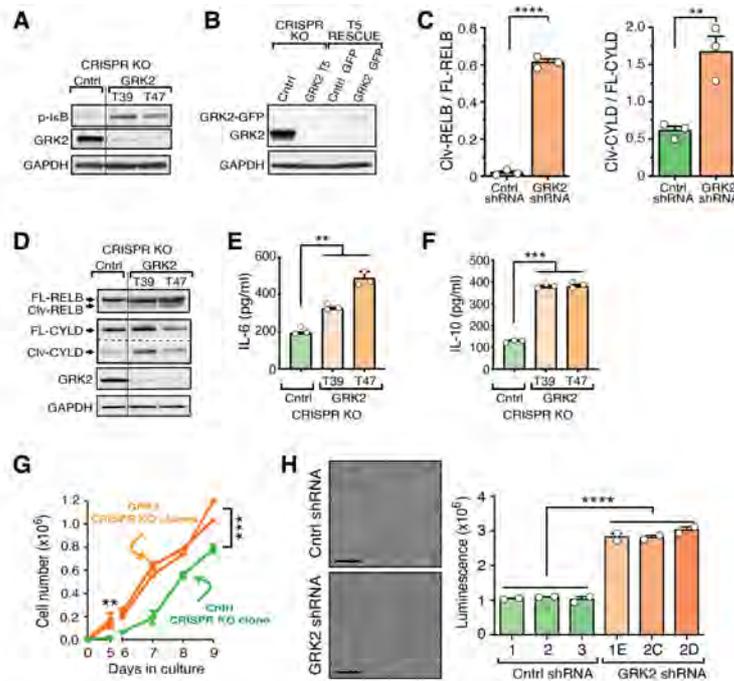
**Supplemental Figure 8. Targeted knockout (KO) of GRK2 leads to enhanced MALT1 activity, MALT1-dependent cytokine secretion and proliferation in ABC-DLBCL cell line OCI-Ly3.** (A) GRK2 KO leads to increased basal IκB phosphorylation in additional OCI-Ly3 clones (T39 and T47). OCI-Ly3 cells with GRK2 KO were made using Cas9/gRNA. GRK2 KO was confirmed by western blot. Blots are representative of at least 3 experiments. A vertical line is included in the figure to indicate that lanes were run on the same gel but were non-contiguous. (B) Rescue of GRK2 was achieved using lentiviral WT GRK2-GFP in GRK2 KO OCI-Ly3 clone T5 (n=3). (C) Densitomeric analysis of RelB and CYLD cleavage using Alphaview for Figure 8B. Results are expressed as the mean ± SEM (n=3). **P<0.01, ****P<0.0001. (D) GRK2 KO leads to increased cleavage of RELB and CYLD in additional OCI-Ly3 clones (T39 and T47). Blots shown are representative of n=3. A vertical line is included in the figure to indicate that lanes were run on the same gel but were non-contiguous. Clv, cleaved; FL, full-length. (E and F) GRK2 KO leads to increased IL-6 and IL-10 production in additional OCI-Ly3 clones (T39 and T47). IL-6 and IL-10 secretion were determined by ELISA (n=3). **P<0.01, ***P<0.001. (G) GRK2 KO leads to increased proliferation in additional OCI-Ly3 clones (T39 and T47). Results are expressed as the mean ± SEM (n=3). ***P<0.001 by two way ANOVA and Dunnett's multiple comparisons test (significance for the end time points is shown). (H) shRNA-mediated GRK2 knockdown leads to increased cellular aggregation and adhesion of OCI-Ly3 cells. Cells were cultured for 72 hours without agitation. Attached cells were imaged using the IncuCyteZOOM instrument (x20) after unattached cells were carefully removed with the culture supernatant. Scale bars: 200μm. Cells attached to the bottom of the culture dish were quantified using luminescence detection. Results are expressed as the mean ± SEM, ****P<0.0001. Control clones (1, 2, and 3) and GRK2 KD clones (1E, 2C, and 2D) were analyzed separately (total of n=6 for both control and for GRK2 KD). Statistical significance for panels C, E, F, and H was evaluated by unpaired, two-tailed Student's T test.
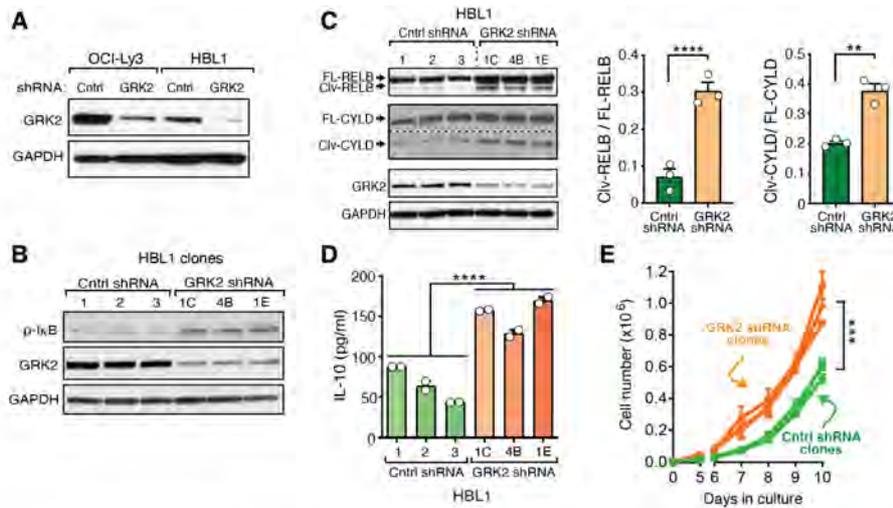
**Supplemental Figure 9. Knockdown of GRK2 results in enhanced MALT1-dependent activity in another ABC-DLBCL cell line (HBL1).** (A) As with OCI-Ly3 cells, GRK2 can be targeted for knockdown by shRNA in HBL1 cells. (B) GRK2 knockdown leads to increased basal IκB phosphorylation in HBL1 cells. Stable HBL1 cells with GRK2 knockdown were made using shRNA-encoding lentivirus (3 GRK2 knockdown clones are shown; 1C, 4B, and 1E). GRK2 knockdown was confirmed by western blotting. Blots are representative of at least 3 experiments. (C) Stable knockdown of GRK2 in HBL1 cells results in increased cleavage of RELB and CYLD. Blots shown are representative of three experiments. Densitometric analysis of cleavage using Alphaview is shown on the right (n=3). **P<0.01, ****P<0.0001 by unpaired, two-tailed Student's T test. Clv, cleavage; FL, full-length. (D) GRK2 knockdown leads to increased IL-10 production in HBL1 cells. IL-10 secretion was determined by ELISA. Control clones (1, 2, and 3) and GRK2 KD clones (1E, 2C, and 2D) were analyzed separately (total of n=6 for both control and for GRK2 KD). ****P<0.0001, by unpaired, two-tailed Student's T test. (E) GRK2 knockdown leads to increased proliferation of HBL1 cells (n=3). Two-way ANOVA and Sidak's multiple comparison test were performed to show proliferation differences between the GRK2 KD and control groups. ***P <0.001.